


### III. ACCELERATOR PHYSICS AND EXOTIC BEAM TECHNOLOGY

#### OVERVIEW



This chapter presents the results of R&D being carried out by the group at Argonne that was working on concepts for the U.S. Rare Isotope Accelerator Project (RIA). This R&D is now mostly directed towards components and concepts for a facility that is approximately half the cost of RIA, the Advanced Exotic Beam Laboratory (AEBL). That work has now also been generalized to projects related to advanced exotic beam facilities world-wide, and has also been extended to include work related to other accelerator projects such as the 8-GeV proton driver project at Fermi Lab and the International Linear Collider (ILC) Project.

The topics covered in this chapter are arranged in three main sub-sections: (A) Superconducting RF, (B) Beam Dynamics and Injectors, and (C) Rare Isotope Production and Separation.

Highlights of developments during 2006 include:

- Significant progress on the construction of a prototype RIA-type drift-tube cryomodule that will be used for an ATLAS Energy Upgrade Accelerator Improvement Project.
- Initial operation of the new clean room and surface processing facility in building 208 which was constructed as a joint FNAL/ANL project.
- Continued work on several aspects of the FNAL proton driver project including extensive studies of the beam dynamics of the full 8-GeV linac.
- Continued development of the beam dynamics for a high-power heavy-ion driver linac based on a 345-MHz triple-spoke resonator including studies to quantify the effects of misalignment and RF setting errors, and the development of algorithms for optimization and tuning of multiple-charge-state beams.
- Complete an updated design of the  $m/q = 240$  injector for an exotic beam post accelerator.
- Full power tests of the prototype module of a cw RFQ for the high-power driver linac.
- Significant progress towards completion of a prototype two-charge-state low energy beam transport system.

- Construction of a prototype system to demonstrate a thin film liquid lithium stripper for use with high intensity uranium beams in the driver linac.
- Simulation tools for large acceptance fragment separator designs have been developed as extensions of the COSY Infinity high-order optics code.
- Significant progress has been made in the development of techniques for inclusion of full 3-D effects of large aperture magnets in COSY Infinity.
- Methods to prepare samples of  $UC_x$  with density over  $5 \text{ g/cm}^3$  and thermal conductivity over  $10 \text{ w/m-k}$  have been developed.
- A beamline for high intensity tests of the large-scale prototype gas catcher has been constructed and used for first evaluations.
- Detailed simulations of an alternative gas catcher geometry, the "inverse-cyclotron" concept, have shown that there are several problems with the approach.



## A. SUPERCONDUCTING RF

### a.1. Joint ANL/FNAL Superconducting Cavity Surface Processing Facility (SCSPF) (M. Kelly, S. Gerbick, and K. W. Shepard)

Cavity electropolishing at the joint ANL/FNAL SCSPF began in 2006 on a set of six new quarter-wave resonators as part of an energy upgrade to the ATLAS accelerator. Electropolishing, together with clean assembly, is a key to achieving the best possible

performance in today's bulk niobium SRF cavities. Figure III-1 shows the two major sub-assemblies of the quarter-wave resonator that were electropolished separately and will be electron beam welded together to form the complete niobium cavity.

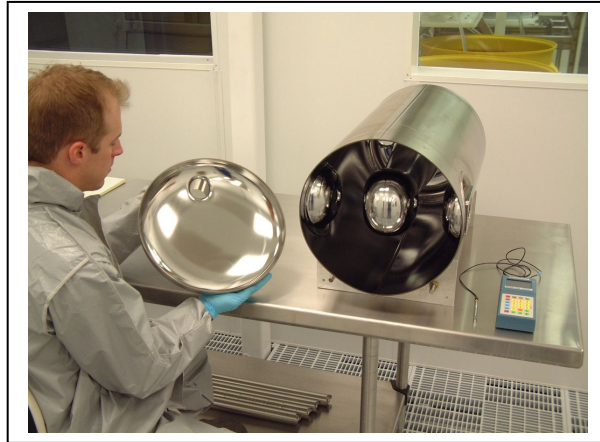


*Fig. III-1. The two major sub-assemblies of an ANL quarter-wave cavity immediately after electropolishing and prior to the final electron beam closure weld.*

The facility will also support R&D for the International Linear Collider. Shown in Fig. III-2 is a nearly complete engineering design for a new electropolishing system for 1.3 GHz elliptical cell cavities to be housed

in the ANL portion of the joint facility. First operations are planned for the summer of 2007. The system is also planned to meet most of the electropolishing needs for ILC cavities in the U.S. for the next two years.

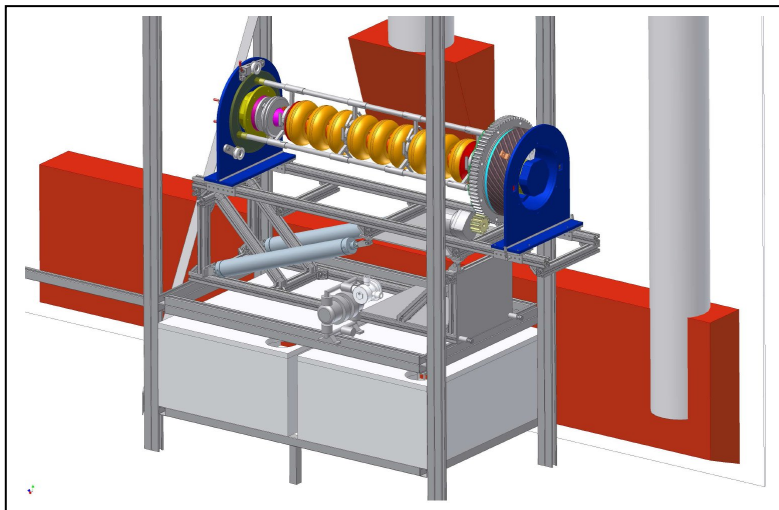


*Fig. III-2. A 1.3 GHz elliptical cell cavity electropolishing system designed at ANL for the joint ANL/FNAL SCSPF.*

### a.2. Fast Mechanical Tuner Development for AEBL (Z. A. Conway, J. Fuerst, M. P. Kelly, S. I. Sharamentov, K. W. Shepard, and G. Zinkann)

The superconducting spoke cavities in the proposed Advanced Exotic Beams Laboratory (AEBL) driver linac will be highly sensitive to mechanical deformations due to their small beam-loaded bandwidth. RF eigenfrequency variations due to microphonics which are a large fraction of the loaded cavity bandwidth result in RF field phase and amplitude errors. The phase and amplitude control system must tolerate this RF frequency variation. This can be accomplished by increasing the output power from the RF power source, and/or controllably deforming the cavity with a fast mechanical tuner to introduce a controllable RF frequency variation. The sum of the microphonic and the controllable mechanical tuner induced RF frequency variations will be less than the total microphonic RF frequency variations, reducing the RF power required to control the cavity RF field amplitude and phase.

The performance of two prototype fast mechanical tuners was characterized by measuring the coupled tuner/cavity transfer function. The transfer function correlates the amplitude and frequency of the tuner drive signal with the cavity RF frequency modulation. This was done by sweeping the frequency of the signal

driving the fast tuner and simultaneously recording the phase and amplitude of the resulting cavity RF frequency modulation.

The fast tuners were mounted on the spoke cavities by bolting the actuator assembly to a conflat flange on the integral stainless steel helium jacket. During operation the fast tuner actuator expands and contracts, pushing between the niobium wall of the cavity and the stainless-steel helium jacket.

The first mechanical tuner tested was a piezoelectric actuated fast tuner. The mechanical tuner incorporated an APC International Ltd. PSt 1000/25/100 actuator mounted in an ANL designed guide assembly. The transfer function for this tuner mounted on the  $\beta = 0.5$  triple-spoke cavity is shown in Fig. III-3.

The second tuner tested was a magnetostrictive actuated fast tuner. The mechanical tuner incorporated an Energen Inc. actuator supplied to ANL under an SBIR grant. The actuator was mounted in an ANL designed guide assembly. The transfer function for this tuner mounted on the  $\beta = 0.5$  triple-spoke cavity is shown in Fig. III-4.

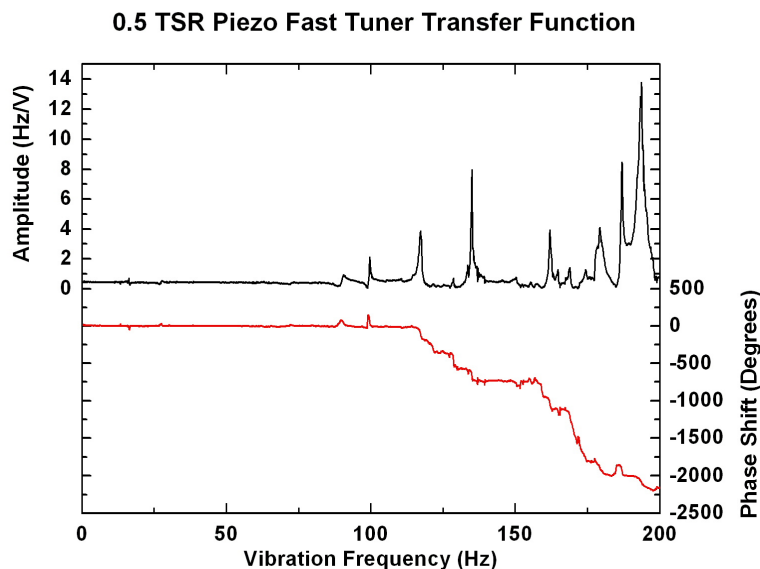


Fig. III-3. Transfer function amplitude and phase for the combined  $\beta = 0.5$  triple spoke resonator and piezoelectric fast tuner system.

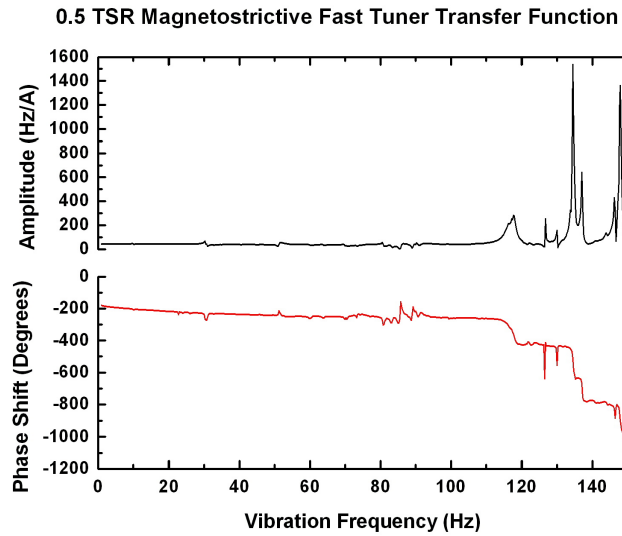


Fig. III-4. Transfer function amplitude and phase for the combined  $\beta = 0.5$  triple spoke resonator and magnetostrictive fast tuner system.

The piezoelectric fast tuner was also used to damp the RF frequency variations due to microphonics in the  $\beta = 0.5$  triple-spoke cavity. The piezoelectric fast tuner was operated in a negative feedback loop with the control signal proportional to the RF frequency

deviation of the cavity from an external stable oscillator. The probability density and the spectrum of the RF frequency variations with and without the piezoelectric fast tuner negative feedback are shown in Figs. III-5 and III-6, respectively.

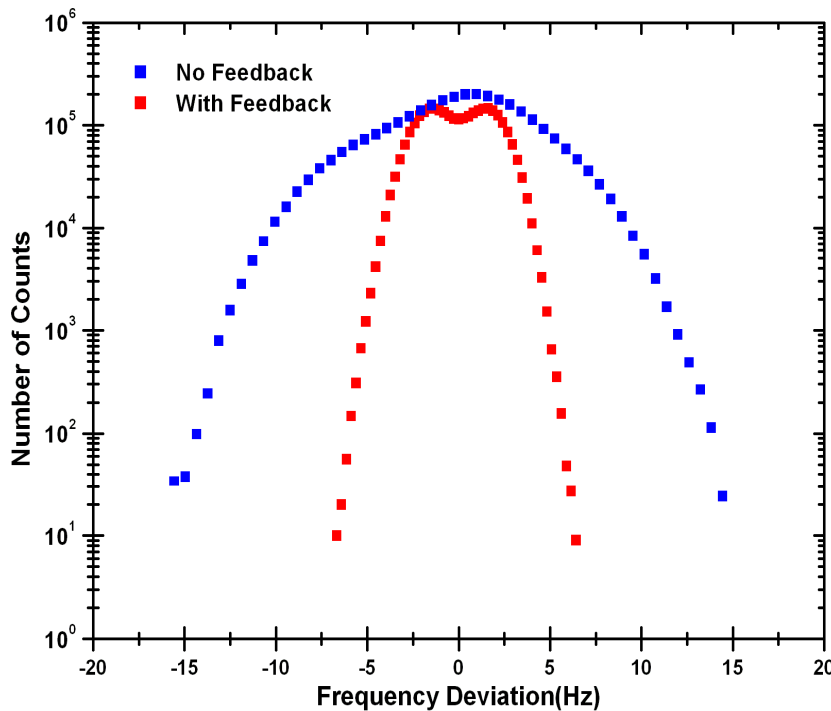


Fig. III-5. Probability density of the  $\beta = 0.5$  triple spoke resonator microphonic induced RF frequency variations with and without negative feedback.

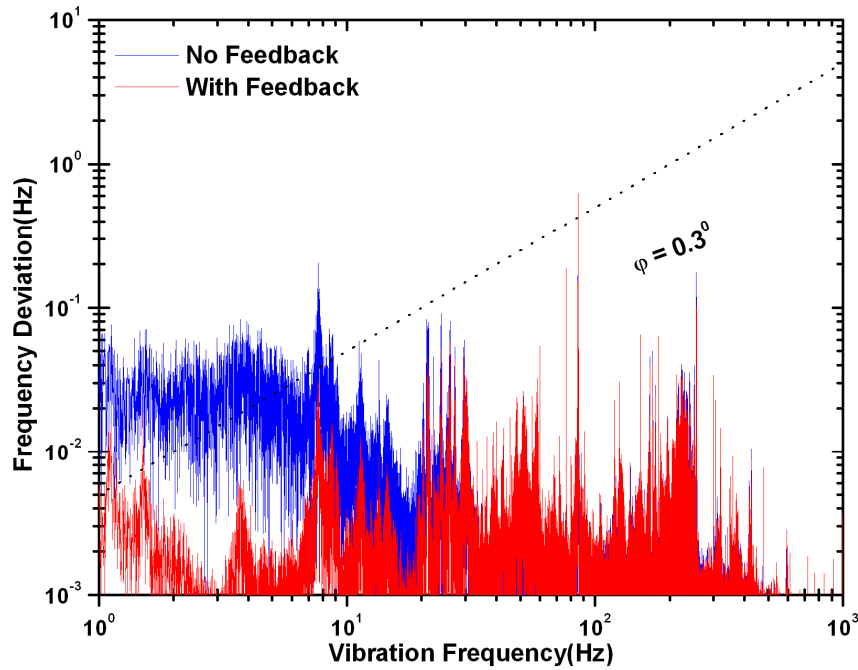


Fig. III-6. Frequency spectrum of the  $\beta = 0.5$  triple spoke resonator microphonic induced RF frequency variations with and without negative feedback.

**a.3. Cavities and Cryomodule for the ATLAS Upgrade** (Z. Conway, J. Fuerst, M. Kedzie, M. Kelly, S. MacDonald, and K.W. Shepard)

The remaining six quarter-wave cavities for the ATLAS upgrade cryomodule are nearing completion. Major subassemblies have been electron beam welded together in preparation for final assembly. Figure III-7

(left) shows cavity housings and center conductors while (right) shows a center conductor and toroid end ready for electron beam welding.

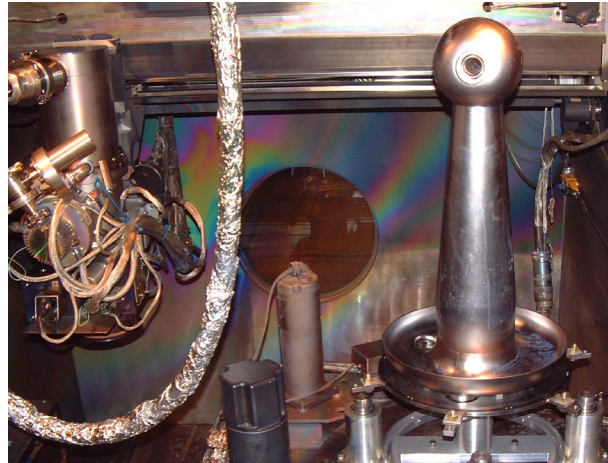


Fig. III-7. Housing/re-entrant nose subassemblies together with center conductor subassemblies for six quarter-wave cavities (left). Center conductor and upper toroid subassemblies are fixtured in vacuum chamber for electron beam welding (right).

The cavities must resonate at the proper frequency to perform in the accelerator. During fabrication, frequency is tuned within one part in ten million by adjusting the cavity geometry. Major subassemblies are periodically clamped together to measure the resonant frequency, factoring in the predicted impact of future construction steps such as weld shrinkage and chemical processing. Figure III-8 (left) shows a typical

frequency measurement setup. To save on fixturing costs and, more importantly, to avoid the possibility of tool bit inclusions which could lead to weld blowout, we have made extensive use of wire EDM to trim subassemblies to length during tuning. Figure III-8 (right) shows a housing and center conductor, together with trim rings cut off as part of the tuning process.



*Fig. III-8. Cavity assembly clamped together for frequency measurement (left). Cavity housing and center conductor together with rings of material sliced off using wire EDM for frequency adjustment (right).*

Cryomodule engineering tests have been performed to verify thermal shield performance. Future tests of the cryogenic systems are planned. Additional subsystems

such as input couplers and mechanical slow tuners are approaching final design and will be fabricated next year.





## B. BEAM DYNAMICS AND INJECTORS

### b.1. Development and Test of a Grid-Less Multi-Harmonic Buncher (P. N. Ostroumov, V. N. Aseev, A. Barcikowski, B. Clifft, R. Pardo, S. I. Sharamentov, and M. Sengupta)

Currently, ATLAS is being upgraded with the Californium Rare Ion Breeder Upgrade (CARIBU). To avoid beam losses associated with the existing gridded multi-harmonic buncher (MHB), we have developed and built a grid-less four-harmonic buncher with a fundamental frequency of 12.125 MHz. The side cross-section and side view of the MHB are shown in Fig. III-9. This configuration allowed us to use the multi-harmonic RF electronics and vacuum box of the old buncher. The multi-harmonic buncher must produce a saw-tooth modulation of the beam energy which produces a short bunch width at the entrance of the first PII cavity. The energy gain of a charged particle passing through the grid-less MHB depends on the transit time factor which is a function of both the particle velocity and harmonic number. Determination of the exact harmonic mix and beam dynamics simulations has been performed using the TRACK code. The main concern in a grid-less bunching system is the uniformity of the longitudinal electric field over the radial direction. As follows from the TRACK simulations there is no noticeable effect of the beam size in the MHB on the quality of beam bunching.

The performance of the new MHB has been measured by studying the beam bunch width using a Fast Faraday Cup located at the first accelerating resonator in the

ATLAS linac. Beams of  $^{40}\text{Ar}^{9+}$ ,  $^{58}\text{Ni}^{15+}$ , and  $^{16}\text{O}^{6+}$  were used in these bunching tests at an energy of 35 keV/u. Using the  $^{40}\text{Ar}^{9+}$  beam, the performance of the buncher was compared to TRACK calculations. The bunch width was measured to be  $(0.7 \pm 0.2)$  ns FWHM, as seen in Fig. III-10, in good agreement with TRACK predictions which is 1 nsec.

The harmonic buncher operates in conjunction with a 24.25 MHz spiral loaded 2-gap resonator which rebunches the beam to reduce the bunch width into the first resonator further and to reduce the sensitivity to space charge. Nominally, the additional "magnification" from this buncher was expected to be approximately 0.3. The two bunchers can operate such that the second buncher is presented with either a "virtual" or a "real" waist from the harmonic buncher. TRACK calculations predicted that the virtual waist would be the better operating mode. This was tested using a  $^{58}\text{Ni}^{15+}$  beam at low ( $\sim 1.5$  eμA) beam current. The transmission through the first section of the linac (18 resonators accelerating the beam to approximately 1.5 MeV/u) was observed for both cases. For the virtual waist condition the best transmission achieved is 73% of the original DC beam and only 68% for the real waist configuration. TRACK calculations predicted 75% and 65% for the two situations respectively.

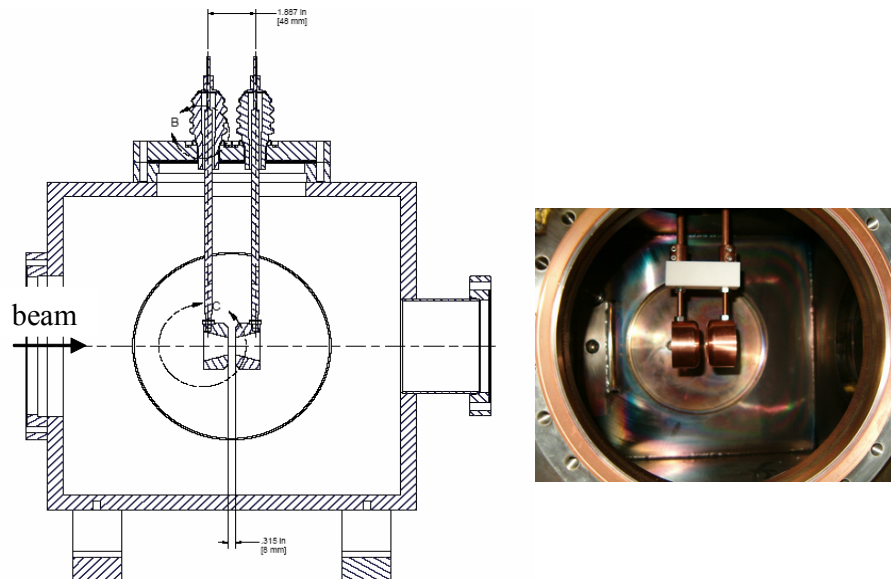


Fig. III-9. The side cross-section (left) and the side view (right) of the buncher.

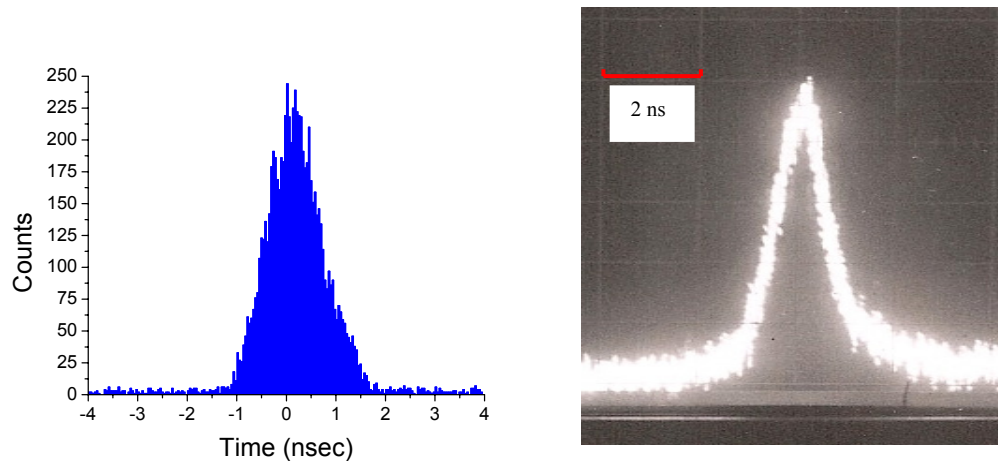


Fig. III-10. Simulated (on the left) and measured (on the right) bunch intensity distribution at the PII entrance for the low current ( $0.3 \mu\text{A}$ )  $^{40}\text{Ar}^{9+}$  ion beam.

### b.2. High Power Tests of a 57-MHz CW RFQ (P. N. Ostroumov, A. Barcikowski, M. Bracken, B. Clift, S. A. Kondrashev, and S. I. Sharamentov)

A Continuous Wave (CW) Radio Frequency Quadrupole (RFQ) accelerator has been designed for the RIA Driver Linac and reported previously. The high-power tests were performed using a 20-kW triode amplifier. After several hours of outgassing, the inter-vane voltage was increased to 75 kV, limited by the amplifier power. To increase available power, the triode circuit was tuned to the cavity frequency to produce 22 kW into a dummy load. When full RF power was applied, the cavity was operated with vacuum in the medium  $10^{-6}$  Torr range. Due to the restricted capacity of the cooling system, the cavity can be operated at a high power level only in self-excited mode. At the highest available power the eigenfrequency of the cavity drops by 240 kHz and the cavity temperature increases by  $20^\circ\text{C}$ .

Inter-vane voltage calibration was performed by two methods: (a) using power-loss measurements and (b) X-ray end-point energy measurements. The pick-up loop power was measured directly by a power meter. The results are shown in Fig. III-11. So far, no sparking has been observed in the cavity when the available RF power is limited by the amplifier. Table III-1 shows the calculated and measured cavity parameters. Simulations by HFSS and MWS have been performed using exact 3D model of the cavity.

We observed multipacting in the cavity at 200-230 Watts power level. This level of RF power corresponds to the voltage required for acceleration of

protons when the design voltage for the uranium beam is 68.5 kV. Our experiments suggest that the design voltage for uranium beams can be chosen to be at least  $\sim 85$  kV, which makes the RF power required for proton acceleration equal to 320 W. We can, therefore, conclude that the RFQ cavity will provide stable acceleration of any ions, from hydrogen to uranium.

Currently, we are restricted in cavity cooling capacity: the design flow of the water is 50 GPM at 8 kW while we have operated at 9 GPM. As a consequence, there is an appreciable frequency shift which primarily occurs due to displacement of the vane tips. To observe vane tip displacement we have installed a CCD camera and taken images of the vane tips through a vacuum window as RF power is increased. Figure III-12 shows the intensity of the image signal taken in horizontal plane along the horizontal direction. We have detected  $\sim 120 \mu\text{m}$  change of the distance between the vane tips at 8.6 kW compared to the  $40 \mu\text{m}$  design value. We expect that with increased cooling capabilities the displacement of the vane tips and frequency shift can be significantly reduced.

The basic design concepts, namely, 100% OFE copper structure machined prior to the assembly with high accuracy, and brazing in high temperature hydrogen atmosphere furnace have proven extremely successful, as evidenced by the voltages achieved and RF power requirements in initial tests of the RIA driver RFQ. So far, no sparking has been observed in the cavity when

operating up to the limit of available RFQ power.

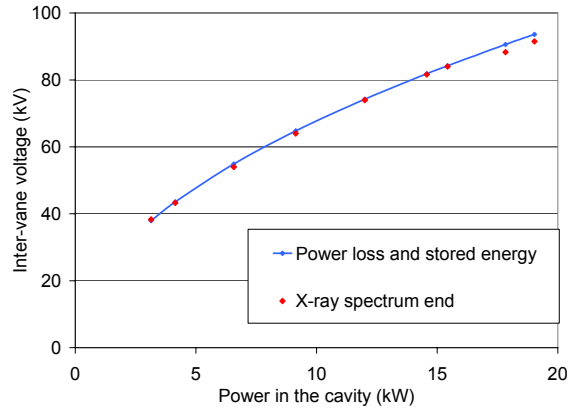


Fig. III-11. RFQ inter-vane voltage as a function of forward RF power measured by two methods.

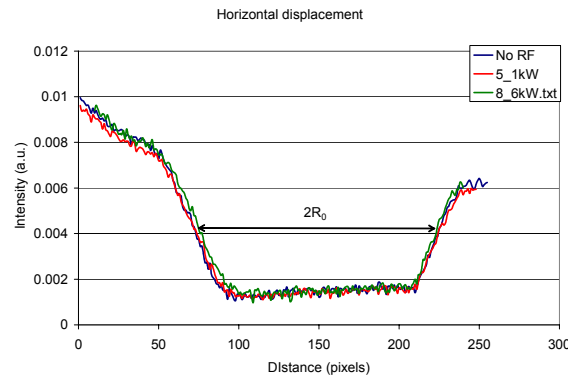


Fig. III-12. CCD image intensity along the horizontal plane.  $2R_0$  is the distance between the vane tips.

Table III-1. Comparison of the simulated and measured parameters of one-segment RFQ cavity.

Parameter	Simulated	Measured
Frequency, MHz	55.62	55.863
Quality factor	9317	8688
Stored energy ( $V_0 = 68.5$ kV), J	0.254	-
P (kW) to obtain $V_0 = 68.5$ kV, kW	9.5	10.2
P (kW) to obtain $V_0 = 91.5$ kV, kW	17.6	19.0

### b.3. Production of a $^{209}\text{Bi}$ Beam in an All Permanent Magnet ECR Ion Source (R. H. Scott, S. A. Kondrashev, and P. N. Ostroumov)

During the past year the 700 W, 12.75-14.5 GHz TWT RF amplifier has been repaired on the BIE-100 all permanent magnet (PM) ECR ion source.<sup>1</sup> When combined with the 2 kW, 14 GHz klystron, two

frequency operation has been restored. An easily replaceable commercial oven<sup>2</sup> for production of metal ions was added to the source as well (Fig. III-13).

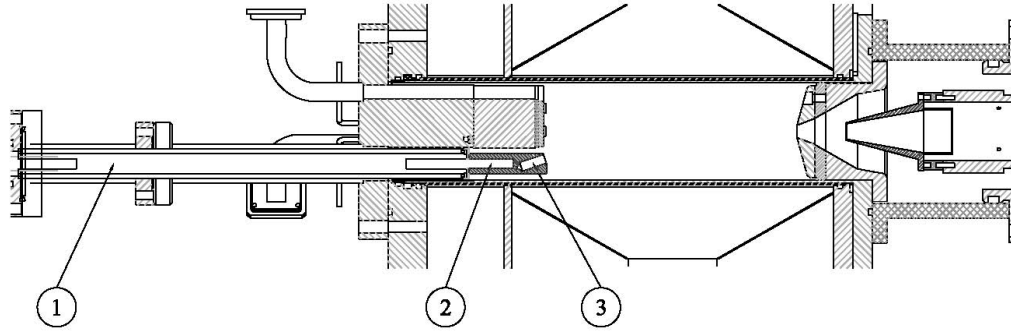


Fig. III-13. BIE-100 with (1) oven support assembly, (2) cartridge heater insertion point and (3) sample material.

The oven can operate up to a temperature of  $800^{\circ}\text{C}$ , which is enough to evaporate a wide range of metals. The frequency of TWT RF amplifier, biased disc potential and oven power are controllable from outside of the high voltage cage. Bismuth, with an operating temperature near  $550^{\circ}\text{C}$ , has been used for the tests. Only the bottom half of crucible was filled with bismuth to minimize material heating by RF and sputtering by plasma ions. Oxygen was used as a support gas to enhance charge states of  $^{209}\text{Bi}$  ions.

The bismuth ion beam was first extracted by applying 15 kV potential and accelerated by 60 kV potential of the HV platform. The 20 mm input aperture Faraday cup (FC) equipped with a suppression ring was installed

downstream of the  $90^{\circ}$  magnet to record the currents of different charge states. The distribution of  $^{209}\text{Bi}$  ion currents for different charge states obtained after a few days of the source conditioning and tuning is shown in Fig. III-14.

One can see that  $^{209}\text{Bi}^{19+}$  and  $^{209}\text{Bi}^{20+}$  ions are the most abundant in the distribution. Intensities of the  $^{209}\text{Bi}^{20+}$  -  $^{209}\text{Bi}^{24+}$  ions are in the range of 1-2.5  $\mu\text{A}$ . The source also produces  $\text{O}^{1+}$  and  $\text{O}^{2+}$  ions with the current up to 350  $\mu\text{A}$ . The quality and intensity of bismuth ions are entirely adequate to verify multiple-charge state acceleration technique<sup>3</sup> using the new set-up of the multiple-charge state LEBT.<sup>4</sup>

<sup>1</sup>D. Z. Xie, Rev. Sci. Instrum. **73**, 531 (2002).

<sup>2</sup>National Electrostatics Corp., www.pelletron.com.

<sup>3</sup>P. N. Ostroumov *et al.*, Phy. Rev. Lett. **86**, 2798 (2001).

<sup>4</sup>N. E. Vinogradov *et al.*, Proc. of LINAC-2006, Knoxville, TN, August 2006, p. 336.

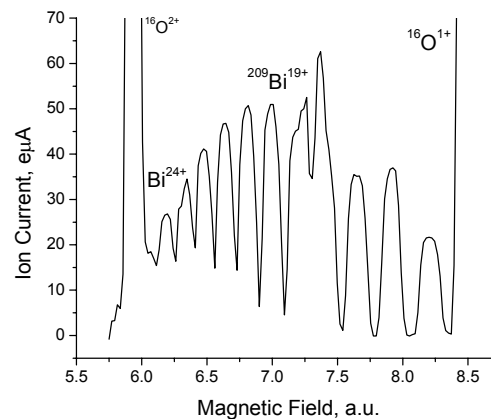


Fig. III-14. Bismuth beam intensities at different charge states.

#### b.4. High Current Regime of an All Permanent Magnet ECR Ion Source

(S. A. Kondrashev, A. Barcikowski, J. A. Nolen, P. N. Ostroumov, and R. H. Scott)

Stability tests of the windowless liquid lithium stripper for AEBL<sup>1</sup> require 400 W bunched light ion beams in the energy range from 100 keV/u to 200 keV/u. The multiple-charge-state LEBT being constructed in the Physics Division can be upgraded to obtain 150 keV/u beams by adding a second accelerating tube. A 3 mA dc beam current in a single charge state is required to achieve 400 Watts on the target. Helium and hydrogen were used as working gases to verify the performance of the BIE-100 all permanent magnet ECR ion source.

The ion beams were extracted by 15 kV potential and accelerated by 60 kV potential of the HV platform. The 20 mm input aperture Faraday cup equipped with a suppression ring was used to record ion beam intensity downstream of the 90° magnet. The distributions of helium and hydrogen ion beam intensities obtained after two days of source conditioning and tuning are shown in Fig. III-15. A 3.3 mA dc proton beam was successfully generated which is entirely suitable to form a bunched and well focused beam on the target.

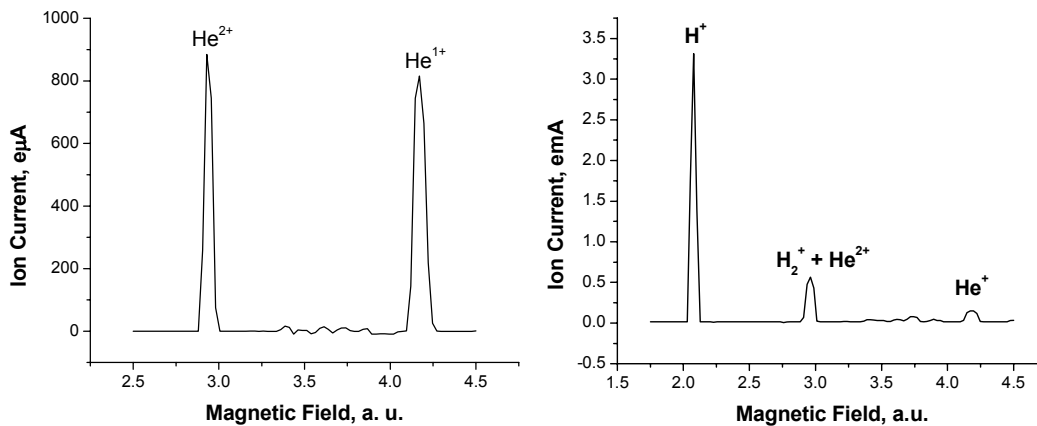


Fig. III-15. Helium (on the left) and hydrogen (on the right) ion beam intensities as a function of the magnet field.

<sup>1</sup>J. A. Nolen, C. B. Reed, V. J. Novick, J. R. Specht, and Y. Momozaki, Development of Windowless Liquid Lithium Stripper for RIA, Physics Division Annual Report 2005, p. 146.

#### b.5. Scintillator Screen Based CW Beam Emittance Measurements (S. A. Kondrashev, A. Barcikowski, B. Mustafa, P. N. Ostroumov, and R. H. Scott)

Fast emittance measurements can be performed using a beam imaging system placed downstream of a “pepper pot” plate. The pepper pot method has the advantage of giving the possibility to extract emittances for both vertical and horizontal planes using the same single image. Micro channel plates (MCP) and scintillator screens are normally used as an imaging system. However, scintillator screens are preferable due to their simplicity and wide dynamic range. Such an approach was used to measure emittances of ion beams<sup>1</sup> with energy higher than 100 keV/u or intense (above 10 mA) pulsed low energy (below 100 keV/u) ion beams.<sup>2</sup> As far as we know, there are no data on scintillator screen sensitivities for low intensity (0.1-10 eµA/cm<sup>2</sup>) low

energy (below 100 keV/u) CW beams typically generated by ECR ion sources.

The main goal of this study is to find whether the pepper pot - scintillator screen (PPSS) method can be used to measure emittances of CW beams generated by ECR ion sources. The BIE-100 all permanent magnet ECR ion source was used to generate ion beams of various elements from hydrogen to bismuth. The PPSS assembly, shown in Fig. III-16, was placed downstream of the 90° magnet and movable faraday cup (FC). The pepper pot plate has 100 pinholes with 200 µm diameter and 4-mm spacing between the holes horizontally and vertically covering a working area of

$36 \times 36 \text{ mm}^2$ . The CsI (Tl) crystal was chosen as a scintillator screen because it has shown the highest sensitivity for high energy proton beams.<sup>3</sup> The diameter and thickness of the crystal are 80 mm and 3 mm respectively. A grounded fine metal mesh with transparency above 50% is attached to the crystal surface irradiated by ions to prevent potential raise caused by ion beam charge. The distance between the pepper pot and scintillator screen is 100 mm. A COHU 2600 monochrome CCD camera connected to a PC was used to acquire and save beam images. The pepper pot plate is isolated from ground and its potential can be varied in the range of  $\pm 1 \text{ kV}$  to study the effect of

secondary electrons on the emittance. The FC was used as a shutter and detector of the ion beam current. In our measurements, the beam energy is 75 keV per unit charge for all elements used.

It was found that CsI (Tl) has a high sensitivity for a variety of ion species from protons to heavy ions. Pepper pot images were recordable for proton and bismuth beams with current densities below  $1 \text{ e}\mu\text{A}/\text{cm}^2$ . A typical image of a  $^{129}\text{Xe}^{14+}$  ion beam with current density of  $7 \text{ e}\mu\text{A}/\text{cm}^2$  is shown in Fig. III-16.

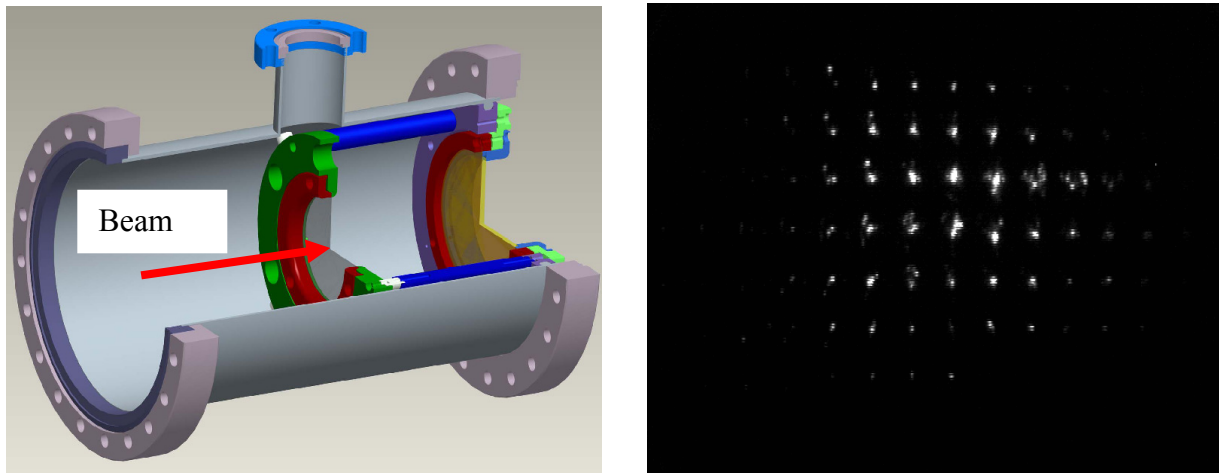


Fig. III-16. Cut-out view of pepper pot – scintillator screen assembly (on the left) and image of a  $^{129}\text{Xe}^{14+}$  ion beam (on the right).

The analysis of captured images was performed using a software developed at Brookhaven National Laboratory for their emittance meter.<sup>4</sup> The results obtained for the  $^{129}\text{Xe}^{14+}$  ion beam is presented in Fig. III-17.

The linearity of the CsI (Tl) crystal for different input

current densities and its life-time under irradiation by CW ion beams will be studied in the near future. A new mask with 100  $\mu\text{m}$  pinholes spaced by 3 mm in both directions is being developed to improve the resolution. A software for on-line emittance measurements is under development as well.

<sup>1</sup>M. Domke *et al.*, A Single Shot Emittance Measuring System for Intense Heavy Ion Beams, GSI-Preprint-97-64, October 1997.

<sup>2</sup>A. Balabaev *et al.*, Rev. Sci. Instrum. **73**, 1121-1124 (2002).

<sup>3</sup>R. Jung, G. Ferioli, and S. Hutchins, Single Pass Optical Profile Monitoring, Proceedings of the DIPAC 2003, Mainz, Germany.

<sup>4</sup>A. Pikin *et al.*, Pepper Pot Emittance Meter, BNL note C-A/AP/#244, July 2006.

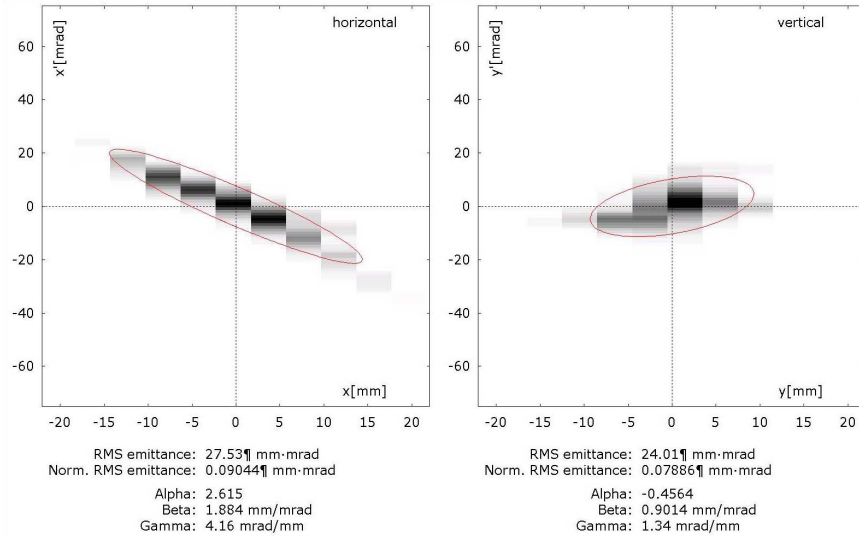


Fig. III-17. Horizontal and vertical emittances of  $^{129}\text{Xe}^{14+}$  beam. The 4-rms emittance ellipses are plotted in red.

**b.6. A Parallel 3D Poisson Solver in Cylindrical Coordinates** (J. Xu, P. N. Ostroumov, and J.A. Nolen)

In beam dynamics simulations, the space charge effects due to electrostatic forces between charged particles, become prominent when the density of particles is high. Since many accelerator devices have cylindrical geometry, a 3D Poisson solver in the Cylindrical Coordinate System (CYLCS) has wide applications. Particularly, we are interested in a 3D solver in CYLCS for the parallel beam dynamics code PTRACK.<sup>1</sup> In these simulations, it is very important to accurately calculate beam halo which can produce beam losses along the accelerator. While it is relatively simple to solve Poisson's equation in the Cartesian Coordinate

System (CARTCS), it is more complicated to develop a 3D Poisson solver in the CYLCS. In the CYLCS, Poisson's equation has the following form:

$$\nabla^2 \phi(r, \theta, z) = \frac{\partial^2 \phi}{\partial r^2} + \frac{1}{r} \frac{\partial \phi}{\partial r} + \frac{1}{r^2} \frac{\partial^2 \phi}{\partial \theta^2} + \frac{\partial^2 \phi}{\partial z^2} = -\frac{\rho}{\epsilon_0}$$

Figure III-18 shows the 3D and 2D meshes used in the CYLCS. In order to avoid singularity at the center, Gauss-Lobatto-Radau integration points have been adopted.

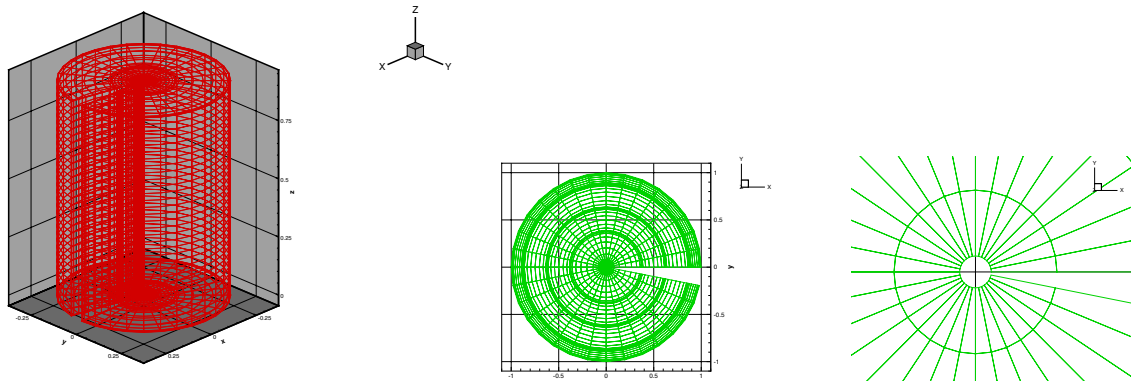


Fig. III-18. Cylindrical mesh (3D & 2D).

The new Poisson solver has been used to substitute the Cartesian Poisson solver implemented in the PTRACK

last year. PTRACK is the parallel version of the beam dynamics code TRACK, which has been developed

during the past several years in the Physics Division.<sup>2</sup> The PTRACK algorithm for the space charge calculation is shown in Fig. III-19 and a particle-in-cell

(PIC) method has been similarly implemented in the CYLCS, as shown in Fig. III-20.

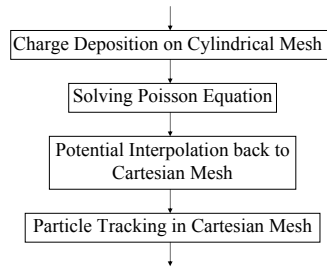


Fig. III-19. Algorithm for the Poisson solver in the CYLCS.

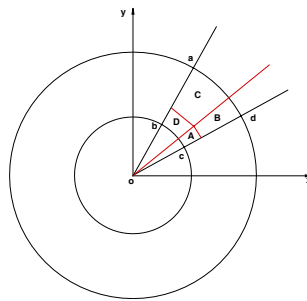


Fig. III-20. PIC in the CYLCS.

We have applied domain decomposition in the longitudinal (z) and circumferential ( $\theta$ ) directions, as shown in Fig. III-21. The particles have been distributed evenly to different processors. Figure III-22 shows the scaling of the parallel Poisson solver in the CYLCS on different platforms; good scaling can be achieved up to 256 processors. Super-linear scaling has been observed on IBM SP machines due to large cache and memory.

beam transport section between the RFQ and the first 4 superconducting accelerating cavities (MEBT4CAV). We have compared our parallel simulation results with the PTRACK using a Cartesian Poisson solver. The results in CARTCS and CYLCS (see Fig. III-23) are close for the particular application, as expected. In general, the Poisson solver in the CYLCS is more accurate, especially for the halo particles.

The new solver has been used for the simulation of a 8-GeV proton linac which includes the medium energy

The new Poisson solver has nearly the same speed as the Cartesian Poisson solver on  $64^3$  mesh, and can be run on thousands of processors on BG/L.

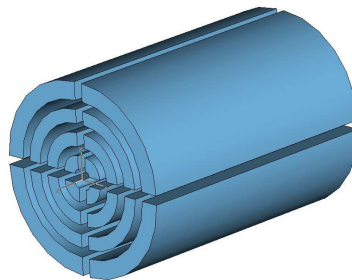


Fig. III-21. Parallel model for the code TRACK.



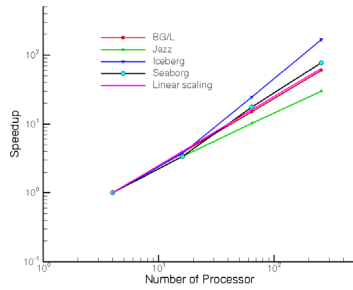


Fig. III-22. Scaling on different platforms.

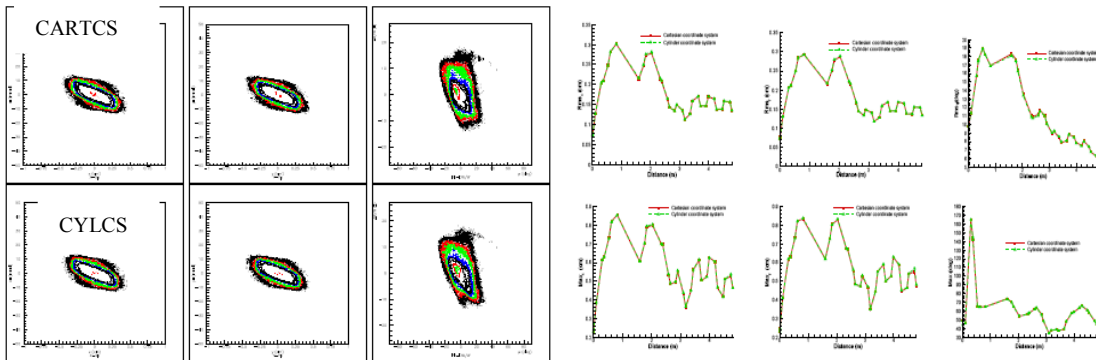


Fig. III-23. Comparison of the results obtained by the Cartesian and Cylindrical Poisson solvers. The left plots compare contours in phase space and the right plots compare beam rms and maximum envelopes.

<sup>1</sup>J. Xu, B. Mustapha, V. N. Aseev, and P. N. Ostroumov, Parallelization of a Beam Dynamics Code and First Large Scale RFQ Simulations, Phys. Rev. ST Accel. Beams **10**, 014201 (2007).

<sup>2</sup>P. N. Ostroumov and V. N. Aseev, TRACK-a Code for Beam Dynamics Simulations in SC Linac with 3D Electric and Magnetic Fields, ANL Technical Report (2003).

<sup>3</sup>P. N. Ostroumov, V. N. Aseev, and B. Mustapha, Beam Loss Studies in High-Intensity Heavy-Ion Linacs, Phys. Rev. ST. Accel. Beams **7**, 090101 (2004).

### b.7. Concept for an Ion LINAC for the Future Electron-Ion Collider (P. N. Ostroumov)

Currently, the Jefferson Lab is leading the effort to develop a high-luminosity Electron-Ion Collider (ELIC) with variable center-of-mass energy in the range of 20 to 65 GeV.<sup>1</sup> The ELIC consists of a heavy-ion synchrotron and storage ring which requires a pulsed linear accelerator with the parameters listed in Table III-2. The linac is designed for acceleration of a

wide variety of polarized and unpolarized ions from H<sup>-</sup> (285 MeV) to <sup>208</sup>Pb<sup>67+</sup> (100 MeV/u). The block-diagram of the proposed linac is given in Fig. III-24. Cost-effective acceleration of lead ions up to 100 MeV/u requires a stripper. The optimum stripping energy is 13 MeV/u.

Table III-2. Basic parameters of the linac.

	Parameter	Value
1	Ion species	From Hydrogen to Lead
2	Ion species for the reference design	$^{208}\text{Pb}$
3	Kinetic energy of lead ions	100 MeV/u
4	Maximum beam current averaged over the pulse	2 mA
5	Pulse repetition rate	10 Hz
6	Pulse length	0.25 msec
7	Maximum beam pulsed power	680 kW
8	Fundamental frequency	115 MHz
9	Total length	150 m

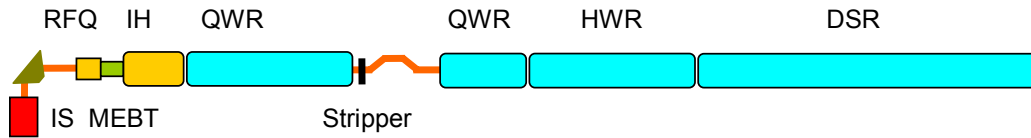


Fig. III-24. Block-diagram of the linac. IS is the ion source, RFQ is the NC radio frequency quadrupole accelerator, MEBT is the medium energy beam transport, IH is the NC interdigital structure, QWR is the RIA-type quarter-wave SC resonator operating at 115 MHz,  $\beta_G = 0.15$ , HWR is the RIA-type quarter-wave SC resonator operating at 230 MHz,  $\beta_G = 0.26$ , and DSR is the RIA-type double-spoke SC resonator operating at 345 MHz,  $\beta_G = 0.4$ .

The linac includes a normal conducting (NC) RFQ and an interdigital IH structure operating at a fixed velocity profile. These two structures are very effective up to  $\sim 5$  MeV/u, especially for pulsed machines. In the proposed linac, the NC section provides 4.8 MeV/u beam energy for all ion species. This section of the linac is similar to the CERN Lead injector linac<sup>2</sup> and to BNL's pulsed heavy-ion injector being constructed.<sup>3</sup> The

4.8 MeV/u ion beams will be injected into the superconducting (SC) linac which comprises three different types of accelerating cavities to cover the velocity range from  $0.1c$  to  $0.5c$  similar to those developed at ANL for RIA. All these cavities have been built and tested providing excellent quality as is reported in Ref. 4 and later publications of the ANL SRF group.

The linac comprises 119 SC cavities. For the current

application, 30 MV/m surface field in all SC cavities is proposed as a design parameter. The SC cavities will be combined into cryostats with the length of about 6 m together with SC focusing quadrupoles. After stripping, a dog leg system is necessary to clean ions with unwanted charge states. The linac is design to provide optimal voltage gain for lead ions (see Fig. III-25) and can be re-phased to accelerate any ions from hydrogen to lead.

The linac requires a total of 7 RF amplifiers: 4 amplifiers for the NC section and 3 amplifiers for the SC section. The SC section of the linac can be fed just from 3 RF amplifiers operating at three different harmonics of the fundamental frequency 115 MHz. The power will be distributed to the cavities through ferrite vector modulators (FVM) to adjust phase and amplitude of the accelerating fields in each cavity.

<sup>1</sup>A. Afanasev *et al.*, Zeroth-Order Design Report for the Electron-Light Ion Collider at CEBAF, [http://casa.jlab.org/research/elic/elic\\_report.shtml](http://casa.jlab.org/research/elic/elic_report.shtml).

<sup>2</sup>H. D. Haseroth, Pb Injector at CERN, Proceedings of LINAC-1996, p. 283.

<sup>3</sup>J. Alessi *et al.*, Status of the EBIS Project at Brookhaven, Proceedings of LINAC-2006, p. 385.

<sup>4</sup>K. W. Shepard, Status of Low and Intermediate Velocity Superconducting Accelerating Structures, Proceedings of PAC-2003, p. 581.

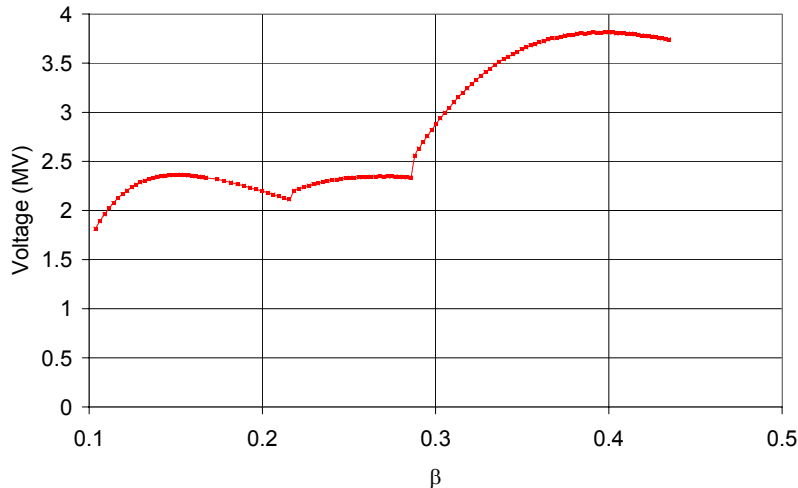


Fig. III-25. Voltage gain per resonator as a function of Lead ion velocity.

### b.8. Developments Related to the Low-Q Post-Accelerator (P. N. Ostroumov, J. A. Nolen, and K. W. Shepard)

Both Super CARIBU and AEBL projects require acceleration of radioactive ions at a charge state 1+ or 2+. The post-accelerator includes a normal conducting (NC) section comprising three RFQs to provide 75 keV/u for all ion species and a superconducting (SC) section to achieve 1 MeV/u for heaviest ions.

We are developing NC prototype RFQ operating at 12.125 MHz for initial acceleration of ions with charge-to-mass ratio of 1/238 and higher. The new set of electrodes capable of accelerating  $^{238}\text{U}^{+1}$  will be fabricated and installed into the vacuum enclosure of the existing 12 MHz split-coaxial RFQ resonator.<sup>1</sup> The design of the new RFQ vanes has the following features:

- Average radius of the RFQ is 7.0 mm, required inter-vane voltage is 82 kV.
- Water cooling of vanes will be provided.
- Higher accuracy of alignment will be implemented.

Figure III-26 shows the engineering model of the 12 MHz RFQ with a new electrode set. The existing 27 kW RF amplifier should be sufficient to achieve the design inter-electrode voltage of 82 kV. We have completed engineering design and development of fabrication drawings of the new set of RFQ vanes and will proceed with fabrication as soon as appropriate funding becomes available.

The SC section of the linac is designed for ions with the lowest charge-to-mass ratio  $q/A = 1/66$  to achieve the stripping energy  $\sim 1$  MeV/u for the heaviest ions<sup>2</sup> and it is based on interdigital drift-tube SC niobium cavities. This type of SC cavities has been used at PII for two decades and can typically provide  $\sim(3-4)$  MV/m of accelerating fields in this velocity range. Progress in electromagnetic and mechanical design tools, fabrication technology and RF surface processing techniques related to TEM-class SC cavities suggests that the accelerating gradients  $\sim 8$  MV/m are entirely feasible. With these high accelerating gradients, a total of 39 SC interdigital four-gap resonators, in three classes, are required for the first four cryostats of the new injector linac. The three resonator classes have matched velocities of 0.017c, 0.026c, and 0.038c and are similar in concept to the resonators now used in PII, but with significantly improved design details. Using modern technology for design, fabrication and processing of SC cavities will significantly reduce the cost of the post-accelerator compared to the original estimate made for the RIA project.

The low charge-state beams require stronger transverse focusing than is used in existing SC ion linacs. A FODO focusing lattice composed from SC quadrupole magnets is proposed. SC quads with the effective length of 15 cm, 30 mm aperture diameter and moderate gradients below 100 T/m are required.

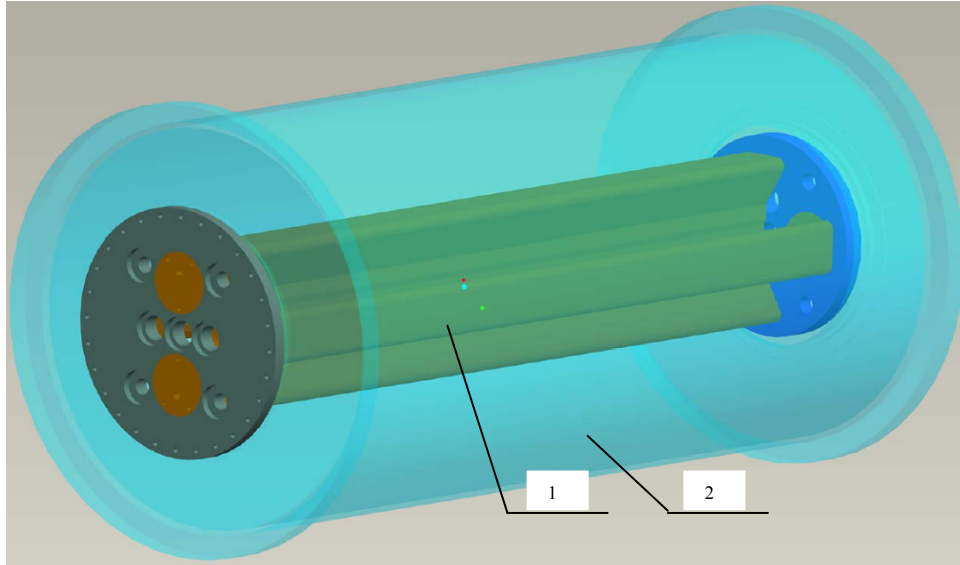


Fig. III-26. Engineering model of the new set of RFQ vanes (1) in the vacuum tank of the existing 12 MHz RFQ (2).

Beam dynamics end-to-end simulations of the post-accelerator have been performed and reported in reference.<sup>2</sup> Recently we have updated the design of the SC section. Figure III-27 shows rms and full envelopes of the ion beam with  $q/A = 1/66$  in the SC section of the

linac. The proposed FODO focusing structure and SC cavities with 20-mm aperture diameter provide normalized transverse acceptance of  $0.2 \pi \mu\text{m}$ . The expected emittances downstream of the high-resolution mass-separator are less than  $0.05 \pi \mu\text{m}$ .

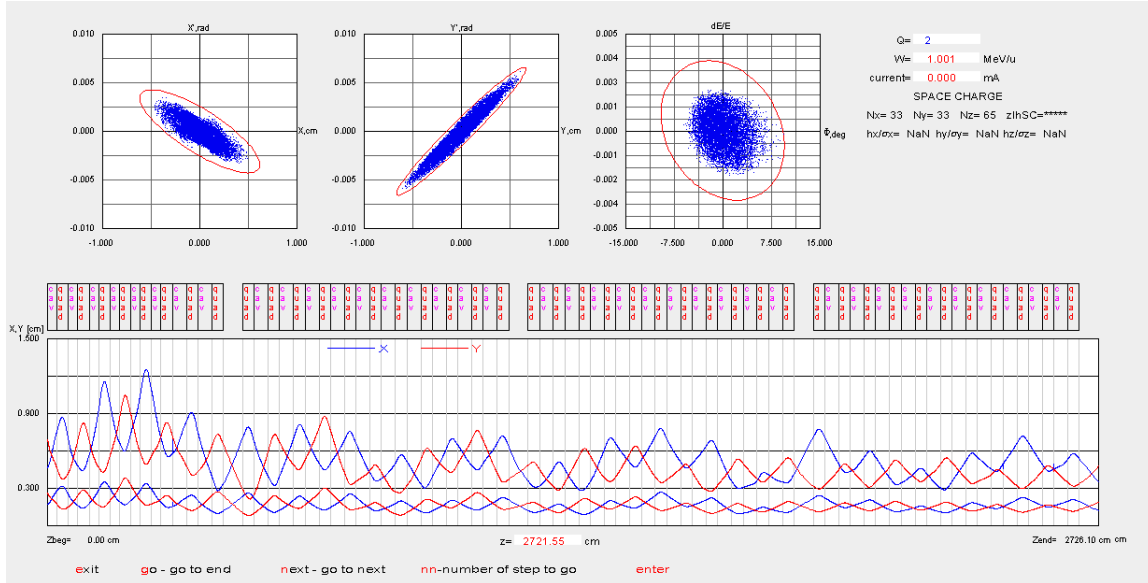


Fig. III-27. Beam rms and full envelopes in the SC section of the low-q linac and phase space plots of the accelerated ions with  $q/A = 1/66$ .

<sup>1</sup>K. W. Shepard and W. C. Sellyey. Proceedings of the LINAC 96, p. 68.

<sup>2</sup>P. N. Ostroumov, V. N. Aseev, and A. A. Kolomiets, Heavy-Ion Beam Dynamics in the RIA Post-Accelerator, Proceedings of the PAC-2005, p. 3301.

### b.9. Realistic Corrective Steering in the Front-End of the Fermilab Proton Driver Linac (B. Mustapha, P. N. Ostroumov, and V. N. Aseev)

When considering element misalignment errors in an accelerator it is often required to apply corrective beam steering to compensate for these errors and periodically re-center the beam position and angle to avoid beam loss. A realistic correction procedure would use the reading from beam position monitors (BPM's) and adjust the strengths of the correctors (dipole coils) to re-center the beam. The number and location of BPM's and correctors should in principle be carefully studied during the design phase of an accelerator. After describing the correction procedure implemented into the beam dynamics code TRACK<sup>1</sup> we present the results of its application to the front-end of the Fermilab proton driver (FNAL-PD) linac.

We consider an accelerator section with  $N_m$  BPM's and  $N_c$  correctors. To simplify the discussion we consider only the correction of the horizontal beam position ( $x$ ). The formalism could be generalized to include the vertical beam position ( $y$ ) and the horizontal and vertical beam divergences or angles ( $x'$  and  $y'$ ). In order to be able to correct the beam center we should first determine the response function of the BPM's to the correctors. Such a response function could be written in matrix form as:  $F(C) = M$  where  $C$  is the vector of strengths of the  $N_c$  correctors and  $M$  is the vector of beam positions measured on the  $N_m$  BPM's. In the ideal case without any misalignments or measurement errors we should have  $M = M_0 = 0$  because the beam should be centered on all BPM's and  $C = C_0 = 0$  because we should not need any correction. In this case the response function is  $F = F_0$  such that

$F_0(0) = 0$  and it should be linear for small deviations about the beam axis:  $F_0(C) = A \times C = M$ , where  $A$  is a  $N_c \times N_m$  matrix. For the case with misalignment errors before applying corrections ( $C = 0$ ) the beam should not be centered on most BPM's and we have  $F(0) = B$  where  $B$  is the vector of beam position measured on the  $N_m$  BPM's before correction. Notice that  $B$  would depend from the actual misalignment of all the elements in the considered section. So the general form of the monitors response function to the correctors is  $F(C) = A \times C + B = M$  where  $B$  is purely coming from misalignment errors whereas  $A$  is independent from misalignment. The response function is now reduced to the response matrix  $A$  and the vector  $B$  characterizing the actual misalignment. Reading the BPM's before correction ( $C = 0$ ) we can determine the vector  $B$ . By switching on one corrector ( $i_c$ ) at a time we should be able to determine the response of every BPM ( $i_m$ ) downstream using:  $A(i_c, i_m) = (M(i_m) - B(i_m)) / C(i_c)$ . The upstream BPM's should not be affected. Knowing the response function  $A \times C + B = M$  we can determine the set of corrector strengths  $C$  required to re-center the beam on all BPM's ( $M = 0$ ). This could in principle be fulfilled by solving the matrix equation  $A \times C + B = 0$  for  $C$ . For arbitrary  $N_m$  and  $N_c$ , which may lead to multiple solutions for  $N_c > N_m$  or an over-determined problem for  $N_c < N_m$ , and to be able to set an upper limit for correctors strengths and to include measurement errors for BPM's, the solution is better performed using least-square minimization. The function to minimize in this case is:

$$f(C_{i_c}, i_c = 1, N_c) = \sum_{i_m=1}^{N_m} \frac{(\sum_{i_c=1}^{N_c} A_{i_c, i_m} * C_{i_c} + B_{i_m})^2}{\sigma_{BPM}^2}; \text{ for } |C_{i_c}| \leq C_{\max}$$

This procedure was implemented for the beam positions ( $x$  and  $y$ ) and divergences ( $x'$  and  $y'$ ) into the code TRACK using the minimization package MINUIT<sup>2</sup> of the CERN Library. The procedure was successfully applied to the front-end of the FNAL-PD linac shown on Fig. III-28. After multiple iterations, the appropriate number and location of BPM's and correctors were found. Figure III-29 shows the location of correctors and monitors for different linac sections. The correction procedure is then applied for up to 200 different sets of randomly generated misalignment errors. Figure III-30 shows beam positions and

divergences along the linac front-end before and after correction. We clearly see the reduction in the spread (largest deviation from center) of the beam positions and angles. Figure III-31 shows the effect of correction on the transverse beam emittances and envelopes. Figure III-32 shows the distribution of integrated field strength ( $B*L$ ) required for the correction. A maximum value of  $B*L = 1250$  Gs\*cm should be enough for effective correction. Figure III-33 shows the effect of the BPM's measurements errors on the quality of the correction. For appropriate and effective correction a BPM error of  $\sigma_{BPM} \sim 30 \mu\text{m}$  is required.

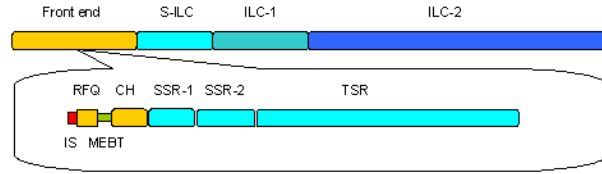


Fig. III-28. Schematic layout of the FNAL-PD linac showing more details about the front-end.

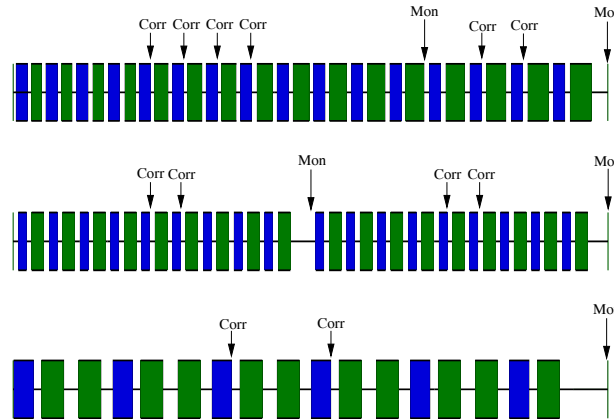


Fig. III-29. Number and location of correctors and monitors for appropriate correction in the room-temperature section (CH: top), in the first single-spoke section (SSR-1: middle) and in the second single-spoke section (SSR-2: bottom).

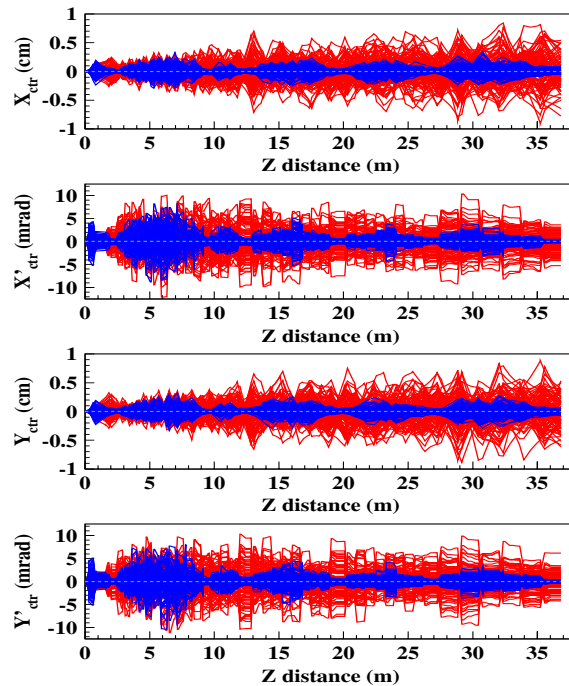


Fig. III-30. Beam central transverse positions and angles along the front-end of the FNAL PD linac (up to SSR-2) before (red) and after (blue) correction for 200 different sets of misalignment errors.

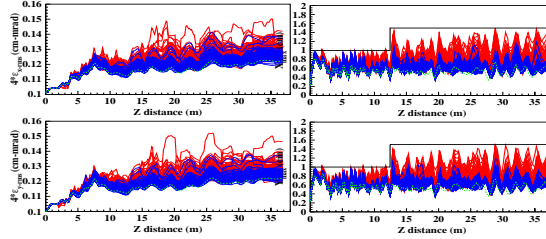


Fig. III-31. Beam transverse emittances (left) and envelopes (right) along the front-end of the FNAL-PD linac (up to SSR-2) before (red) and after (blue) correction for 200 different sets of misalignment errors.

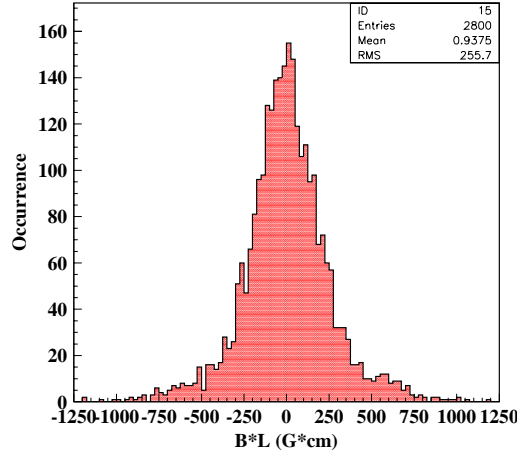


Fig. III-32. Correctors integrated field strengths used in the correction procedure for the front-end of the FNAL-PD linac.

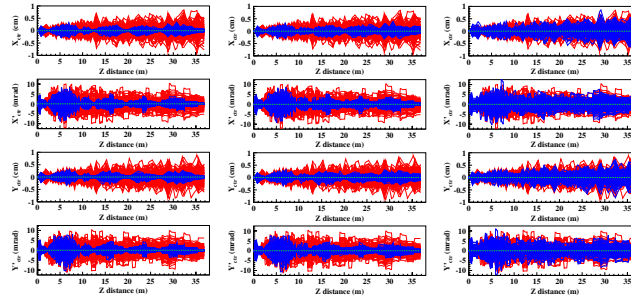


Fig. III-33. Effect of BPM measurement errors on the effectiveness of the correction procedure. The left plot is for  $\sigma_{BPM} = 10 \mu\text{m}$ , the center is for  $\sigma_{BPM} = 30 \mu\text{m}$  and the right for  $\sigma_{BPM} = 100 \mu\text{m}$ .

<sup>1</sup>“TRACK, the New Beam Dynamics Code”, V. N. Aseev *et al.*, in Proceedings of PAC-05.

<sup>2</sup>MINUIT–Function Minimization and Error Analysis, CERN Program Library Long Writeup D506.

**b.10. First Track Simulations of the SNS Linac** (B. Mustapha, J. Xu, V. N. Aseev, P. N. Ostroumov, D. Jeon,\* and S. D. Henderson\*)

In this collaborative effort between ANL and ORNL, we meant to expand the domain of applicability of the code TRACK<sup>1</sup> to new elements not previously included such as long Drift Tube Linac (DTL) and to benchmark

the code against the commissioning data from the SNS linac. This work constitutes a first of many developmental steps towards the realization of the concept of the "Model Driven Accelerator", where

TRACK could be used to fully support machine operations in the SNS linac or any future facility based on linear accelerators.

The SNS accelerator facility<sup>2</sup> is designed to provide a 1 GeV, 1.4 MW proton beam to a liquid mercury target for neutron production. The accelerator complex consists of a H<sup>+</sup> injector capable of producing 38 mA peak current, a 1 GeV linac, an accumulator ring and

associated beam transport lines to experimental areas. The linac consists of a 2.5 MeV, 38mA H<sup>+</sup> front-end injector, a six-tank 402.5 MHz DTL to accelerate the beam to 87 MeV, a four-module 805 MHz Coupled Cavity Linac (CCL) to accelerate the beam to 187 MeV, and a superconducting linac (SRF) to accelerate the beam to 1 GeV. Figure III-34 shows a schematic layout of the SNS linac.

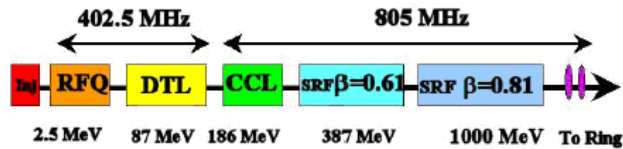


Fig. III-34. Schematic layout of the SNS linac.

The DTL section is composed of 6 tanks with a total of 216 cells to accelerate the beam from 2.5 MeV to 87 MeV. Each DTL tank is driven by a separate 402.5 MHz, 2.5-MW klystron. The focusing is provided by permanent magnet quadrupoles (PMQs) positioned within specific drift tubes. The focusing lattice is FFODDO where every third drift tube is kept empty for possible beam diagnostic devices. The cell length is equal to  $\beta\lambda$  and the transverse focusing period length is  $6\beta\lambda$ . Before being able to simulate the DTL using TRACK, three major steps need to be performed. They are:

- Preparation of 3D electromagnetic fields for every cell including fringe fields.
- Building the lattice with the exact dimensions (length and aperture) as well as electric and magnetic field strengths for every cell.
- Implementation of a special tracking routine for the DTL where a whole DTL tank is considered as a single element with many cells.

Every DTL cell contains an accelerating RF gap and one or two PMQs as shown in Fig. III-35.

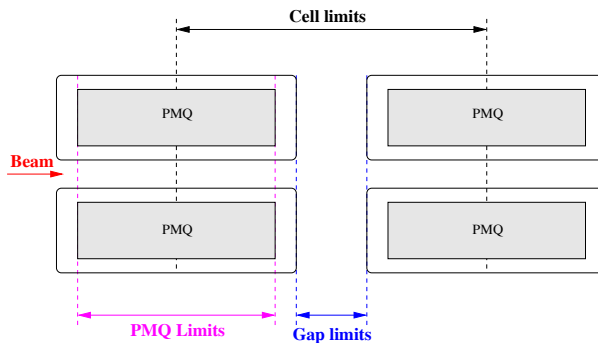


Fig. III-35. Approximate geometry of a DTL cell.

2D electric field (E) tables for the RF gaps are computed using Superfish.<sup>3</sup> Using the cylindrical symmetry we can determine the 3D E-field at any point within the aperture. Figure III-36 shows the E-field components in the first cell along the Z axis at  $X = Ra/2$  and  $Y = Ra/4$  where  $Ra = 1.25$  cm is the aperture radius of the DTL.

The magnetic field (B) from the PMQs is calculated using the field formula's used in Trace-3D<sup>4</sup> for Bx and By whereas the Bz component is taken from the original paper by Halbach.<sup>5</sup> The results of the formulas were confirmed using EM-studio for the exact geometry and material properties of the PMQ. Figure III-37 shows the B-field components for the same conditions as Fig. III-36 (first cell at  $X = Ra/2$  and



$Y = Ra/4$ ) where the first PMQ has a field gradient (tube).  
 $G = -3.7$  kG/cm and the second with  $G = 0$  (empty drift

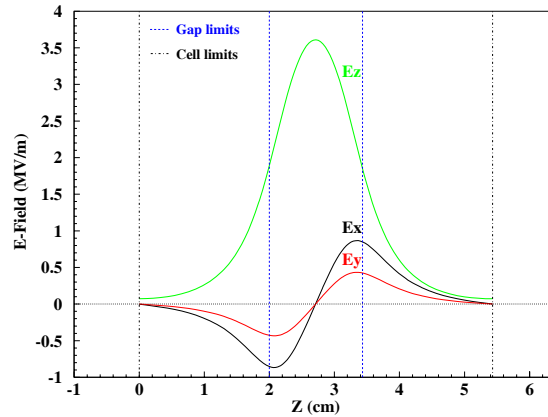


Fig. III-36. Electric field components in a DTL cell.

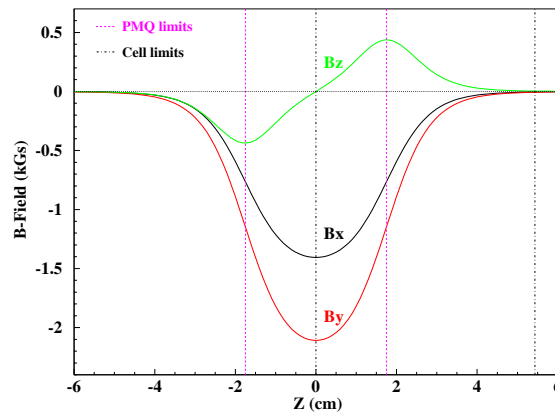


Fig. III-37. Magnetic field components in a DTL cell.

In TRACK's main lattice input a DTL tank is represented by a single line specifying the total length, a harmonic number, a global E-field scaling factor, the input phase, the number of cells and a file number with more detailed cell information. The cell information file contains the length, aperture, E-field strength, B-field strength for both PMQs for every cell in the tank (1 line per cell). In this way we have the flexibility of changing any parameter which is especially important when we want to input measured values for field strengths. Because every DTL tank is driven by a single klystron, no phase setting is allowed for individual cells for which the phases are set by the geometrical design. The DTL tracking routine is based on the existing RFQ routine described in Ref. 6. When the beam enters a new cell, the corresponding field data are loaded and the tracking performed by integrating the equation of motion for every particle in the 3D

external and internal space charge fields.

Figure III-38 and Fig. III-39 show a detailed comparison between TRACK and PARMILA<sup>7</sup> simulations results for the DTL section (MEBT + 6 Tanks). In this case, a 38 mA  $H^-$  beam is simulated by tracking  $10^5$  particles. The E and B field strengths are set to the experimentally measured values. A good overall agreement is obtained; the differences could be explained by the fringe fields from the PMQs and a possible difference in the space charge calculations. As discussed earlier, fringe fields could cause a beam mismatch which is visible on the transverse beam parameters in Fig. III-38. Starting from the second DTL tank ( $Z \sim 14$  m) we notice a longitudinal mismatch on TRACK results. We believe that this difference is due to a phase ramping procedure used in PARMILA to adjust the phases of the first and

last cells in a DTL tank to ensure phase matching between successive tanks. This procedure is not directly reflected on the design geometry used as input

to TRACK. This phase mismatch is responsible for producing a more pronounced beam tail on the phase space plots of Fig. III-39.

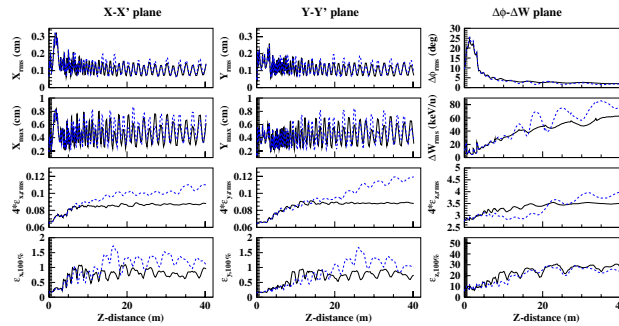


Fig. III-38. Comparison of PARMILA and TRACK simulation results of the SNS-DTL section. The plots show and compare the evolution of most important beam parameters along the DTL. The solid-black curves correspond to PARMILA and the dashed-blue curves to TRACK.

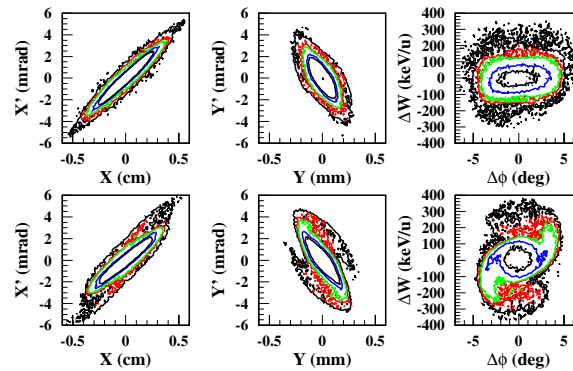


Fig. III-39. Comparison of phase space plots at the exit of the SNS-DTL section obtained using PARMILA and TRACK. The top plots are from PARMILA and the bottom ones are from TRACK. The colored contours represent different levels of particle density.

\*Oak Ridge National Laboratory.

<sup>1</sup>V. N. Aseev *et al.*, Proceedings of the PAC-05 Conference, Knoxville, TN, May 16-20, 2005.

<sup>2</sup>N. Holtkamp, Proceedings of the PAC-03 Conference, Portland, OR, May 12-16, 2003.

<sup>3</sup>J. H. Billen and L. M. Young, Poisson-Superfish Manual, Report LA-UR-96-1834, Los Alamos, 1996 (Revised 2005).

<sup>4</sup>K. R. Crandall, TRACE-3D Manual, Report LA-11054-MS, Los Alamos, 1987.

<sup>5</sup>K. Halbach, Nucl. Instrum. Methods **187**, 109-117 (1981).

<sup>6</sup>P. N. Ostroumov, V. N. Aseev, and A. A. Kolomiets, J. of Instr., JINST **1**, P04002, 2006.

<sup>7</sup>J. H. Billen and H. Takeda, PARMILA Manual, Report LA-UR-98-4478, Los Alamos, 1998 (Revised 2004).

### b.11. Automatic Transverse Tuning of a Multiple-Charge-State Heavy-Ion Beam

(B. Mustapha and P. N. Ostroumov)

In most existing accelerators, beam tuning or retuning after an element failure or to change the beam

parameters or specie is usually done manually step by step. This is due to the lack of a realistic model of the

machine that could fully support the machine operations which often results in excessive time wasted in beam tuning. The ultimate goal of this effort is to produce automatic and realistic beam tuning tools that could be incorporated into a realistic beam dynamics code which could be used for machine operations. This problem is especially important for SC linacs due to the presence of several different focusing lattice structures.

Extensive end-to-end beam dynamics simulations of the RIA driver linac<sup>1</sup> using the beam dynamics code TRACK<sup>2</sup> and including all sources of machine errors and detailed beam loss analysis showed that the losses could be significantly reduced for a fine-tuned linac. For this purpose we have developed an automatic longitudinal tuning procedure for multiple charge state heavy-ion beams.<sup>3</sup> For a complete tuning tool, we have recently developed an automatic transverse tuning procedure to produce smooth transverse beam dynamics

$$F = X_{rms}^0 + \sum_i \frac{(X_{rms}^i - X_{rms}^0)^2}{\Delta X_{rms}^2} + Y_{rms}^0 + \sum_i \frac{(Y_{rms}^i - Y_{rms}^0)^2}{\Delta Y_{rms}^2}$$

where  $X_{rms}^0$  and  $Y_{rms}^0$  are the RMS beam sizes at the entrance of the section or after the first focusing period, the sum index  $i$  runs over the focusing periods in a given section and  $\Delta X_{rms}$  and  $\Delta Y_{rms}$  are the allowed errors on the RMS beam sizes. In the case of a multiple charge state beam we use the parameters of the total beam. The procedure could very well be used for a single charge state beam. A similar procedure could be implemented to smooth out the longitudinal beam parameters, if needed. The minimization is performed using the CERN-LIB optimization package MINUIT<sup>4</sup> modified to consider a large number of fit parameters. The fit parameters in this case are the magnetic field strengths of all focusing elements in the section.

Figure III-40 shows the X- and Y-rms beam sizes before and after applying the automatic tuning procedure. We clearly notice the reduction in the

by minimizing the RMS beam sizes after each focusing period. In addition to improving an existing tune, this powerful automatic beam tuning tool can be used to retune the linac and restore the beam after one or more element failures and to develop new tunes for ion beams with different Q/A ratios.

The transverse tuning procedure consists of producing smooth transverse beam dynamics by optimizing the field strengths in the focusing elements. This is done by minimizing the fluctuations in RMS beam sizes along the considered section. Large fluctuations in the RMS beam sizes are usually induced by mismatch between sub-sections of the linac which could eventually lead to beam losses. This method is general and should produce good results for both regular (periodic) or non regular accelerating structures. The function to minimize in this case is:

fluctuations of the RMS beam sizes; the low-frequency oscillations due to beam mismatch were removed after applying the tuning procedure. In this case, the tuning is done for a two-charge state uranium beam in the first section of the RIA driver linac by tracking a small number of particles (typically 100 for each charge state) using the code TRACK. Space charge forces are negligible in this case. The matrix approach like in TRACE-3D<sup>5</sup> did not produce good results because of significant deviations when performing full beam dynamics simulations using realistic 3D fields. Tuning is done better by tracking particles through realistic 3D and space charge fields. In the case where space charge forces should be included, the typical number of particles would be at least  $10^5$ . Since the optimization process involves multiple iterations, large scale computing will be required.

<sup>1</sup>P. N. Ostroumov, V. N. Aseev, and B. Mustapha, Phys. Rev. ST. Accel. Beams **7**, 090101 (2004).

<sup>2</sup>“TRACK, The New Beam Dynamics Code”, V. N. Aseev *et al.*, in Proceedings of the PAC-05.

<sup>3</sup>B. Mustapha and P. N. Ostroumov, Phys. Rev. ST. Accel. Beams **8**, 090101 (2005).

<sup>4</sup>MINUIT—Function Minimization and Error Analysis, CERN Program Library Long Writeup D506.

<sup>5</sup>K. R. Crandall, TRACE-3D Manual, Report LA-11054-MS, Los Alamos, 1987.

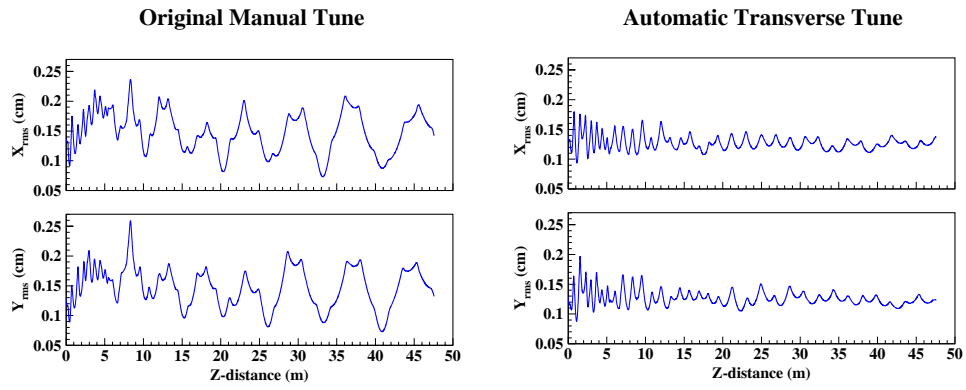


Fig. III-40. X- and Y-rms beam sizes before and after applying the automatic transverse tuning procedure. The beam is a two-charge state uranium beam in the first section of the RIA driver linac.

## C. RARE ISOTOPE PRODUCTION AND SEPARATION

### c.1. Development of a Windowless Liquid Lithium Stripper (J. A. Nolen, Y. Momozaki,\* C. B. Reed\*)

#### Windowless Liquid Lithium Stripper Overview

This section summarizes the on-going development of windowless liquid lithium strippers for advanced exotic beam facilities and other high current heavy ion accelerators that can withstand the large power density deposited by the intense heavy ion beams. The objective of the current phase of the work is to develop a film thickness diagnostic that can be used to initially measure the flowing film thickness and, later in the operating stripper system, to provide real time feedback of the film thickness for a variety of uses. Liquid lithium is considered a primary candidate for a stripper for high atomic number heavy ion beams in high intensity driver linacs because it has good nuclear physics properties in stripping electrons from beams such as uranium in the 10-20 MeV/u energy regime and good thermal properties in removing very high heat loads while maintaining sufficiently low vapor pressure. Preliminary nuclear physics calculations indicate that liquid lithium films in the range of 10-20  $\mu\text{m}$  thick are required. In addition, preliminary thermal calculations show that the film velocity needs to be at  $\geq 50$  m/s. To measure the exact thickness of a flowing liquid lithium film, a special diagnostic technique must be developed and demonstrated in high temperature ( $\sim 350^\circ\text{C}$ ), at high vacuum ( $\sim 10^{-7}$  -  $10^{-8}$  Torr), in contact with lithium vapor, and with possible

exposure to lithium splashing.

Previous work found that measuring the transmission of a low energy electron beam through the liquid lithium thin film was the best approach to measure the film thickness. A layout of the measurement setup was determined; critical components in the setup include an electron gun with appropriate energy and current output, beam transfer line, beam steering, focusing and bending devices, electron collector, precision current meter, and controller. An electron gun of  $\sim 30$  keV maximum energy is needed to penetrate advanced exotic beam accelerator strippers which may require liquid lithium thin film thicknesses in the range of  $\sim 10$   $\mu\text{m}$  to  $20+$   $\mu\text{m}$ . A suitable e-gun was identified and the procurement package prepared.

Formation of the film and factors affecting its stability and appearance were also studied. High speed (6 k and 12 k frames/sec) digital video movies were recorded of both the startup and steady state flow of the film. Figure III-41 identifies the basic elements of the thin film system. In Fig. III-42, one can see the initial film formation and, for example, the detrimental role played by the very large puddle of lithium clinging to the deflector plate.

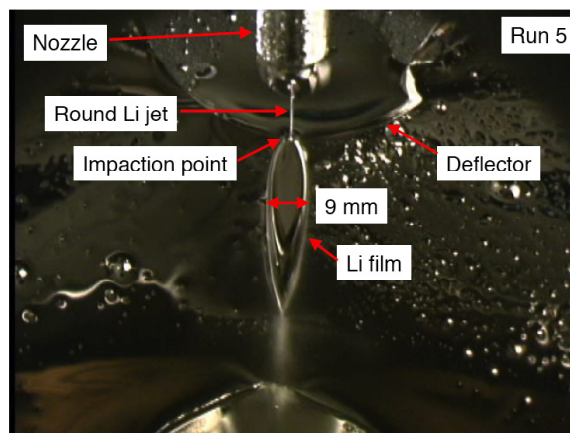


Fig. III-41. Liquid lithium thin film.

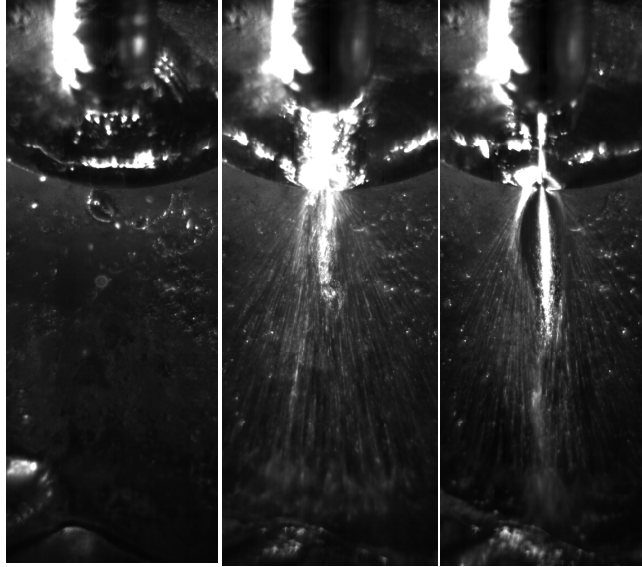


Fig. III-42. HS video clips of film formation.

#### Thermal Analysis of a Second Stripper for the Rare Isotope Accelerator

Thermal analysis calculations were made on the second stripper to be used in the driver linac of the Rare Isotope Accelerator (RIA). Both liquid (Sodium) and solid (Titanium and Vanadium) stripper concepts were considered. These calculations were intended to provide basic information to evaluate the feasibility of liquid (thick film) and solid (rotating wheel) second strippers. Nuclear physics calculations to estimate the volumetric heat generation in the stripper material were performed by “LISE for Excel”. In the thermal calculations, the strippers were modeled as a thin 2D plate with uniform heat generation within the beam spot. Then, temperature distributions were computed by assuming that the heat spreads conductively in the plate in the radial direction without radiative heat losses to surroundings.

A schematic of the second stripper is shown in Fig. III-43. The stripper was modeled as a slab moving at velocity  $v$ , which could be a liquid or a solid. An incident U beam at the charge state of  $72+$ , flux of 4 particle  $\mu\text{A}$ , and energy of 85 MeV/nucleon passes through the stripper material and deposits some energy as heat within it. Expected beam diameter is 1 mm.

Introducing some simplifications into this problem made it possible to use an analytical solution for a heat conduction problem of a moving, solid body. Since the stripper is very thin, the problem may be treated as a 2-D problem (Pittaway, 1964). In this analysis, a heat source that had a Gaussian distribution was moving at the velocity,  $v$  m/s on a thin stripper material. The stripper has a constant, uniform, background temperature of  $T_\infty$ . For simplicity, it was assumed that no heat transfer from the surfaces of the stripper takes place.

The initial background temperature for Na was taken to be 381 K. That is 10 K above the melting point of Na. Example results of the thermal calculations for the spatial temperature distribution of the Na film along the beamline for a Na film velocity of 10 m/s are shown in Fig. III-44. This figure shows that for a once-through Na stripper system, the calculated maximum temperatures of the Na film are  $\sim 1800$  K for Na film velocity of 10 m/s. This temperature would cause excessive evaporation of Na, implying that a much higher velocity,  $\sim 30 - 50$  m/s, is required.

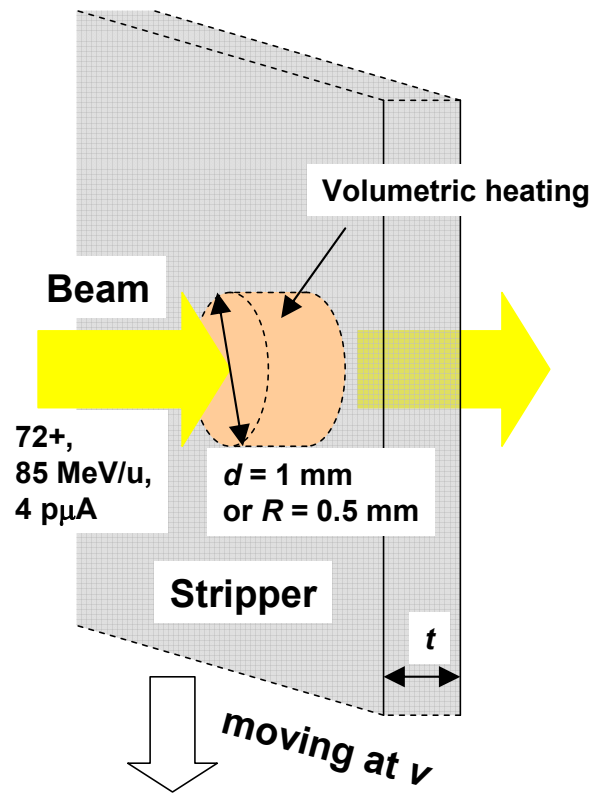


Fig. III-43. Schematic of second stripper.

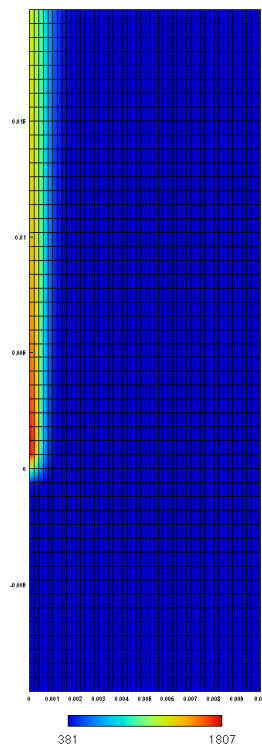


Fig. III-44. 2D spatial temperature distribution (Na at 10 m/s).

### Collaboration with the Israeli Soreq/SARAF Group

In 2006, an opportunity to collaborate with the Israeli Soreq/SARAF group, who are building a high power thin lithium target, arose. The collaboration included our support in target design, assembly and commissioning, followed by our participation in high power testing of the target with intense proton beams. This will be the first test at the high power densities possible with this new facility (CW beams with the Bragg peak in the target) to investigate the onset of bubble formation inside a windowless lithium jet. This is considered a huge windfall since the Israeli's are paying for essentially all of the hardware. We provided immediate assistance to the Soreq/SARAF group on developing their high-power liquid-lithium target system in order to meet the scheduled Phase I completion of the SARAF accelerator. The on-line availability of the SARAF target system during phase one is scheduled only for the second six months of calendar year 2007. Then there will be a 1-2 year down period for the installation of the rest of the accelerator (Phase 2). The Soreq/SARAF (Phase 1) research combines a demonstrated technique, successfully and intensively used for nuclear astrophysics, with ANL's windowless liquid lithium target technology to reach higher fluxes than available up to now. The successful development and utilization of a liquid lithium target in real conditions of a physics experiment, not realized so far, is expected to bring a unique and invaluable experience for advanced exotic beam facilities before their implementation there. In 2006, several meetings at ANL and at Soreq were held to plan and discuss target system issues, and we began helping the Soreq/SARAF group in developing the infrastructure necessary (design, choice of materials, construction, safety reviews and training procedures) for a windowless liquid lithium target to be usable in the

field for physics experiments. Also, two PhD students from The Hebrew University of Jerusalem were sent to ANL for six months at their expense to learn the engineering aspects of alkali metal technology and windowless target design and operation.

In summary, the aspects of the lithium target development at SARAF that are of great benefit to the US exotic beam programs are:

1. The practical installation and operation of a high-power liquid lithium target system in a nuclear physics/accelerator facility. Complete safety reviews and detailed operating procedures will be significant accomplishments.
2. Traps to control radiological contaminants such as  $^7\text{Be}$  will be incorporated into the system and tested in practice.
3. At the beam currents available at SARAF (4 mA of protons) the power density at the Bragg peak inside the target will be higher than ever demonstrated previously in such targets. The practical limitations of such targets will be determined by the on-set of bubble formation within the target. Detailed simulations of this limit are very uncertain and this test will be an invaluable experimental demonstration and benchmark for such simulations.

We produced a number of EM pump designs coupled with estimated hydraulic characteristics of the SARAF target loop. These include yoke design, magnet and yoke material selection, pump duct design to minimize stress, stress analysis and handling the freeze-thaw issue. An example compact, inexpensive DC EM pump design is shown in Fig. III-45.

\*Nuclear Engineering Division, Argonne National Laboratory.

<sup>1</sup>Claude B. Reed, Jerry A. Nolen, and Yoichi Momozaki, "A Liquid Lithium Thin Film Stripper for RIA", Seventh International Conference on Radioactive Nuclear Beams (RNB7), Cortina d'Ampezzo, Italy, July 3-7, (2006).

<sup>2</sup>Y. Momozaki and J. A. Nolen, "On a Thermal Analysis of a Second Stripper for Rare Isotope Accelerator," ANL-06/10, (2006).

<sup>3</sup>L. G. Pittaway, "The Temperature Distributions in Thin Foil and Semi-Infinite Targets Bombarded by an Electron beam," Brit. J. Appl. Phys. **15**, 967-982 (1964).



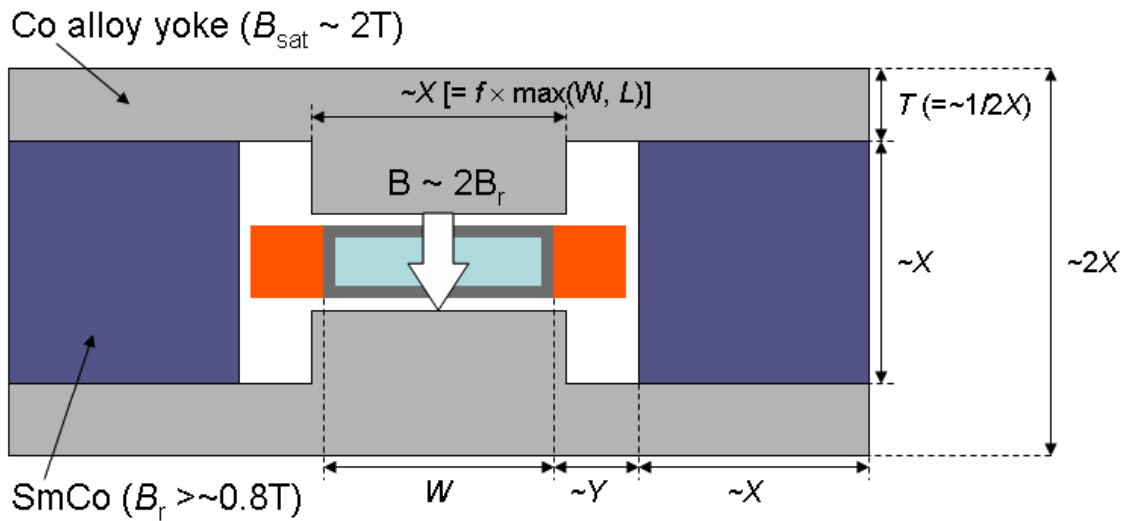


Fig. III-45. Example DC EM pump.

### c.2. Fragment Separator Design (B. Erdelyi, J. Nolen, L. Bandura, and J. Maloney)

Using a combination of beam optics symmetry theories we have worked to design the optical layout for the fragment separator of an exotic isotope accelerator. The achievement of large acceptance and high resolution is a challenge in the presence of large aperture superconducting magnets. The primary motivation for the design was criteria for the fragment separator in the proposed Rare Isotope Accelerator (RIA), but the design methods which were developed can readily be applied to a much broader range of systems.

The design was developed by taking advantage of basic symmetries in the design layout, including the geometry of the components. The effects of the separator's components were calculated by determining a Taylor expansion for the transfer map for isotopes traveling from the beginning through the end of the fragment separator. At first order (*i.e.*, the terms with linear dependence on the initial 6-dimensional phase space vector) this map becomes a matrix. The components of the transfer map can be used to measure resolution and aberrations of the optical design for the separator.

Because no fields in the separator are explicitly time dependent and all components of the separator have

geometric symmetry about the mid-plane above and below the optical axis, half of the terms in the transfer map are cancelled. Other less obvious symmetries were also considered, including the symplectic symmetry that arises from the Hamiltonian nature of the particle motion within the separator, and mirror symmetry about certain points in the separator. The combination of these symmetries allows explicit calculation of the minimum number of multipoles necessary to minimize the aberrations in the final beam.

The linear layout, depicted in Fig. III-46, consisted of two identical cells with dipoles and quadrupoles. Each cell maintains symmetry about the middle of the bending dipole. The system also focuses point-to-parallel and parallel-to-point at the middle of the dipole. Both the dispersive and achromatic images focus point-to-point and parallel-to-parallel. It was calculated by using a Mathematica notebook to determine the spacing of the magnetic components. COSY Infinity was used to calculate the final magnetic pole tip fields necessary to focus the system. The development of this design involved extensive testing of a variety of possible layout configurations seeking to maximize resolution while minimizing the maximum beam size anywhere in the system, and the quadrupole strengths.

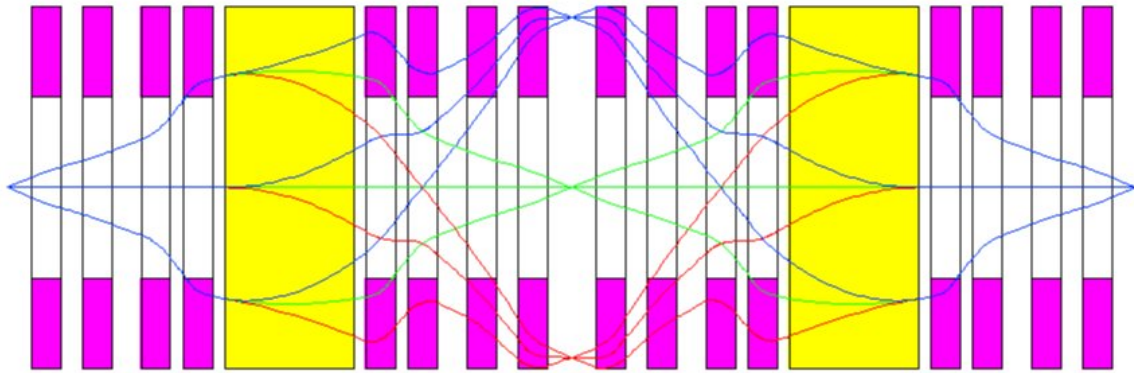


Fig. III-46. First order layout of the (first stage of the) proposed ion optics of the fragment separator.

After the linear layout system was designed, corrections had to be made for the higher order aberrations of the system, as well as the effect of fringe fields. Again, the use of symmetry theories, in particular the combination of mirror and symplectic symmetry, allowed determination of the minimum number of multipoles necessary to minimize the aberrations. We were able to

show how aberrations in the optical system could be minimized by minimizing an explicit list of transfer map coefficients. The final layout, shown in Fig. III-47, successfully minimized all aberrations through third order. The residual aberrations were calculated through fifth order to show that their effect was minimal.

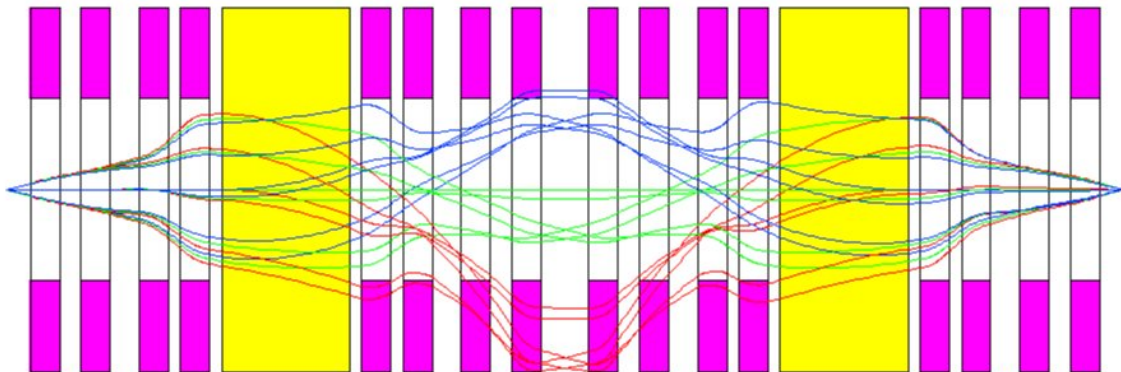


Fig. III-47. Third order layout of the (first stage of the) proposed ion optics of the fragment separator.

Additionally, we have been working on a modified layout using the principles from our original research which could be used to separate isotopes such as  $^{15}\text{O}$ . This system, shown in Fig. III-48, also utilizes the same

basic symmetries as the original design, but also minimizes aberrations at the dispersive image at higher orders.

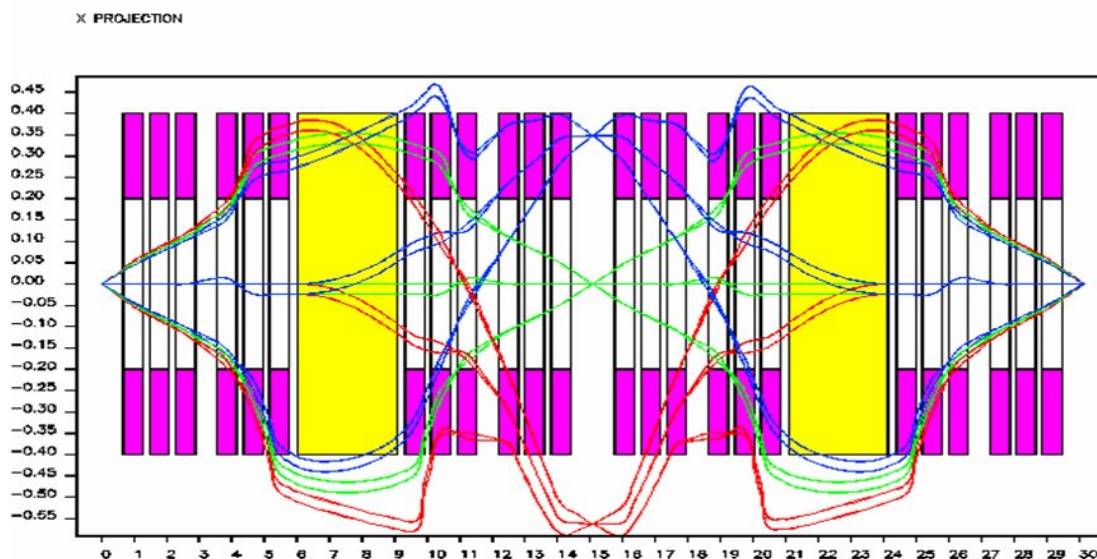


Fig. III-48. Second order alternate layout of the (first stage of the) proposed ion optics of the fragment separator.

### c.3. Effects of the Wedge Absorber in Fragment Separators (B. Erdelyi, J. Nolen, L. Bandura, and J. Maloney)

Next-generation fragment separators for the study of exotic nuclei possess some design challenges due to the large emittances that result from the reaction kinematics in the target. In order to achieve separation in mass and charge, an absorber wedge must be used. As isotopes pass through the wedge, the amount of energy loss varies according to the isotope's specific mass and charge. This ensures that only one species is selected at the end of the fragment separator. In addition to complications resulting from the beam interactions in the target, the introduction of an absorber wedge into the fragment separator creates undesirable optical effects that must be eliminated. A computational framework to model these beam-material interactions and their effects on the operation of the fragment separator has been developed and implemented.

We have used COSY Infinity to model the beam-material interactions in the target and absorber in combination with the charged particle optics. COSY Infinity is a general purpose nonlinear dynamics code based on Differential Algebra (DA). We have integrated several stand-alone codes into COSY, which were necessary to look at energy loss and other nuclear physics processes. The codes we have utilized are EPAX for calculation of fragmentation cross sections, GLOBAL for charge state evolution of the beam, and

ATIMA for energy loss and energy and angular straggling within the target and absorber. These codes are now available as simple calls to intrinsic functions within COSY.

A fission model has been developed to accurately model the dynamics of the secondary beam in the fragment separator and to correctly predict the cross sections of the fission products from a uranium primary beam at various energies. The fission and fragmentation database has been constructed from data generated by the nuclear physics code MCNPX. Production cross sections were provided for four primary beam energies and polynomial interpolations were used to obtain the cross sections of all isotopes in the 200-1500 MeV/u energy regime. In order to accurately model the beam dynamics in the fragment separator, the kinematics of the fission products, upon emergence from the target, were needed. In Fig. III-49, the phase space coordinates of  $^{132}\text{Sn}$  particles produced by a 200 MeV/u  $^{238}\text{U}$  beam in a carbon target are shown. The coordinates of all fission products are represented by similar "fuzzy" spherical shells. Several data points from MCNPX were collected and polynomial interpolations in mass, charge, and energy were used to obtain the initial coordinates of any secondary beam.

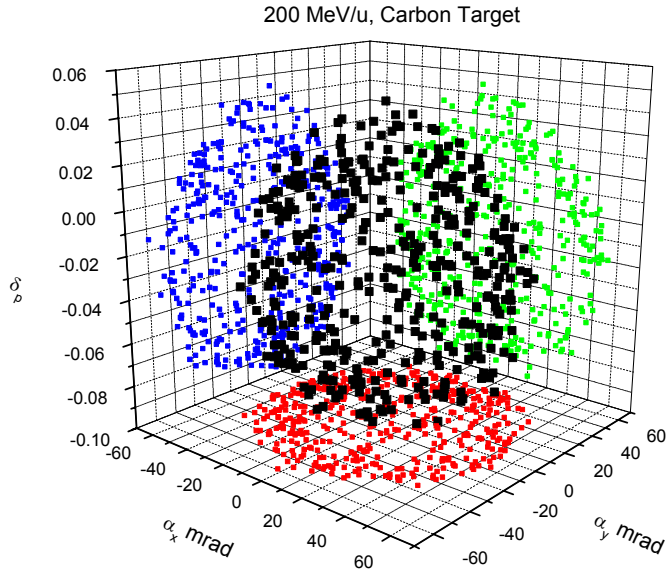


Fig. III-49. Initial coordinates of  $^{132}\text{Sn}$  produced by 200 MeV/u  $^{238}\text{U}$  on  $^{12}\text{C}$  target.

A detailed study of the optical effects induced by the introduction of the absorber into the fragment separator has been performed. Using an unshaped absorber, we have analyzed how the magnification and dispersion change as functions of absorber thickness and projectile energy. The ideal thickness and shape of the absorber have been calculated such to maximize resolution and transmission for a 400 MeV/u  $^{132}\text{Sn}$  beam. Figure III-50 shows the resolution of the fragment separator as a function of the absorber thickness. We have also investigated the dependence of resolution on initial beam emittance.

As an unshaped absorber produces aberrations in an otherwise low-aberration separator, higher order shaping of the entrance and exit surfaces is needed for their correction. Without shape correction, aberrations due to even a thin wedge can be on the order of several centimeters. Using optimizers from within COSY, we have fit the higher order surface coefficients such to minimize aberrations in the horizontal plane. We have succeeded in cancelling all of the aberrations (<1 mm) to third order for a wedge that is optimized for transmission and resolution.

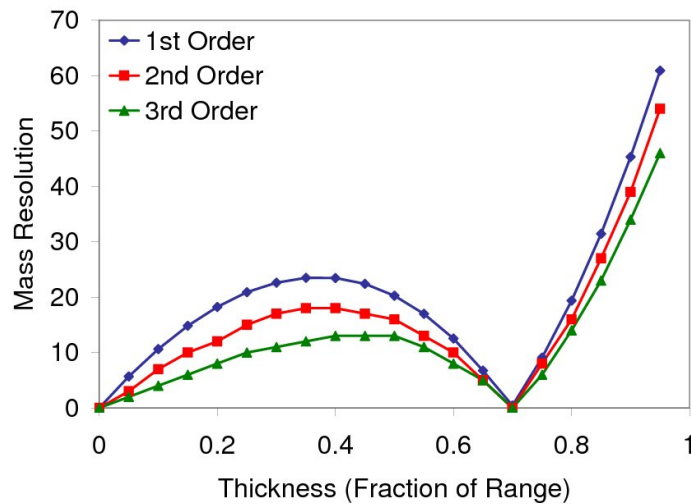


Fig. III-50. Mass resolution of fragment separator at 400 MeV/u.

Two modes have been implemented in order to look at different effects of the absorber. In “map mode” the deterministic effects are easily modeled. When the absorber is viewed as an optical element, the map approach can capture the average energy loss of a particle which is dependent on the projectile-absorber material combination, the energy of the reference particle, the shape of the absorber and the initial conditions of the particle. In map mode the optimization of the wedge shape to minimize aberrations in the system is fast.

In “Monte-Carlo mode” one may track all isotopes produced in the target and wedge. In this mode we

divide the target and wedge into thin slices. For each slice, the incident particle sees a drift with energy loss. At the end of the slice, new particles can be created and primary particles are deleted. Coordinates must be assigned to the new particles based on the parent particle. For new particles which are not produced by a uranium nucleus, the new coordinates are determined by invoking the “fireball method”. If the parent particle is uranium, then coordinates are found by interpolation using the fission database. It should be noted that MC mode also incorporates all of the features of map mode. Since MC mode allows us to track all isotopes in the fragment separator, we will perform separation purity studies by this approach.

**c.4. Large Aperture Magnet Maps to Optics Maps (S. Manikonda, J. Nolen, M. Berz,\* and K. Makino\*)**

Next-generation radioactive beam facilities like the proposed AEBL facility in the U.S. require the use of large aperture air-core type superconducting quadrupole magnets. Since the charged particle beams used in such facilities are wider in the dispersive plane than the transverse plane, it is cost efficient to utilize magnets with elliptic cross sections. We have proposed a new design for a quadrupole magnet with an elliptic cross section and with tunable higher order multipoles.

The design consists of eighteen superconducting racetrack coils placed on two hollow concentric rhombic prism support structures, with the ratio of the

diagonals of the rhombus equal to 2. The cross section view showing the arrangement of the current coils on the support structure is shown in Fig. III-51. The positioning of the coils in the first quadrant is given in Table III-3. The signs “+” and “-” indicate the direction of the current to produce a positive multipole terms. The superconducting racetrack coils on the inner rhombic prism produce quadrupole and octupole fields. The racetrack coils on the outer rhombic prism produce hexapole and decapole fields, and also allow for a limited dipole field for correction purposes. The length of the magnet is 1m.

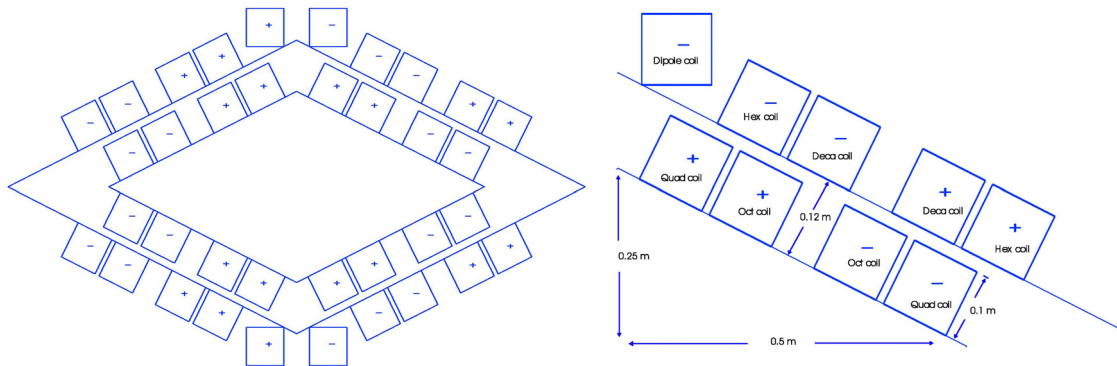


Fig. III-51. The cross section view of the full magnet and coil description in the first quadrant.

In order to study the proposed design new numerical tools to compute the multipole expansion of the magnetic field starting from the Biot-Savart law and Ampere’s law have been implemented using the

Differential Algebraic (DA) framework available in the code COSY Infinity. Some of the features of these tools are:

- Racetrack type current coil and infinitely long current wire of rectangular cross section have been implemented to do the 3D and 2D design of air-core type magnets.
- The computation of high-order multipole decomposition of the field is done using the DA techniques. Using orders around 10, accuracy of about 14 digits can be achieved using these tools.
- The currents and geometric design factors can be set as parameters for the field computation. This leads to high-order parameter dependent local expansion of the magnetic field, which can be used to study and further optimize the design.
- The multipole decomposition of the field obtained from these tools can be combined with the existing DA based transfer map extraction tools in the code COSY Infinity. Fringe fields can now be treated exactly and no approximation by the analytic Engle model is needed.

Table III-3. The center position of the coils in the first quadrant.

Coil Description	Position of Coils	
	X (m)	Y (m)
<i>Inner Coils</i>		
Quadrupole (-)	0.4473	0.8222E-01
Octupole (-)	0.3473	0.1322
Octupole (+)	0.1973	0.2072
Quadrupole (+)	0.9736E-01	0.2572
<i>Outer Coils</i>		
Hexapole (+)	0.5591	0.1604
Decapole (+)	0.4591	0.2104
Decapole (-)	0.3091	0.2854
Hexapole (-)	0.2091	0.3354
Dipole Corrector (-)	0.8385E-01	0.4172

The feasible range of multipole strengths that the proposed magnet can achieve is shown in Fig. III-52. The strengths are computed at the horizontal half

aperture and the current density was varied between  $\pm 10^8 \text{ A/m}^2$ .

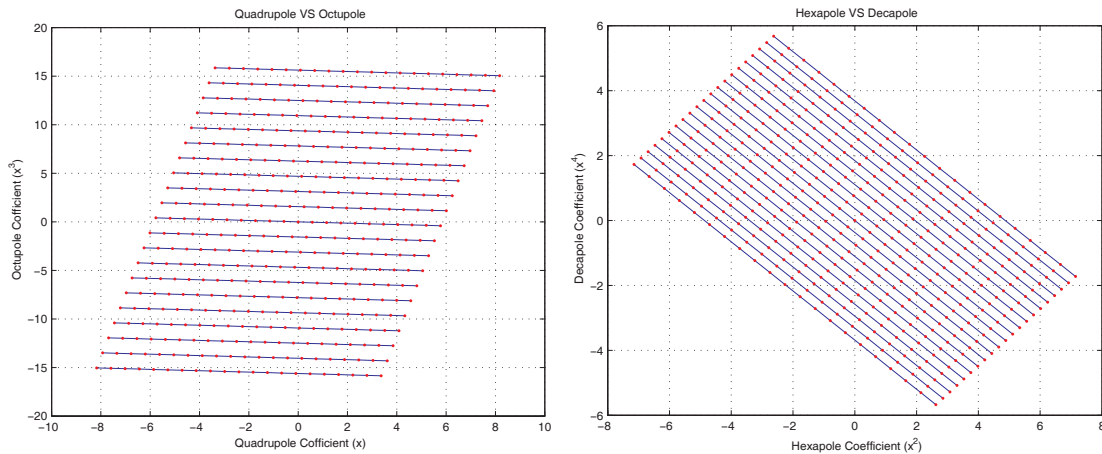


Fig. III-52. The operational plots for different multipoles.

The magnetic field on the central cross section of the magnet is shown in the Fig. III-53. As expected, the

magnetic field is purely transverse ( $B_z = 0$ ) here. The y-component of the magnetic field on the mid plane of

the magnet, showing the fringe field region, is plotted in Fig. III-54.

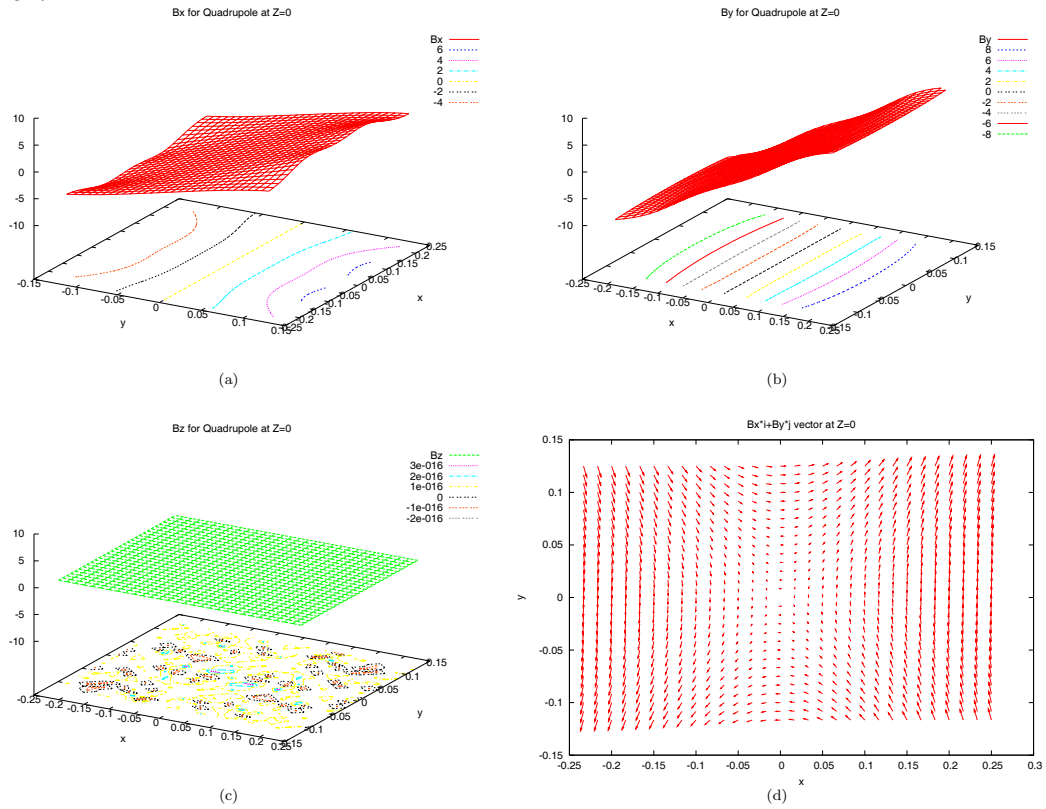


Fig. III-53. The magnetic field on the central cross section of the magnet ( $z = 0m$ ).

By for Quadrupole at Y=0 plane

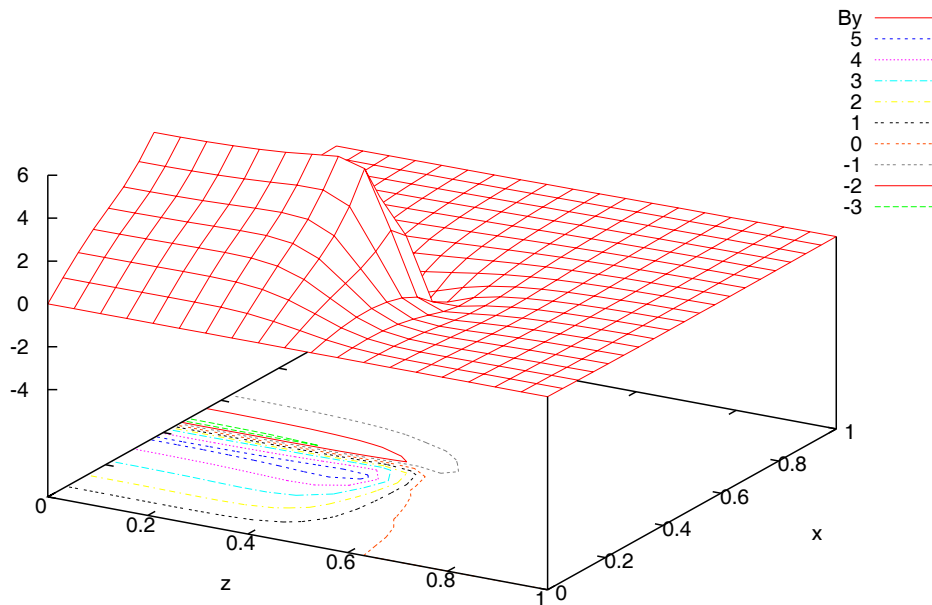


Fig. III-54. The plot of y-component of magnetic field on the midplane.

\*Michigan State University.

### c.5. Development of Uranium Carbide Material for High Power ISOL Applications (J. P. Greene, J. A. Nolen, and T. Burtseva\*)

One option as a high power isotope separator on-line (ISOL) production target proposed for the Advanced Exotic Beam Laboratory (AEBL) will be one based on fission from uranium or a compound of uranium to produce ion species far from stability.<sup>1</sup> The two-step target design employs neutrons first generated in a cooled, refractory, primary target which then induce fission in a surrounding assembly of uranium carbide.

The prototype target design was done by TechSource, Inc.<sup>2</sup> with the fine-grained, high thermal conductivity  $UC_2$  target material to be supplied by Argonne National Laboratory (ANL). The primary target will be a liquid cooled tungsten cylinder, irradiated by the AEBL driver beam. The small energy deposition rate in the surrounding  $UC_2$  secondary target material is not sufficient to heat the target to the desired operating conditions (1600 to 2100 C) necessary to promote effective release of fission products. Thermal conductivities on the order of 2 W/m-K (or greater) over the operating temperature range are required for a viable secondary target design.

The thermal conductivity measurements are carried out on sample disks prepared using  $UC_2$  powder together with carbon (ratio of 8:1) in the form of exfoliated graphite obtained through Superior Graphite which avoids the need for a binder. Densities of 5 g/cc and greater have been achieved, meeting design specifications.

These thin sample pellets then have their thermal

conductivity measured using the method of electron bombardment.<sup>4</sup> The sample is heated on the bottom face by a vertical electron beam source installed within a vacuum evaporator. After achieving thermal equilibrium, the temperature of both faces of the sample was measured with the aid of a two-color pyrometer. Modifications to the original design were recently performed adding ceramic rod supports and an intermediate tungsten collimator installed beneath the pellet support to prevent beam halo from hitting the Ta sample holder. New measurements were performed of the thermal conductivities for our  $UC_2$  samples which exhibit properties comparable to values found in the literature. A thermal analysis was made on these heated disks using the code FlexPDE,<sup>5</sup> solving the heat flow partial differential equations and extracting the thermal conductivity as a check of the method.

As the original material used for this research is no longer commercially available, an effort was immediately mounted for preparation in-house by the method of arc melting.<sup>3</sup> Recently, alternative commercial sources for uranium carbide supply have come to our attention. One company, IBI Labs, which was contacted after the last collaboration meeting at Oak Ridge National Laboratory (ORNL), has provided us with a supply of commercially available  $UC_2$  material having a grain size down to -325 mesh. This material will be fashioned into disks for thermal conductivity determinations and also release measurements. A photomicrograph of this new material is seen in Fig. III-55.

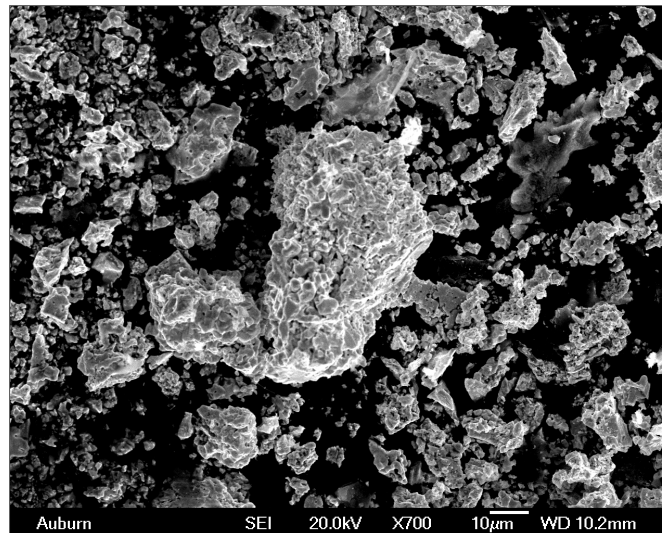


Fig. III-55. Photomicrograph of the -325 mesh uranium carbide powder purchased from IBI Labs.



Another avenue of manufacture has been undertaken by Refrac Systems using the method of hydriding, starting with depleted metal reacted in a hydrogen furnace. Over 3 kg of clean depleted uranium metal plate was shipped to Refrac Systems with the reacted product combined with fine graphite powder for the manufacture of  $UC_2$ . Enough uranium carbide material has now been manufactured to meet the requirements for the TechSource target design. In addition, as part of the compaction/carbonization process several disks having significantly higher densities (in the range of 8-11 g/cc) were prepared and are now being characterized for thermal properties and radioactive release. One of the prepared target disks is shown in Fig. III-56.

The desired release of the fission products produced under sample irradiation is also being explored as a function of density. The target/ion source (UNISOR) facility is being used for characterization of the secondary target material release properties. We are working closely with Dan Stracener and Ken Carter at ORNL and  $UC_2$  manufactured from our fine grain size material has been shipped there for these measurements. Analysis of the experimental data on the release properties of radioactive ions from this intermediate density, smaller grain size pellets is being performed. This work is presently ongoing as we are

awaiting beam time when available.

With verification of the thermal properties coupled with new data from ORNL on the release properties eventually from the high density material, we hope to move towards fabricating actual secondary target disks using custom designed dies and available large area press.

As an alternate method to make the large diameter disks needed for the actual target, we are investigating the use of a electrocompaction process that was recently demonstrated by an ANL/Superior Graphite collaboration. Under an agreement between the two parties, the ANL Physics Division has now taken possession of the equipment and is presently developing the required radiation safety documentation with the Energy Technology Division to operate it using uranium carbide. With Superior Graphite personnel, large diameter sample disks of WC/exfoliated graphite have been successfully pressed to high density as a demonstration of the process. It is believed that the densities and thermal conductivity achieved for  $UC_2$  samples using this process will be sufficient for a prototype high-power ISOL target, including a tilted spallation target for manufacture and testing under actual experimental conditions.

\*Energy Technology Division, Argonne National Laboratory.

<sup>1</sup>Report to ATLAS Users Facility, ANL-ATLAS-99-1, March (1999).

<sup>2</sup>W. Talbert *et al.*, TechSource, Inc. (SBIR Grant).

<sup>3</sup>J. Crane, F. B. Litton, and H. S. Kalish, Arc Skull Melting and Casting of Uranium Carbide, ASM Trans. Quarterly **56**, 176 (1963).

<sup>4</sup>J. P. Greene, A. Levand, J. Nolen, and T. Burtseva, Nucl. Phys. **A746**, 425c-428c (2004).

<sup>5</sup>FlexPDE 4.2.7s (student version) [www.pdesolutions.com](http://www.pdesolutions.com).

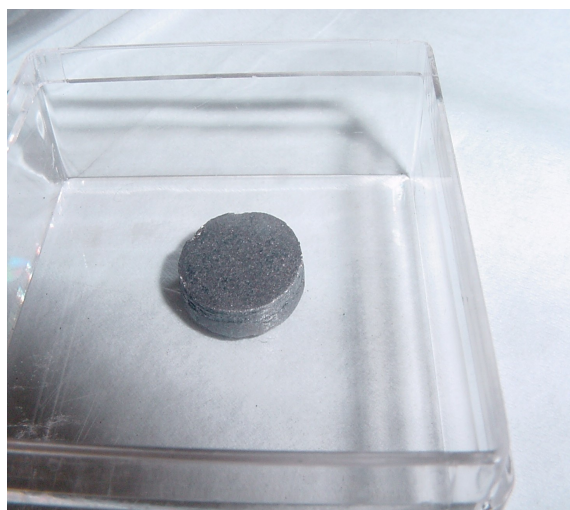


Fig. III-56. Picture of a high-density uranium carbide sample produced by Refrac, Inc.

### c.6. A Study of the Cyclotron Gas Stopper Concept (M. Sternberg and G. Savard\*)

The proposed cyclotron gas-stopping scheme (see Fig. III-57) for the efficient thermalization of intense rare isotope beams has been examined. Simulations expand on previous studies completed by Bollen *et al.*<sup>1</sup>

and expose many complications of such an apparatus arising from physical effects either not accounted or not accounted properly for in previous work. Below is a schematic of the device, as proposed by Bollen *et al.*

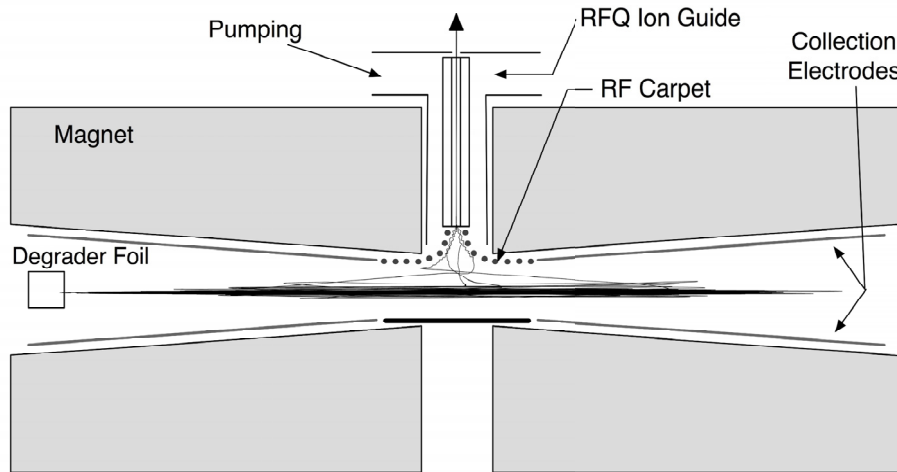


Fig III-57. Schematic layout of the proposed cyclotron catcher concept.

The proposed design uses a gas-filled weakly focusing cyclotron magnet with a 4 cm pole gap to thermalize energetic beams produced by fragmentation. After passing the ions through a degrader foil they can become confined within the cylindrical gas-filled magnetic region where current gas-stopping techniques can be used to cool ions to thermal energies using 10 mbar of high purity He. As the ions collide with and ionize the He gas they lose energy and their orbits within the magnet field shrink about the center of the magnet causing them to stop finally within a small cylindrical region in the center of the magnet. Simulations by Bollen *et al.* have shown this method to produce a clear separation between the He<sup>+</sup> ions concentrated in a donut shaped region surrounding the center and the cooled ions in the center within a 4 cm pole gap. It has been suggested that such a technique may be able to overcome space charge limitations inherent in other gas-cell designs by removing the highly concentrated He ions with a ring of charge collection electrodes allowing for operations at greater beam intensities, while the cooled ions in the middle could be extracted with the use of a DC gradient combined with an RF carpet followed by an RFQ-ion guide.

Such simulations suggested a large possible improve-

ment on currently allowed beam intensities. However, these simulations failed to properly include many physical phenomena that were either neglected, mistreated, or improperly determined to be negligible. Of particular concern was their assertion that, “these [small angle scattering and energy straggling] effects are relatively small for ions stopping in helium and are small compared to the initial beam parameters.” While the effects of energy straggling are very small, simulations performed in SRIM suggest an average lateral stopping range of 37 cm for the test case used by Bollen *et al.* and it is not immediately clear that the effects of multiple scattering could be neglected when stopping ions within a 4 cm pole gap.

Our approach was to first reproduce the results of Bollen *et al.* then systematically improve on these simulations by:

- Correcting the charge-changing collision method used in the paper.
- Including proper charge state of ions in solids for beam exiting the degrader.
- Adding angular straggling.

- Performing simulations with larger phase-space for the incoming beam.
- Investigating alternative means of focusing.

Figure III-58 shows a plot of our results for stopping efficiency as a function of pole gap for the design proposed by Bollen *et al.* using two different models for the cyclotron's B-field. As one can see, the originally proposed cyclotron gas-stopper geometry with a 4 cm pole gap was found to have a near null efficiency (the original study reported a 100% stopping efficiency), with the largest loss in efficiencies coming from the

inclusion of angular straggling and properly treating charge-state straggling. We extended these simulations to devices with modified geometry and a much larger pole gap and could achieve a stopping efficiency approaching roughly 90%, but at the expense of many engineering difficulties. The advantages that were, however, incorrectly predicted in previous simulations for high intensity operation of this device are severely compromised. In addition, we have demonstrated the validity of our simulation methods by reproducing experimental data from experiments involving ion collisions in gas-filled magnets. These results have been submitted for publication in NIM.

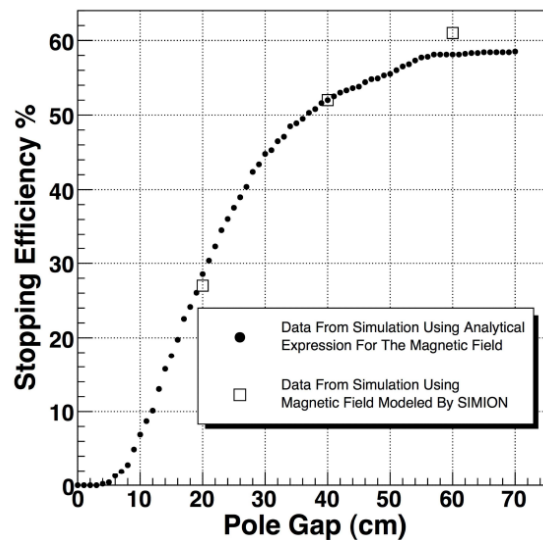


Fig. III-58. Calculated stopping efficiency as a function of the magnet pole gap.

\*Argonne National Laboratory and University of Chicago.

<sup>1</sup>G. Bollen *et al.*, Nucl. Instrum. Methods **A550**, 27 (2005).

### c.7. The High-Intensity AEBL/RIA Gas Catcher Test at ATLAS (G. Savard, J. Clark,\* S. Gerbick, J. P. Greene, A. Levand, N. Scielzo, K. S. Sharma,† M. Sternberg, and B. J. Zabransky)

Both theoretical and experimental work has continued on the RIA prototype gas catcher and resulted in a breakthrough in performance at high intensity for such devices. Detailed calculations we performed identified radial losses due to positive space charge build up in the gas catcher as the main loss mechanism in high intensity operation. The incoming ions create ion-electron pairs by losing energy while they slow down. The electrons have higher drift velocity in the gas and

are removed quickly. The remaining positive ions, mostly helium, remain behind and their space charge repels the positive radioactive ions which must then move in the combined DC fields from the electrodes and the space charge distribution. At low and moderate intensity, the ions reach the RF cone and are rechanneled to the nozzle and extracted; this is one of the great advantages over the DC only approach where there is no recovery mechanism and these ions are lost

even at fairly low intensity. At the highest intensities, however, the radioactive ions can be lost radially even before they get to the RF cone. To overcome this difficulty, we added an RF structure similar to that in the RF cone along the body of the gas catcher in regions where medium ionization is present and developed a novel structure for operation in the highest ionization regions. The complex electrodes for these body RF sections were built, chemically polished, cleaned and assembled together with their resonating RF feeding system and used to replace the existing electrodes in the AEBL/RIA prototype body sections.

In parallel to these efforts, the high-intensity beamline in construction in experimental area II at ATLAS to test high-intensity operation of the RIA/AEBL gas catcher by reproducing beam properties expected after the final degrader behind a RIA-type fragment separator was completed. This beamline utilizes a high-power rotating target for isotope production and a large bore superconducting solenoid to refocus all isotopes produced at an angle below 10 degrees to the entrance of the gas catcher. A movable zero-degree beamstop lets through scattered tails of the beam so that RIA-like ionization densities can be reached inside the gas catcher. This new beamline was commissioned in August 2006.

The RIA gas catcher prototype, retrofitted with the new RF body sections combined with the existing large RF cone, was installed in the new high-intensity beamline in experimental area II at ATLAS (see Fig. III-59) and connected to the diagnostics line from the CPT Penning trap injection system. A 25 cm diameter all-metal thin window is used to isolate the beamline vacuum from the gas catcher high purity helium gas. The modified gas catcher was first tested with fission products from a  $^{252}\text{Cf}$  source with which the device was shown to operate properly and the body RF sections shown to be

effective at focusing radioactive ions. Even at low intensity, the body RF was shown to increase the extracted radioactive ion yield by about 7% over the nominal 45% efficiency obtained under previous operating conditions. This increase is believed to be coming from fission products stopped very close to the body electrodes that were lost under the previous configuration where no RF repulsion along these electrodes was available to counteract fringe field effects. A first high intensity test of the gas catcher took place in September 2006 with activity from a fission source extracted from the gas catcher system being measured while ions from the new beamline were simultaneously injected into the gas catcher. Initial results indicate that the efficiency of the gas catcher under these conditions was reduced by 2% with an incoming ion flux of  $3 \times 10^7$  per second, the maximum ion flux we could obtain from the new beamline in this initial run. This very positive result validated our approach and a second test where activity from the incoming beam was monitored as a function of intensity, with intensity in the  $10^7 - 10^9$  ions/second range, took place at the end of 2006. Figure III-60 summarizes the results of this test.

The results from the initial high-intensity test shown in Fig. III-60 indicate that the device, with its new RF focusing structures, can operate without loss in efficiency at incoming ion intensity up to  $10^8$  ions per second and still has an efficiency of about 10% at  $10^9$  incoming ions per second. This represents successful operation at about four orders of magnitude higher intensity than previously demonstrated and within shooting distance of the original RIA goal of 20% efficiency at  $10^9$  ions per second. This is the first demonstration of operation in a regime anywhere close to that required at AEBL/RIA and the further refinement that will be incorporated in the coming year should allow us to reach or surpass this goal.

---

\*Yale University, †University of Manitoba, Winnipeg, Manitoba.



Fig. III-59. Aerial view of the large gas catcher inside its high-voltage shielding cage (on the right) in location at the end of the new beamline built to reproduce the ion properties expected after the final degrader in a RIA-type fragment separator. The main optical element in that beamline is a 65 cm bore superconducting solenoid shown in blue at the left of the picture.

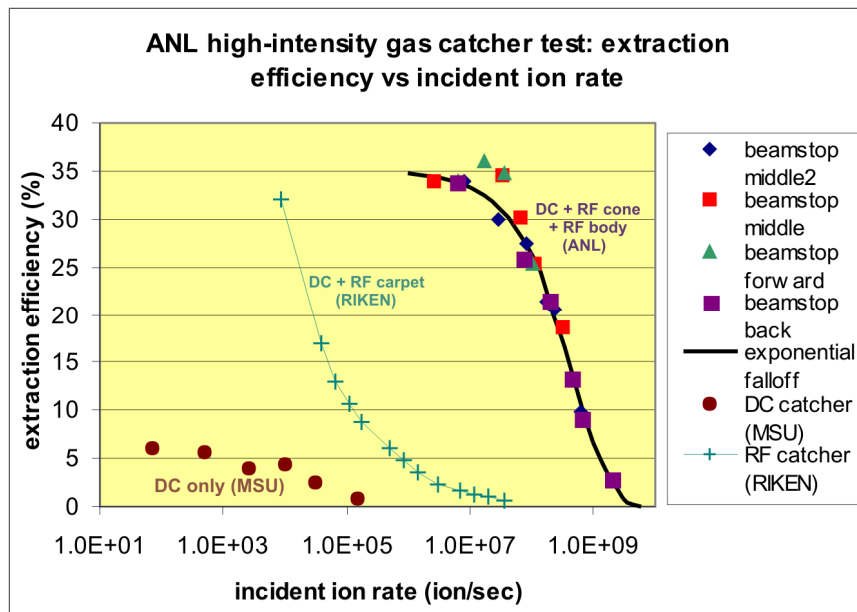



Fig. III-60. Efficiency for the extraction of the stopped radioactive ions versus the incoming ion rate. The addition of the new RF focusing structures allows successful operation at four or more orders of magnitude higher intensity than other approaches used so far.



## IV. MEDIUM-ENERGY NUCLEAR PHYSICS RESEARCH

### OVERVIEW



The overall goals of the Medium-Energy Physics research program in the Argonne Physics Division are to test our understanding of the structure of hadrons and nuclei and provide tests of the Standard Model. In addition, we develop and exploit new technologies for high-impact applications in nuclear physics as well as other national priorities. In order to test our understanding of the structure of hadrons and the structure of nuclei within the framework of quantum chromodynamics, the medium-energy research program emphasizes the study of nucleons and nuclei on a relatively short distance scale. Because the electromagnetic interaction provides an accurate, well-understood probe of these phenomena, primary emphasis is placed on experiments involving electron scattering, real photons and Drell-Yan processes. The electron beams of the Thomas Jefferson National Accelerator Facility (JLab) are ideally suited for studies of nuclei at hadronic scales and represent one center of the experimental program. Staff members have had a key role in the development of experimental equipment and development of the scientific program at JLab. During the past year, the MEP group had a major responsibility for four new proposals for the 12-GeV physics program. We have continued to develop the optical trap program and have applied this new technique to the study of neutron-rich light nuclei and began preparations for the search for a non-zero electric dipole moment in a nucleus.

Recently, staff members have focused increasingly on studies of the nucleon and the search for exotic phenomena. Preparations were begun for a super-Rosenbluth measurement for electron-proton elastic scattering at JLab. In the past year, analyses were completed for the search for pentaquark partners and for polarization in deuteron photodisintegration; while preliminary analyses were completed for the EMC effect in light nuclei, the  $x > 1$  experiment in nuclei, and for transparency in  $\rho$  electroproduction in nuclei.

The HERMES experiment in the HERA electron ring at DESY-Hamburg has two novel features: (1) polarized electron scattering from internal polarized or unpolarized atomic gas targets, and (2) a dual-radiator ring imaging Cerenkov counter (RICH). Deep inelastic scattering has been measured with polarized electrons on polarized hydrogen, deuterium and  $^3\text{He}$ . Argonne has concentrated on the hadron particle identification of HERMES, a unique capability compared to other spin structure experiments. In 1999 and under Argonne leadership, the RICH was brought into operation at the design specifications to provide complete hadron identification in the experiment. In recent months, HERMES entered its final year of operation. During its last year HERMES plans a program of measurements for unpolarized targets. These results are expected to provide new and significant data for deeply virtual Compton scattering as well as accurate  $d/u$  ratios in the valence region.

Measurements of high mass virtual photon production in high-energy proton-induced reactions have determined the flavor dependence of the sea of antiquarks in the nucleon. These measurements gave insight into the origin of the nucleon sea. In the same experiment, the high- $x$  absolute Drell-Yan cross sections were measured. During the past year the angular distribution of the Drell-Yan process in free proton-proton scattering was determined as a constraint on the Boer-Mulders structure function of the proton. In Fiscal Year 2001, a new initiative was approved by the FNAL PAC to continue these measurements with much higher luminosity at the FNAL Main Injector. These Drell-Yan experiments not only provide the best means to measure anti-quark distributions in the nucleon and nuclei, but represent an outstanding opportunity to perform these measurements at an ideal proton beam energy of 120 GeV. During the past year, the FNAL PAC re-affirmed the importance of these Drell-Yan measurements. In addition, a technical, cost and schedule review of the Drell-Yan project was conducted during the past year.

The technology of laser atom traps provides a unique environment for the study of nuclear and atomic systems and represents a powerful new method that is opening up exciting new opportunities in a variety of fields, including nuclear physics. In particular, the group has continued the development and improvement in efficiency of a high-sensitivity magneto-optical trap for rare, unstable isotopes of krypton as a means for dating ancient groundwater. In 2004, a highlight was the optical trapping of single atoms of  $^6\text{He}$  and performing precision laser spectroscopy on the individual atoms to determine the charge radius of  $^6\text{He}$  nuclei. During the past year, the helium atom trap efficiency was improved by more than an order of magnitude. The helium trap was successfully moved and brought into operation at GANIL in preparation for the  $^8\text{He}$  charge radius measurement.

Preparations for the search for an electric dipole moment (EDM) of  $^{225}\text{Ra}$  are in progress. The ultimate goal is to search for a non-zero EDM for  $^{225}\text{Ra}$  and improve the sensitivity for nuclear EDM searches by approximately two orders of magnitude. This test of time-reversal symmetry represents an outstanding opportunity to search for new physics beyond the Standard Model. Not only were radium-225 atoms successfully optically trapped, but the beneficial effect of blackbody radiation on the trap was discovered.





## A. HADRON PROPERTIES

### a.1. Precision Measurements of the Proton Electromagnetic Form Factors and Two-Photon Exchange Effects (J. Arrington, K. Hafidi, R. J. Holt, P. E. Reimer, P. Solvignon, and the JLab E05-017 Collaboration)

Polarization transfer measurements of the proton form factors showed a significant difference between the charge and magnetization distributions of the proton. These results contradict previous Rosenbluth separation measurements, and the explanation is now believed to be due to two-photon exchange (TPE) corrections. While these corrections are small, typically 5% or less, they have a significant impact on the Rosenbluth extraction of  $G_{Ep}$ .

We have been trying to better understand the TPE corrections and to provide better extractions of the nucleon form factors. A review article on nucleon form factors was prepared and published in collaboration with Craig Roberts of the theory group.<sup>1</sup> We have also completed and are about to submit a detailed extraction of the form factors, including TPE corrections.<sup>2</sup> Finally, we have been studying the possible effects on TPE corrections on other exclusive processes, such as the extraction of the pion form factor, the measurement of the strangeness form factors of the nucleon through parity violating electron-proton scattering, and the impact of the electromagnetic form factors on neutrino scattering measurements.<sup>3,4</sup>

We also have a significant experimental program aimed at better understanding two-photon exchange. JLab Experiment E01-001<sup>5</sup> used a modified technique to make an extremely high precision Rosenbluth extraction of  $G_{Ep}/G_{Mp}$ . This conclusively demonstrates the disagreement between the techniques, and provided a measure of the size of the TPE effects needed to explain the disagreement. A new measurement, E05-017,<sup>6</sup> is underway at JLab. These new data will provide information on the size of the TPE corrections at larger  $Q^2$  than previous measurements, as well as providing much greater sensitivity to deviations from the linear cross section dependence associated with pure one-photon exchange. In addition, the measurement will reach values of  $Q^2$  where the contribution of the electric form factor is extremely small, allowing for a clean separation of the magnetic form factor and the TPE corrections. These data will

allow for more reliable corrections at large  $Q^2$  as well as reducing the uncertainty associated with TPE calculations at lower  $Q^2$ .

A more direct way of isolating the TPE corrections is a comparison of positron-proton and electron-proton scattering. Such data provide some evidence for two-photon exchange corrections,<sup>7</sup> and we have two new experiments that will make improved comparisons of positron-proton and electron-proton scattering.<sup>8,9</sup> Figure IV-1 shows the proposed scheme for generation of a secondary mixed positron/electron beam in Hall B. For the JLab measurement, a test run was completed in Hall B in October 2006. We demonstrated a significant decrease in the background rates with modifications to the physical layout of the photon tagging system, as well as an improved shielding configuration. We were able to run with luminosities that allowed us to observe and reconstruct positron-proton and electron-proton elastic scattering using the secondary combined electron/positron beam. As a result, a full proposal was submitted and approved by the JLab PAC, and is expected to run in 2008-2009. For the Novosibirsk measurement, there will be a run in summer 2007, which will commission the new internal hydrogen target and the additional calorimetry added to the large angle detectors.

Finally, we also participated in new polarization transfer measurements at low momenta,<sup>10</sup> taken as calibration for recent polarization measurements on deuterium. This demonstrated the ability to make extremely high precision measurements in this region, which has led to a proposal (PR07-004, conditionally approved) to improve the precision and  $Q^2$  coverage of this measurements in the region of low  $Q^2$ , where there is a gap between the extremely precise Rosenbluth measurements for  $Q^2 < 0.1 \text{ GeV}^2$ , and polarization transfer measurements at  $Q^2 > 1 \text{ GeV}^2$ . In addition, we will participate in the upcoming high  $Q^2$  form factor measurements (E04-108) and TPE studies (E04-109) using polarization transfer.

<sup>1</sup>J. Arrington, C. D. Roberts, and J. M. Zanotti, *J. Phys. G: Nucl. Part. Phys.* **34**, S23 (2007).

<sup>2</sup>J. Arrington and W. Melnitchouk, to be submitted to *Phys. Rev. C*.

<sup>3</sup>J. Arrington and I. Sick, submitted to Phys. Rev. C, arXiv:nucl-th/0612079 (2006).

<sup>4</sup>R. Bradford, A. Bodek, H. Budd, and J. Arrington, Nucl. Phys. Proc. Suppl. 159:127 (2006), arXiv:hep-ex/0602017.

<sup>5</sup>JLab experiment E01-001, "New Measurement of  $G_E/G_M$  for the Proton", J. Arrington and R. Segel, spokespersons.

<sup>6</sup>JLab experiment E05-017, "A Measurement of Two-Photon Exchange in Unpolarized Elastic Electron-Proton Scattering", J. Arrington, spokesperson.

<sup>7</sup>J. Arrington, Phys. Rev. C **69**, 032201(R) (2004).

<sup>8</sup>J. Arrington *et al.*, nucl-ex/0408020.

<sup>9</sup>JLab experiment E06-116, "Beyond the Born Approximation: A Precise Comparison of Positron-Proton and Electron-Proton Elastic Scattering in CLAS," A. Afanasev, J. Arrington, W. K. Brooks, K. Joo, B. A. Raue, and L. B. Weinstein, spokespersons.

<sup>10</sup>G. Ron *et al.*, arXiv:0706.0128 (2007).

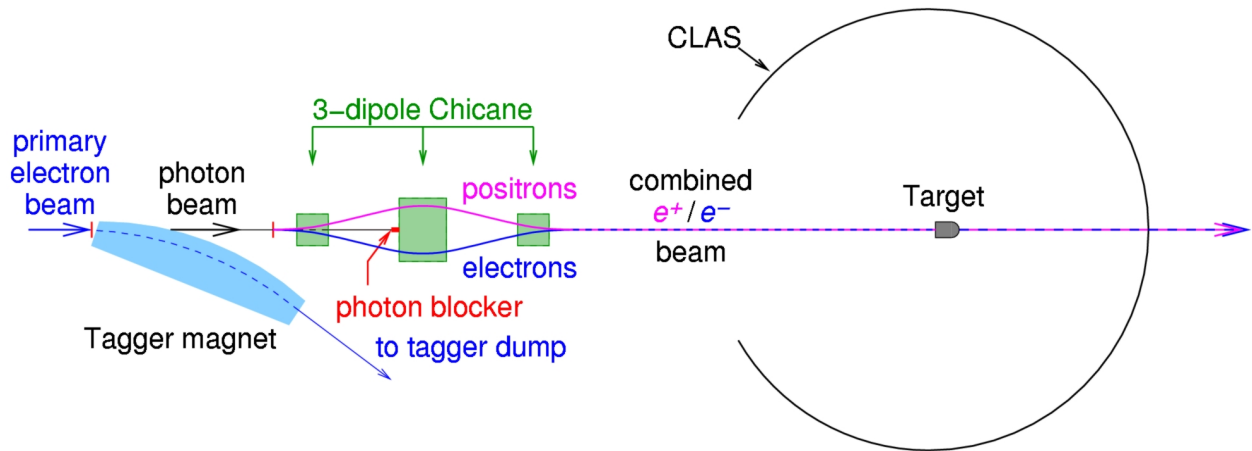


Fig IV-1. Overview of the secondary production of the mixed positron/electron beam in Hall B at JLab.

### a.2. Parity Violating Electron-Proton Scattering and the Strangeness Content of the Nucleon (J. Arrington, K. Hafidi, P. E. Reimer, X. Zheng, and the JLab E99-115, E00-114, and E05-109 Collaborations)

Given precise knowledge of the nucleon electromagnetic form factors, parity violating electron-proton scattering can be used to probe the nucleon strange quark form factors. In 2004, the HAPPEX collaboration made a high precision measurement of parity violating  $e-p$  scattering at  $Q^2 = 0.1 \text{ GeV}^2$ , as a measure of the strangeness contribution to the magnetic moment of the proton. In addition, elastic scattering from  $^4\text{He}$  was measured, which provides a clean measure of the strangeness radius of the proton. The results have been published<sup>1</sup> and indicate that  $G_{Es}$  and  $G_{Ms}$  are smaller than previously believed at  $Q^2 = 0.1 \text{ GeV}^2$ . A proposal to extend these measurements to higher precision at  $Q^2 = 0.5 \text{ GeV}^2$  (E05-109) was approved.

While the parity violating asymmetry is largely insen-

sitive to the effects of two-photon exchange,<sup>2</sup> the isolation of the strange quark contribution requires precise knowledge of the electromagnetic form factors. An analysis of low- $Q^2$  nucleon form factors, including two-photon exchange effects from the calculation of Blunden *et al.*,<sup>3</sup> was recently completed.<sup>4</sup> We provide a prescription for a consistent analysis of the parity violating elastic scattering measurements, accounting for TPE corrections and correlations between the different measurements of the electromagnetic form factors. As part of this work, we provide parameterizations and uncertainties for the low- $Q^2$  form factors of the proton and neutron, appropriate for use in other experiments that require high precision knowledge of the low  $Q^2$  form factors. This will also provide the foundation for a full flavor decomposition of the nucleon form factors into their contributions from

up, down, and strange quarks.

<sup>1</sup>A. Acha *et al.*, Phys. Rev. Lett. **98**, 032301 (2007).

<sup>2</sup>A. Afanasev and C. E. Carlson, Phys. Rev. Lett. **94**, 212301 (2005).

<sup>3</sup>P. G. Blunden, W. Melnitchouk, and J. A. Tjon, Phys. Rev. Lett. **91**, 142304 (2003).

<sup>4</sup>J. Arrington and I. Sick, submitted to Phys. Rev. C, arXiv:nucl-th/0612079 (2006).

### **a.3. The Charged Pion Form Factor** (J. Arrington, K. Hafidi, R. J. Holt, P. E. Reimer, E. C. Schulte, X. Zheng, and the JLab E01-004 and E01-107 Collaborations)

While studies of hadron structure typically focus on the proton, which is easily accessible experimentally, the complicated structure of a three light-quark system makes modeling of the proton in realistic, QCD-based framework, extremely difficult. On the other hand, while the pion is more difficult to access experimentally, its structure is simpler, and can in some cases provide a better meeting ground between theory and experiment in the study of QCD. Calculations led by C. Roberts of the Argonne theory group using the Dyson-Schwinger equations provide realistic representations of the QCD dynamics which can make predictions for both the pion form factors and the pion structure function, which provide complementary information on the pion structure.

Experiment E01-004 extended measurements of the pion form factor to 2.5 GeV<sup>2</sup>. These results were recently published<sup>1</sup> as was a more detailed analysis<sup>2</sup> of the earlier JLab measurement.<sup>3</sup> In addition, it was possible to extract the pion form factor using calibration data from the pion color transparency measurement, E07-107. A draft has been prepared that includes both the extraction of the pion form factor, and as study of the separated longitudinal and transverse cross sections.

Figure IV-2 shows the preliminary results from E07-107, along with the previous world's data. These measurements can be used to test models of hadron structure in a simpler system than the nucleon, where more advanced calculations can be performed.

<sup>1</sup>T. Horn *et al.*, Phys. Rev. Lett. **97**, 192001 (2006).

<sup>2</sup>J. Volmer *et al.*, Phys. Rev. Lett. **86**, 1713 (2001).

<sup>3</sup>V. Tadevosyan *et al.*, Phys. Rev. C **75**, 055205 (2007).

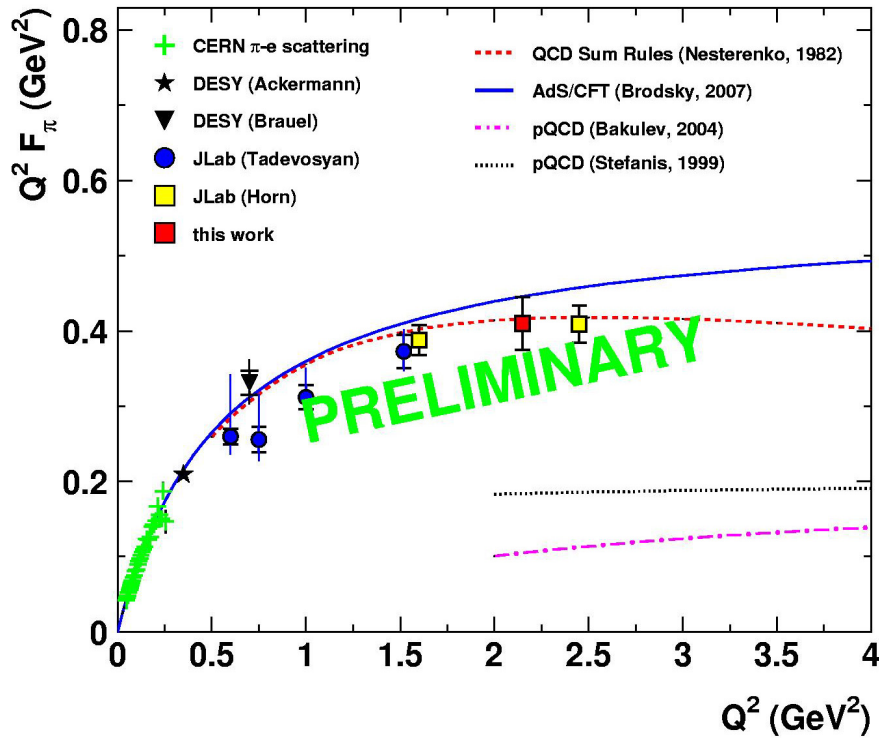


Fig. IV-2. World's data on the pion form factor, including preliminary JLab E07-107 results.

**a.4. Duality and Separated Structure Functions of Nucleons and Nuclei** (J. Arrington, D. Gaskell, D. F. Geesaman, K. Hafidi, R. J. Holt, D. H. Potterveld, P. E. Reimer, E. C. Schulte, P. Solvignon, X. Zheng, and the JLab E94-110, E99-118, E00-002, E00-108, E00-116, E04-001, E06-009 Collaborations)

Inclusive electron scattering in the deeply inelastic scattering (DIS) regime allows us to extract the quark distributions in nucleons or nuclei. In the resonance region, the simple picture of electron-quark scattering is not valid and the scattering is better understood in terms of resonance excitations and pion electroproduction. The unpolarized structure function has been measured precisely in both regions,<sup>1,2</sup> and the data show precise quark-hadron duality. In this case, duality results in the observation that the structure function at lower energies shows resonance structure, but when averaged over the resonances, reproduces the DIS structure function when taken as a function of the Nachtmann scaling variable,  $\xi$ . Using  $\xi$  provides an approximate treatment of target mass corrections, although additional studies using explicit treatment of these corrections yields the same conclusions.

Recently, such measurements have been extended to both the longitudinal and transverse separated structure

functions, and to semi-inclusive pion electroproduction. For the proton and deuteron separated structure functions, the initial resonance region results (E94-110) have been reanalyzed after finding a potential model dependence in the analysis. The final results did not change significantly, and the initial paper<sup>3</sup> has been updated and resubmitted. In addition, an analysis of the separated DIS structure functions at low  $Q^2$  (E99-118) have been finalized and published.<sup>4</sup> Additional studies of the resonance region structure functions, one focused on extremely low  $x$  values (E00-002) and one making precise measurements of duality at high  $x$  and  $Q^2$  (E00-116) are close to having final results. Measurements looking at the separated structure functions for deuterium and nuclear targets (E04-001 and E06-009), aimed to study duality in nuclei and provide cross sections at low  $x$  and  $Q^2$  as input to upcoming neutrino scattering measurements were started in 2005, and additional data is currently being taken.

The results from the semi-inclusive measurement, E00-116, were finalized and published.<sup>5</sup> They show duality in pion electroproduction over a significant range in  $x$  and  $z$ , at relatively low  $Q^2$ , indicating that

duality is a global phenomenon, and providing significant evidence that factorization should hold fairly precisely for higher energy measurements planned for the 12 GeV upgrade.

<sup>1</sup>E. D. Bloom and F. J. Gilman, Phys. Rev. Lett. **25**, 1140 (1970).

<sup>2</sup>I. Niculescu *et al.*, Phys. Rev. Lett. **85**, 1182 (2000).

<sup>3</sup>Y. Liang *et al.*, nucl-ex/0410027 (2004).

<sup>4</sup>V. Tvaskis *et al.*, Phys. Rev. Lett. **98**, 142301 (2007).

<sup>5</sup>T. Navasadyan *et al.*, Phys. Rev. Lett. **98**, 022001 (2007).

#### a.5. Search for Additional Pentaquark States at JLab (P. E. Reimer, J. Arrington, K. Hafidi, E. C. Schulte, X. Zheng, and the JLab E04-012 Collaboration)

All experimentally observed hadrons can be placed into two categories: mesons with valence quark-antiquark pair mesons ( $\bar{q}q$ ) and baryons composed of three valence quarks ( $qqq$ ). These are, however, not the only configurations of quarks and antiquarks allowed by the underlying theory, Quantum Chromodynamics and other configurations not fitting into the meson and baryon framework are known as “exotics”. One possible exotic configuration is the pentaquark state with four quarks and an antiquark ( $qqqq\bar{q}$ ). Recently, experimental evidence and theoretical work have suggested the existence of a pentaquark state, known as the  $\Theta^+$  with a mass near 1540 MeV. Within the Chiral Soliton model, the  $\Theta^+$  is a member of a set of 10 pentaquark states known as an antidecuplet. Using Hall A at JLab, E04-012<sup>1</sup> looked for evidence of an exotic isospin partner state, the  $\Theta^{++}$ , in the  $H(e,e'K^-)X$

reaction, as well as the  $\Sigma^0$  and  $N^0$  members of the antidecuplet in the reactions  $H(e,e'K^+)X$  and  $H(e,e'\pi^+)X$ , by reconstructing the missing mass of the system. Although the  $\Sigma^0$  and  $N^0$  states are not explicitly exotic, the discovery of a narrow state would be a valuable confirmation of the existence of an antidecuplet of states. The experiment used collected data in May and June, 2004, using the HRS spectrometers to detect the scattered electron and the  $K^-$ , and  $K^+$  and  $\pi^+$  respectively. No evidence for any narrow resonances within the candidate regions. The cross section upper limits,  $\sigma_{\max}$ , depend on the exact mass and width of the resonance. In the relevant mass regions and a maximum width of  $\Gamma = 10$  MeV at 90% confidence,  $\sigma_{\max}(\Theta^{++}) < 4.0$  nb/sr,  $\sigma_{\max}(\Sigma^0) < 17.5$  nb/sr and  $\sigma_{\max}(N^0) < 10.0$  nb/sr,<sup>2</sup> with lower limits on  $\sigma_{\max}$  for narrower resonances.

<sup>1</sup>J. P. Chen *et al.*, "High Resolution Study of the 1540 Exotic State," Proposal 04012 to the JLab PAC, P. E. Reimer, and B. Wojtsekhowski, spokespersons, December 2, 2003.

<sup>2</sup>Y. Qiang, Phys. Rev. C (to appear) arXiv: hep-ex/0609025.



## B. HADRONS IN THE NUCLEAR MEDIUM

### b.1. Measurement of the EMC Effect in Very Light Nuclei (J. Arrington, L. El Fassi, K. Hafidi, R. J. Holt, D. H. Potterveld, P. E. Reimer, E. C. Schulte, P. Solvignon, X. Zheng, and the JLab E03-103 Collaboration)

For more than twenty years, it has been known that the quark momentum distribution of nuclei is not simply the sum of the quark distributions of its constituent protons and neutrons. The structure function is suppressed in heavy nuclei at large values of  $x$  (corresponding to large quark momenta), and enhanced at lower  $x$  values. Measurements to date indicate that the overall form of this modification is the same for all nuclei, but the magnitude of the enhancement and suppression is larger for heavier nuclei. Many attempts have been made to explain the EMC effect, but none of the proposed models can fully reproduce the observed modifications, and there is still no consensus on which effect or combination explain the data.

Experiment E03-103<sup>1</sup> ran in Hall C in late 2004 and measured the EMC effect for <sup>3</sup>He, <sup>4</sup>He, and a series of heavier nuclei. Because <sup>4</sup>He has an anomalously large density for a light nucleus, it is the most sensitive test to determine if the EMC effect scales with  $A$  or with nuclear density. More importantly, these measurements of the EMC effect can be compared to exact few body calculations. If the EMC effect is caused by few nucleon interactions, the universal shape observed in heavy nuclei may be a result of a saturation of the effect, and the shape may be different in few-body nuclei. Several calculations<sup>2</sup> predict that the  $x$ -dependence will be significantly different in these few-body nuclei. By making precise measurements in light nuclei, we will be able to distinguish between different models of the EMC effect based on their predictions for few-body nuclei.

Preliminary results are shown in Fig. IV-3. These results suggest that the EMC effect in <sup>4</sup>He is nearly identical to that of <sup>12</sup>C, suggesting that nuclear dependence of the EMC effect scales with density. The <sup>3</sup>He results suggest a larger effect than one would assume based on a density-scaling model. However, the <sup>3</sup>He result has a large isoscalar correction, which is model dependent, especially at large  $Q^2$ . The correction applied to the preliminary results is not from the best extraction of the neutron structure function, but it is consistent with what was used for the heavy nuclei in from previous measurements. By varying the n/p model, we change both the <sup>3</sup>He and heavy nuclei results in opposite ways, and can thus use these data to study the tradeoff between neutron cross section model and  $A$ -dependence of the extracted nuclear effects.

Finally, a measurement of  $A \leq 4$  nuclei will help constrain models of the EMC effect in deuterium. Models of nuclear effects in deuterium and <sup>3</sup>He must be used to extract information on neutron structure, and a high precision measurement including <sup>1</sup>H, <sup>2</sup>H, <sup>3</sup>He, and <sup>4</sup>He will give a single set of data that can be used to evaluate these models in several light nuclei. This will help to quantify the model dependence of the neutron structure functions inferred from measurements on <sup>2</sup>H and <sup>3</sup>He. We are working with members of the Argonne theory group to perform a global comparison of the realistic few-body calculations with existing data on the proton and deuteron, as well as our new results on <sup>3</sup>He and <sup>4</sup>He.

<sup>1</sup>JLab experiment E03-103, "A Precise Measurement of the Nuclear Dependence of the EMC Effect in Light Nuclei", J. Arrington and D. Gaskell, spokespersons.

<sup>2</sup>G. I. Smirnov *et al.*, Eur. Phys. J. C **10**, 239 (1999); V. V. Burov *et al.*, Phys. Lett. **B466**, 1 (1999); I. R. Afnan *et al.*, Phys. Rev. C **68**, 035201 (2003); O. Benhar, private communication.

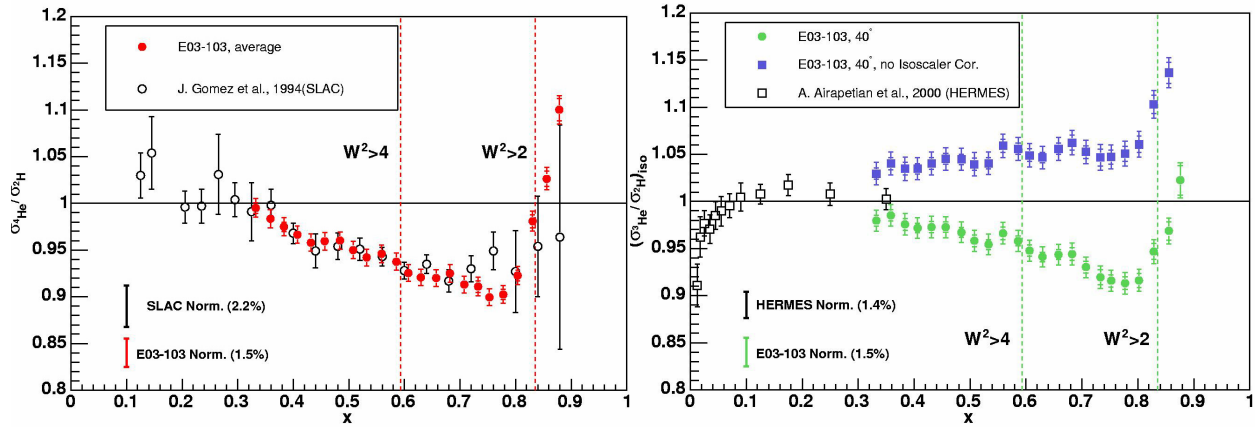


Fig. IV-3. Preliminary EMC ratio for  $^4\text{He}$  and  $^3\text{He}$ . Hollow points are previous data, solid points are the E03-103 preliminary results showing only the statistical uncertainties. For  $^3\text{He}$ , the blue squares are the raw  $^3\text{He}/^2\text{H}$  ratio, while the green circles show the ratio after applying the isoscalar correction due to the excess proton.

## b.2. Search for the Onset of Color Transparency: JLab E02-110 Experiment (K. Hafidi, J. Arrington, L. El Fassi, D. F. Geesaman, R. J. Holt, B. Mustapha, D. H. Potterveld, P. E. Reimer, and the JLab Hall-B Collaboration)

According to QCD, point colorless systems, such as those produced in exclusive processes at high  $Q^2$  have quite small transverse sizes. Therefore, they are expected to travel through nuclear matter experiencing very little attenuation. This phenomenon is known as Color Transparency (CT). An analogous mechanism is well known in QED: the interaction cross section of an electric dipole is proportional to its square size. As a result, the cross section vanishes for objects with very small electric dipole moments. Since color in QCD is equivalent to the charge in QED, the cross section of a color-neutral dipole, as formed by a pair of oppositely colored quarks for instance, is also predicted to vanish for small sized hadrons. Color transparency cannot be explained by Glauber theory and calls upon quark degrees of freedom. Earlier measurements were mainly focused on quasi-elastic hadronic  $(p, 2p)^1$  and leptonic  $(e, e'p)^2$  scattering from nuclear targets. None of these experiments were able to produce evidence for CT up to  $Q^2 \sim 8 \text{ GeV}^2$ . The strongest evidence for CT so far comes from Fermilab experiment E791 on the  $A$ -dependence of coherent diffractive dissociation of 500 GeV/c pions into dijets.<sup>3</sup> A recent measurement performed by the HERMES collaboration using exclusive  $\rho^0$  electroproduction from nitrogen adds further evidence for the existence of CT.<sup>4</sup>

The main goal of E02-110 experiment<sup>5</sup> is to search for

the onset of CT in the incoherent diffractive  $\rho^0$  electro and photoproduction on deuterium, carbon and copper. In this process, the virtual photon fluctuates into  $q\bar{q}$  pair which travels through the nuclear medium evolving from its small initial state with a transverse size proportional to  $1/Q$ , to a "normal size" vector meson detected in the final state. Therefore, by increasing the value of  $Q^2$  one can squeeze the size of the produced  $q\bar{q}$  wave packet. The photon fluctuation can propagate over a distance which is known as the coherence length  $l_c$ . The coherence length can be estimated relying on the uncertainty principle and Lorentz time dilatation as  $l_c = 2v / (Q^2 + M_{q\bar{q}}^2)$ , where  $v$  is the energy of the virtual photon and  $M_{q\bar{q}}$  is the mass of  $q\bar{q}$  pair dominated by the  $\rho^0$  mass in the case of the exclusive  $\rho^0$  electroproduction. What is measured in the reaction is how transparent the nucleus appears to "small size"  $\rho^0$  by taking the ratio of the nuclear per-nucleon ( $\sigma_A/A$ ) to the free nucleon ( $\sigma_N$ ) cross sections, which is called nuclear transparency  $T_A = \sigma_A/A\sigma_N$ . Consequently, the signature of CT is an increase in the nuclear transparency  $T_A$  with increasing hardness ( $Q^2$ ) of the reaction. Recent theoretical calculations by Kopeliovich *et al.*,<sup>6</sup> predicted an increase of more than 40% at  $Q^2 \sim 4 \text{ GeV}^2$ . However, one should be careful about other effects that can imitate this signal. Indeed, measurements by HERMES have shown that  $T_A$  increases when  $l_c$  varies from long to short compared to



the size of the nucleus for moderate  $l_c$  values. This so-called coherence length effect (CL) can mock the signal of CT and should be under control to avoid confusing it with the CT effect. Therefore, the experiment E02-110 intends to measure the  $Q^2$  dependence of the transparency  $T_A$  for small  $l_c$  values where no CL effect is expected.

The experiment was performed using the CEBAF Large Acceptance Spectrometer (CLAS)<sup>7</sup> in Hall B at Jefferson Lab. The data were taken with both 4 and 5 GeV electron beams incident on 2 cm liquid deuterium target and a solid target (0.4 mm thick  $^{56}\text{Fe}$  and 1.72 mm thick  $^{12}\text{C}$ ) simultaneously to reduce

systematic uncertainties. In these measurements we are interested in the scattered electron and the two pions from the  $\rho^0$  decay in the low  $t$  region below  $0.5 \text{ GeV}^2$ . Figure IV-4 shows the normalized invariant mass of the two charged pions for hydrogen, deuterium and iron. A clean  $\rho^0$  peak is obtained for the three targets. The  $Q^2$  dependence of the pion absorption is found to be of the order of 7%. The background contributing to the  $\rho^0$  peak which is mainly coming from  $\Delta^{++}$ ,  $\Delta^0$  and the non resonant background was subtracted using Genova Monte Carlo. The data was also corrected for Radiative corrections using DIFFRAD<sup>8</sup> code. As shown in Fig. IV-5, no CL dependence was found for Fe data. Preliminary results for Fe and C are expected soon.

<sup>1</sup>A. S. Carroll *et al.*, Phys. Rev. Lett. **61**, 1698 (1988); Y. Mardor *et al.*, Phys. Rev. Lett. **81**, 5085 (1998);

A. Leksanov *et al.*, Phys. Rev. Lett. **87**, 212301 (2001).

<sup>2</sup>N. C. R. Makins *et al.*, Phys. Rev. Lett. **72**, 1986 (1994); T. G. O'Neill *et al.*, Phys. Lett. **B351**, 87 (1995);

D. Abbott *et al.*, Phys. Rev. Lett. **80**, 5072 (1998); K. Garrow *et al.*, Phys. Rev. C **66**, 044613 (2002).

<sup>3</sup>E. M. Aitala *et al.*, Phys. Rev. Lett. **86**, 4773 (2001).

<sup>4</sup>A. Airapetian *et al.*, Phys. Rev. Lett. **90**, 052501 (2003).

<sup>5</sup>JLab experiment E02-110, "Q<sup>2</sup> Dependence of Nuclear Transparency for Incoherent  $\rho^0$  Electroproduction," K. Hafidi, B. Mustapha, and M. Holtrop, spokespersons.

<sup>6</sup>B. Kopeliovich *et al.*, Phys. Rev. C **65**, 035201 (2002).

<sup>7</sup>B. Mecking *et al.*, Nucl. Instrum. Methods **A503/3**, 513 (2003).

<sup>8</sup>I. Akushevich, Eur. Phys. J. C **8**, 457 (1999); Website: [www.jlab.org/RC](http://www.jlab.org/RC).

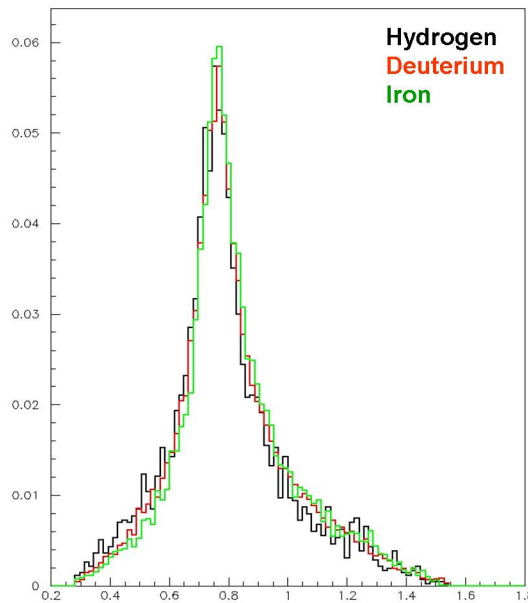


Fig. IV-4. Normalized  $\pi^+\pi^-$  invariant Mass for  $^1\text{H}$ ,  $^2\text{H}$  and  $^{56}\text{Fe}$  targets.

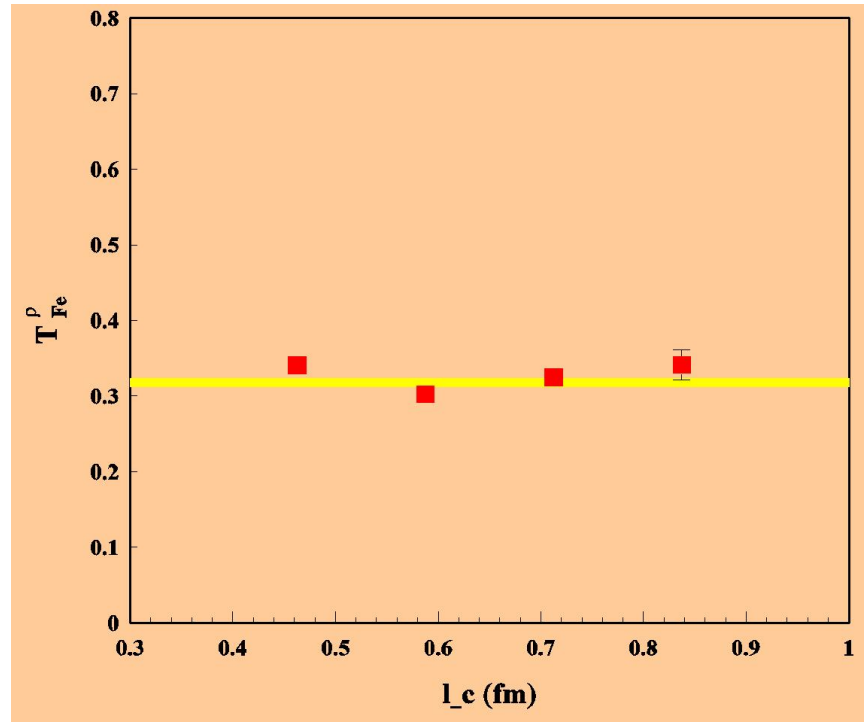


Fig. IV-5. Fe nuclear transparency as a function of  $l_c$  for 5 GeV electron beam.

**b.3. Study of Color Transparency in Exclusive Vector Meson Electroproduction Off Nuclei: JLab E12-06-106 Experiment** (K. Hafidi, J. Arrington, L. El Fassi, D. F. Geesaman, R. J. Holt, B. Mustapha, D. H. Potterveld, P. E. Reimer, and the JLab Hall-B Collaboration)

The nature of hadronic interactions can be investigated *via* tests of the prediction of “color transparency”. Color transparency (CT) is one of few direct manifestations of the underlying color degrees-of-freedom in nuclear physics. Under the right conditions, two quarks, each of which (alone) would have interacted very strongly with nuclear matter, could from an object that passes undisturbed through the nuclear medium. A similar phenomenon occurs in QED, where an  $e^+e^-$  pair of small size has a small cross section determined by its electric dipole moment. In QCD, a  $q\bar{q}$  or  $qqq$  system with a small color dipole moment is predicted to have similar reduced interactions due to the cancellation of the color fields of the quarks. Color transparency can be observed experimentally by measuring a reduced attenuation of particles as they exit a nucleus. These transparency measurements will allow us to study the necessary ingredients: formation of small sized configuration, the reduced color interactions of these configurations, and the evolution of these exotic configurations back into ordinary hadrons.

The E12-06-106 experiment<sup>1</sup> is a natural extension of the E02-110<sup>2</sup> experiment performed within CLAS detector using a 5 GeV electron beam. The E02-06-106 experiment will use 11 GeV electron beam and the CLAS12 detector. Its main goal is to study CT in the incoherent diffractive vector meson electroproduction on deuterium, C, Fe and Sn. In this process, the virtual photon with a four momentum  $Q$ , fluctuates into  $q\bar{q}$  pair which travels through the nuclear medium evolving from its small initial state with a transverse size proportional to  $1/Q$ , to a “normal size” vector meson detected in the final state. Therefore, by increasing the value of  $Q^2$  one can squeeze the size of the produced  $q\bar{q}$  wave packet. JLab 12 GeV upgrade will allow for significant increase in the momentum and energy transfer involved in the reaction. Therefore, one expects to produce smaller configurations that live longer; the optimum parameters for CT studies. Figure IV-6 shows the expected errors bars of the nuclear transparency  $T_A = \sigma_A/A\sigma_N$  for Fe target, extending the previous measurements into the very

important higher  $Q^2$  region up to  $5.5 \text{ GeV}^2$ . The curve is a theoretical calculation by Kopeliovich *et al.*<sup>3</sup> The same accuracy is expected for C and Sn targets.

<sup>1</sup>JLab experiment E12-06-106, "Study of Color Transparency in Exclusive Vector Meson Electroproduction Off Nuclei," K. Hafidi, L. El Fassi, B. Mustapha, and M. Holtrop, spokespersons.

<sup>2</sup>JLab experiment E02-110, " $Q^2$  Dependence of Nuclear Transparency for Incoherent  $\rho^0$  Electroproduction," K. Hafidi, B. Mustapha, and M. Holtrop, spokespersons.

<sup>3</sup>B. Kopeliovich *et al.*, Phys. Rev. C **65**, 035201 (2002).

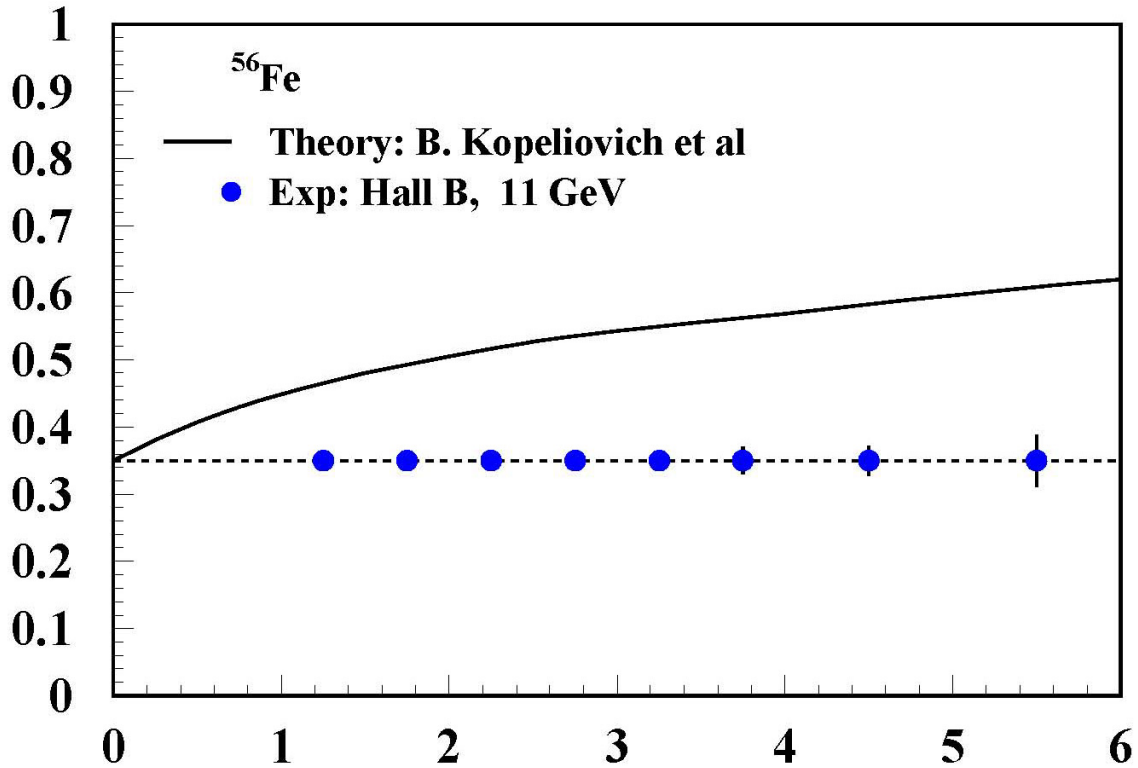


Fig. IV-6. Expected error bars for the Fe nuclear transparency. The solid curve is the model prediction by Kopeliovich *et al.*<sup>3</sup>

#### b.4. Search for Color Transparency in Pion Electroproduction (J. Arrington, L. El Fassi, X. Zheng, and the JLab E01-107 Collaboration)

Argonne also participated in an experiment to search for color transparency in pion electroproduction. Measurements were made for the  $A(e,e'\pi)$  reaction from  $^2\text{H}$ ,  $^{12}\text{C}$ ,  $^{63}\text{Cu}$ , and  $^{197}\text{Au}$  over a range in  $Q^2$ . As with production of vector mesons, color transparency is expected to set at lower  $Q^2$  than in the case of  $A(e,e'p)$  measurements, and there is some hint of color transparency in pion photoproduction for similar pion momenta.<sup>1</sup>

Experiment E01-107 was performed at Jefferson Lab Hall C in late 2004. The experiment measured the

exclusive electroproduction of pions from nuclei by detecting the scattered electron and the knocked out pions in coincidence. The nuclear transparency is extracted by comparing the pion production from heavy nuclei to that from deuterium. The analysis of the data is complete and the results show a  $Q^2$  dependence that is consistent with color transparency. A draft showing the extracted transparency as a function of  $A$  and  $Q^2$  has been completed and is being circulated among the collaboration. A separate paper, detailing the separated structure function and addressing issues related to the pion electroproduction reaction mechanism is also

being circulated.

<sup>1</sup>D. Dutta *et al.*, Phys. Rev. C **68**, 021001 (2003).

**b.5. Dynamics of Hadronization from Nuclear Semi-Inclusive Deep-Inelastic Scattering: JLab E02-104 Experiment** (K. Hafidi, J. Arrington, L. El Fassi, D. F. Geesaman, R. J. Holt, S. Johnston, G. Larsen, B. Mustapha, D. H. Potterveld, P. E. Reimer, and the JLab Hall-B Collaboration)

Hadronization is the mechanism by which the quark, when ejected from a nucleon neutralizes its color to form many hadrons in the final state. The description of hadronization in terms of fragmentation functions is known in the vacuum, but the physical information on its dynamics is still a mystery. The time-space evolution of the hadron formation is unknown due to the fact that it is a non perturbative process and, therefore, is hard to calculate at the most fundamental level. Unfortunately, Lattice QCD calculations are not yet helpful in this matter. To access this dynamic, the nucleus will play the role of the detector since the

production length is comparable with the nuclear size. The nuclear environment provides a unique opportunity to look at the early stage of hadronization a few Fermi from the origin. Therefore, by studying the properties of leading particles emerging from deep inelastic scattering (DIS) on a range of nuclei, important information on the characteristic time distance-scales of hadronization can be determined as a function of several variables.

A primary experimental observable is the hadronic multiplicity ratio:

$$R_M^h(z, \nu, p_T^2, Q^2) = \left\{ \frac{N_h^{DIS}(z, \nu, p_T^2, Q^2)}{N_e^{DIS}(\nu, Q^2)} \right\}_A / \left\{ \frac{N_h^{DIS}(z, \nu, p_T^2, Q^2)}{N_e^{DIS}(\nu, Q^2)} \right\}_D$$

$N_h^{DIS}$  and  $N_e^{DIS}$  denote the number of hadrons and electrons measured in DIS kinematics,  $\nu$  is the virtual photon energy,  $z = E_h/\nu$  is the fraction of the photon energy carried by the hadron,  $Q^2$  is the four-momentum transfer, and  $p_T$  is the transverse momentum of the hadron relative to the virtual photon direction. The second experimental quantity is called the transverse momentum broadening  $\langle \Delta p_T^2 \rangle = \langle p_T^2 \rangle_A - \langle p_T^2 \rangle_D$ , where  $\langle p_T^2 \rangle$  is the  $p_T^2$  averaged. The dependence of the multiplicity ratio on several kinematical variables offers a wealth of information on quark propagation in

the nuclear medium and hadron formation. Studying the transition from high to low  $\nu$  dependence is correlated with the transition from quark propagation to hadron propagation in nuclei while the  $z$  dependence controls the broadening effects. In addition, the transverse momentum broadening provides valuable information on the parton energy loss which is believed to play an important role in predicting signatures of the quark gluon plasma at RHIC<sup>1</sup> through the phenomenon of jet quenching.<sup>2</sup>

<sup>1</sup>J. Adams *et al.*, (STAR collaboration), Phys. Lett. **B616**, 8 (2005).

<sup>2</sup>Xin-Nian Wang, Phys. Lett. **B579**, 299 (2004).

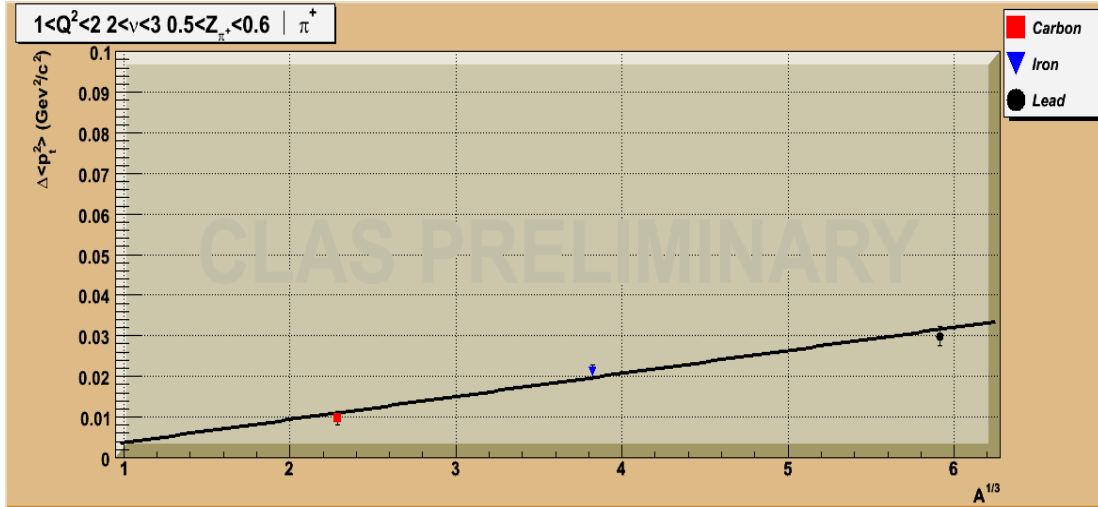


Fig. IV-7. Preliminary  $\pi^+$  data from CLAS EG2 run for  $\Delta p_T^2$  vs.  $A^{1/3}$  for carbon, iron and lead for one bin in  $Q^2$ ,  $z$ , and  $v$ . The line is a linear fit.

Jefferson Lab offers unique capabilities to study hadron production in DIS. Measurements with the CEBAF Large Acceptance Spectrometer (CLAS) provide data on the widest possible range of nuclear target masses at high luminosity. Data at 5 GeV were taken in 2003 with  $10^{34}$  cm<sup>-2</sup>s<sup>-1</sup> luminosity using two targets simultaneously on (the liquid deuterium target and one solid target; alternating between C, Fe and Pb) to reduce systematic errors in the multiplicity ratio. Figure IV-7 shows preliminary  $\pi^+$  data from the CLAS EG2 experiment at 5.0 GeV. These data are for  $z$  from 0.5 to 0.6,  $Q^2$  from 1 to 2 GeV<sup>2</sup> and  $v$  from 2 to 3 GeV. The plot shows a linear behavior of the transverse momentum broadening as a function of the nuclear

radius within the statistical uncertainties. These are the first direct and precise measurements of  $p_T$  broadening on several nuclei, confirming that the quark energy loss has a quadratic dependence on the quark path length in the nuclear medium in this kinematical regime. This is consistent with the non Abelian analog of the LPM effect in QED.<sup>1</sup> An example of preliminary hadronic multiplicity ratio results is given in Fig. IV-8. The plot is for  $Q^2$  from 1 to 1.25 GeV<sup>2</sup> and  $v$  from 2.2 to 3 GeV for C, Fe and Pb. The high statistics collected in this experiment allow measuring the multiplicity ratio with significantly smaller uncertainties than HERMES experiment.<sup>2</sup>

<sup>1</sup>B. Z. Kopeliovich, J. Nemchik, E. Predazzi, and A. Hayashigaki, Nucl. Phys. **A740**, 212 (2004).

<sup>2</sup>A. Airapetian *et al.*, (HERMES Collaboration), Eur. Phys. J. C **20**, 479 (2001).

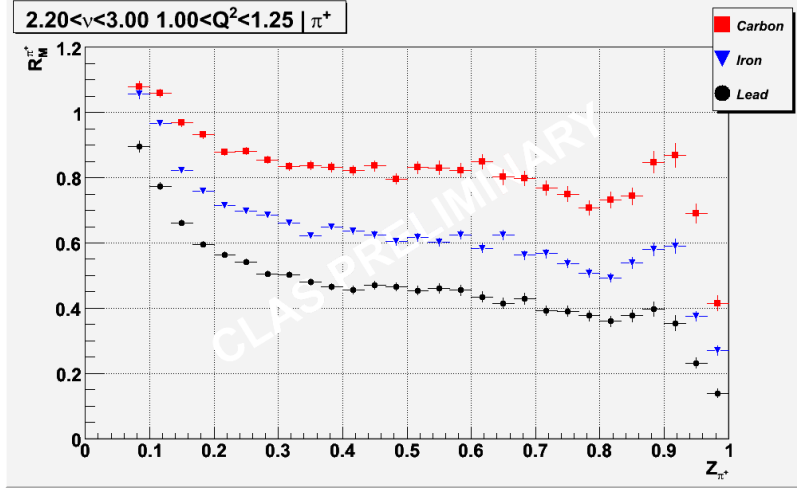


Fig. IV-8. Preliminary data from the CLAS EG2 run for the hadronic multiplicity ratio  $R_M^{\pi^+}$  for positive pions in carbon (top), iron, and lead (bottom).

### b.6. Quark Propagation and Hadron Formation: JLab E12-06-117 Experiment

(K. Hafidi, J. Arrington, L. El Fassi, D. F. Geesaman, R. J. Holt, S. Johnston, G. Larsen, B. Mustapha, D. H. Potterveld, P. E. Reimer and the JLab Hall-B Collaboration)

The properties of isolated quarks are generally experimentally inaccessible due to quark confinement in hadrons. In hard interactions, such as in deep inelastic scattering, the struck quark in a nucleon must separate from the rest of the residual system. When this separation distance is comparable to nuclear radii, it is possible to study the properties of the propagating quark by varying the radii of nuclear targets and observing modifications of the final hadronic states. The time interval (called the formation time) over which the struck quark transforms into a new hadron can be characterized as a function of multiple variables. This provides completely new information on how the

color field of the hadron is restored in real time through the fundamental process of gluon emission. If the formation time is much smaller than the nuclear transit time, then the hadron that carries the struck quark will strongly interact with the nuclear medium. If on the other hand, the formation time is much longer than the nuclear transit time, then the formed hadron will not interact with the nuclear medium. In this way, hadron absorption by nuclei can be used to estimate the time scales of the hadron of the hadronization process. The observable that is used to quantify this absorption is the hadronic multiplicity ratio:

$$R_M^h(z, \nu, p_T^2, Q^2) = \left\{ \frac{N_h^{DIS}(z, \nu, p_T^2, Q^2)}{N_e^{DIS}(\nu, Q^2)} \right\}_A \bigg/ \left\{ \frac{N_h^{DIS}(z, \nu, p_T^2, Q^2)}{N_e^{DIS}(\nu, Q^2)} \right\}_D$$

$N_h^{DIS}$  and  $N_e^{DIS}$  denote the number of hadrons and electrons measured in DIS kinematics,  $\nu$  is the virtual photon energy,  $z = E_h/\nu$  is the fraction of the photon energy carried by the hadron,  $Q^2$  is the four-momentum transfer, and  $p_T$  is the transverse momentum of the hadron relative to the virtual photon direction. The second experimental quantity is called the transverse momentum broadening  $\langle \Delta p_T^2 \rangle = \langle p_T^2 \rangle_A - \langle p_T^2 \rangle_D$ , where  $\langle p_T^2 \rangle$  is the  $p_T^2$  averaged. The dependence of the multiplicity ratio on several kinematical variables offers a wealth of information on quark propagation in

the nuclear medium and hadron formation. Studying the transition from high to low  $\nu$  dependence is correlated with the transition from quark propagation to hadron propagation in nuclei while the  $z$  dependence controls the broadening effects. In addition, the transverse momentum broadening provides valuable information on the parton energy loss which is believed to play an important role in predicting signatures of the quark gluon plasma at RHIC<sup>1</sup> through the phenomenon of jet quenching.<sup>2</sup>

The E12-06-117 experiment presents a broad program to determine the mechanism of confinement in forming systems. It will use 11 GeV electron beam and CLAS12 detector. From these measurements, the quark production time will be determined and hadron formation times will be extracted for a series of 15 hadrons.

These measurements will provide two to three orders of magnitude more data than any previous measurement in this energy range, and will include a much larger collection of hadron species. The availability of

11 GeV beam in combination with the high rate capability of CLAS12 allows access to the ranges in  $\nu$ ,  $Q^2$  and  $p_T$ , that are crucially needed to determine the production time and to isolate the correct physical picture. These data will enable the multi-dimensional analysis that is crucial for discriminating between the competing models for these observables. By producing a high-statistics (see Fig. IV-9), multi-dimensional analysis, the models with the correct physical picture can be validated and significant new information on the mechanism of QCD confinement in forming systems will be obtained.

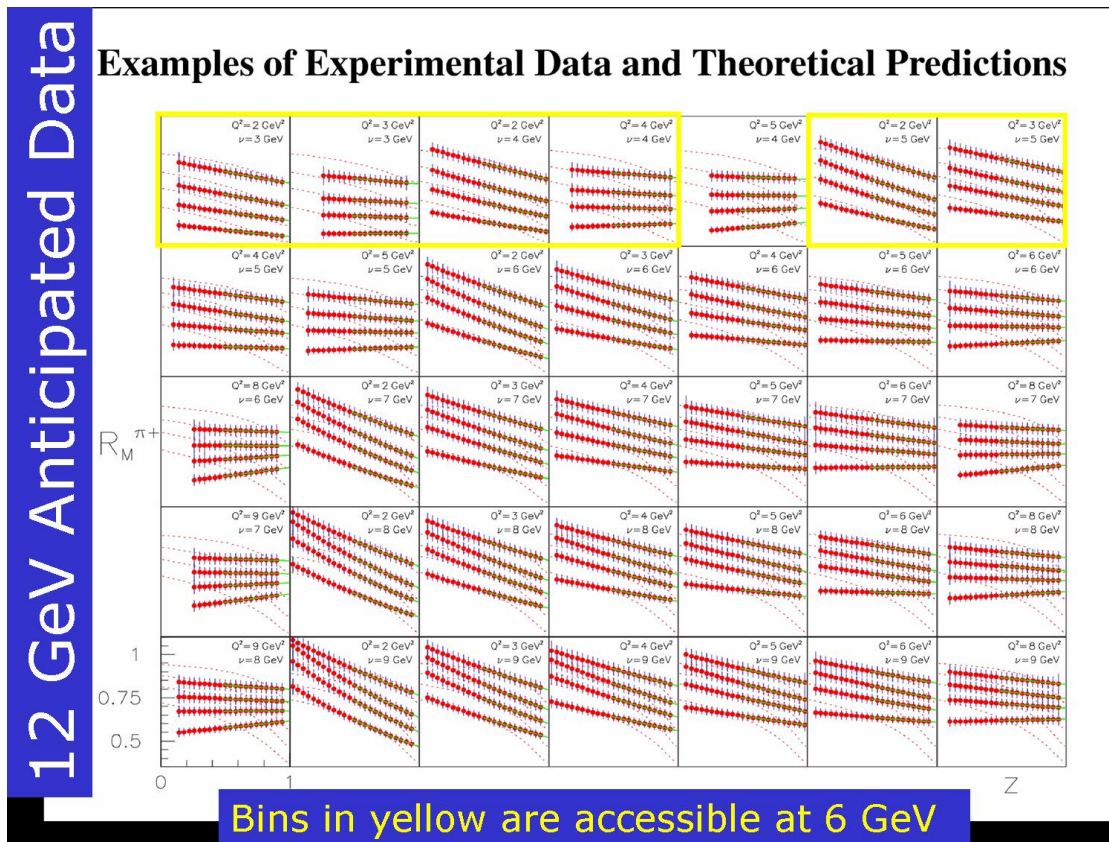


Fig. IV-9.  $Z$  dependence of the hadronic multiplicity ratio for (top to bottom in each plot)  $^{14}\text{N}$ ,  $^{40}\text{Ar}$ ,  $^{84}\text{Kr}$ ,  $^{197}\text{Au}$  for 35 bins in  $\nu$  and  $Q^2$ . The solid line is a gluon bremsstrahlung model<sup>3</sup> calculation for  $z > 0.5$  for pions. The dotted line shows the parameterization based on HERMES 27 GeV data,<sup>4</sup> which is independent of  $Q^2$ .

<sup>1</sup>J. Adams *et al.*, (STAR Collaboration), Phys. Lett. **B616**, 8 (2005).

<sup>2</sup>Xin-Nian Wang, Phys. Lett. **B579**, 299 (2004).

<sup>3</sup>B. Z. Kopeliovich, J. Nemchik, E. Predazzi, and A. Hayashigaki, Nucl. Phys. **A740**, 212 (2004).

<sup>4</sup>A. Airapetian *et al.*, (HERMES Collaboration), Eur. Phys. J C **20**, 479 (2001).

**b.7. Measurement of High Momentum Nucleons in Nuclei** (J. Arrington, L. El Fassi, K. Hafidi, R. J. Holt, D. H. Potterveld, P. E. Reimer, E. C. Schulte, P. Solvignon, X. Zheng, and the JLab E02-019 Collaboration)

Inclusive scattering from nuclei at low energy transfer (corresponding to  $x > 1$ ) is dominated by quasielastic scattering from nucleons in the nucleus. As the energy transfer decreases, the scattering probes nucleons of increasing momentum allowing us to map out the distribution of high momentum nucleons. Because the high momentum nucleons are dominantly generated by short-range correlations (SRCs), these data allow us to examine the strength of two-nucleon and multi-nucleon correlations in heavy nuclei.

Experiment E02-019<sup>1</sup> ran in late 2004 and measured inclusive scattering at large  $Q^2$  over a broad range in  $x$ . The high  $Q^2$  values in this experiment should simplify the extraction of the high momentum components, as effects such as final state interactions are reduced at large  $Q^2$ . The measurement focused on  $^2\text{H}$ ,  $^3\text{He}$ , and  $^4\text{He}$ , but data were also taken on several heavier nuclei. Measurements with few-body nuclei allow contact with theoretical calculations via essentially "exact" calculations for few-body systems. Data on heavy nuclei can then be used to constrain the high momentum components of their spectral functions, as well as allowing an extrapolation to infinite nuclear matter.

We are working with Fritz Coester and T.-S. Harry Lee from the Theory Group to extract information on the

neutron structure and nuclear effects on few-body nuclei. With a realistic calculation of the deuteron, a comparison of proton and deuteron results from this and previous high- $Q^2$  measurements allows one to extract the ratio of neutron to proton cross sections. One can then take this extracted neutron structure function and calculate the  $^3\text{He}$  and  $^4\text{He}$  structure functions, both at  $x > 1$ , which is sensitive to the spectral function used, and for  $x < 1$ , which tests the nuclear effects in the calculation.

Direct comparisons<sup>2</sup> of heavy nuclei to deuterium at large  $x$  will allow us to map out the strength of two-nucleon correlations in both light and heavy nuclei. Just as the ratio of heavy nuclei to deuterium at  $x \gtrsim 1.5$  shows that the distribution in heavy nuclei is dominated by two-nucleon correlations, similar ratios of heavy nuclei to  $^3\text{He}$  at  $x \gtrsim 2.5$  provide a measure of the strength of three-nucleon correlations.

Beyond probing nucleon distributions and short-range correlations, these data fill in a significant void in our knowledge of nuclear structure functions. Data at large  $x$  are important in the study of scaling and duality in nuclei.<sup>3</sup> In addition, the structure function at  $x > 1$  must be included in studies of the energy-momentum sum rule and analysis of the QCD moments.<sup>4</sup>

<sup>1</sup>JLab experiment E02-019, "Inclusive Scattering from Nuclei at  $x > 1$  and High  $Q^2$  with a 6 GeV Beam,"

J. Arrington, D. B. Day, A. F. Lung, and B. W. Filippone, spokespersons.

<sup>2</sup>J. Arrington, D. B. Day, D. Higinbotham, and P. Solvignon, "Precision Measurements of Scattering from Three-Nucleon Short Range Correlations in Hall A at  $1.6 < Q^2 < 1.9 \text{ GeV}^2$ ".

<sup>3</sup>J. Arrington, R. Ent, C. E. Keppel, J. Mammei, and I. Niculescu, Phys. Rev. C **73**, 035205 (2006).

<sup>4</sup>I. Niculescu, J. Arrington, R. Ent, and C. E. Keppel, Phys. Rev. C **73**, 045206 (2006).

**b.8. Short Range Correlations in Nuclei** (J. Arrington, P. Solvignon, and the JLab E01-015 Collaboration)

While inclusive measurements at large  $x$  are sensitive to short range correlations in nuclei, previous measurements have been limited. The first extracted ratios from SLAC<sup>1</sup> required combining data from deuterium and nuclear targets from different experiments, requiring interpolation of the cross sections, and increasing the systematic uncertainties compared to direct ratio measurements. Measurements using CLAS<sup>2,3</sup> at Jefferson Lab were able to improve on

this, but were only able to take ratios to  $^3\text{He}$ , and were limited to relatively low  $Q^2$  values. This was the first precision extraction for the ratio in the three-nucleon correlation region, but the  $Q^2$  value was relatively low, and there was no way to determine if these data are in the scaling region.

While E02-019 measured these ratios at higher  $Q^2$  with both deuterium and  $^3\text{He}$  targets, the data for the highest



$x$  values was somewhat limited. For this experiment, we used short (4 cm) He targets, and the subtraction of the contribution from the Al endcaps becomes very large as one approaches  $x = 3$ , the kinematic endpoint for scattering from  ${}^3\text{He}$ . To improve on this, we submitted an informal proposal<sup>4</sup> for a short measurement in Hall A, designed to run with two to three days of beamtime during the present or upcoming running using the 20 cm  ${}^3\text{He}$  targets in Hall A. By reducing the relative contribution from the endcaps and moving to slightly lower  $Q^2$ , we should be able to obtain high precision ratios in a minimal amount of time. The experiment was tentatively scheduled to run during the summer of 2007, but delays in the schedule mean that we will most likely have to wait until running later in the year.

While inclusive scattering provides the greatest sensitivity and kinematic range for such measurements,

coincidence measurements can provide more detailed information about the structure of the correlations. Another measurements in Hall A at Jefferson Lab used two-nucleon knockout measurements,  $A(e,e'pN)$ , to study the isospin-dependence of the correlations. Initial results for the two-proton knockout channel have been analyzed and submitted.<sup>5</sup> Preliminary results for the comparison of pn to pp channels suggests that the correlations in this kinematic region are strongly dominated by pn correlations, which are a factor of five or more larger than pp SRCs. This was explained in terms of the tensor structure of the two-nucleon interaction.<sup>6</sup> Using the Argonne theory group's variation Monte Carlo calculation for the structure of few-body nuclei, it was shown that for the region of nucleon momentum probed in the experiment, 300-600 MeV/c, the SRCs are dominated by  $n$ - $p$  pairs, due to the tensor force which is important for the  $n$ - $p$  pairs, which largely in deuteron-like states.

<sup>1</sup>L. L. Frankfurt, M. I. Strikman, D. B. Day, and M. Sargsian, Phys. Rev. C **48**, 2451 (1993).

<sup>2</sup>K. Egiyan *et al.*, Phys. Rev. C **68**, 014313 (2003).

<sup>3</sup>K. Egiyan *et al.*, Phys. Rev. Lett. **96**, 082501 (2006).

<sup>4</sup>J. Arrington, D. B. Day, D. Higinbotham, and P. Solvignon, "Precision Measurements of Scattering from Three-Nucleon Short Range Correlations in Hall A at  $1.6 < Q^2 < 1.9 \text{ GeV}^2$ ".

<sup>5</sup>R. Shneor *et al.*, nucl-ex/0703023 (2007), submitted to Phys. Rev. Lett.

<sup>6</sup>R. Schiavilla *et al.*, Phys. Rev. Lett. **98**, 132501 (2007).

### **b.9. Mapping Out the Distribution of Super-Fast Quarks in Nuclei** (J. Arrington, K. Hafidi, R. Holt, P. Reimer, P. Solvignon, and the JLab E12-06-105 Collaboration)

While previous measurements of inclusive scattering at  $x > 1$  at energies up to 6 GeV allow us to study high momentum nucleons and short range correlations, higher energy measurements will allow us to study extremely high momentum quarks, which allow us to study non-hadronic degrees of freedom in nuclei, and look for signs of modification of the internal structure of the nucleons at high density.

A 12 GeV proposal<sup>1</sup> was submitted and approved to PAC30, to extend inclusive measurements at  $x > 1$  to higher energy. At these energies, the scattering is no longer dominated by quasielastic scattering from individual nucleons, but by scattering from super-fast quarks. The highest momentum quarks come from the high- $x$  quarks in the highest momentum nucleons. These high momentum nucleons are generated by short range  $N$ - $N$  interactions and in conventional models, the strength above  $x = 1.2$  is very small and falls off extremely rapidly. However if there is significant interaction between the quarks in these highly

overlapping nucleons, it is much easier for the quarks in the nucleons to share momentum, and the distribution of these super-fast quarks increases dramatically. This is an extremely sensitive way to look for nuclear effects at high density that involve a breakdown of the individual nucleons' identities.

Such modification of the nucleon internal structure has been suggested as a possible explanation (or at least contribution) to the EMC effect. An example of this is the suggestion that a pair of overlapping nucleons spend some fraction of the time in a 6-quark bag, rather than remaining as two separated objects whose internal degrees of freedom (quarks) do not interact. Figure IV-10 shows the calculated structure function for a deuteron assuming that the structure function is simply the convolution of the proton and neutron structure functions (dashed red line), and assuming that there is a 5% contribution from a 6-quark bag state (solid blue line). In the region of the EMC effect,  $0.3 < x < 0.9$ , the inclusion of the 6q bag contribution

modifies the structure function by at most a few percent (left panel). However, for  $x > 1$ , the admixture of a 6q bag contribution increases the structure function by an order of magnitude or more (right panel). This behavior is not sensitive only to the presence of a 6-quark component. Any new mechanism by which quarks in the nucleons can directly exchange momentum when the nucleons have significant overlap will yield a significant excess in the distribution of quarks at  $x > 1$ .

The solid blue points in the right had plot show projected measurements and uncertainties (on the scale of the size of the points) for the 12 GeV measurement. The data will not be entirely in the DIS regime, but we expect to be sensitive to the quark distributions up to  $x = 1.2-1.3$  or higher, more than enough to see a significant signal from such non-hadronic components to the nuclear wavefunction.

<sup>1</sup>JLab experiment E12-06-105, "Inclusive Scattering from Nuclei at  $x > 1$  in the Quasielastic and Deeply Inelastic Regimes," J. Arrington and D. B. Day, spokespersons.

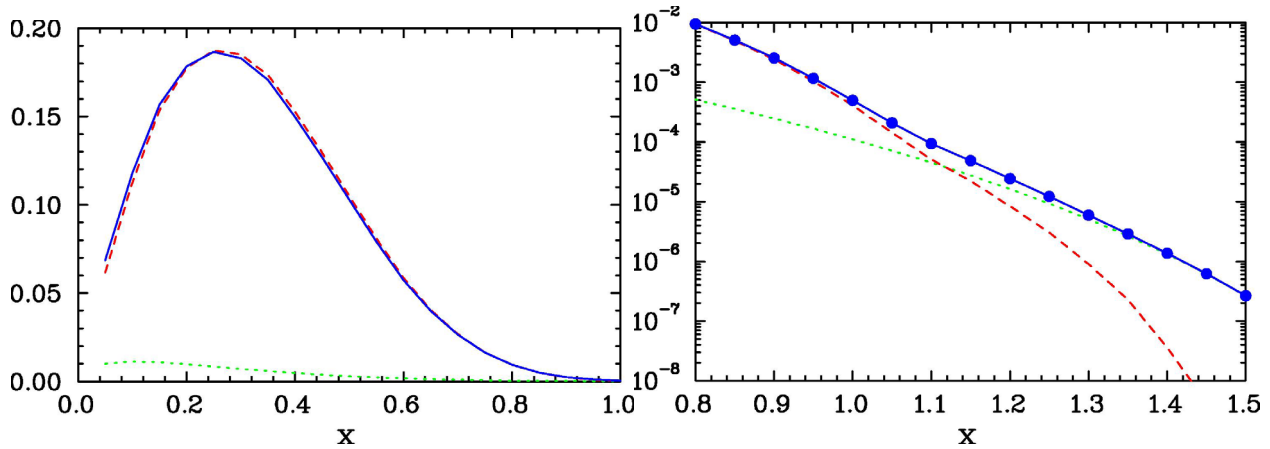


*Fig. IV-10. Structure function for deuterium calculated as a convolution of the proton and neutron quark distributions (dashed red line), and with the inclusion of a 5% contribution from a 6-quark bag configuration (solid blue line). The calculated structure function is only for the valence quarks. The dashed green line shows the contribution of the 6-quark bag.*

## C. QUARK STRUCTURE OF MATTER

### c.1. Studies of Nucleon Spin Structure and Related Measurements of Deep-Inelastic Scattering at HERA (H. E. Jackson, A. El Alaoui, K. G. Bailey, T. P. O'Connor, P. E. Reimer, Y. Sanjiev, and the HERMES Collaboration)

With the termination of operations at the HERA accelerator on July 1, 2007, the HERMES experiment will end over a decade of experimental measurements directed at probing the partonic structure of the proton. HERMES, HERA measurement of spin, is an international collaboration of 30 institutions which was formed to address a basic question of hadron structure. How do the spins of its constituent quarks combine with the spin of the glue and the angular momentum of the partons to give the proton its spin of  $1/2$ ? The HERMES experiment uses polarized internal targets in the HERA 30 GeV  $e^+e^-$  storage ring at the DESY Laboratory. Although semi-inclusive deep-inelastic scattering (DIS) in which an identified hadron is observed in coincidence with the scattered lepton is emphasized, the program includes measurements of polarized inclusive cross sections which have established a new standard of precision, as well as studies of parton propagation in nuclear matter using data accumulated with unpolarized DIS. The HERMES program has and continues to produce a rich spectrum of new results on the partonic structure of hadrons.

A major milestone in the HERMES program was the completion of a quark-flavor decomposition of the spin of the proton based on measurements of semi-inclusive double spin asymmetries<sup>1</sup> which avoids the need for use of data from hyperon decay and the assumption of SU(3) symmetry. The data provided the first separate determinations of the polarizations of the up, down, and strange quarks. They show that the largest contribution to the nucleon spin comes from the valence region, while contrary to previous indications, the polarizations of the sea quarks are all consistent with zero. To probe the properties of the quark sea in more detail, a novel technique has been developed to measure directly the polarization of the strange quark sea using inclusive and semi-inclusive charged kaons asymmetries for a deuteron target. To increase the sensitivity and precision of the flavor decomposition, HERMES is expanding the database in this analysis to include neutral pions and kaons. A final full flavor decomposition of expanded scope including all HERMES measurements is planned. During the final running period in 2006-2007 HERMES is exploring the possibilities of probing the parton angular momenta by

measuring spin asymmetries in hard exclusive reactions which leave the target nucleon intact.

The intense interest in these exclusive processes stems from their description in terms of Generalized Parton Distributions (GPDs) which are expected to provide access to the quark total angular momentum content of the nucleon. HERMES already has studied several exclusive reactions, including exclusive production of charged and neutral pions, and of  $\rho$  mesons. Recent measurements of deeply virtual Compton scattering (DVCS) include the first measurements of a beam-charge asymmetry. However, these measurements have been limited by the relatively poor missing mass resolution for real photons which is dominated by the resolution of the HERMES calorimeter. To improve the exclusivity of the events the collaboration decided to install a recoil detector around the storage cell target used in the HERA ring. Construction and installation of the detector was completed in 2006. The commissioning was completed in early 2007, and the remaining beam time until final shutdown is devoted to exploitation of this instrument. It will provide an order of magnitude improvement in resolution, in addition to higher acceptance and background rejection. Exploitation of this new capability is the highest priority for the beam time which remains. The enhanced selectivity of these measurements will provide a unique opportunity to assess the promise of GPDs as the next step in understanding the spin structure of the nucleon.

A major effort continues to study the third structure function, transversity, required to describe nucleon spin structure in leading order. Because it is odd under chirality transformations, it can only be probed by processes involving additional chiral-odd structure, such as chiral-odd fragmentation in semi-inclusive DIS. Data taken during HERA Run II with a transversely polarized target provide access to transversity and probe other effects of transverse motion of the quarks including measurement of the Sivers function which describes distribution of unpolarized quarks as a function of their transverse momentum distribution. This function must vanish in the absence of quark orbital angular momentum. The new data set which

includes results for neutral pions and charged kaons is of much greater statistical precision than that which was the basis for the first observation<sup>2</sup> of the Collins and Sivers asymmetries reported by HERMES.

A unique opportunity to explore a number of topics in unpolarized DIS is provided by dedicated running exclusively for HERMES during the last hour of each fill of the HERA  $e^+/e^-$  storage ring. Because the target density is limited during this period only a beam lifetime much shorter than normal, measurements can be made with very high luminosities. Studies of quark propagation in nuclear matter including measurements of the ratio of multiplicities for selected hadron types in heavy targets to those in deuterium continue. Data on the multiplicities measured for proton and deuteron

targets currently under analysis provide accurate measurements of quark fragmentation functions specifically at HERMES kinematics, and test factorization. Charged-pion production in semi-inclusive DIS(SIDIS) on hydrogen and deuterium targets has been used to extract the ratio of u valence to d valence quarks in the proton. Hard exclusive electroproduction of charged pions have been measured and their production cross sections compared with predictions of models generated by generalized parton distributions.

The HERA accelerator will continue operations through July 1, 2007. Every effort is being made to maximize the impact of the beam time that remains. Highlights of recent results are presented below.

<sup>1</sup>A. Airapetian *et al.*, Phys. Rev. D **71**, 012003 (2005).

<sup>2</sup>A. Airapetian *et al.*, Phys. Rev. Lett. **94**, 012002 (2005).

### c.1.1. Commissioning and Operation of the HERMES Recoil Detector (H. E. Jackson, A. El Alaoui, K. G. Bailey, T. P. O'Connor, P. E. Reimer, Y. Sanjiev, and the HERMES Collaboration)

The partonic structure of the nucleon has been traditionally described in terms of Parton Distribution Functions (PDFs) of the parton's momentum as a function of the nucleon's "infinite momentum". In the context of the rapid theoretical developments of the last decade, PDFs have been subsumed within Generalized Parton Distributions (GPDs) which relate directly to exclusive processes that involve at least one additional vertex, yet leave the target nucleon intact. PDFs and nucleon elastic form factors appear as kinematic limits and moments of GPDs, respectively. Strong interest in the formalism of GPDs and their experimental constraint emerged when GPDs were found to possess properties related to the total (including orbital) angular momentum carried by the quarks in the nucleon. Exclusive deep virtual Compton scattering (DVCS) is the simplest example of a reaction which is described by GPDs. Certain measurable asymmetries attributed to the interference between DVCS and Bethe Heitler processes provide constraints on GPDs. HERMES has already measured transverse-target-spin azimuthal asymmetries for the first time. By comparing the results with model calculations using GPDs it has been possible to place model-dependent constraints on the total angular momentum carried by the quarks.

However, the energy resolution for the electrons/positrons and the photons of the existing HERMES spectrometer is not sufficient to isolate a clean sample of the exclusive process, and the spectrometer has no acceptance for the detection of the recoil particles at large angles. To alleviate these limitations, a recoil detector has been designed to upgrade the spectrometer to study specifically exclusive DVCS. Its objectives are positive identification of recoiling protons, measurement of the momenta of these particles to improve the resolution of the transverse momentum, and improved rejection of non-exclusive background events. The detector is shown in Fig. IV-11. It consists of three components: a silicon detector surrounding the target cell inside the beam vacuum, a scintillating fiber tracker and a photon detector with three layers of tungsten and scintillator bars in three different orientations. All three detectors are located inside a solenoidal magnet which provides a 1 T longitudinal magnetic field to trap beam generated low energy electrons. The detector was installed and commissioned in 2006 and has been in routine operation since September of 2006. Data taking will continue until the HERA shutdown on July 1, 2007.

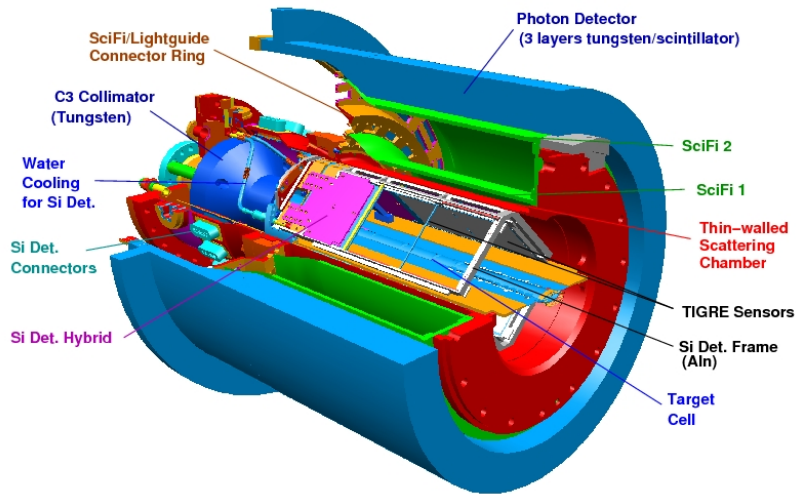


Fig. IV-11. Schematic overview of the HERMES Recoil Detector.

### c.1.2. Strange Quark Parton Distributions in the Proton from Semi-Inclusive Deep-Inelastic Scattering on the Deuteron (H. E. Jackson, A. El Alaoui, K. G. Bailey, T. P. O'Connor, P. E. Reimer, Y. Sanjiev, and the HERMES Collaboration)

The internal structure of the nucleon is embodied in parton distributions of its constituent quarks and gluons. The spin-averaged parton distribution functions (PDFs)  $q(x)$  of quarks and antiquarks of flavors  $q = (u, d, s)$  describe the parton momentum distributions, where  $x$  is the dimensionless Bjorken scaling variable representing the momentum fraction of the target carried by the parton in the frame where the target has "infinite" momentum. They are sums of the number densities of the partons,  $q(x) = q^+(x) [q^-(x)]$ , with their spins in the same [opposite] direction as the nucleon. The differences, or helicity distributions,  $\Delta q(x) = q^+(x) - q^-(x)$  describe the flavor dependent contributions of the constituent partons to the spin of the nucleon. The features of the parton distributions reflect the QCD dynamics of the constituents at the confinement scale. Strange quarks are of special interest as purely sea objects which reflect directly properties of the nucleon sea.

In the absence of significant experimental constraints, current global QCD analyses of PDFs assume the strange quark and antiquark momentum distributions  $s(x)$  and  $\bar{s}(x)$  to be given by  $s(x) = \bar{s}(x) = r[\bar{u}(x) + \bar{d}(x)]/2$  with  $r \approx 1$  at some low factorization scale. Much of the information on the helicity distributions of strange quarks is based on analysis of inclusive deeply inelastic scattering (DIS) and hyperon decay under the assumption of SU(3) symmetry among the structures of the octet baryons. In these inclusive experiments the

first moment of the helicity distribution for strange quark was one of the principal results. The strange quark sea was observed to have a substantial negative polarization. The violation of the Ellis-Jaffe sum rule, a characteristic feature of the inclusive experiments was attributed to this negative polarization. In contrast to the inclusive measurements, recent data from semi-inclusive DIS at HERMES<sup>1</sup> suggest that the strange sea is unpolarized. A full 5 flavor decomposition using data from proton and deuteron targets, although not sensitive to the  $\Delta \bar{s}(x)$ , yielded  $\Delta s = 0.028 \pm 0.033 \pm 0.009$  for the first moment of the strange quark helicity density. A separate extraction from DIS data on the deuteron alone gave  $\Delta s + \Delta \bar{s} = 0.129 \pm 0.042 \pm 0.129$  where the large systematic error reflected lack of knowledge of kaon fragmentation functions.

HERMES is carrying out a new isoscalar extraction of both  $s(x) + \bar{s}(x)$  and  $\Delta s(x) + \Delta \bar{s}(x)$  which is based on data obtained from polarized DIS on a deuterium target. Because strange quarks carry no isospin the strange seas in the proton and the neutron are identical. In the deuteron, an isoscalar target, the fragmentation process in DIS can be described without any assumptions regarding isospin dependent fragmentation. Aside from isospin symmetry between the proton and the neutron, the only symmetry assumed is charge-conjugation invariance in fragmentation. The data for the analysis were recorded with a longitudinally nuclear-polarized deuteron gas target internal to the E = 27.6 GeV HERA

positron storage ring. Scattered beam leptons and coincident hadrons are detected by the HERMES spectrometer. Leptons are identified with an efficiency exceeding 98% and a hadron contamination of less than 1% using an electromagnetic calorimeter, a transition-radiation detector, a preshower scintillation counter and a Cerenkov detector. Charged kaons are identified using a dual-radiator ring-imaging Cerenkov detector. Events were selected subject to the kinematic requirements  $Q^2 > 1 \text{ GeV}^2$ ,  $W^2 > 10 \text{ GeV}^2$  and  $y < 0.85$ , where  $W$  is the invariant mass of the photon-nucleon system, and  $y = \nu/E$ . Coincident hadrons were accepted if  $0.2 < z < 0.8$  and  $x_F \approx 2p_L/W > 0.1$ , where  $p_L$  is the longitudinal momentum of the hadron with respect to

the virtual photon direction in the photon-nucleon center of mass frame.

Analysis of the data is nearly complete. Inclusive and semi-inclusive-charged-kaon spin asymmetries have been analyzed to extract the LO parton distributions of the strange sea in the proton. The partial moment of the non strange fragmentation function needed for the LO analysis has been extracted directly from the same data. The momentum densities are softer than previously assumed. The helicity densities are consistent with zero and the moment octet axial combination is observed to be substantially less than the axial charge extracted from hyperon decays under the assumption of SU(3) symmetry.

<sup>1</sup>A. Airapetian *et al.*, Phys. Rev. D **71**, 012003 (2005).

### c.1.3. Inclusive Longitudinal Spin Asymmetries for the Proton and Deuteron

(H. E. Jackson, A. El Alaoui, K. G. Bailey, T. P. O'Connor, P. E. Reimer, Y. Sanjiev, and the HERMES Collaboration)

Using inclusive longitudinal spin asymmetries HERMES has measured the spin structure function  $g_1(x, Q^2)$  of the proton and the deuteron in the kinematic range  $0.0041 < x < 0.90$  and  $0.18 \text{ GeV}^2 < Q^2 < 20 \text{ GeV}^2$ . The final result for  $g_1(x, Q^2)$  from all data taken with longitudinally polarized hydrogen and deuterium targets is presented in Fig. IV-12, left panel. The statistical precision of the proton data is comparable to that of the hitherto most precise data from SLAC and

CERN in the same  $x$  range, while the deuteron data provide the most precise determination of  $g_1^d(x, Q^2)$  compared to previous measurements. The right panel of Fig. IV-12 shows the integrals of  $g_1^{p,d,n,NS}$  over the range  $0.021 < x < 0.9$ , corresponding to the event selection  $Q^2 > 1 \text{ GeV}^2$ , as a function of the low- $x$  limit integration evaluated at  $Q_0^2 = 5 \text{ GeV}^2$  for  $x < 0.04$ ,  $g_1^d(x, Q^2)$  becomes compatible with zero and its measured integral shows saturation. Based on the

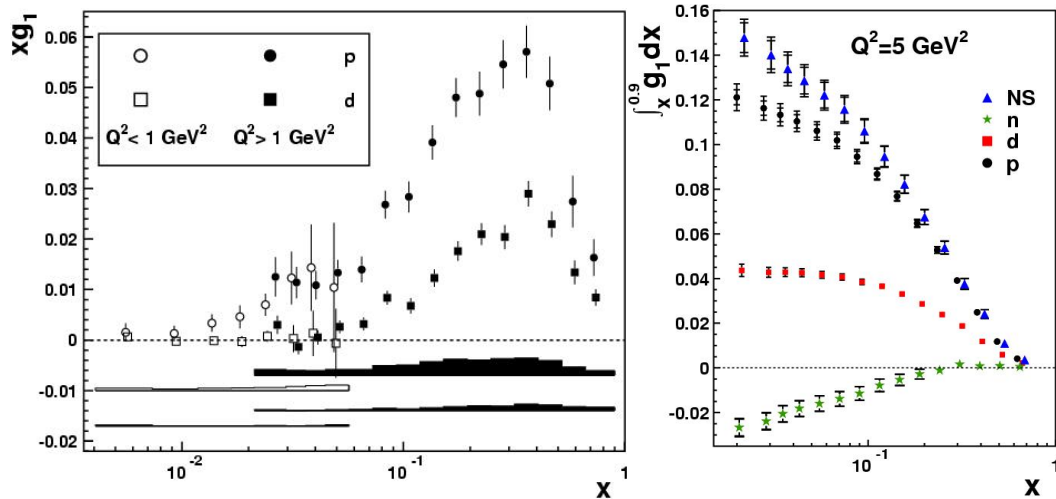


Fig. IV-12. HERMES results for  $xg_1$  vs  $x$  for the proton and the deuteron (left) and the integrals of  $g_1^{p,d,n,NS}$  over the range  $0.021 < x < 0.9$  as a function of the low- $x$  limit of integration.

assumed saturation of the integral of  $g_i^d(x, Q^2)$ , the flavor-singlet axial charge has been determined in the  $\overline{\text{MS}}$  scheme at  $Q_0^2 = 5 \text{ GeV}^2$  using only the integral of  $g_i^d(x, Q^2)$  and the axial charge  $a_8$  as inputs giving  $a_0 = 0.330 \pm 0.011(\text{theo.}) \pm 0.025(\text{exp.}) \pm 0.028(\text{evol.})$ . In this factorization scheme, the result can be

interpreted as the contribution  $\Delta\Sigma$  of quark spins to the spin of the nucleon. The data, therefore, suggest that the quark helicities contribute a substantial fraction to the nucleon helicity, but there is still a need for a major contribution from gluons and/or angular momentum.

**c.1.4. Collins and Sivers Asymmetries for Charged Pions and Kaons with a Transversely Polarized Target** (H. E. Jackson, A. El Alaoui, K. G. Bailey, T. P. O'Connor, P. E. Reimer, Y. Sanjiev, and the HERMES Collaboration)

At leading twist, the quark structure of the nucleon is described by three parton distribution functions: the momentum distribution  $q(x, Q^2)$ , the known helicity distribution  $\Delta q(x, Q^2)$ , and the unknown transversity distribution  $\delta(x, Q^2)$ . In the helicity basis, transversity is related to a quark-nucleon forward scattering amplitude involving helicity flip of both nucleon and quark. Because it is chiral-odd it cannot be probed in inclusive measurements. At HERMES transversity in conjunction with the chiral-odd Collins fragmentation function is accessible in azimuthal single-spin asymmetries (SSA) in semi-inclusive DIS in a transversely polarized target. The Collins fragmentation function describes the correlation between the transverse polarization of the struck quark and the transverse momentum of the hadron produced. The Sivers mechanism can also produce a SSA. The T-odd Sivers distribution function describes the correlation between the transverse polarization of the nucleon and the transverse momentum of the quarks within. A non-zero Sivers effect signals a nucleon spin flip without quark helicity flip, which must therefore involve orbital angular momentum inside the nucleon.

The characteristic signature of the Collins (Sivers) effect is a  $\sin(\varphi + \varphi_S)$  [ $\sin(\varphi - \varphi_S)$ ] modulation of the cross section in the distribution of the azimuthal angle  $\varphi$  of the pion around the virtual photon direction and relative to the lepton scattering plane, and  $\varphi_S$ , the angle between the scattering plane and the transverse spin component of the target nucleon. In the years 2002-2005 HERMES has taken data with a transversely polarized target. The azimuthal asymmetries are evaluated in two dimensions ( $\varphi$  and  $\varphi_S$ ) and the amplitudes for the Collins and Sivers processes were extracted simultaneously. Preliminary results for charged pions and kaons, based on the data taken in the years 2002-2004 which correspond to about 30% of the total statistics and supersede the published result<sup>1</sup> are shown in Fig. IV-13. The average Collins amplitude is positive for  $\pi^+$  and negative for  $\pi^-$  with a magnitude for  $\pi^-$  comparable to or larger than the one for  $\pi^+$ . One explanation could be a substantial magnitude for the disfavored Collins fragmentation function with an opposite sign to the favored one. These non-zero Collins asymmetries provide clear evidence for the existence of both the transversity distribution and the Collins fragmentation function. The significant positive Sivers amplitudes for  $\pi^+$  and  $K^+$  provide the first evidence for a T-odd parton distribution function in leptonproduction and imply a non-vanishing orbital angular momentum of the quarks inside the nucleon.

HERMES has already published data<sup>1</sup> on a transversely polarized target which allowed extraction of Collins and Sivers moments for charged pions. Measurements with a transversely polarized target allow one to distinguish between the Collins and Sivers processes.

<sup>1</sup>A. Airapetian *et al.*, Phys. Rev. Lett. **94**, 012002 (2005).

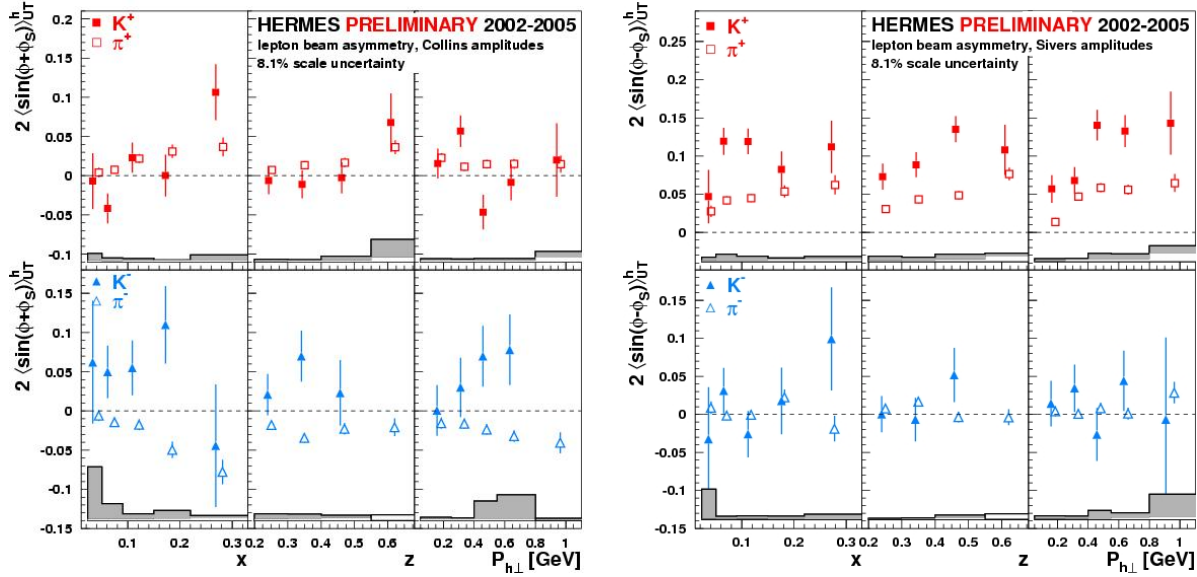


Fig. IV-13. Measured Collins moments (left) and Sivers moments (right) of charged pions and kaons obtained with a transversely polarized target. The error band represents the maximal systematic uncertainties in the measurement.

### c.1.5. Transverse Target-Spin Asymmetries in Deeply-Virtual Compton Scattering at HERMES (H. E. Jackson, A. El Alaoui, K. G. Bailey, T. P. O'Connor, P. Reimer, Y. Sanjiev, and the HERMES Collaboration)

An exciting new field has opened with measurements of hard exclusive production of mesons and real photons (Deep Virtual Compton Scattering, DVCS). The parton correlation functions (known as Generalized Parton Distributions, GPDs) accessible in these processes are related to the total angular momentum of the quarks contributing to the spin of the nucleon. Thus, with prior knowledge of the spin contribution of the quarks from other experiments, the orbital angular momentum carried by the quarks may become accessible. Such studies appear to mark a major advance in unraveling the spin structure of the nucleon. DVCS provides the cleanest access to GPDs. DVCS amplitudes can be determined through a measurement of the interference between the DVCS and Bethe Heitler (BH) processes, in which the photon is radiated from a parton and from the lepton, respectively. Measuring the  $\phi$ -dependence of a cross section asymmetry with respect to the charge

(spin) of the lepton beam provides information about the real (imaginary) part of the DVCS amplitude.

HERMES has already measured azimuthal asymmetries with respect to the beam helicity,<sup>1</sup> and to the target helicity<sup>2</sup> and w.r.t. the beam charge.<sup>3</sup> New results have been obtained for the beam-spin asymmetry measured on nuclear targets. A very exciting observable is the DVCS transverse target-spin asymmetry (TTSA) shown in Fig. IV-14 as obtained from the HERMES data accumulated in 2002-2004 using a transversely polarized hydrogen target. This asymmetry provides direct access to the total angular momentum  $J_{u,d}$  within a certain GPD model that parameterizes the GPDs using  $J_u$  and  $J_d$  as free parameters. In this particular GPD model, the data favor a non-zero value of  $J_u$  of order of 0.4 assuming  $J_d = 0$ .

<sup>1</sup>HERMES Collaboration, A. Airapetian *et al.*, Phys. Rev. Lett. **87**, 182001 (2001).

<sup>2</sup>M. Kopytin (for the HERMES Collaboration), AIP Conf. Proc. **792**, 424-427 (2005).

<sup>3</sup>HERMES Collaboration, A. Airapetian *et al.*, hep-ex/0605108.



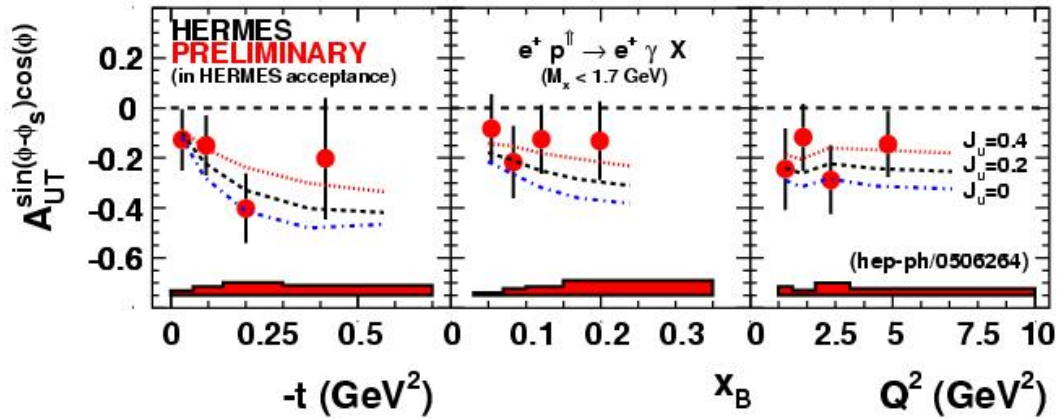


Fig. IV-14. HERMES results for the transverse target asymmetry in DVCS compared to GPD model calculations (see text)

### c.1.6. Determination of the Gluon Polarization from High- $p_T$ Hadron Electroproduction (H. E. Jackson, A. El Alaoui, K. G. Bailey, T. P. O'Connor, P. Reimer, Y. Sanjiev, and the HERMES Collaboration)

A direct model dependent extraction of  $\Delta g/g$  has been performed by studying charged hadron production at large transverse momenta  $p_T$  relative to the direction of the virtual photon. The high statistics data sample of antitagged (vetoed by the beam particle) inclusive charged hadrons was used. To relate the measured longitudinal double-spin asymmetry to the gluon polarization  $\Delta g/g$ , information on the relative contributions of the various subprocesses to the inclusive hadron production cross section, their asymmetries and variation with  $p_T$  was obtained from detailed Monte Carlo simulation using Pythia 6.2 and parameterizations of the spin dependent parton distributions of the nucleon and the photon. This information is used to obtain the signal asymmetry

which still contains a convolution of  $\Delta g(x)/g(x)$  with the hard subprocess cross section. Two methods have been applied to extract the average  $\langle \Delta g/g \rangle (p_T)$  from the signal asymmetry using different assumptions on the shape of  $\Delta g(x)/g(x)$ . Method I assumes that  $\Delta g(x)/g(x)$  is constant in the measured range of  $x$  while Method II employs a functional form for  $\Delta g(x)/g(x)$ . A value of  $\Delta g/g = 0.071 \pm 0.034$  (stat.)  $\pm 0.010$  (sys-exp)  $\pm 0.127$  (sys-models) has been obtained for  $\langle x \rangle = 0.22$  and  $\langle \mu^2 \rangle = 1.35$  GeV<sup>2</sup>. This result is shown in Fig. IV-15 together with previous determinations of  $\Delta g/g$  and is compared there with several different parameterizations obtained from NLO-QCD fits. The data favor a very small  $\Delta g/g$  or one with a node near  $x \approx 0.1$ .

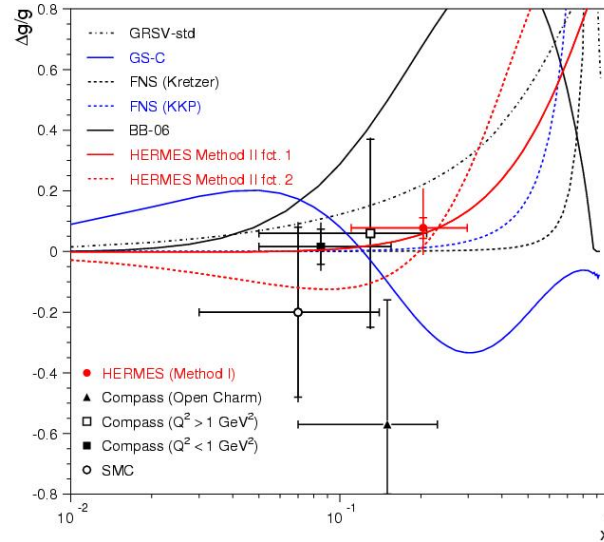


Fig. IV-15. HERMES results for  $\Delta g/g$  compared with a compilation of world data. The curves represent two fit functions from Method II (see text) and the results of several NLO-QCD fits.

### c.1.7. Hadronization in Semi-Inclusive Deep-Inelastic Scattering on Nuclei (H. E. Jackson, A. El Alaoui, K. G. Bailey, T. P. O'Connor, P. Reimer, Y. Sanjiev, and the HERMES Collaboration)

A series of semi-inclusive deep-inelastic scattering measurements on deuterium, helium, neon, krypton, and xenon targets has been performed in order to study quark hadronization. The data were collected with the HERMES detector at the DESY HERA accelerator using a 27.6 GeV positron or electron beam. Hadron multiplicities on nucleus  $A$  relative to those on the deuteron  $R_A^h$  were determined for pions, kaons and protons of all charges as a function of the virtual-photon energy  $\nu$ , the fraction of this energy transferred to the hadron  $z$ , the photon virtuality  $Q^2$ , and the hadron transverse momentum squared  $p_T^2$ . The data reveal a systematic decrease of  $R_A^h$  with the mass number  $A$  for each hadron type  $h$ . Furthermore,  $R_A^h$  increases (decreases) with increasing values of  $\nu(z)$ , increases

slightly with increasing  $Q^2$ , and is almost independent of  $p_T^2$ , except at large values of  $p_T^2$ . For pions two-dimensional distributions have also been obtained. These indicate that the dependences of  $R_A^h$  on  $\nu$  and  $z$  can largely be described as a dependence on a single variable  $L_c$ , which is a combination of  $\nu$  and  $z$ . The dependence on  $L_c$  suggests in which kinematic conditions partonic and hadronic mechanisms may be dominant. The behavior of  $R_A^h$  at large  $p_T^2$  constitutes tentative evidence for a partonic energy-loss mechanism. The  $A$ -dependence of  $R_A^h$  has also been investigated as a function of  $\nu, z$ , and  $L_c$ . It follows approximately an  $A^\alpha$  with  $\alpha \approx 0.5-0.6$ . A report of this work is in press (Nucl. Phys. B).

### c.2.1. Drell-Yan Measurements with 120 GeV Protons, FNAL E906 (P. E. Reimer, D. F. Geesaman, J. Arrington, K. Hafidi, R. J. Holt, D. H. Potterveld and the FNAL E906 Collaboration)

Although many of the properties of the proton may be attributed to its three valence quarks, it is, in fact, much

more complicated, with over 50% of its momentum carried by the non-valence (sea) quarks and gluons. To

understand the structure of the proton, it is necessary to understand the sea quarks, their origins and their interactions with the gluons that bind the proton together. The Fermilab E906 experiment is specifically designed to use Drell-Yan scattering to probe the sea quarks of the proton.<sup>1,2</sup>

The Drell-Yan mechanism provides a powerful tool to study the structure of the proton at the quark level. In Drell-Yan scattering a quark (or antiquark) in the proton beam annihilates with an antiquark (or quark) in the target, resulting in the production of a virtual photon that decays into a pair of leptons, which are detected in the spectrometer. The kinematics of the detected leptons can be used to select interactions between beam valence quarks and target antiquarks. This was successfully exploited by Fermilab E866/NuSea using an 800 GeV/c proton beam provided new insight into the antiquark sea in the proton<sup>3,4</sup> and nuclear dependence phenomena.<sup>5</sup> Fermilab E906 has been approved by Fermilab to extend Drell-Yan measurements to larger values of Bjorken- $x$  using the new 120 GeV Main Injector at Fermilab.

Vacuum polarization accounts for the creation of a flavor symmetric sea. Previous E866 Drell-Yan data, however, exhibit a large asymmetry between  $\bar{d}$  and  $\bar{u}$  for  $x < 0.25$ , clearly indicating a non-perturbative origin to the sea. Above  $x > 0.28$  these data, albeit with poor statistical uncertainty, indicate the ratio  $\bar{d}/\bar{u}$  returns to unity. This result dramatically changed the sea quark parton distribution fits and was completely unpredicted by meson cloud and other non-perturbative models. The return of  $\bar{d}/\bar{u}$  to unity clearly signals a change in the mechanism by which the sea is generated.<sup>3,4,6</sup> The current parton distributions now reproduce the previous Drell-Yan data for  $0.28 < x < 0.3$ , but parameterize  $\bar{d}/\bar{u} < 1$  as  $x$  increases above 0.3. This is not expected by *any* models of the proton and is simply indicative of the complete lack of data. Fermilab E906 will determine  $\bar{d}/\bar{u}$  and  $\bar{d} - \bar{u}$  for  $0.1 \leq x \leq 0.45$ , encompassing the non-perturbative region and extending well into the region where the sea appears to return to symmetry, as shown in Fig. IV-16.

Very little is known about the regime in which only one parton carries much of proton's momentum – different theoretical treatments prescribe different behaviors as  $x \rightarrow 1$  and very little data is available to serve as a guide. Through the partons in the beam proton, Fermilab E906 will access these distributions. The Drell-Yan cross section is dominated by the distribution of  $4u(x) + d(x)$  as  $x \rightarrow 1$ . E906 will extend the data provided by Fermilab E866 to higher  $x$  and provide

much more precise *proton* data than is currently available.

Models based on the hypothesis that nuclear binding is governed by the exchange of mesons have been used to quite successfully describe the nuclear force. Given the success of these models, it is natural to look for direct experimental evidence for the presence of these mesons in nuclei. Thus far, however, no direct evidence has been found.<sup>7</sup> If present, these mesons will lead to an enhancement of antiquarks in the nucleus. Drell-Yan is ideally suited to measure this enhancement. Fermilab E906 will collect data using nuclear targets, in addition to hydrogen and deuterium to look for these effects.

From deep inelastic scattering (DIS) experiments, we know that the quark level structure of a nucleon within a nucleus is different from that of a free nucleon. In the range  $0.10 < x < 0.25$ , a surplus of quarks (approximately 2-4%) in nuclei, known as antishadowing, is clearly observed in DIS data. To understand these phenomena, it is important to determine if it is a general property of the quark and antiquark distributions, or just a property of the valence or sea quarks. Drell-Yan, with its ability to measure sea-only quark effects, is the ideal reaction in which to measure this. Early Drell-Yan data indicate that this surplus might not be present<sup>7</sup> but with poor statistical uncertainty (3-5%). Fermilab E906's measurements will clearly determine if there is antishadowing in the sea, with statistical uncertainties of less than 1% throughout this region (see Fig. IV-16).

Using the same nuclear target data, Fermilab E906 will also study the propagation of colored partons in strongly interacting, cold nuclear matter. By comparing the Drell-Yan yields from different nuclear targets and looking for apparent shifts in the beam parton's momentum distributions between nuclei, E906 will be able to measure the beam parton's energy loss. Previous Drell-Yan studies have placed upper limits on parton energy loss.<sup>8</sup> With increased sensitivity from the 120 GeV beam and better statistical accuracy, Fermilab E906 will turn these upper limits into measurements. These measurements will aid in the understanding of jet suppression data from RHIC.

FNAL E906 is able to make these improvements over previous measurements because of the lower beam energy available at the Fermilab Main Injector. For fixed  $x_{\text{beam}}$  and  $x_{\text{target}}$  the cross section scales as the inverse of the beam energy. Thus a factor of seven more events for the same integrated luminosity can be achieved. At the same time, the primary background to

the measurement, muons from  $J/\psi$  decays, decreases with decreasing beam energy, allowing for an increase in instantaneous luminosity by another factor of seven. These two factors combine to provide roughly 50 times more events for the same beam time.

FNAL E906 has been approved by the Fermilab PAC and will begin collecting data in late 2009. Much of the reconfigured spectrometer will come from detector elements recycled from the E866 Drell-Yan

spectrometer. To increase the rate and triggering capabilities of the spectrometer, some new detectors will be fabricated. In addition, because of the significantly different kinematics of the 120 GeV experiment, the new spectrometer will require new coils to be fabricated for the first magnet in the spectrometer to focus the Drell-Yan muons. Current efforts are focused on the design of the coils of the new magnet, which is almost complete.

<sup>1</sup>J. Arrington *et al.*, (Fermilab E906 Collaboration), "Drell-Yan Measurements of Nucleon and Nuclear Structure with the Fermilab Main Injector: E906," Proposal Update to the Fermilab PAC, September 29, 2006.

<sup>2</sup>L. D. Isenhower *et al.*, (Fermilab E906 Collaboration), "Proposal for Drell-Yan Measurements of Nucleon and Nuclear Structure with the FNAL Main Injector," Proposal to the Fermilab PAC, April 1, 2001.

<sup>3</sup>E. A. Hawker *et al.*, (Fermilab E866/NuSea Collaboration), Phys. Rev. Lett. **80**, 3715 (1998).

<sup>4</sup>R. S. Towell *et al.*, (Fermilab E866/NuSea Collaboration), Phys. Rev. D **64**, 05202 (2001).

<sup>5</sup>M. J. Leitch *et al.*, (Fermilab E866/NuSea Collaboration), Phys. Rev. Lett. **84**, 3256 (2000).

<sup>6</sup>J.-C. Peng *et al.*, (Fermilab E866/NuSea Collaboration), Phys. Rev. D **58** 092004 (1998).

<sup>7</sup>D. M. Alde *et al.*, Phys. Rev. Lett. **64**, 2479 (1990).

<sup>8</sup>M. A. Vasiliev *et al.*, (Fermilab E866/NuSea Collaboration), Phys. Rev. Lett. **83**, 2304 (1999).

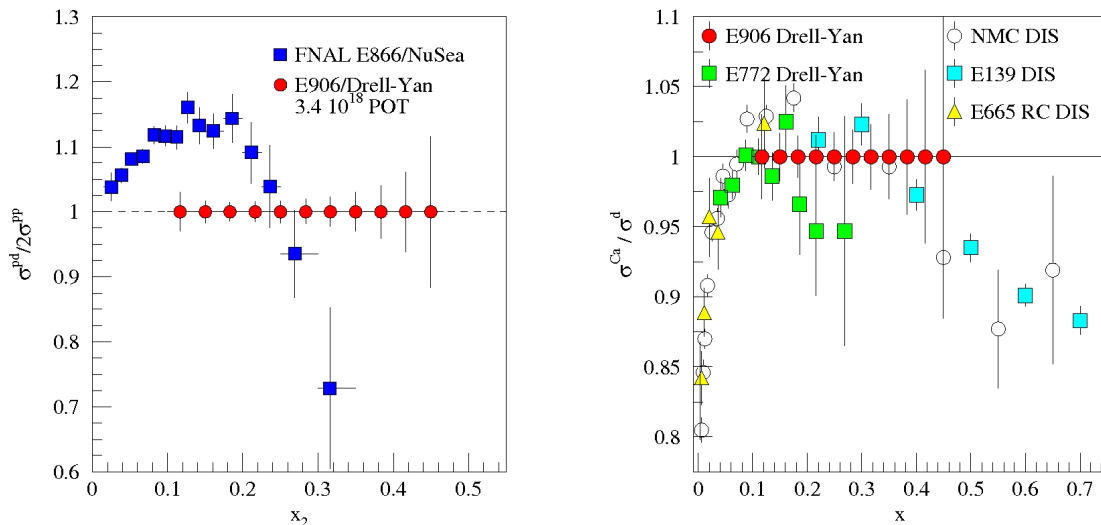


Fig. IV-16. The statistical uncertainty of the proposed E906 measurement of the ratio of hydrogen to deuterium cross sections (arbitrarily plotted at 1) compared with the E866 measurements of the same quantity (left). The statistical uncertainty of E906's measurement of the ratio of deuterium to Calcium cross sections (arbitrarily plotted at 1) compared with previous Drell-Yan and deep inelastic scattering (DIS) measurements (right).

### c.2.2. Measurement of the Drell-Yan Angular Distributions (P. E. Reimer, D. F. Geesaman, S. B. Kaufman, N. C. R. Makins, B. A. Mueller and the FNAL E866/NuSea Collaboration)

In leading order QCD, the Drell-Yan process is the annihilation of a quark-antiquark pair into a virtual photon. The virtual photon then decays into a lepton-

antilepton pair that is detected. The general expression for the angular distribution for Drell-Yan scattering is given by

$$d\sigma \sim 1 + \lambda \cos^2\theta + \mu \sin 2\theta \cos 2\phi + \nu/2 \sin^2\theta \cos 2\phi.$$

Theoretically, for massless quarks or a transversely polarized virtual photon in a reference frame with  $\theta$  defined relative to the quark-antiquark annihilation axis,  $\lambda = 1$  and  $\mu = \nu = 0$ . More generally, in any reference frame, the Lam-Tung rule,  $1 - \lambda = 2\nu$ , is expected to hold.

Experimentally, these angular distributions have only been studied in pion-induced Drell-Yan scattering experiments using nuclear targets. In both cases, the data indicate the Lam-Tung rule is violated and sizeable  $\cos 2\phi$  contributions to the angular distributions were observed. These results were more pronounced at large

transverse momentum ( $p_T$ ).

We have studied 800 GeV proton-induced Drell-Yan data collected by Fermilab E866/NuSea. The angular distributions from these data reveal no significant  $\cos 2\phi$  dependence, and within statistical uncertainties, the Lam-Tung sum rule is valid.<sup>1</sup> The lack of any observed effect can be used to constrain the *sea-quark* transverse-momentum-dependent Boer-Mulders structure function  $h_1^\perp$ . We are also studying the possibilities of more precise measurements of the angular distributions with future Drell-Yan experiments such as Fermilab E906.

<sup>1</sup>L. Zhu *et al.*, (E866/NuSea Collaboration), "Measurement of Angular Distributions of Drell-Yan Dimuons in  $p + d$  Interactions at 800 GeV/c," submitted to Phys. Rev. Lett., arXiv: hep-ex/0609005.

### c.3. 12-GeV Proposal to Determine the d/u Ratio in the Proton at High $x$ (R. J. Holt, D. F. Geesaman, J. Arrington, K. Hafidi, R. J. Holt, D. H. Potterveld, and the JLab Hall A Collaboration)

A proposal was presented to the first 12-GeV JLab PAC to perform deep inelastic scattering from the  $^3\text{H}$  and  $^3\text{He}$  mirror nuclei.<sup>1</sup> The proposed experiment will provide first measurements of the EMC effect in  $^3\text{H}$ , a determination of the ratio of the neutron to proton inelastic structure functions, and the ratio of the down to up quark distributions in the proton at relatively large Bjorken  $x$ . The  $F_2^n/F_2^p$  ratio will be extracted from the measurement of the inelastic cross section ratio of the two mirror nuclei. This ratio is expected<sup>2</sup> to be nearly free of nuclear effects, which have plagued previous extractions from deuteron structure function data. The d/u ratio at high  $x$  is particularly sensitive to the underlying quark structure of the nucleon.<sup>3</sup> These data

will provide a stringent test of non-perturbative QCD-based models of the nucleon. The nucleon structure function data at high  $x$  are also essential to understand the QCD background expected at high-energy colliders such as the LHC. The expected data quality from this proposed experiment are indicated in Fig. IV-17.

Experiment E12-06-018 was conditionally approved by the JLab PAC 30. The condition was essentially a successful safety review of the tritium target design. Efforts are underway to design a safe 5000 Ci cooled-gas tritium target for this experiment.

<sup>1</sup>G. G. Petratos *et al.*, (JLab MARATHON Collaboration), "Measurement of the F2n.F2p, d/u Ratios, and A = 3 EMC Effect in the Deep Inelastic Scattering from the Tritium and Helium Mirror Nuclei", JLab PR12-06-118.

<sup>2</sup>I. R. Afnan *et al.*, Phys. Rev. C **68**, 35201 (2003).

<sup>3</sup>N. Isgur, Phys. Rev. D **59**, 34013 (1999); S. J. Brodsky, M. Burkardt, and I. Schmidt, Nucl. Phys. **B441**, 197 (1995); W. Melnitchouk and A. W. Thomas, Phys. Lett. **B377**, 11 (1996).

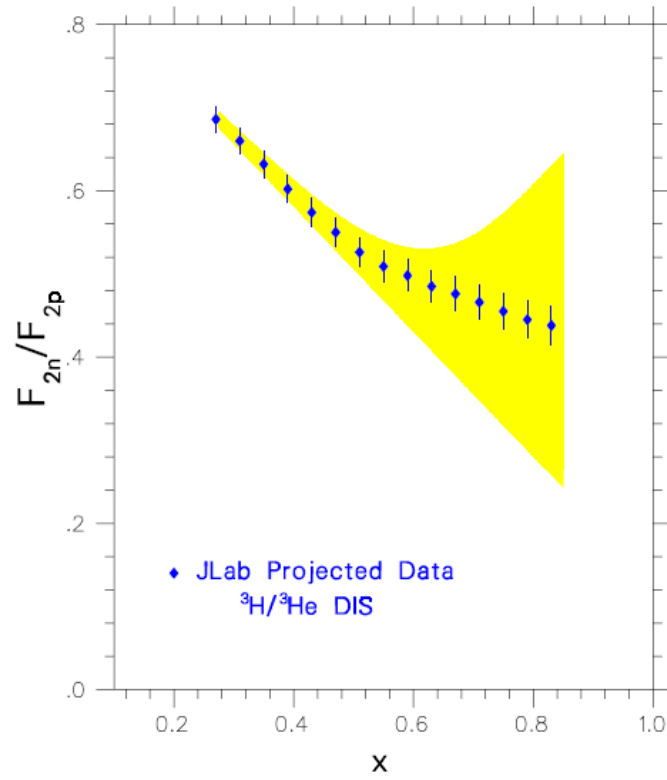


Fig. IV-17. Expected data for the ratio as a function of Bjorken  $x$ . The yellow band indicates the present uncertainty in the ratio from previous extraction of the ratio from deep inelastic scattering data from the proton and the deuteron.

## D. FUNDAMENTAL SYMMETRIES IN NUCLEI

### d.1. Laser Trapping of the Octupole-Deformed $^{225}\text{Ra}$ with Repumping by Black-Body Radiation (J. R. Guest, I. Ahmad, K. Bailey, J. P. Greene, R. J. Holt, Z.-T. Lu, T. P. O'Connor, and J. W. Wang)

Permanent electric dipole moments (EDMs) in atoms or molecules are a signature of Time (T)-and Parity (P)-violation and represent an important window onto physics beyond the Standard Model. We are developing a next-generation EDM search around laser-cooled and -trapped  $^{225}\text{Ra}$  ( $t_{1/2} = 15$  d) atoms. Due to octupole deformation of the nucleus,  $^{225}\text{Ra}$  is predicted to be two to three orders of magnitude more sensitive to T-violating interactions than  $^{199}\text{Hg}$  (stable), which currently sets the most stringent limits in the nuclear sector. The scheme is to collect  $^{225}\text{Ra}$  atoms in a magneto-optical trap (MOT), and then transfer the sample to an optical dipole trap where the atoms will be polarized by optical pumping and the EDM measurement will be performed.

In 2005, we showed for the first time that radium atoms can be laser-cooled and trapped. The feasibility was demonstrated on the long-lived  $^{226}\text{Ra}$  ( $t_{1/2} = 1600$  yr). Building upon this success, in 2006 we succeeded in laser-trapping of  $^{225}\text{Ra}$ ,<sup>1</sup> the candidate isotope for the EDM experiment now under development. Using a  $\sim 1$  mCi of  $^{225}\text{Ra}$  ( $\sim 25$  ng) purchased from the ORNL Isotope Program, we realized a trap loading rate of 20 atoms per second, and a trap loading efficiency of  $7 \times 10^{-7}$ . Improvements including a longer transverse cooling region and a much higher vacuum ( $10^{-11}$  Torr) in the trap chamber are being implemented so that the number of  $^{225}\text{Ra}$  atoms in the trap can reach  $1 \times 10^4$  for an EDM measurement.

We have performed precision laser spectroscopy on the trapped  $^{225}\text{Ra}$  and  $^{226}\text{Ra}$  atoms (Fig. IV-18), and measured the isotope shifts and hyperfine structures of the transitions relevant to the control of atoms. Figure IV-19 shows the spectroscopy study on the repump transition,  $6d\ ^3D_1 - 7p\ ^1P_1$ , at 1429 nm. The hyperfine structure A-coefficients of  $^{225}\text{Ra}$  have been determined to be  $4687.7 \pm 1.5$  MHz for the  $6d\ ^3D_1$  level, and  $2797.3 \pm 1.5$  MHz for the  $7p\ ^1P_1$  level.

As indicated by the spectrum inset in Fig. IV-18, room-temperature blackbody radiation can also redistribute population between the  $^3P_1$ ,  $^3D_2$ ,  $^3D_1$ , and  $^3P_0$  levels. This effect was discovered in the course of our trapping experiment, and has been demonstrated by observing the slow transfer on the milli-seconds scale of population among the levels while the lasers are turned off. In practice, this blackbody mechanism eases the requirements on the repumping laser fields because atoms which decay from the  $^3D_1$  level to the metastable  $^3P_0$  level will be recycled to the  $^3D_1$  level by the thermal radiation and be exposed to the repumping laser again. This is particularly significant for the trapping of  $^{225}\text{Ra}$ , which can be efficiently repumped by exciting from only one of the hyperfine manifolds. To our knowledge, this is the first demonstration that blackbody radiation can serve as an effective repump source. This mechanism may find more uses in laser-trapping of other elements with complex structure.

<sup>1</sup>J. R. Guest, N. D. Scielzo, I. Ahmad, K. Bailey, J. P. Greene, R. J. Holt, Z.-T. Lu, T. P. O'Connor, and D. H. Potterveld, Phys. Rev. Lett. **98**, 093001 (2007).

<sup>2</sup>N. D. Scielzo, J. R. Guest, E. C. Schulte, I. Ahmad, K. Bailey, D. L. Bowers, R. J. Holt, Z.-T. Lu, T. P. O'Connor, and D. H. Potterveld, Phys. Rev. A **73**, 010501(R) (2006).

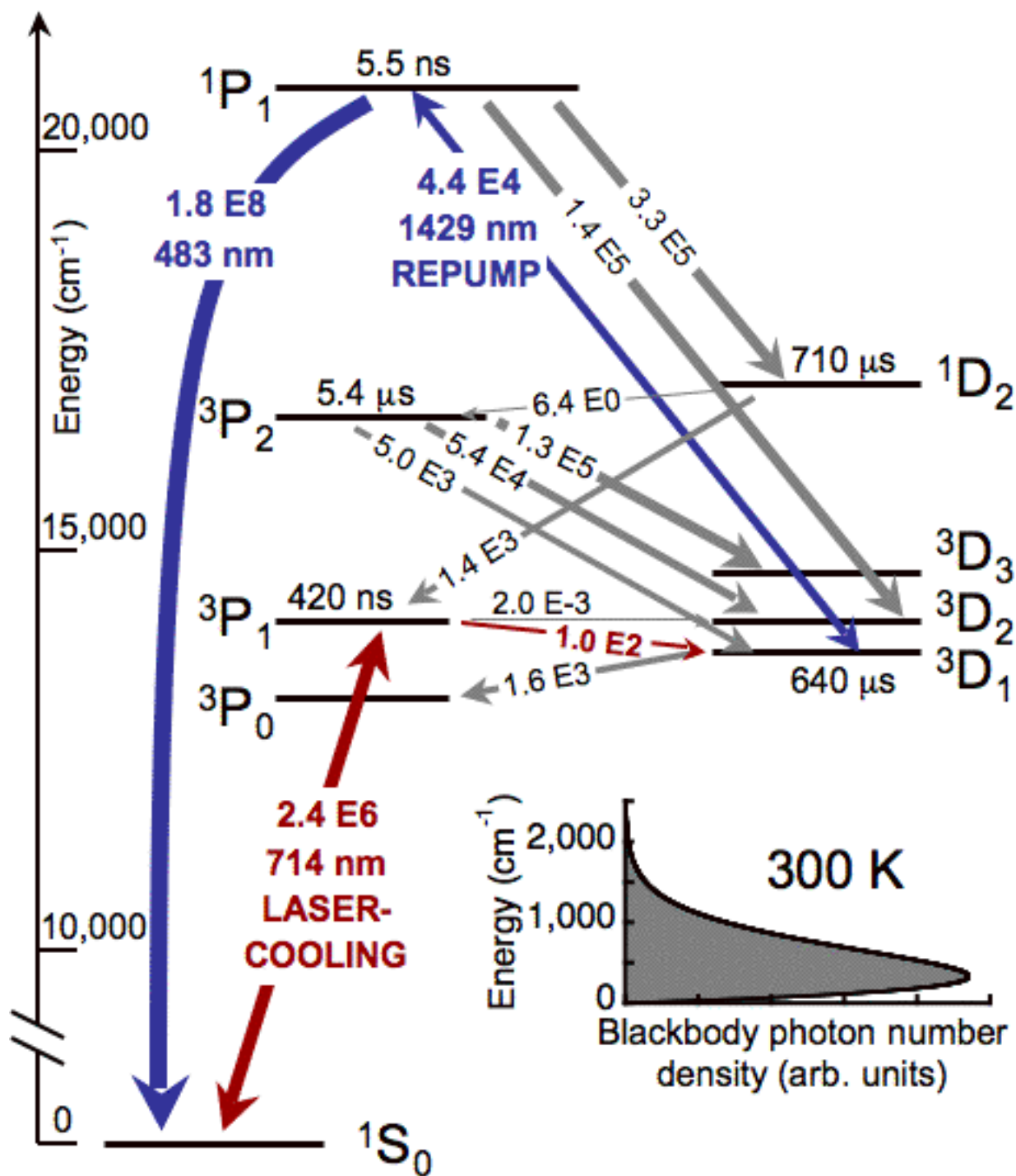


Fig. IV-18. Energy level diagram and decay rates for radium. Energies are indicated at the left, and calculated decay rates are shown ( $^3P_1$  lifetime comes from experiment).<sup>2</sup> The room-temperature (300 K) blackbody photon number density is shown on the same energy scale in the inset.



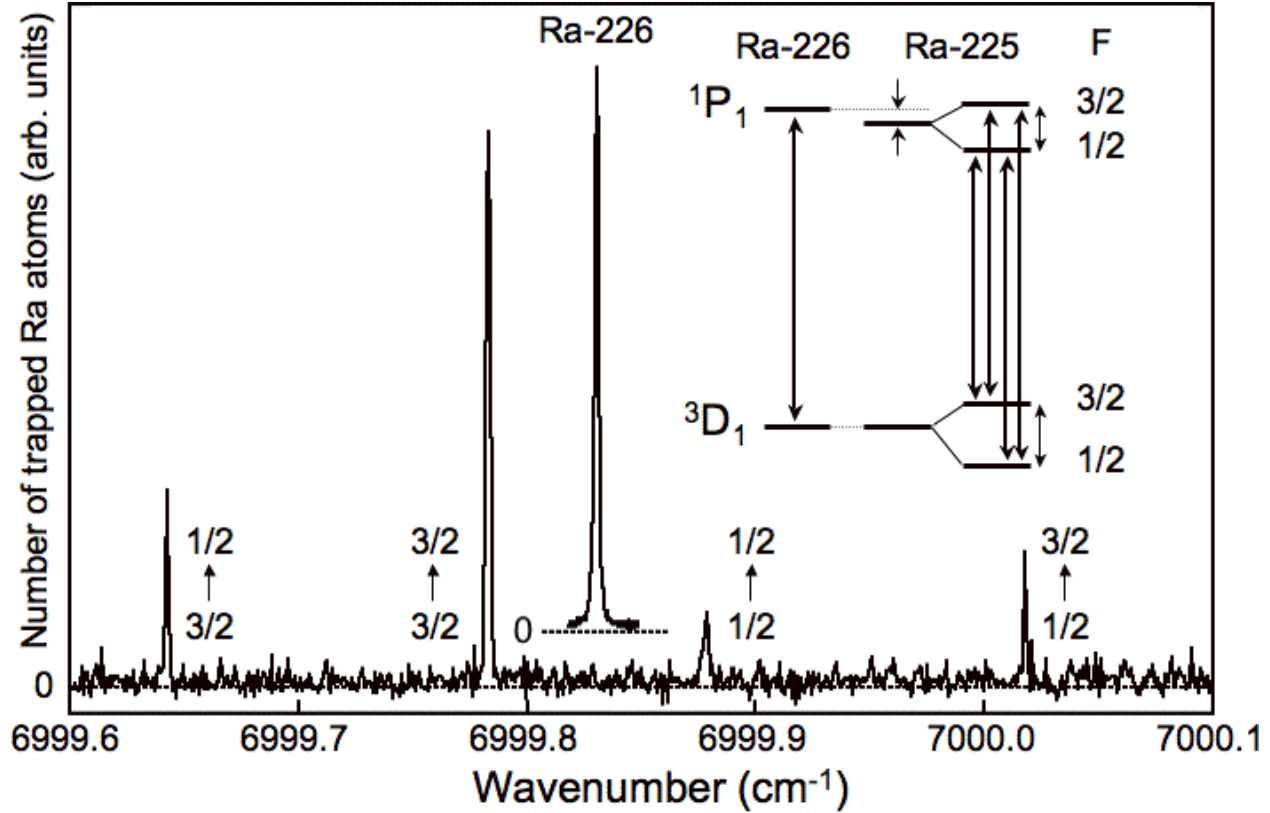


Fig. IV-19. Number of  $^{225}\text{Ra}$  and  $^{226}\text{Ra}$  atoms in the trap, as measured by fluorescence at 714 nm, vs. the wavenumber of the 1429 nm repump laser recorded by the wavemeter. The  $^{225}\text{Ra}$  data are scaled by 100 to compare to  $^{226}\text{Ra}$ , which is offset on the vertical scale for clarity. The repump resonances are indicated in the inset level schematic.

#### d.2. Measurement of $\sin^2\theta_W$ Through Parity Violation in Deep-Inelastic Scattering (PV DIS) on Deuterium (P. E. Reimer, X. Zheng, J. Arrington, K. Hafidi, R. J. Holt, H. E. Jackson, and D. H. Potterveld)

In the Standard Model of the electro-weak interaction,  $\sin^2\theta_W$  represents the relative strength of the weak and electromagnetic forces. The Standard Model predicts the observed value  $\sin^2\theta_W$  will vary (or run) as a function of  $Q^2$ , the energy squared at which it is probed, due to radiative corrections. At  $Q^2 = M_Z^2$  (the mass of the Z-boson)  $\sin^2\theta_W$  is well measured; for  $Q^2 < M_Z^2$ , however, only a few measurements exist. One way to probe  $\sin^2\theta_W$  at lower  $Q^2$  is by measuring the parity violating (PV) asymmetry in polarized deep inelastic scattering (DIS). The asymmetry ( $A_d$ ) is relatively large ( $A_d \approx 10^{-4} Q^2$ ), making it experimentally quite accessible. The sensitivity to  $\sin^2\theta_W$  is through the product of the axial Z-electron and vector Z-quark couplings ( $C_{1q}$ ) and the product of the vector Z-electron and axial Z-quark couplings ( $C_{2q}$ ). A program of DIS

parity violation measurement at Jefferson Lab with both 6 and 11 GeV electron beams is being developed.

A preliminary measurement at JLab with a 6 GeV beam has been approved (E05-007).<sup>1</sup> These data will provide a measurement of  $(2C_{2u} - C_{2d})$ . Current experimental knowledge of this quantity has an uncertainty of 180%, and is subject to model dependence in their interpretation. The complete measurement at 6 GeV will reduce this uncertainty by a factor of five. In addition, the 6 GeV experiment will explore the contribution of higher-twist effects to the asymmetry, providing crucial guidance to interpreting this data and future PV-DIS measurement with the 12 GeV upgrade to JLab. As a critical step toward the realization of this experiment, a scaler-based counting DAQ has been

designed and will be tested in the next year with beam at JLab.

Once the JLab 12 GeV upgrade is completed, a measurement of both  $\sin^2\theta_W$  and  $(2C_{2u} - C_{2d})$  will be completed using the baseline equipment. A Letter of Intent was submitted to the JLab PAC as a stand alone measurement in Hall C<sup>2</sup> and a full proposal is being developed for this measurement. Because of the large parity violating asymmetry, this measurement can be completed with only two to three weeks of beam time

and will provide a measurement of  $\delta\sin^2\theta_W/\sin^2\theta_W = \pm 0.26\% (stat) \pm 0.36\% (sys)$ , competitive with other off measurements below  $M_z^2$ .

Finally, investigations are underway construct a large-acceptance solenoid-based spectrometer to use DIS-Parity to not only measure  $\sin^2\theta_W$  but also probe parton distributions at large- $x$ . This spectrometer would also take advantage of the 11 GeV polarized electron beam at JLab.

<sup>1</sup>J. Arrington *et al.*, " $\bar{e}$  -<sup>2</sup>H Parity Violating Deep Inelastic Scattering at CEBAF 6 GeV," proposal 05007 to the JLab PAC, P. E. Reimer and X. Zheng, spokespersons, December 6, 2004.

<sup>2</sup>J. Arrington *et al.*, "Precision Measurement of the Parity-Violating Asymmetry in Deep Inelastic Scattering Off Deuterium Using Baseline 12 GeV Equipment in Hall C," Letter of Intent submitted to the JLab PAC, K. Paschke, P. E. Reimer, and X. Zheng spokespersons, July 9, 2006.

## E. ATOM TRAP TRACE ANALYSIS

### e.1. Measuring the Nuclear Charge Radius of $^8\text{He}^1$ (P. Mueller, K. Bailey, R. J. Holt, R. V. F. Janssens, Z.-T. Lu, T. P. O'Connor, J. P. Schiffer, I. Sulai, L.-B. Wang,\* M.-G. Saint Laurent,† J.-Ch. Thomas,† A. C. C. Villari,† O. Naviliat-Cuncic,‡ and X. Flechard‡)

Experimental and theoretical investigations of light nuclei play a complementary role in nuclear physics. A major progress in the theoretical description of nuclei has been the success of *ab-initio* calculations in accurately describing the properties of the lightest nuclei. At the same time, experimental investigations of light nuclei concentrate on precision measurements of these properties to serve as benchmarks for theoretical calculations. These experiments often take advantage of newly developed techniques as well as the highest possible production yields available at online facilities for the short-lived isotopes of interest.

In this line of experiments, we have been concentrating to perform precision measurements of the nuclear charge radius of the two short-lived isotopes of helium,  $^6\text{He}$  and  $^8\text{He}$ . Both isotopes exhibit a nuclear structure with a loosely bound neutron halo around a  $^4\text{He}$ -like core. The charge radius provides a measure of the correlation of the halo neutrons and gives insight into nuclear binding in very neutron rich systems. In particular, it probes the isospin dependence of the three nucleon potentials that are a key component of the *ab-initio* calculations.

Previously, we have determined the nuclear charge radius of  $^6\text{He}$  with a relative uncertainty of 0.7%.<sup>2</sup> The experiment was based on a measurement of the atomic isotope shift between  $^6\text{He}$  and  $^4\text{He}$  using high resolution laser spectroscopy of single helium atoms cooled and confined in a magneto-optical trap. The resulting rms charge radius value of 2.054(14) fm corroborated the neutron halo structure of  $^6\text{He}$  and verified the strong correlation between the halo neutrons predicted by theory.

Currently, we are working towards extending our technique to also measure the nuclear charge radius of  $^8\text{He}$ , which has the highest neutron-to-proton ratio of all known nuclei. The main experimental challenge of this effort is the production of  $^8\text{He}$  with sufficient yield and its efficient detection with the laser spectroscopic setup.

We have selected the GANIL facility (Grand Accelérateur National d'Ion Lourds) in Caen, France as the online source for our  $^8\text{He}$  experiment. At GANIL  $^8\text{He}$  is produced by impinging a  $\sim 70$  MeV/u  $^{13}\text{C}$  beam of up to 2.2  $\mu\text{A}$  current on a carbon target optimized for helium isotope production. The helium is subsequently ionized, mass separated and delivered into the experimental area as a low energy ( $\sim 20$  keV) ion beam with a  $^8\text{He}$  flux of up to  $6 \times 10^5 \text{ s}^{-1}$ . In addition, the overall detection efficiency of the spectroscopic setup was improved by up to a factor of 20 as compared to the  $^6\text{He}$  measurement through a number of experimental refinements.

In January 2007 the laser spectroscopic setup was moved from Argonne to GANIL and was subsequently reinstalled and commissioned during the time period from February to May 2007. A new helium neutralizer and transfer line was tested during a "parasitic" online run in April 2007 with a relatively low yield of  $\sim 200$   $^8\text{He}$ /s available in this mode. The transfer efficiency for  $^8\text{He}$  from the ion beam to the atomic beam apparatus was measured to be 25% in agreement with expectations. Currently, the optimization of the trap efficiency and the calibration of the isotope shift measurement are under way to prepare for a full online  $^8\text{He}$  run scheduled from June 12th to June 19th 2007.

\*Los Alamos National Laboratory, †Grand Accelérateur National D'Ion Lourds (GANIL), Caen, France,

‡Laboratoire de Physique Corpusculaire (LPC), Caen, France.

<sup>1</sup>Project homepage: <http://www-mep.phy.anl.gov/atta/>.

<sup>2</sup>L.-B. Wang *et al.*, Phys. Rev Lett. **93**, 142501 (2004).

**e.2. ATTA-3: The Next-Generation Instrument for  $^{81}\text{Kr}$ -Dating** (Y. Ding, K. Bailey, A. M. Davis,\* R. W. Dunford,† S.-M. Hu,‡ Z.-T. Lu, P. Mueller, T. P. O'Connor, N. C. Sturchio,§ and L. Young†)

We have made a breakthrough in the optical excitation of Kr that will allow us to complete the development of the next-generation instrument, ATTA-3, with an efficiency leading to a 100-fold reduction in sample size. This reduction in sample size will help make ATTA an essential analytical instrument in earth sciences.

Due to the lack of a cw, narrow-bandwidth laser at 124 nm, laser trapping of krypton atoms can only be realized with atoms at the metastable  $5s[3/2]^0_2$  level (Fig. IV-20). In ATTA-2, the excitation of Kr atoms to

the metastable level is done by colliding atoms and electrons in a plasma discharge, which poses a serious limitation to the analyzer. The discharge source has a low excitation efficiency ( $\text{Kr}^*/\text{Kr} \sim 10^{-4}$ ); the collision process causes the atomic beam to diverge; in the plasma,  $\text{Kr}^+$  ions are slowly imbedded into surfaces, causing a loss of sample, only to re-emerge later in subsequent analyses, and thereby inducing cross-sample contamination; moreover, a discharge requires a certain minimum gas pressure to operate, which raises the minimum amount of sample needed to support the operation of the discharge.

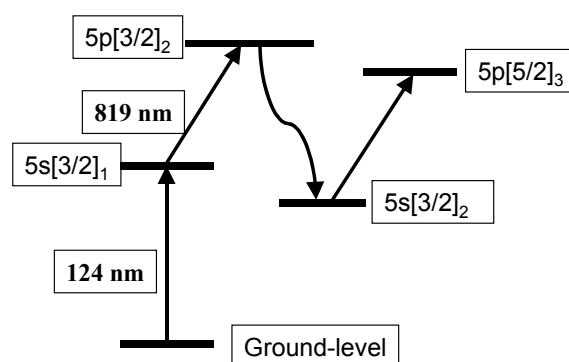


Fig. IV-20. Atomic energy diagram of Kr. The new optical excitation scheme (124 nm + 819 nm) is shown.

In order to avoid these problems and improve both the atom counting rate and counting efficiency, we have been investigating alternative sources of metastable  $\text{Kr}^*$  atoms. It had been previously demonstrated that Kr atoms can be transferred from the ground level to the metastable level via a two-photon excitation process (Fig. IV-20): excitation with a vacuum ultraviolet photon at 124 nm and an infrared photon at 819 nm, followed by a spontaneous decay at 760 nm.<sup>1</sup> All three transitions are of the allowed E1 type. Based on this scheme, we have recently realized, for the first time, a beam of metastable  $\text{Kr}^*$  atoms produced by photon excitation.<sup>2</sup> In the experiment, a vacuum ultraviolet Kr lamp was used to generate the 124 nm photons that are

resonant with Kr atoms at the ground level. The 819 nm light was supplied by a diode laser system. At the optimum lamp and laser conditions, the metastable  $\text{Kr}^*$  beam has reached a flux comparable to that produced with a RF-discharge in ATTA-2. With better engineering controls such as a liquid-nitrogen-cooled Kr atom source and a longer optical excitation path, we believe that a higher  $\text{Kr}^*$  beam intensity can be reached. This optical production scheme is a clean and efficient way of producing a well-collimated beam of metastable  $\text{Kr}^*$  atoms, and will enable the analysis of small sample size required by many geochemical and cosmochemical applications.


\*University of Chicago, †Chemistry Division, Argonne National Laboratory, ‡Hefei National Laboratory, Anhui, China, University of Science and Technology of China, Hefei, Anhui, China, §University of Illinois at Chicago.

<sup>1</sup>L. Young *et al.*, J. Phys. **B35**, 2985 (2002).


<sup>2</sup>Y. Ding *et al.*, Rev. Sci. Instrum. **78**, 023103 (2007).

## V. THEORETICAL PHYSICS

### OVERVIEW



Our research addresses the key questions that comprise the Nation's nuclear physics agenda. We place heavy emphasis on the prediction of phenomena accessible at Argonne's ATLAS facility, at JLab, and at other laboratories; and on anticipating and planning for a future rare isotope beam facility (FRIB). In theoretical and computational nuclear astrophysics our program addresses such issues as the origin of the elements from hydrogen through the actinides and the nature of the basic mechanisms of supernova explosions, and serves to identify critical nuclear parameters and systematic properties to be explored with an advanced exotic beam laboratory. We employ quantum chromodynamics to explore hadron properties: in vacuum, as relevant to programs such as those pursued at JLab; and in-medium, as appropriate to the early universe, compact astrophysical objects, and the RHIC program. Dynamical coupled-channel models are developed to investigate the structure of nucleon resonances by using meson production data from; *e.g.*, JLab, Bonn and Mainz, and also to predict neutrino-nucleus reaction cross sections necessary for analyzing the data from experiments measuring neutrino properties. The structure of atomic nuclei is explored in *ab-initio* many-body calculations based on the realistic two- and three-nucleon potentials we have constructed. These potentials give excellent fits to nucleon-nucleon elastic scattering data and the properties of light nuclei. We use quantum Monte Carlo methods to, *e.g.*, compute nucleon-nucleus scattering phase shifts, transition amplitudes, and a variety of electroweak reactions important to astrophysics. Our nuclear structure and reaction program includes: coupled-channels calculations of heavy-ion reactions near the Coulomb barrier; studies of breakup reactions involving nuclei far from stability, the determination of radiative capture rates from Coulomb dissociation experiments, and studies of the effects of *np*-pairing on nuclei near the proton dripline and of the heaviest elements, using many-body wavefunctions. Our programs provide much of the scientific basis for the drive to physics with rare isotopes. Additional research in the Group focuses on: atomic and neutron physics; fundamental quantum mechanics; quantum computing; and tests of fundamental symmetries and theories unifying all the forces of nature, and the search for a spatial or temporal variation in Nature's basic parameters. The pioneering development and use of massively parallel numerical simulations using hardware at Argonne and elsewhere is a major component of the Group's research.





## A. NUCLEAR DYNAMICS WITH SUBNUCLEONIC DEGREES OF FREEDOM

The objective of this research program is: to investigate the role of quark-gluon degrees of freedom in hadron structure and interactions, and in nuclear dynamics; to explore the properties and phase structure of hot, dense Quantum Chromodynamics (QCD) and its possible consequences for the structure of compact astrophysical objects; to develop theoretical methods and tools to place reliable constraints on the variation of Nature's fundamental parameters and physics beyond the Standard Model; the development and application of reaction theories for use in exploring hadron structure using the data from meson and nucleon-resonance production experiments at modern experimental facilities; and to investigate relations of Poincaré covariant dynamics specified by mass operators to complementary dynamics specified by Green functions.

At the level of quark-gluon degrees of freedom, the Dyson-Schwinger equations (DSEs) provide a Poincaré covariant, nonperturbative method for studying QCD in the continuum. A hallmark of present-day DSE applications in hadron physics is the existence of a symmetry preserving truncation that enables the simultaneous exploration of phenomena such as: confinement, dynamical chiral symmetry breaking, and bound state structure and interactions. In addition, the DSEs provide a generating tool for perturbation theory and hence yield model-independent results for the ultraviolet behavior of strong interaction observables. This means that model studies facilitate the use of physical processes to constrain the long-range behavior of the interaction between light-quarks in QCD, which is poorly understood and whose elucidation is a key goal of modern experimental programs. The last year saw numerous noteworthy applications and successes. For example, we presented arguments which support a view that chiral perturbation theory is inapplicable for pion-like meson masses greater than  $m_{\theta^-} \sim 0.45$  GeV; that a unique signal for the restoration of chiral symmetry via excitation of mesons is equality between the pole residues for  $\theta^-(nS)$  and  $\theta^{++}(nS)$  states when  $n$ , the radial quantum number, is large; that chiral symmetry and its dynamical breakdown in QCD even place constraints on properties of mesons composed of two heavy-quarks; and we also provided a prediction for the ratio of neutron electric and magnetic form factors.

At the level of meson and baryon degrees of freedom, we continue our effort to develop a dynamical coupled-channels model for use in analyzing the very extensive set of data for electromagnetic meson production reactions. A primary objective is the development of an interpretation for this data in terms of the quark-gluon substructure of nucleon resonances ( $N^*$ ). We aim to draw the connection between this data and the predictions made by QCD-based hadron models and numerical simulations of lattice-regularized QCD. In the past year we completed a major stage of this project by determining the hadronic interactions in the model by fitting pion-nucleon scattering data up to 2 GeV. We predicted the effect of a meson cloud on the form factors describing the transition to all known low-lying nucleon resonances. Methods for determining the resonance parameters from the partial-wave amplitudes were developed. We also made progress on projects focused on  $\eta$  and  $\omega$  photoproduction, which aim at discovering highly excited resonances with masses close to 2 GeV. In addition, we continued to play a leading role in directing operations of the Excited Baryon Analysis Center (EBAC) at Jefferson Laboratory.

Relativistic quantum dynamics requires a unitary representation of space-time symmetries (Poincaré group) and localization of states, such that states localized in relatively space-like regions are causally independent. We have recently focused on the application and elucidation of complementary mathematical representations of hadron phenomena, and on a consistent treatment of medium energy electromagnetic few-body processes.

### a.1. Space-Time Variation of Strong Interactions and Fine Structure Constant (V. V. Flambaum\*)

Grand Unification Models suggest that the fundamental masses ( $m_{electron}$ ,  $m_{quark}$ ) and the strong interaction scale  $\Lambda_{QCD}$  may vary much faster than the QED fine structure constant  $\alpha$ . A number of theoretical and experimental papers devoted to temporal variation of  $m/\Lambda_{QCD}$  were recently published. There is some evidence for this parameter variation in Big Bang nucleosynthesis, quasar absorption spectra and Oklo natural nuclear reactor data. The need for an interpretation of these measurements and the search for new, enhanced effects have created a topical field of research: strong interaction calculations of the dependence of nuclear parameters on quark masses. We have been active in this area.

We showed<sup>1</sup> that the relative effects of a variation in  $\alpha$  and  $m_{quark}/\Lambda_{QCD}$  are enhanced by 5-6 orders-of-magnitude in a very narrow ultraviolet transition between the ground and first excited state in <sup>229</sup>Th (energy  $\sim 5$  eV). An experiment capitalizing on this can potentially improve sensitivity to a variation in Nature's fundamental parameters by 7-10 orders-of-magnitude (exposing a variation of up to  $10^{-23}$ /year).

We demonstrated<sup>2</sup> that atomic scattering lengths, which can be measured in Bose-Einstein condensate and Feshbach molecule experiments, are extremely sensitive to the variation of Nature's fundamental

constants, in particular, to the electron-to-proton mass ratio ( $m_e/m_p$ ). Based on a single- and two-channel scattering model, we showed how this variation in the mass ratio is communicated to the scattering length. Our results suggest that a variation in  $m_e/m_p$  on the level of  $10^{-11} \sim 10^{-13}$  can be detected near a narrow magnetic or an optical Feshbach resonance by monitoring the scattering length on the 1% level. The formulae we have derived may also be used to estimate the isotopic shift in the scattering length.

We calculated<sup>3</sup> the dependence of nuclear magnetic moments on the current-quark masses, including an estimate of the effect of spin-spin interactions, and obtained limits on the variation of  $\alpha$  and ( $m_{quark}/\Lambda_{QCD}$ ) by using recent atomic clock experiments that examine the hyperfine transitions in H, Rb, Cs, Yb<sup>+</sup> and Hg<sup>+</sup> and the optical transition in H, Hg<sup>+</sup> and Yb<sup>+</sup>.

We found<sup>4</sup> that the relative effect of a variation in  $\alpha$  on microwave transitions between very close and narrow rotational-hyperfine levels may be enhanced by 2-3 orders-of-magnitude in diatomic molecules with unpaired electrons, such as LaS, LaO, LuS, LuO, YbF, and similar molecular ions. The enhancement results from cancellation between the hyperfine and rotational intervals.

\*Argonne Fellow, Physics Division, and University of New South Wales, Sydney, Australia.

<sup>1</sup>V. V. Flambaum, Phys. Rev. Lett. **97**, 092502 (2006).

<sup>2</sup>C. Chin and V. V. Flambaum, Phys. Rev. Lett. **96**, 230801 (2006).

<sup>3</sup>V. V. Flambaum and A. F. Tedesco, Phys. Rev. C **73**, 055501 (2006).

<sup>4</sup>V. V. Flambaum, Phys. Rev. A **73**, 034101 (2006); V. V. Flambaum and M.G. Kozlov, Phys. Rev. Lett., to appear.

### a.2. Coulomb Problem for Vector Bosons (V. V. Flambaum\* and M. Yu. Kuchiev†)

There is a difficulty with the Coulomb problem for vector bosons. Indeed, soon after Proca formulated a theory for vector particles it became clear that it produces inadequate results for the Coulomb problem.

This inspired Corben and Schwinger to modify Proca's theory, tuning the Lagrangian and the equations of motion so as to force the vector boson's gyromagnetic ratio to acquire the value  $g = 2$ . (N.B.  $g = 2$  is the



Standard Model value for  $W_{\pm}$ ). They obtained a simple Sommerfeld-type formula for the spectrum valid up to  $Z\alpha = 1/2$ .

However, the problem has not completely disappeared: for  $j = 0$  states the charge of the boson localized in the vicinity of the attractive Coulomb center remains infinite. We re-derived<sup>1</sup> these results for the spectrum and wavefunction starting from the Standard Model and then displayed a clear way to properly formulate the Coulomb problem for vector particles. Our main observation is that the polarization of the QED vacuum has a profound impact on the problem, forcing the density of charge of a vector boson to decrease exponentially at the origin thus making the Coulomb problem stable and well defined.

At first glance this result may be surprising because the vacuum polarization increases the strength of the attractive field at the origin. Moreover, the vacuum polarization for spinor and scalar particles in the Coulomb field is known to produce only small, perturbative effects. In contrast, we find for the vector particle a *strong reduction* in its charge density near the origin. To grasp the physical mechanism involved it is necessary to notice that the equation of motion for vector particles contains a particular term, which has no counterparts for scalars and spinors; namely, the last term in the following equation:

$$(\partial^2 + m^2) W^\mu + 2ie F^{\mu\nu} W_\nu + (ie/m^2) \partial^\mu (j_\nu W^\nu) = 0$$

This additional term is responsible for a strong repulsion arising from the vacuum polarization and makes the Coulomb problem stable. The effective potential becomes large and positive when  $r \rightarrow 0$ ; viz.,  $U(r) \approx Z^2 \alpha^3 \beta / (m^2 r^4)$ .

Here the factor  $\beta$  is the lowest coefficient of the Gell-Mann-Low function. Both the Standard Model and experimental data indicate that  $\beta > 0$ , presumably, up to the Grand Unification limit. Hence the vacuum polarization results in an intense repulsion near the origin for even arbitrarily small values of  $Z^2 \alpha^3$ .

The wavefunction decreases exponentially at small distances:  $\varphi(r) \sim \exp(-Z\alpha (\alpha\beta)^{1/2} / [m r])$ , so that the charge density of the W-boson also decreases exponentially at the origin. Thus, accounting for the QED vacuum polarization eliminates the difficulty related to the infinite charge of a vector boson located at the Coulomb center.

For small  $Z$  the energy shift of discrete energy levels owing to the vacuum polarization is found to be small, which makes the Sommerfeld formula applicable for the spectrum of vector bosons.

In addition we have recently found that the charge density of a positively charged vector boson, e.g., the  $W^+$ -boson, may be negative.<sup>2</sup> The effect manifests itself even for a free propagation; when the energy of the W-boson is higher than  $\sqrt{2}m$  and the standing-wave is considered. The charge density of W also changes sign in the vicinity of a Coulomb center. For an arbitrary vector boson, this effect depends on the g-factor. We traced the origin of this surprising effect to the electric quadrupole moment and spin-orbit interaction of vector particles; their contributions to the current have a polarization nature. The corresponding charge density  $\mu_{Pol} = -\nabla P$ , where  $P$  is an effective polarization vector that depends on the quadrupole moment and spin-orbit interaction. The density oscillates in space, producing zero contribution to the total charge.

\*Argonne Fellow, Physics Division, and University of New South Wales, Sydney, Australia, †University of New South Wales, Sydney, Australia.

<sup>1</sup>M. Yu. Kuchiev and V. V. Flambaum, Mod. Phys. Lett. A **21**, 781 (2006).

<sup>2</sup>V. V. Flambaum and M. Yu. Kuchiev, Phys. Rev. Lett. **98**, 181805 (2007).

### a.3. Quark Deconfinement in Neutron Star Cores: The Effects of Spin-Down (P. Jaikumar, J. Staff,\* and R. Ouyed†)

We studied the role of spin-down of isolated neutron stars in driving quark deconfinement in its high-density core. We concluded that light neutron stars ( $\leq 1.6$  solar massive neutron stars ( $\geq 1.8$  solar masses) can enter a quark phase only if they are spinning faster than about 3 milliseconds as observed now.

We created sequences of neutron star models using numerical methods developed specifically to treat rapidly rotating neutron stars. We obtained typical timescales to reach quark deconfinement in the core of neutron stars that are born with Keplerian frequencies.

We found this time to be least for equations of state that support the largest minimum mass at zero spin, unless the moment of inertia is very high. For each equation of state, we also determined the minimum and maximum neutron star masses, as well as the current minimum spin periods that will allow for deconfinement in a Hubble time via spin-down only.

Our results directly address the issue of forming a quark

star in the spin-down epoch of a neutron star, and present a window in mass and spin-periods in which observers are likely to discover quark stars. They also suggest that the existence of quark stars is predicated upon having a low deconfinement threshold of less than five-times the saturation density of nuclear matter.

An article describing this work was published.<sup>1</sup>

\*Purdue University, †University of Calgary, Alberta, Canada.

<sup>1</sup>J. Staff, R. Ouyed, and P. Jaikumar, *Astrophys. J. Lett.* **645**, L145-L148 (2006).

#### a.4. **Quark Matter in Neutron Stars: An Aperçu** (P. Jaikumar, S. Reddy,\* and A. W. Steiner†)

Deconfined quark matter may exist in a stable phase in the interior of a neutron star, where densities are as much as five times that of nuclei. We reevaluated the possibility for the existence of deconfined quark matter in the light of recent observations that, for the first time, determined the mass and radius of the same neutron star; *viz.*, the X-ray binary EXO 0748-676. We concluded that the rather large inferred values of mass and radius of this object conflicts with a scenario in which significant softening occurs owing to a phase transition to quark matter at high density. However, strange stars that are made entirely of quark matter and hybrid stars that are composed of a quark core with a relatively stiff equation of state remain viable.

We reviewed recent observations of thermally emitting neutron stars, whose surface temperatures are accurately known, in order to determine if rapid neutrino cooling processes characteristic of quark

matter could operate in such stars. We found that the data do not support any rapid cooling mechanism; instead, they are satisfactorily explained by neutrino emission in superfluid nucleonic matter. However, a cold neutron star in the supernova remnant 3C58 and the growing number of such remnants with low observed luminosity may well suggest that some neutron stars require a rapid cooling mechanism.

Based on a broad evaluation of transient phenomena in neutron stars, taken together with mass-radius and spin-period measurements, we emphasized the need to understand the long-term evolution of neutron stars within a consistent picture. In particular, we pointed out that it would be premature to rule out quark matter in neutron stars on the basis of mass-radius measurements alone.

An article describing this work was published.<sup>1</sup>

\*Los Alamos National Laboratory, †Michigan State University.

<sup>1</sup>P. Jaikumar, S. Reddy, and A. W. Steiner, *Mod. Phys. Lett. A* **21**, 1965 (2006).

#### a.5. **Surface Structure of Quark Stars with Magnetic Fields** (P. Jaikumar)

Bare quark stars are a proposed class of compact stars that are composed entirely of deconfined quark matter. An observational confirmation of their existence would be conclusive evidence of quark deconfinement at large baryon densities, a phenomena anticipated from Quantum Chromodynamics (QCD). We outlined the main observational characteristics of bare quark stars as determined by their photon luminosity, including the effects of a strong magnetic field at the surface.

We studied the modifications of a quark star's surface charge distribution owing to a magnetic field in a force-free approximation, employing a Thomas-Fermi model to solve the Poisson equation. We found an exponentially decaying charge distribution at large distance from the surface, contrary to the  $1/r$  fall off in the non-magnetic case. For magnetic fields  $B \sim 10^{14}$  G, or more, quantization of electrons into Landau orbits was found to significantly affect the charge distribution.

We showed that the flux and the spectrum of photons from quark stars is determined by  $e^+e^-$  pair-emission at high temperatures ( $T > 10^9$  K) and by bremsstrahlung and other  $2 \rightarrow 3$  processes for  $T < 10^9$  K. The resulting non-thermal spectrum is different from that of a cooling neutron star, allowing for an observational distinction to be made. It was established that strong magnetic fields

of  $B \sim 10^{14}$  G or more induce a collective response of the surface material that strongly diminishes the reflectivity from the unmagnetized case and also polarizes the emitted photons.

An article describing this work was published.<sup>1</sup>

<sup>1</sup>P. Jaikumar, *Pramana-Indian J. of Phys.* **67**, 937 (2007).

#### a.6. **Nucleosynthesis in Decompressing Neutron Star Matter** (P. Jaikumar, B. Meyer,\* K. Otsuki,† and R. Ouyed‡)

The rapid neutron capture process ( $r$ -process) makes approximately half of the heavy elements above  $^{56}\text{Fe}$ . The astrophysical site for the  $r$ -process is not yet known with any certainty, although Type-II supernovae are the most promising candidates. We proposed an alternative site: decompressing neutron-rich material from the surface of a neutron star that undergoes a quark-hadron phase transition. We performed network calculations that are adapted to decompression and which match to dynamical  $r$ -process calculations at densities below neutron drip ( $4 \times 10^{11}$  g/cc).

We studied the sensitivity of the final abundance pattern of heavy elements to heating from nuclear reactions and expansion timescale of the ejecta. We found that heating was an essential factor in producing

the prominent peaks of the  $r$ -process and that a slow expansion rate of the ejecta was able to best reproduce the observed relative abundance of  $r$ -process elements in our galaxy, as shown in Fig.V-1.

We estimated the frequency of decompression events in our galaxy and found it to be significantly smaller than that of Type II supernovae but comparable to binary neutron star mergers. We highlighted the distinguishing features of the decompression scenario by contrasting it with conventional nucleosynthesis sites such as Type II supernovae and neutron star mergers, especially in the context of heavy-element compositions of extremely metal-deficient stars.

An article describing this work was submitted.

\*Clemson University, †University of Chicago, ‡University of Calgary, Alberta, Canada.

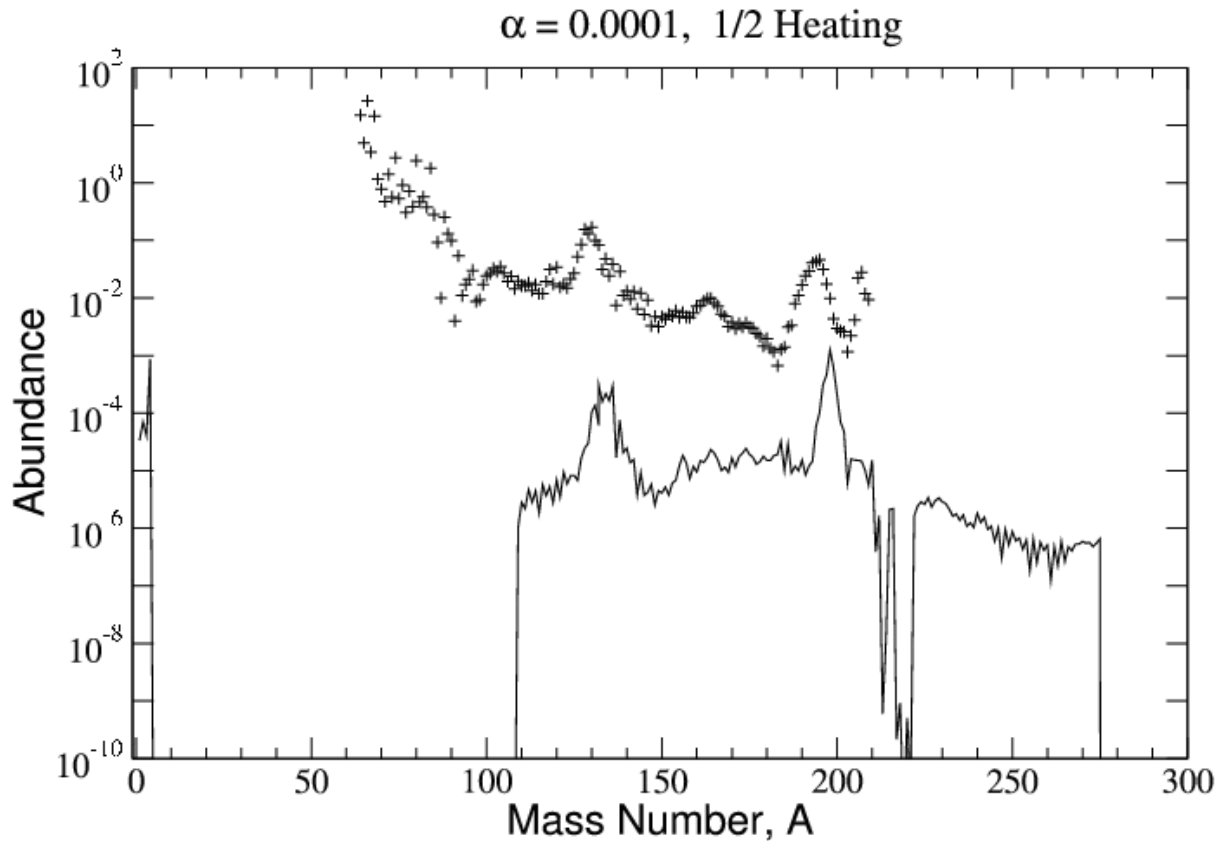


Fig. V-1. The final abundance distribution as a function of mass number in a decompression calculation for the slowest parameterized ejecta expansion rate  $\alpha = 0.0001$  and 50% local energy deposition from nuclear reactions.

#### a.7. Nucleon Weak and Strong Form Factors (C. D. Roberts, S. V. Wright, and A. Höll\*)

The framework we have developed for the Poincaré covariant study of nucleon electromagnetic form factors can naturally also be employed to calculate weak and strong form factors of the nucleon, which are sensitive to different aspects of quark-nuclear physics and should prove useful, *e.g.*, in constraining coupled-channel models for medium-energy production reactions on the nucleon.

We obtained preliminary results in the chiral limit for three such form factors: the axial-vector,  $G_A(Q^2)$ , and

pseudoscalar,  $G_P(Q^2)$ , nucleon form factors, which appear in the axial-vector-nucleon current, and the pion-nucleon coupling,  $g_{\pi NN}(Q^2)$ . These first calculations were based on an axial-vector nucleon vertex constructed from components that are necessary but not sufficient to ensure fulfillment of the axial-vector Ward-Takahashi identity for on-shell nucleons. Work on improvement is underway.

An article describing these results was published.<sup>1</sup>

\*Universität Rostock, Germany.

<sup>1</sup>A. Höll, C. D. Roberts, and S. V. Wright, AIP Conf. Proc. **857**, 46 (2006).

### a.8. Dynamical Chiral Symmetry Breaking and a Critical Mass (M. S. Bhagwat, C. D. Roberts, S. V. Wright, L. Chang,\* and Y.-X. Liu†)

Dynamical chiral symmetry breaking (DCSB) is the creation, via interactions with the gauge field alone, of a fermion mass gap: whose magnitude exceeds, perhaps by a great amount, the mass-scale in the action set by the fermion's bare mass; and which persists when that bare-mass-scale vanishes, namely, in the chiral limit. It is fundamentally important in strong interaction physics. For example, DCSB is responsible for the generation of large constituent-like masses for dressed-quarks in QCD. This is a longstanding prediction of Dyson-Schwinger equation (DSE) studies, which has recently been confirmed in numerical simulations of lattice-regularized QCD. DCSB is also the keystone in the realization of Goldstone's theorem through pseudoscalar mesons in QCD, and thereby the remarkably small value of the ratio of  $\pi$ - and  $\rho$ -meson masses, and the weak  $\pi\pi$  interaction at low energies. A large body of efficacious QCD phenomenology is built on an appreciation of the importance of DCSB. Nevertheless, not all facets of DCSB have been elucidated. We uncovered novel aspects of the interplay between explicit and dynamical chiral symmetry breaking.

On a bounded interval of current-quark mass,  $D(m) = \{m \mid 0 \leq m < m_{cr}\}$ , realistic models of QCD's gap equation can simultaneously admit two inequivalent dynamical chiral symmetry breaking (DCSB) solutions for the dressed-quark mass-function,  $M_{\pm}(p^2)$ , and a solution that is unambiguously connected with the realization of chiral symmetry in the Wigner mode,  $M_W(p^2)$ . The DCSB solutions are distinguished by their value at the origin:  $M_+(p^2) > 0$  and  $M_-(p^2) < 0$ . In the ultraviolet all three solutions coincide with the running current-quark mass.

The pointwise values of all solutions evolve continuously with current-quark mass within  $D(m)$ . However, things change at the upper boundary. The  $M_W$  solution, whose chiral limit value is perturbative in the coupling, becomes identical to the essentially nonperturbative solution  $M_-$  that is actually characteristic of DCSB. Moreover, both disappear for  $m > m_{cr}$ , a domain whereupon the current-quark mass is large enough to completely destabilize these solutions.

Only the positive  $M_+$  solution exists on this domain. Furthermore, we demonstrated that the upper boundary of  $D(m)$  also defines the radius of convergence for an expansion of  $M_+$  in current-quark mass around its DCSB chiral-limit form.

The pointwise values of all solutions evolve continuously with current-quark mass within  $D(m)$ . However, things change at the upper boundary. The  $M_W$  solution, whose chiral limit value is perturbative in the coupling, becomes identical to the essentially nonperturbative solution  $M_-$  that is actually characteristic of DCSB. Moreover, both disappear for  $m > m_{cr}$ , a domain whereupon the current-quark mass is large enough to completely destabilize these solutions. Only the positive  $M_+$  solution exists on this domain. Furthermore, we demonstrated that the upper boundary of  $D(m)$  also defines the radius of convergence for an expansion of  $M_+$  in current-quark mass around its DCSB chiral-limit form, see Fig. V-2.

Thus one has the coalescing of two qualitatively distinct solutions at  $m_{cr}$ , the persistence of only one essentially nonperturbative solution for  $m > m_{cr}$  plus the breakdown of a chiral expansion for this solution, and, as we also showed, the simultaneous loss of a well-defined mass-dependent quark condensate. This behavior supports an interpretation of  $m_{cr}$  as the upper bound on the domain within which a perturbative expansion of physical quantities in the current-quark mass around their chiral-limit values can uniformly be valid. In a phenomenologically efficacious renormalization-group-improved rainbow-ladder truncation of QCD's DSEs, the critical current-quark mass corresponds to a mass  $m_{cr} \sim 0.45$  GeV for a pseudoscalar meson constituted of equal mass current-quarks. (NB. Irrespective of the current-mass of the other constituent, a meson containing one current-quark whose mass exceeds  $m_{cr}$  is never within the domain of uniform convergence.) This scale also marks the boundary below which observables should exhibit that curvature as a function of pion-like pseudoscalar-meson mass which is characteristic of chiral effective theories. This work was published.<sup>1</sup>

\*Peking University, Beijing, China, †Peking University, Beijing, China; The Key Laboratory of Heavy Ion Physics, Ministry of Education, Beijing, China; Center of Theoretical Nuclear Physics, National Laboratory of Heavy Ion Accelerator, Lanzhou, China.

<sup>1</sup>L. Chang, Y.-X. Liu, M. S. Bhagwat, C. D. Roberts, and S. V. Wright, Phys. Rev. C **75**, 015201 (2007).

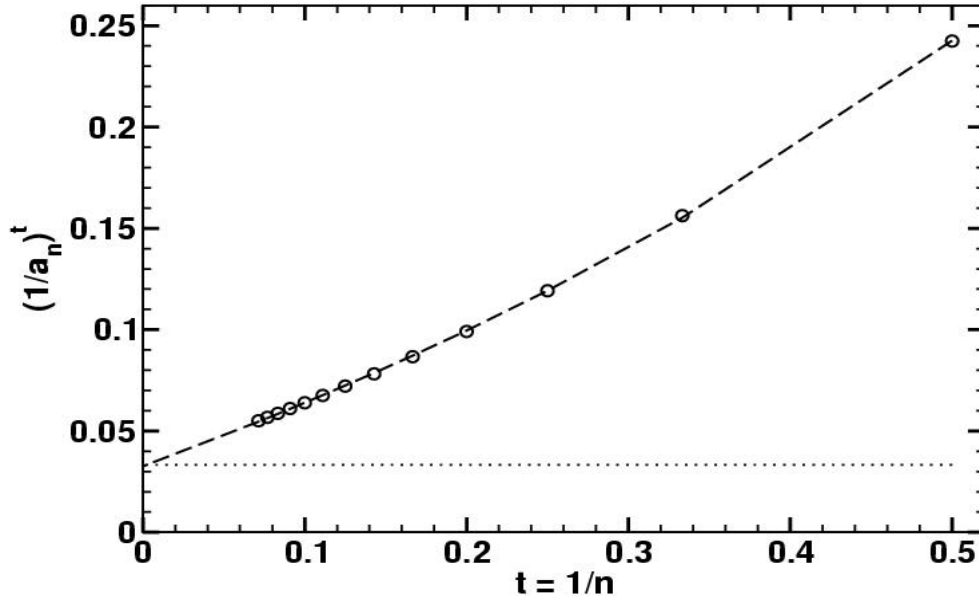


Fig. V-2. Reciprocal of the  $n$ -th roots of the coefficients in a chiral expansion of the DCSB solution,  $M_+$ , around  $m = 0$ , as a function of  $t = 1/n$ , where  $n$  is the order of the expansion. Dotted curve –  $m_{cr} = 0.033$  (in units of model's mass-scale). Dashed curve –  $[1,1]$  Padé approximant, from which one can infer the chiral expansion's radius of convergence; viz., the ordinate intercept.

### a.9. Studies of Meson Properties (M. S. Bhagwat, C. D. Roberts, S. V. Wright, A. Höll,\* A. Krassnigg,† and P. Maris‡)

We examined properties of pseudoscalar and scalar mesons using a practical and symmetry preserving truncation of QCD's Dyson-Schwinger equations.

One study<sup>1</sup> provided a comparison between properties of ground and radially excited mesons via a calculation of the dependence on current-quark mass of the masses and leptonic decay constants for these systems. We obtained, *e.g.*, predictions for the mass and leptonic decay constant of the first radial excitation of the kaon: namely,  $m_{K(1460)} = 1.52 \pm 0.12$  and  $f_{K(1460)} \sim 10 f_{\pi(1300)}$ , where  $\pi(1300)$  is the pion's first radial excitation; and the mass of the  $\chi_{c0}(2P)$  meson; viz., 3.88 GeV. Moreover, we found that up till the  $c$ -quark mass, the ordering of meson masses is

$$0^+(1S) < 0^{++}(1S) < 0^+(2S) < 0^{++}(2S).$$

In a related investigation<sup>2</sup> we recalled that it has been conjectured that DCSB notwithstanding, the properties of highly excited pseudoscalar and scalar mesons exhibit a pattern that is consistent with a Wigner

realization of chiral symmetry. These mesons appear as poles in QCD's inhomogeneous pseudoscalar and scalar vertex functions. Such poles are characterized in part by gauge-invariant residues. We argued that a unique signal of the truth of this conjecture is equality between the pole residues for  $0^+(nS)$  and  $0^{++}(nS)$  states when  $n$ , the radial quantum number, is large; *i.e.*,

$$\rho_{\pi^n} = \rho_{\sigma^n}, \text{ for } n \text{ large.}$$

We were also able to prove<sup>3</sup> that chiral symmetry and its dynamical breakdown in QCD place constraints on properties of mesons composed of two heavy-quarks, one of which is an identity relating the gauge invariant residues of these states in the inhomogeneous pseudovector and pseudoscalar vertex functions, mentioned above, in the heavy-quark limit; viz.,

$$\rho_{\pi^n}(QQ) = f_{\pi^n}(QQ) m_{\pi^n}(QQ) \text{ for } m_Q \rightarrow \infty.$$

In illustrating this identity, we established that the leptonic decay constants for vector and pseudoscalar

heavy-heavy mesons both increase linearly with current-quark mass on a domain that begins at approximately twice the  $c$ -quark mass. This is the result one would obtain for heavy-quarks bound by a Coulomb potential. It therefore suggests that the properties of truly heavy-heavy mesons are determined primarily by the one-gluon exchange potential in QCD and hence, importantly, they are not sensitive to the confinement potential.

Within a Poincaré covariant framework it makes sense to discuss quark orbital angular momentum since, while it is not a Poincaré invariant, if absent in a particular frame, it will inevitably appear in another frame related via a Poincaré transformation. This constraint and feature of covariance is the reason that the Bethe-Salpeter wavefunction for mesons (and the Faddeev

wavefunctions for baryons) is a matrix-valued function with a rich structure. We exhibited<sup>3</sup> the rest-frame angular momentum content of a pseudoscalar meson and its current-quark-mass-dependence. In the neighborhood of the chiral limit, there is a material  $L = 1$  component, which can be characterized by a mixing angle of  $35^\circ$ . The angle decreases with increasing current-quark mass. As measured by this mixing angle, at a given bound state mass the  $L = 1$  admixture is roughly 15% greater in the first radial excitation. However, measured as a function of current-quark mass, the situation is reversed: the angle in the excited state is approximately 1/2 that in the ground state and the ratio increases toward one with increasing current-quark mass. Figure V-3 illustrates these results, which are qualitatively model-independent.

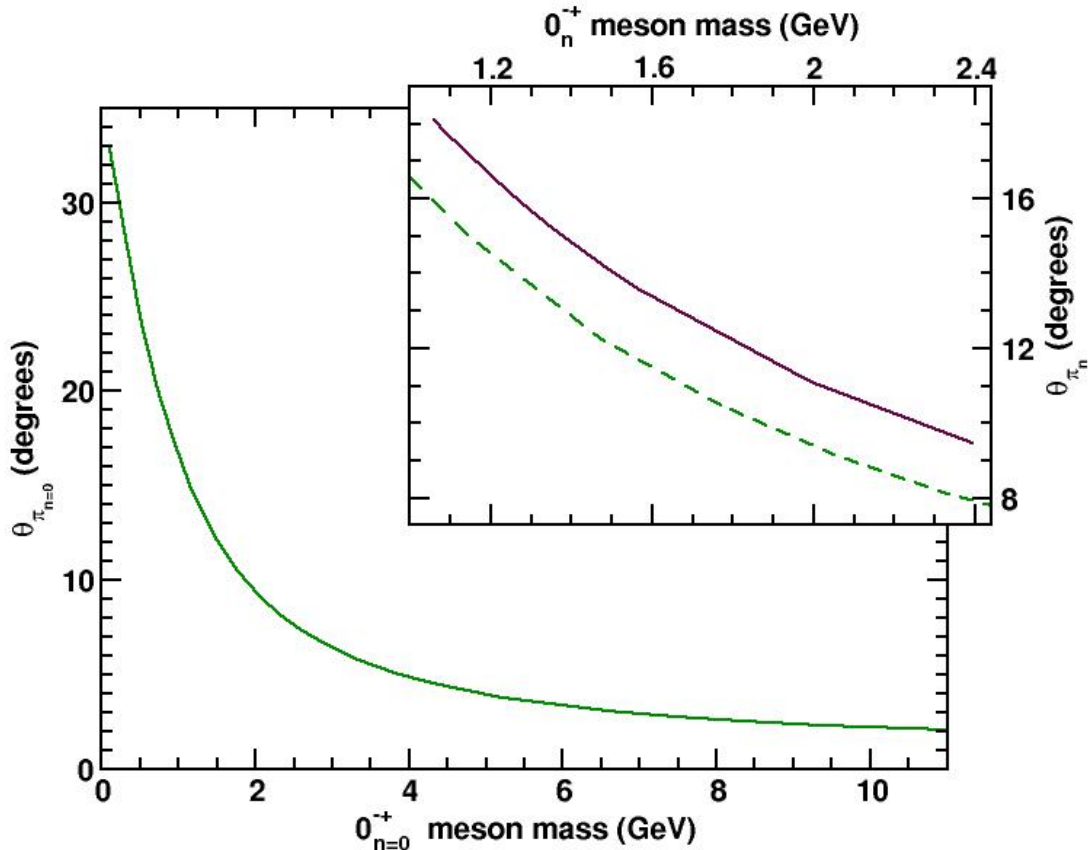


Fig. V-3. Main frame:  $\theta_{\pi,0}$ , which gauges the rest-frame admixture of  $L = 1$  components in the ground state  $O^+$  meson's Bethe-Salpeter wavefunction, plotted as a function of the meson's mass. Inset: Solid curve -- analogue,  $\theta_{\pi,1}$  for the first excited state; dashed curve,  $\theta_{\pi,0}$  for comparison. In the chiral limit the ground state pseudoscalar is naturally massless whereas the calculated mass of the first excited state is 1.04 GeV.

Studies such as we have described in this subsection and their refinement through comparison with extant and forthcoming data are an essential precursor to the

reliable prediction of properties of hybrid and exotic hadrons.

\*Universität Rostock, Germany, †Karl-Franzens-Universität Graz, Austria, ‡University of Pittsburgh.

<sup>1</sup>A. Krassnigg, C. D. Roberts, and S. V. Wright, *Int. J. Mod. Phys. A* **22**, 424 (2007).

<sup>2</sup>M. S. Bhagwat, A. Höll, A. Krassnigg, and C. D. Roberts, *Theory and Phenomenology of Hadrons*, *Nucl. Phys. A* **790**, 10 (2007).

<sup>3</sup>M. S. Bhagwat, A. Krassnigg, P. Maris, and C. D. Roberts, *Eur. Phys. J. A* **31**, 630 (2007).

### a.10. Schwinger Functions and Light-Quark Bound States (M. Bhagwat, C. D. Roberts, S. V. Wright, A. Höll,\* and A. Krassnigg†)

The probability measure plays a crucial role in quantum field theory. In Euclidean space a theory's generating functional can truly be expressed in terms of a probability measure and the properties of such measures make it likely that the rigorous definition of interacting quantum field theories is possible in that case. However, in Minkowski space the probability density becomes a probability *amplitude*, through the appearance of “ $i$ ” in the exponent, and that precludes the formulation of a measure theory.

The moments of a probability measure are  $n$ -point Schwinger functions. They correspond to vacuum expectation values of Euclidean fields and may loosely be termed Euclidean space Green functions. When certain conditions are met, analytic continuation of the Schwinger functions yields the Wightman functions and one may prove the reconstruction theorem; namely, the complete content of a quantum field theory is recovered from the Wightman functions. This is the basis for the contemporary belief that the evaluation of a theory's Schwinger functions is equivalent to solving that theory.

While that may be true in principle one must nonetheless develop practical means by which to extract physical information from the Schwinger functions. The challenge may be illustrated by noting that complete knowledge of a two-point Schwinger function in momentum space corresponds only to direct knowledge of the expectation value at spacelike momenta. A physical particle pole can only appear at timelike momentum. Locating such a pole therefore requires that all the conditions be met for a unique analytic continuation. If the Schwinger function is known only at a discrete set of points; *i.e.*, on a set of measure zero, then that is strictly impossible. In this common instance all that is really possible are

constrained inference and an estimation of the inherent error.

For us a context for these observations is the problem of determining the spectrum of QCD. Much has been learnt about the two-point Schwinger functions for quarks, gluons and ghosts. However, the pointwise behavior of the continuation of these functions to timelike momenta is uncertain. These two-point functions appear in the kernels of the Bethe-Salpeter equations whose solutions provide information about the properties of color-singlet hadrons. The study of ground state mesons in the pseudoscalar and vector channels has met with success. A present challenge is the extension to excited states in these and other channels, and to channels in which the ground state lies above 1 GeV. A veracious analytic continuation of two-point Schwinger functions becomes increasingly important as the bound-state mass becomes larger. The possibility that this continuation might be absent poses the question: can reliable information about bound state properties be obtained directly from the Schwinger functions?

Another context for this question is the numerical simulation of lattice-regularized QCD. That approach is grounded on the Euclidean space functional integral. Schwinger functions are all that it can directly provide. Hence, it can only be useful if methods are found so that the question can be answered in the affirmative.

We analyzed the capacity of Schwinger functions to yield information about bound states, and established that for the ground state in a given channel the mass and residue are accessible via rudimentary methods. When the mass-splitting between the first and second excited states is not significantly smaller than that between the ground and first excited states, these



methods may also reliably provide the same information about the first excited state, so long as the Schwinger function under consideration does actually possess the analytic properties assumed of it. However, simple methods cannot provide dependable information about more massive states in a given channel.

Indeed, there is no easy way to extract such information. An approach based on a correlator matrix can be successful but only if the operators are carefully constructed so as to have large overlap with states of interest in a given channel and statistical errors can be made small; *viz.*,  $\sim 1\%$ . While it is possible in principle to satisfy these constraints, doing so is labor intensive and time consuming. That is, nevertheless, justified in the absence of model-dependence.

We posed the question of whether, in the context of bound-state studies in which model assumptions are made regarding the nature of the long-range interaction between light quarks, labor can be saved and/or

accuracy gained by working solely with Schwinger functions. Our analysis suggested strongly that the answer is *no*. In their formulation the studies of this type explicitly define an analytic continuation of a model into the complex plane. Hence, all momenta are directly accessible. We saw clearly that it is not possible to avoid model artifacts by pretending ignorance of this. Thus, nothing is gained by solving a complex of DSEs for the Schwinger functions associated with numerous carefully tuned interpolating fields. Moreover, capitalizing on the feature that all momenta are directly accessible is the most efficient manner by which to test and improve the model input, and, thereby, to relate experimental data on bound state properties to information about the interaction between light quarks. This is further emphasized by the fact that because excited states are unstable they are characterized by complex pole positions.

An article describing this work was accepted for publication.<sup>1</sup>

\*Universität Rostock, Germany, †Karl-Franzens-Universität Graz, Austria.

<sup>1</sup>M. Bhagwat, A. Höll, A. Krassnigg, C. D. Roberts, and S. V. Wright, *Few Body Systems* **40**, 209 (2007).

### a.11. Nucleon Electromagnetic Form Factors (J. Arrington, M. Bhagwat, C. D. Roberts, A. Höll,\* A. Krassnigg,† and J. M. Zanotti‡)

Elastic electromagnetic nucleon form factors have long provided vital information about the structure and composition of these most basic elements of nuclear physics. The form factors are a measurable and physical manifestation of the nature of the nucleons' constituents and the dynamics that binds them together. Accurate form factor data obtained in recent years using modern experimental facilities has spurred a significant re-evaluation of the nucleon and pictures of its structure; *e.g.*, the role of quark orbital angular momentum, the scale at which perturbative QCD effects should become evident, the strangeness content, and meson-cloud effects. In a review article, we provided a succinct survey of the experimental studies and theoretical interpretation of nucleon electromagnetic form factors.<sup>1</sup>

As described therein, a modern approach to the study of baryons is based on a Poincaré covariant Faddeev equation, which may be viewed as one of the collection of DSEs and an analogue of the Bethe-Salpeter equation that is well-suited to the study of mesons. A merit of the Poincaré covariant Faddeev equation is that a veracious understanding of the structure of dressed-

quarks and -gluons is straightforwardly incorporated; namely, effects owing to and arising from the strong momentum-dependence of these propagators are realized and exhibited. This momentum-dependence, which explains, *e.g.*, the connection between constituent- and current-quark masses, was predicted by Dyson-Schwinger equation studies.

However, the study of baryons using this approach is not at a level of sophistication comparable to that of mesons. It is actually at roughly the same stage as was the study of mesons more than a decade ago; namely, model-building and phenomenology constrained and informed by the best available hadron physics theory.

Notwithstanding this, important predictions are being made. For example, Fig. V-4 shows the calculated<sup>2</sup> ratio

$$\mu_n G_{En}(Q^2)/G_{Mn}(Q^2).$$

(NB. The analogous proton ratio was calculated earlier and it passes through zero at  $Q^2 \approx 6.5 \text{ GeV}^2$ . This is a prediction that will soon be tested by experiment at JLab.) For the neutron, it is noteworthy that in the

neighborhood of  $Q^2 = 0$

$$\mu_n G_{En}(Q^2)/G_{Mn}(Q^2) = -(r_n^2/6) Q^2,$$

where  $r_n^2$  is the neutron's mean-square electric radius. Our calculation shows this to be a good approximation for  $|r_n^2| Q^2 < 1$ , a result which is consistent with the data. The calculated curve omitted pion-loop effects

from the current and therefore underestimated the magnitude of  $r_n^2$ . This is apparent in the figure. It is thus evident that, just as we found in earlier studies of the proton, the small  $Q^2$  behavior of this ratio is materially affected by the neutron's pion cloud.

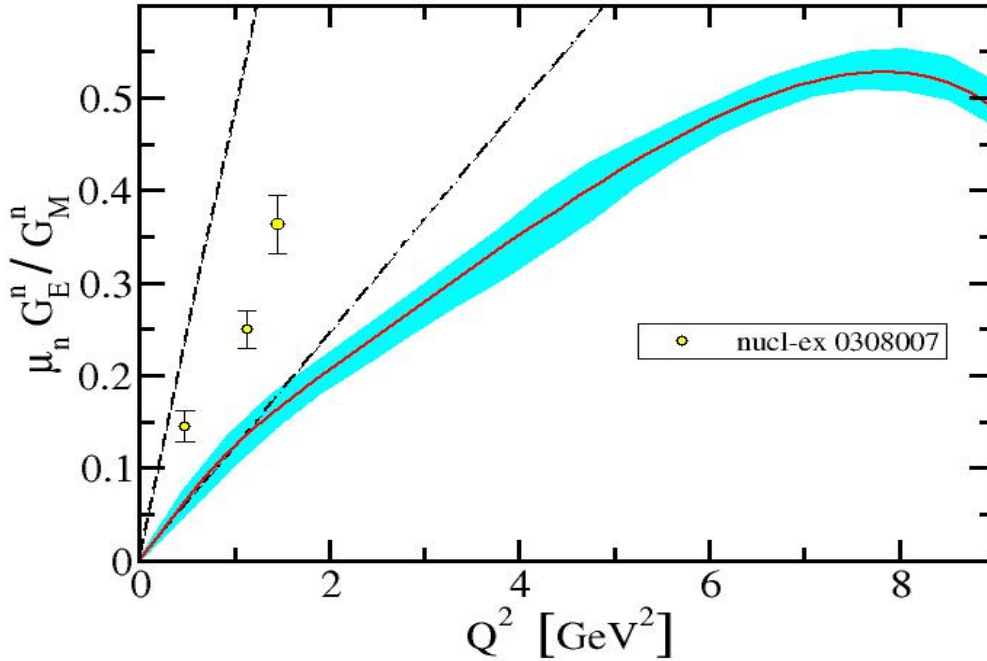


Fig. V-4. Solid curve – calculated result for  $\mu_n G_{En}(Q^2)/G_{Mn}(Q^2)$ . The band shows the response of the ratio to changes in model parameters and also reflects Monte Carlo -integration error. Dashed curve –  $|r_n^2/6|_{\text{expt.}} Q^2$ ; dash-dot curve –  $|r_n^2/6|_{\text{calc.}} Q^2$ . Data from R. Madey et al., *Phys. Rev. Lett.* **91**, 122002 (2003).

Pseudoscalar mesons are not pointlike and, therefore, their contributions to form factors diminish in magnitude with increasing  $Q^2$ . It follows, therefore, that the evolution of  $\mu_n G_{En}(Q^2)/G_{Mn}(Q^2)$  on  $Q^2 > 2$   $\text{GeV}^2$ , is primarily determined by the quark-core of the neutron. This calculation predicts that the ratio will continue to increase steadily until  $Q^2 > 8$   $\text{GeV}^2$ , which is a very different result to that for the proton. Data from JLab that is currently being analyzed will test this prediction out to  $Q^2 > 3.5$   $\text{GeV}^2$ .

In developing an understanding of these results, we returned to the observation that in a Poincaré covariant treatment the quark core of a nucleon is necessarily described by a Faddeev amplitude with nonzero quark

orbital angular momentum. This is why the amplitude is a matrix-valued function with a rich structure that, in a baryons' rest frame, corresponds to a relativistic wavefunction with  $s$ -wave,  $p$ -wave and even  $d$ -wave components. The figure illustrates that while there is some quantitative sensitivity to the model parameters, the gross features of the form factors are primarily governed by correlations expressed in the nucleon's Faddeev amplitude and, in particular, by the amount of intrinsic quark orbital angular momentum. The nature of the kernel in the Faddeev equation specifies just how much quark orbital angular momentum is present in a baryon's rest frame.

\*University of Rostock, Germany, †Karl-Franzens-Universität Graz, Austria, ‡University of Edinburgh, United Kingdom.

<sup>1</sup>J. Arrington, C. D. Roberts, and J. M. Zanotti, *J. Phys. G* **34**, S23-S52 (2007).

<sup>2</sup>M. S. Bhagwat, A. Höll, A. Krassnigg, and C. D. Roberts, *Theory and Phenomenology of Hadrons*, *Nucl. Phys.* **A790**, 10 (2007).

### a.12. Semileptonic Decays of Heavy $\Omega$ Baryons in a Quark Model (M. Pervin, W. Roberts\* and S. Capstick\*)

The semileptonic decays of  $\Omega_c$  and  $\Omega_b$  baryons were treated in the framework of a constituent quark model. The form factors as well as the rates for the semileptonic heavy  $\Omega$  decays were calculated within this model.

Analytic formulae were obtained for the form factors of  $\Omega_b$  in the decays to ground states and a number of excited states of  $\Omega_c$ . A modified fit of non-relativistic and semirelativistic Hamiltonians generated configuration-mixed baryon wavefunctions from the known masses and the measured  $\Lambda_c^+ \rightarrow \Lambda e^+ \nu$  rate, with wavefunctions expanded in both harmonic oscillator

and Sturmian bases. We obtained general agreement with the leading-order constraints of heavy-quark effective theory. Using these configuration-mixed wavefunctions, the decay rates for  $\Omega_b$  to pairs of ground and excited  $\Omega_c$  states related by heavy-quark symmetry are, to a good approximation, in the ratios expected from heavy-quark effective theory. We also calculated numerous branching ratios for other decay modes; e.g.,  $\Omega_c \rightarrow \Omega$ , and provided evidence that our results have only modest model-dependence.

An article describing these results was published.<sup>1</sup>

\*Florida State University.

<sup>1</sup>M. Pervin, W. Roberts, and S. Capstick, *Phys. Rev. C* **74**, 025205 (2006).

### a.13. $\Xi$ Baryons in a Constituent Quark Model (M. Pervin and W. Roberts\*)

The study of hyperon properties can provide important insight into two questions of crucial interest in hadron physics; *viz.*, what are the relevant degrees of freedom in a baryon; and what is the mechanism of confinement? In order to understand the symmetries and dynamics of the strong interaction, the expected multiplet structure of the baryons must be established experimentally. For this, details of their excitation spectrum are crucial.

In this work we studied the multistrange ( $\Xi$ s and  $\Omega$ s) baryon spectrum using a non-relativistic quark model. The experimentally known states [ $\Xi(1318)$ ,  $\Xi(1530)$ ,  $\Xi(1823)$ ,  $\Omega(1672)$ ] are well reproduced by our model, while we predicted the mass and spin-parity assignments for a number of the less-well-known states, such as the  $\Xi(1690)$ . The predictions for the spin-parity of multistrange baryons are very useful since, even for the “well-known” states, many of the quantum numbers have still not been measured.

\*Florida State University.

### a.14. Dynamical Coupled-Channel Model of $\pi N$ Scattering in the $W \leq 2$ GeV Nucleon Resonance Region (T.-S. H. Lee, B. Julia-Diaz,\* A. Matsuyama,† and T. Sato‡)

As a first step to analyze the electromagnetic meson production reactions in the nucleon resonance region, the parameters of the hadronic interactions of a dynamical coupled-channel model, developed in Ref. 1, are determined by fitting the  $\pi N$  scattering data up to

invariant mass  $W = 2$  GeV. The channels included in the calculations are  $\pi N$ ,  $\eta N$  and  $\pi\pi N$  which has  $\pi\Delta$ ,  $\rho N$ , and  $\sigma N$  resonant components. The non-resonant meson-baryon interactions of the model are derived from a set of Lagrangians by using a unitary

transformation method. One or two bare excited nucleon states in each of S, P, D, and F partial waves are included to generate the resonant amplitudes in the fits. The predicted total cross sections of  $\pi N$  reactions and  $\pi N \rightarrow \eta N$  reactions are in good agreement with the

data.

Some of our results are shown in Figs. V-5 and V-6 for the  $\pi N$  amplitudes and in Fig.V-7 for the predicted total cross sections.

\*University of Barcelona, Spain, †Shizuoka University, Japan, ‡Osaka University, Japan.  
<sup>1</sup>A. Matsuyama, T. Sato, and T.-S. H. Lee, Physics Reports **439**, 193 (2007).

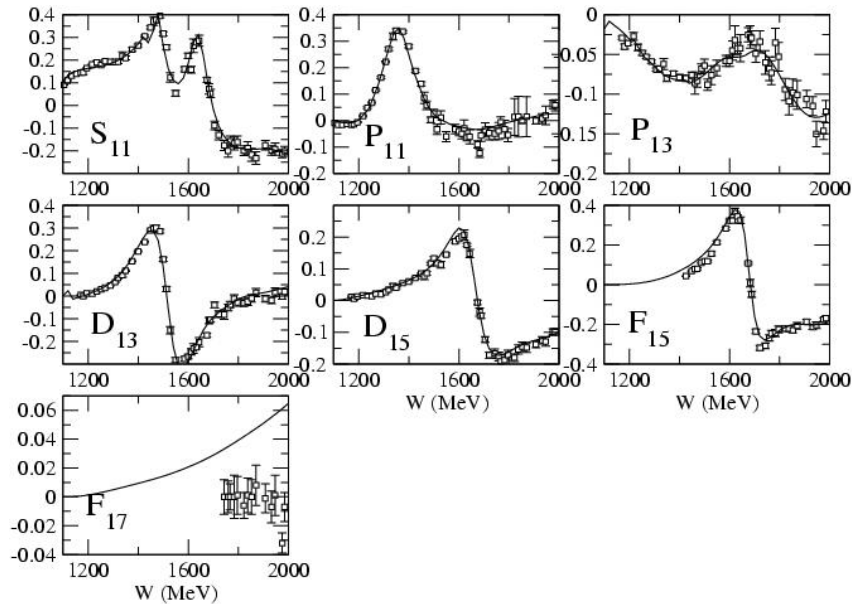


Fig. V-5. Real parts of the calculated  $\pi N$  partial wave amplitudes of isospin  $T = 1/2$  are compared with the energy independent solutions of SAID.

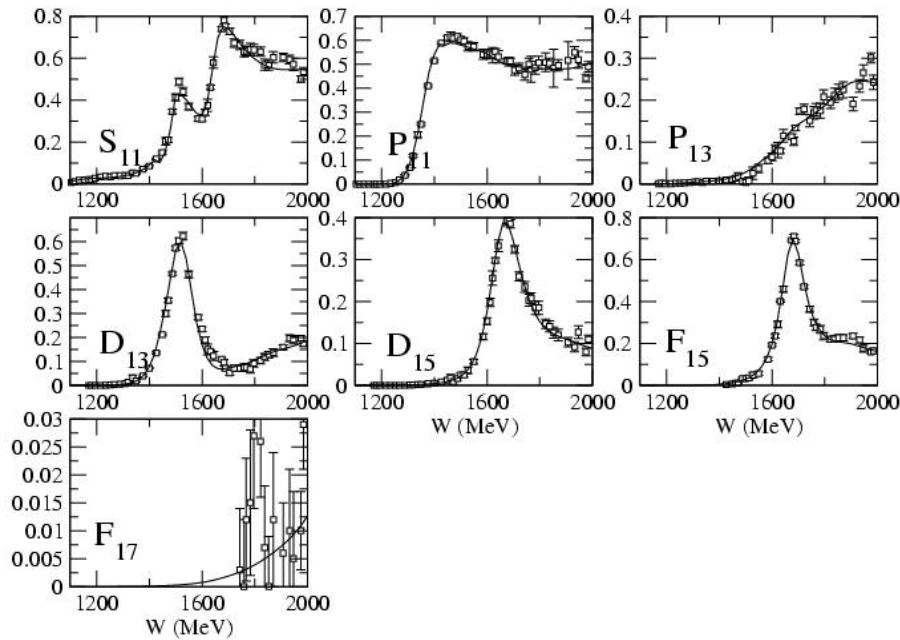


Fig. V-6. Imaginary parts of the calculated  $\pi N$  partial wave amplitudes of isospin  $T = 1/2$  are compared with the energy independent solutions of SAID.

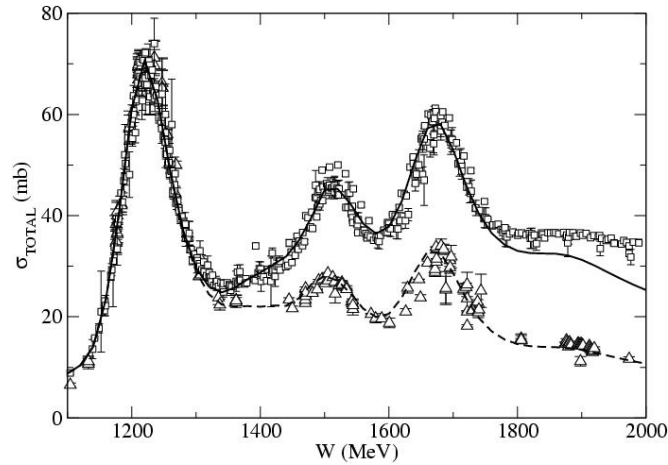


Fig. V-7. The predicted total cross sections of the  $\pi^- p \rightarrow X$  (solid curve) and  $\pi^- p \rightarrow \pi^- p + \pi^0 n$  (dashed curve) reactions are compared with the data.

#### a.15. Extraction and Interpretation of $\gamma N \rightarrow \Delta$ Form Factors within a Dynamical Model (T.-S. H. Lee, B. Julia-Diaz,\* T. Sato,† and C. Smith§)

Within the dynamical model of Ref. 1 we have performed an analysis of recent data of pion electroproduction reactions at energies near the  $\Delta(1232)$  resonance. Figure V-8 shows the extracted  $Q^2$ -dependence of the meson cloud effects on the magnetic  $\gamma N \rightarrow \Delta$  transition form factor. We have

found that the extracted bare form factor (dashed curve) is close to the predictions of relativistic constituent quark models. The predictions from the lattice QCD calculations are only in very qualitative agreement with the extracted dressed form factors (solid curves).

\*University of Barcelona, Spain, †Osaka University, Japan, §University of Virginia.

†T. Sato and T.-S. H. Lee, Phys. Rev. C **54**, 2660 (1996); Phys. Rev. C **63**, 055201 (2001).

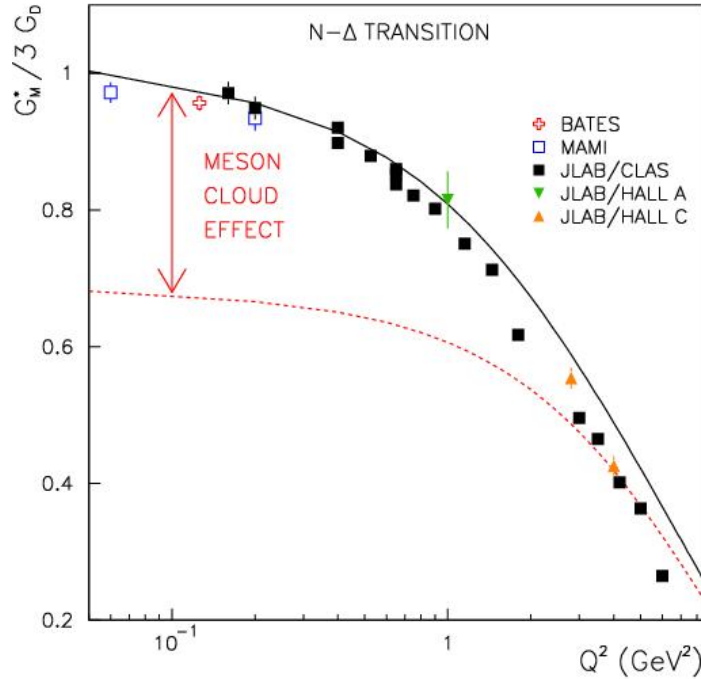


Fig. V-8. The extracted magnetic  $\gamma N \rightarrow \Delta$  transition form factors.

#### a.16. Dynamical Coupled-Channel Analysis of $\pi$ Electroproduction (T.-S. H. Lee, B. Julia-Diaz,<sup>\*</sup> A. Matsuyama,<sup>†</sup> T. Sato,<sup>‡</sup> and C. Smith<sup>§</sup>)

With the  $\pi N$  model constructed in Section a.14, we are now investigating  $\pi$  electroproduction reactions within the dynamical coupled-channel model of Ref. 1. The main focus is to extract the  $\gamma N \rightarrow N^*$  form factors for testing the predictions from QCD-inspired hadron models and lattice QCD. As a first step, we have predicted the meson cloud effects on  $\gamma N \rightarrow N^*(1440)$  form factors. Comparing with the empirical values extracted by the CLAS collaboration, we have found that meson cloud effects account for about 30% for the

Roper  $N^*(1440)$  resonance. The importance of the coupled-channel off-shell effects at short distances has been demonstrated.

Our current effort is to determine the  $\gamma N \rightarrow N^*$  form factors for all of the known low-lying  $N^*$  with mass below 1.6 GeV. This is being done by developing a code to fit the differential cross section data of all of the available data of  $p(e, e'\pi^0)p$  and  $p(e, e'\pi^+)n$  reactions in the  $W = 1.1-1.7$  GeV and  $Q^2 = 0-6$  (GeV/c)<sup>2</sup> region.

<sup>\*</sup>University of Barcelona, Spain, <sup>†</sup>Shizuoka University, Japan, <sup>‡</sup>Osaka University, Japan, <sup>§</sup>University of Virginia.

<sup>1</sup>A. Matsuyama, T. Sato, and T.-S. H. Lee, Physics Reports **439**, 193 (2007).

#### a.17. Speed-Plot and Time-Delayed Methods for Extracting Resonance Parameters (T.-S. H. Lee, O. Suzuki,<sup>\*</sup> and T. Sato<sup>\*</sup>)

Speed-plot method proposed by Hohler and Time-delayed method originated from Wigner have been commonly used to extract the resonance parameters from the empirical partial-wave amplitudes. However, the validity of these methods for the coupled-channel

cases have not been well investigated. Within several exactly soluble models, we reveal that these two methods give poles on different Riemann sheets and clarify the conditions under which we can safely apply these methods. We are currently applying these

methods to extract the poles from the  $\pi N$  scattering amplitudes generated from the dynamical coupled-channel model described in Section a.14. We are also

developing theoretical interpretations of the extracted poles; in particular on their relations with the predictions from hadron models and lattice QCD.

---

\*Osaka University, Japan.

**a.18. On the Sign of the  $\pi$ - $\rho$ - $\omega$  Coupling Constant** (T.-S. H. Lee, K. Nakayama,\* Y. Oh,\* and J. Haidenbauer†)

It is shown that the relative sign between the  $NN\omega$  and  $\pi\rho\omega$  coupling constants can be determined most sensitively from  $\omega$  production processes in  $NN$  collisions. Our results from a distorted-wave impulse approximation calculation are shown in Fig. V-9. Clearly, the recent data favor the sign of the  $\pi\rho\omega$

coupling constant which is opposite to that inferred from studies of the photoproduction reaction in combination with the vector meson dominance assumption. We are currently investigating the consequences of our results in predicting the  $\omega$  photoproduction reactions.

---

\*University of Georgia, †Jülich Research Center, Germany.

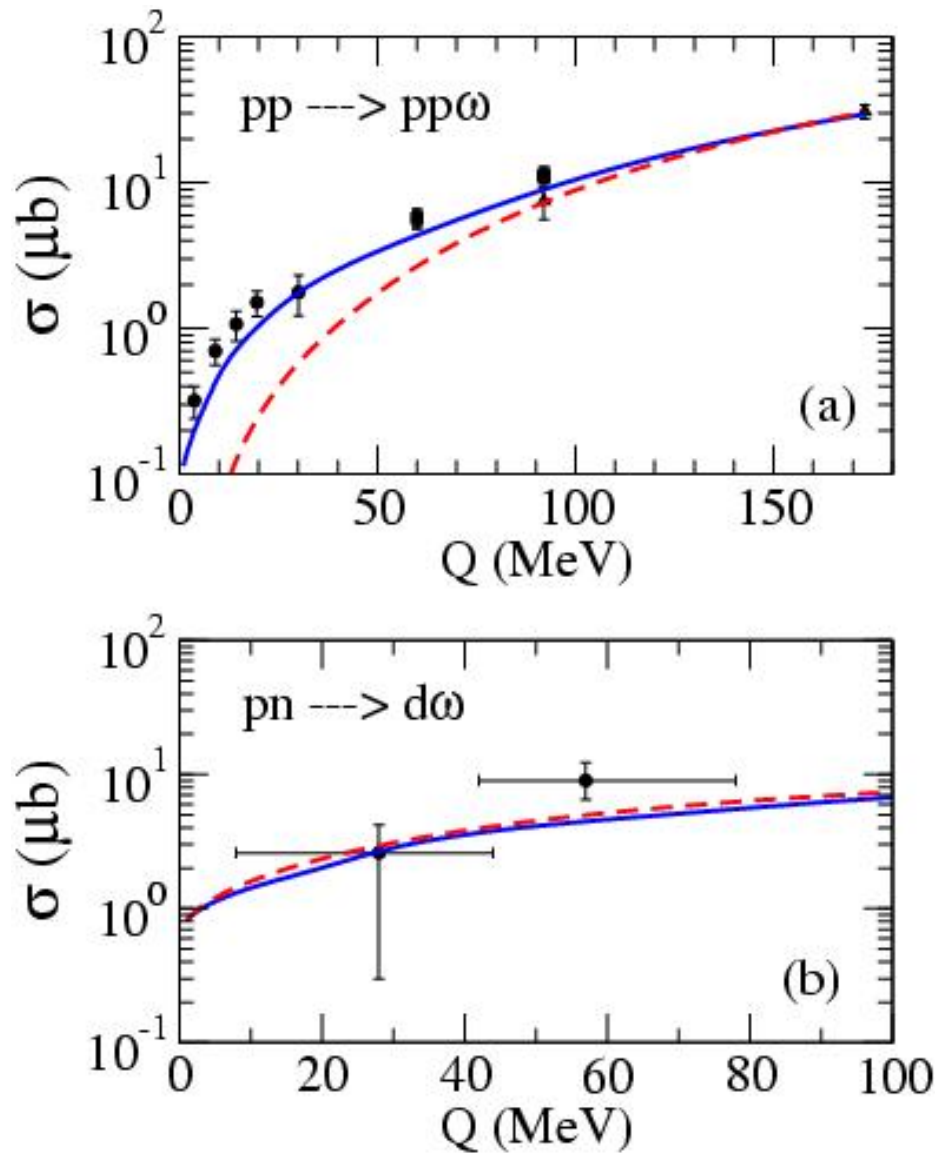


Fig. V-9. Total cross sections of  $\omega$  production in NN collisions. The dashed curves are from the calculations using the sign of  $\pi$ - $\rho$ - $\omega$  coupling conventionally determined by using the vector meson dominance assumption. The solid curves are obtained when the opposite sign is chosen.



## B. NUCLEAR FORCES AND NUCLEAR SYSTEMS

The goal of this program is to achieve a description of nuclear systems ranging in size from deuterium and tritium to nuclear matter and neutron stars using a single parameterization of the nuclear forces. Aspects of our program include both the construction of two- and three-nucleon potentials and the development of many-body techniques for computing nuclear structure and reactions with these interactions. Detailed quantitative, computationally-intensive studies are essential parts of this program.

Quantum Monte Carlo (QMC) calculations of light ( $A \leq 12$ ) nuclei with realistic interactions have been the main focus of our recent efforts. Our nonrelativistic Hamiltonian contains the accurate Argonne  $v_{18}$  two-nucleon ( $NN$ ) potential, which includes charge-independence breaking terms, and either the Urbana IX three-nucleon ( $NNN$ ) potential, or one of several Illinois  $NNN$  models. The QMC calculations include both variational (VMC) and Green's function (GFMC) methods. We begin with the construction of variational trial functions based on sums of single-particle determinants with the correct total quantum numbers, and then act on them with products of two- and three-body correlation operators. Energy expectation values are evaluated with Metropolis Monte Carlo integration and parameters in the trial functions are varied to minimize the energy. These optimized variational wavefunctions can then be used to study other nuclear properties. They also serve as a starting point for the GFMC calculations, which systematically remove higher excited-state components from the trial wavefunctions by propagation in imaginary time.

We are currently studying all  $A \leq 10$  nuclei, including more than 100 ground or excited states, as well as  $^{12}\text{C}$ . These are the first calculations to treat  $A \geq 6$  nuclei directly with realistic  $NN$  and  $NNN$  interactions. In GFMC calculations, with our best Hamiltonian, we can reproduce most of the experimental ground- and excited-state energies to within  $0.6$  MeV.

Many excited states in the light nuclei are not particle stable and should be treated as scattering states, though until recently our efforts treated all of them as bound. A major effort was made in the last two years to extend our GFMC program to nucleon-nucleus scattering, and results for  $^5\text{He}$ , or  $n\alpha$  scattering are in press. These results demonstrate that we can make *ab-initio* calculations of the low-energy scattering cross section, and extract resonance energies and widths.

A new effort this year is to calculate electroweak M1, E2, and GT transition matrix elements in light nuclei. In previous years we had examined a number of transitions and form factors using VMC trial functions, but now we have developed the machinery to use the full GFMC propagated wavefunctions. Initial results have been obtained for a dozen transitions in  $A = 6, 7$  nuclei and good agreement with experiment is obtained in most cases. A major long term goal of the scattering and transition efforts is to use GFMC wavefunctions to predict reaction cross sections for astrophysics as part of the Theory Group's nuclear astrophysics effort.

We used our VMC wavefunctions to investigate the two-nucleon momentum distributions in ground states of light  $A \leq 8$  nuclei as a function of the relative and center-of-mass momenta. We find an order-of-magnitude difference in the number of  $np$  and  $pp$  pairs with relative momenta

above  $1.5 \text{ fm}^{-1}$  when they have vanishing total momentum. This prediction can be tested in two-nucleon knockout electron-scattering experiments at JLab.

We also continued a systematic survey of cluster form factors and spectroscopic factors in the light  $p$ -shell nuclei using VMC wavefunctions. The correlations in these wavefunctions can provide significant quenching of spectroscopic factors compared to traditional shell-model calculations. A specific application was made for a new ( $d, {}^3\text{He}$ ) experiment run at ATLAS. The calculated cluster form factors are used as input to the distorted-wave Born approximation (DWBA) program PTOLEMY, developed here many years ago, to provide the theoretical analysis of the experiments. We are also providing overlap calculations to experimental groups at MSU and TRIUMF.

Calculations with order 1% accuracy of the rms radii of helium isotopes are needed for comparison to experiment but had proven impossible to achieve. This year we made considerable progress in solving this problem and have provided a prediction for a measurement of the  ${}^8\text{He}$  charge radius being made by Argonne experimentalists at GANIL.

A simple but useful guide for understanding the structure of light nuclei was formulated, based on counting the number of interacting pairs in different spin-isospin states for a given spatial symmetry and estimating the overall binding according to the spin-isospin operator expectation value taken from one-pion exchange. The overall binding of light nuclei, various aspects of their excitation structure, and clustering characteristics are all given a simple physical interpretation. This model correlates many of the results from our detailed QMC calculations of the last several years.

The influence of changes of fundamental physical constants on properties of nuclei is of considerable interest. We are studying how nuclear binding energies might change if the underlying nucleon and meson masses vary. This is done by making appropriate modifications of the nuclear Hamiltonian and carrying out VMC calculations for  $A \leq 8$  nuclei. The specific predictions from DSE studies of how the hadron masses vary with the current-quark mass can be used as input, and in turn, the output may be used in astrophysical rate calculations to examine the consequences for primordial nucleosynthesis. These studies may also provide some useful insight into contemporary efforts to extract nucleon-nucleon scattering from lattice QCD calculations.

### **b.1. Quantum Monte Carlo Calculations of Light Nuclei Energies** (S. C. Pieper, R. B. Wiringa, K. M. Nollett, and J. Carlson\*)

We have been studying the ground states and excitation spectra of light nuclei as  $A$ -body problems with realistic nucleon-nucleon ( $NN$ ) and three-nucleon ( $NNN$ ) interactions using advanced quantum Monte Carlo (QMC) many-body methods. Our preferred Hamiltonian contains the Argonne  $v_{18}$   $NN$  potential (AV18), which gives an excellent fit to elastic  $NN$  scattering data and deuteron properties, and the Illinois-2  $NNN$  potential (IL2), which we have fit to binding

energies of  $A \leq 8$  nuclei. The QMC methods include both variational Monte Carlo (VMC), which gives an initial approximate solution to the many-body Schrodinger equation, and Green's function Monte Carlo (GFMC), which systematically improves on the VMC starting solution. The GFMC method produces absolute binding energies that are accurate at the 1-2% level.

The VMC calculations begin with the construction of an antisymmetric Jastrow trial wavefunction that includes single-particle orbits coupled to the desired  $JM$  values of the state of interest as well as pair and triplet correlations. A symmetrized product of two- and three-body spin, isospin, and tensor correlation operators (induced by the  $NN$  and  $NNN$  potentials) is applied to the Jastrow product to produce the full trial function. The wavefunction is diagonalized in the small basis of different spatial symmetry components to project out multiple states with the same quantum numbers.

In GFMC calculations an imaginary-time propagator,  $\exp[-(H-E_0)\tau]$ , where  $H$  is the Hamiltonian,  $E_0$  is an estimate of the eigenvalue, and  $\tau$  is the imaginary time, is applied to the VMC trial function. The excited-state components of the trial function are damped out for large  $\tau$ , leaving the exact lowest eigenfunction with the quantum numbers of the input VMC trial function. The expectation value of  $H$  is computed for a sequence of increasing values of  $\tau$  to determine the convergence.

In 2006 we started work on new versions of the Illinois  $NNN$  potentials. The IL2 parameters we currently use were published in 2001. Since then we have made a

\*Los Alamos National Laboratory.

## b.2. Scattering Methods for Quantum Monte Carlo Calculations (K. M. Nollett, S. C. Pieper, R. B. Wiringa, J. Carlson,\* and G. M. Hale\*)

Our calculations of properties of light nuclei have concentrated on energies of discrete levels, because the quantum Monte Carlo methods have until recently required that unbound states be treated as bound states. We have, therefore, been restricted to bound or narrow states, and unable to compute the widths of resonances. A smaller amount of effort has gone into computing transition probabilities and radiative-capture cross sections using VMC wavefunctions, along with calculations of a few static nuclear properties like RMS radii.

It is desirable to expand the range of the QMC methods to include unbound states treated as such and the computation of phase shifts and reaction cross sections. This will greatly expand the number of observables against which the computational methods and potentials can be tested. It will also open the door to accurate quantitative predictions of reaction cross sections for astrophysics, at least in the light systems important for solar neutrinos, big-bang nucleosynthesis, and seeding

number of improvements in the GFMC propagation and, with the improvements in computer speeds, are routinely doing calculations with much better statistics. This has revealed some difficulties in the IL2 parameters, particularly for  ${}^8\text{He}$ . We are also including  $A = 9$  and  $10$  nuclei in the fitting procedure for the first time. This work is still in progress.

We are part of the "Universal Nuclear Energy-Density Functional" collaboration in the DOE SciDAC program. Most of our work in that will be concerned with changes to the GFMC program to enable efficient  ${}^{12}\text{C}$  calculations on parallel computers with 10,000's of processors. With other groups we will be making benchmark calculations of  ${}^{12}\text{C}$  and other nuclei using various Hamiltonians. The first bench marks will be for  ${}^{4,6,8}\text{He}$  and  ${}^6\text{Li}$  using just a two-nucleon potential. However, realistic  $NN$  potentials do not bind  ${}^{6,8}\text{He}$  without the addition of a  $NNN$  potential. To get around this difficulty, we have made small modifications to the  ${}^3\text{P}$  components of the Argonne  $v_8'$  and a  $v_8'$  projection of the super-soft-core C potential so that the  ${}^{6,8}\text{He}$  and  ${}^6\text{Li}$  separation energies are close to the experimental values. A subroutine for these potentials is available at <http://www.phy.anl.gov/theory/research/av18/>.

the r-process in alpha-rich freeze-out.

We are developing methods to compute unbound states, using an R-matrix-like boundary condition to specify the state being computed. As a first application, we have computed low-energy phase shifts in the first three partial waves in  ${}^4\text{He}$ -neutron scattering.<sup>1</sup> In VMC, the boundary condition is set as a condition on the correlation between the  ${}^4\text{He}$  nucleus and the last neutron. In GFMC, the boundary condition is enforced through a method of images that enforces a specified logarithmic derivative in the wavefunction normal to a specified surface of fixed  ${}^4\text{He}$ -n separation ( $9\text{ fm}$  in most of our calculations). Useful calculations require an accuracy of about  $50\text{ keV}$  or better. This in turn requires careful work to eliminate dependence of the result on the GFMC path constraint, the starting wavefunction, and the radius at which the boundary condition is imposed.

Results after carefully controlling these sources of error

are shown in Fig. V-10 below for the  $J^\pi = 3/2^-$  and  $J^\pi = 1/2^-$   $p$ -wave and the  $J^\pi = 1/2^+$   $s$ -wave scattering partial waves. The results for three different choices of potential demonstrate the importance of the three-nucleon interaction in this system: the AV18 two-nucleon interaction alone provides less splitting between the  $p$ -waves than observed, while including the most up-to-date three-nucleon interaction

(Illinois-2) produces good agreement with measured phase shifts.

This work opens the door to several additional calculations in light nuclei, particularly neutron resonances, states in  ${}^4\text{H}$ , and the  ${}^7\text{Be}(p,\gamma){}^8\text{B}$  radiative capture reaction.

\*Los Alamos National Laboratory.

<sup>1</sup>K. M. Nollett, S. C. Pieper, R. B. Wiringa, J. Carlson, and G. M. Hale, Phys. Rev. Lett. **99**, 022502 (2007).

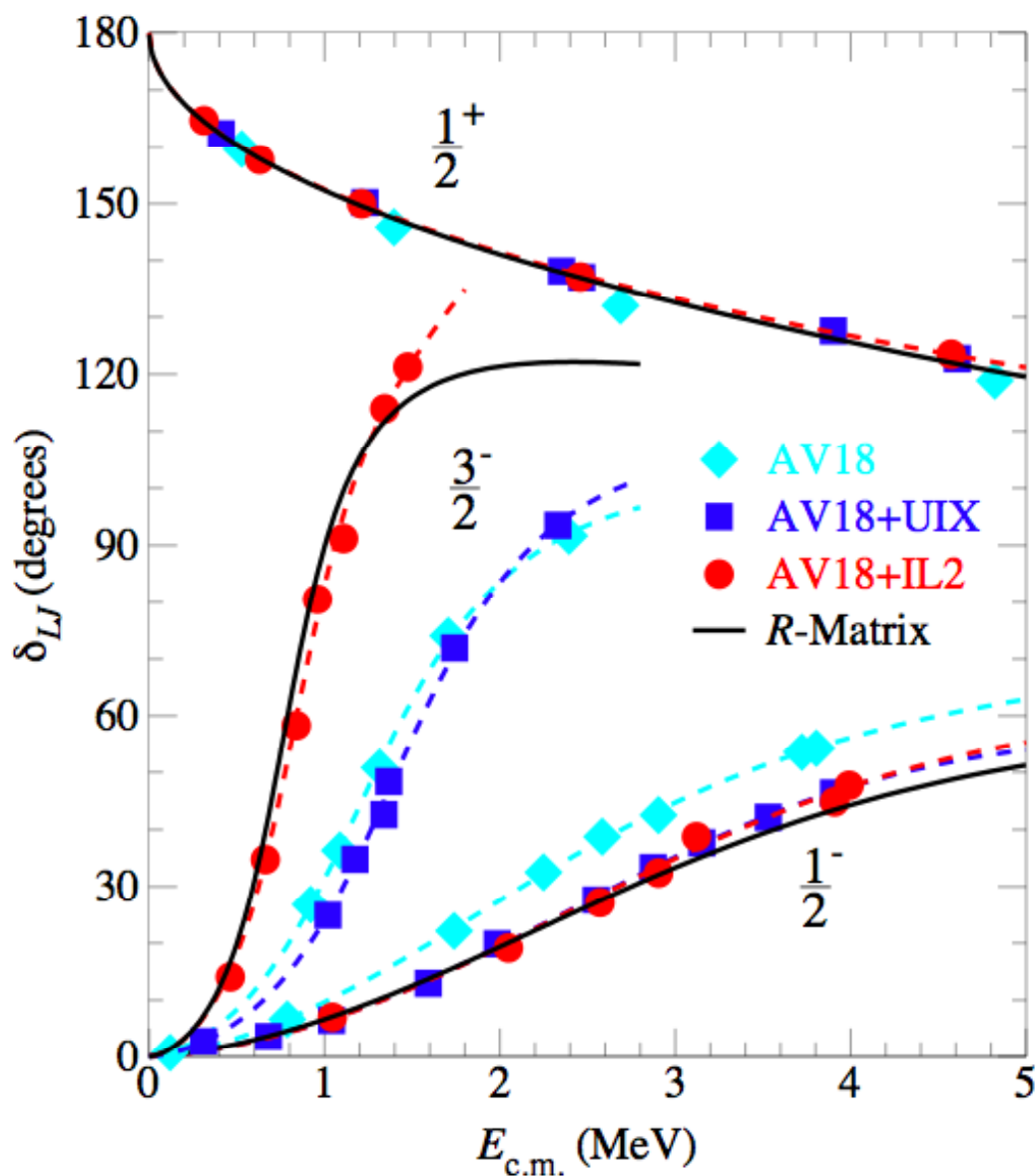


Fig. V-10. Phase shifts for  ${}^4\text{He}$ -neutron scattering with three different potentials, broken down by partial wave. Solid curves are an R-matrix fit to the measured cross sections. Filled symbols joined by dashed curves are results of GFMC calculations.

### b.3. Spectroscopic Factors and Cluster Form Factors of Light Nuclei (R. B. Wiringa, S. C. Pieper, and D. Kurath)

The cluster form factor is defined as the overlap between  $A$ -body and  $(A-1)$ -body nuclear states, either in configuration or momentum space,  $\langle (A-1)_J | a_j | A_J \rangle$ , where  $a_j$  is a nucleon annihilation operator. It is a very useful quantity in analyzing pickup reactions such as  $(p,d)$ , where  $A_J'$  is a ground state, or stripping reactions such as  $(d,p)$ , where  $(A-1)_J$  is a ground state, or nucleon-knockout reactions such as  $(e,e'p)$ . The cluster form factor can be folded into a DWBA calculation to help extract experimental information. The spectroscopic factor  $S$  is just the normalization of this wavefunction overlap, and provides a simple characterization of nuclear structure aspects of such reactions.

We have been calculating the cluster form factors and spectroscopic factors for all  $A \leq 10$  nuclei using VMC wavefunctions from the AV18+UIX Hamiltonian. The spectroscopic factors are being compared to predictions from the Cohen-Kurath (CK) shell model.<sup>1</sup> The CK spectroscopic factors for transitions between stable nuclei were first published in 1967, but many additional transitions are now experimentally accessible with the

<sup>1</sup>S. Cohen and D. Kurath, Nucl. Phys. **A101**, 1 (1967).

### b.4. Calculations of RMS Radii of Helium Isotopes (S. C. Pieper, R. B. Wiringa, and J. Carlson\*)

In October 2004, a group led by the Physics Division's Zheng-Tian Lu published a measurement, with better than 1% accuracy, of the rms charge radius of  ${}^6\text{He}$ . The measurement prompted us to attempt a correspondingly accurate calculation of the  ${}^6\text{He}$  point proton and neutron rms radii. This has proved significantly more difficult than we originally anticipated, but the work is nearing completion.

We first had to improve the GFMC propagation to obtain reliable densities in the neutron halo of  ${}^6\text{He}$ . Even with these improvements we find that GFMC calculations made with different starting wavefunctions can result in binding energies that differ by 50 to 100 keV. Although this is only 0.2% to 0.3% of the binding energy, it is 5% to 10% of the separation energy to  ${}^4\text{He}$  plus two neutrons and the rms radius can

advent of rare-isotope beams at Argonne, MSU, and other facilities.

Two specific applications were made in 2005 as part of experiments carried out at ATLAS: a study of the  ${}^9\text{Li}$  spectrum using the  ${}^8\text{Li}(d,p)$  reaction, and a study of the  ${}^7\text{He}$  spectrum using the  ${}^6\text{He}(d,p)$  reaction. This year we participated in a follow-on experiment on  ${}^7\text{He}$  using the  ${}^8\text{Li}(d,{}^3\text{He})$  reaction. The VMC cluster overlaps between the ground state of  ${}^8\text{Li}$  and the ground and low-lying excited states in  ${}^7\text{He}$  were calculated and used as input to the DWBA program PTOLEMY to obtain differential cross sections. The VMC overlaps predict a specific overall normalization. We also made VMC calculations of the  $\langle d|a_j|{}^3\text{He} \rangle$  and  $\langle d|a_j|t \rangle$  overlaps to improve PTOLEMY calculations of  $(d,{}^3\text{He})$  and  $(d,t)$  reactions. A paper on the experiment is being prepared for publication.

In addition, we have been providing overlap calculations to other experimental groups at both MSU and TRIUMF.

be significantly changed. Thus, in practice, all we can do is produce a narrow band of rms radius versus separation energy. We find that many different calculations, including ones for different Hamiltonians, even those without NNN potentials, lie in this band. The band reproduces the experimental rms radius at the experimental separation energy.

We have made similar calculations for  ${}^8\text{He}$ , lithium isotopes, and other  $A = 9$  and  $10$  nuclei for which rms radii are measured or should be experimentally accessible. Lu's group is in the process of measuring the charge radius of  ${}^8\text{He}$ ; at the experimental  ${}^8\text{He}$  to  ${}^6\text{He}$  separation energy, our band of calculated values predicts a charge radius of 1.94(3) fm, which is 0.11 fm smaller than the  ${}^6\text{He}$  value.

\*Los Alamos National Laboratory.

### b.5. Pair Counting, Pion-Exchange Forces, and the Structure of Light Nuclei (R. B. Wiringa)

A simple but useful guide for understanding the structure of light nuclei has been formulated. It is based on counting the number of interacting pairs in different spin-isospin ( $ST$ ) states for a given spatial symmetry and estimating the overall binding according to the sum of  $\sigma_i \cdot \sigma_j \tau_i \cdot \tau_j$  expectation values. This choice is motivated by long-range one-pion exchange (OPE), which in the microscopic quantum Monte Carlo (QMC) calculations gives about 75% of the net potential energy, although most of the contribution comes from the tensor component of the OPE potential rather than the spin-isospin part. This operator conveys a key feature of  $NN$  forces, namely that they are moderately attractive in ( $ST$ ) = ( $10$ ) and ( $01$ ) pairs, slightly repulsive in ( $11$ ) pairs, and very repulsive in ( $00$ ) pairs.

The number of pairs of different ( $ST$ ) combinations,  $P_A(ST)$  for a given nuclear state can be obtained knowing the total spin, isospin, and spatial symmetry. The energy estimate is

$$E_{OPE} = C[9P_A(00) - 3P_A(01) - 3P_A(10) + P_A(11)]$$

where  $C$  is a scale factor in units of energy. With this estimate, the binding energy of the deuteron, triton, and alpha are  $-3 C$ ,  $-9 C$ , and  $-18 C$ , respectively. This is actually a good estimate of the relative potential energies obtained in our QMC calculations, but not of the total binding because the positive kinetic energy contribution grows less rapidly. However, in the  $p$ -shell something like a virial theorem is established, with the ratio of kinetic to potential energy having a fairly constant value  $0.76-0.80$ , so  $E_{OPE}$  does become a binding energy estimator.

<sup>1</sup>R. B. Wiringa, Phys. Rev. C **73**, 034317 (2006).

### b.6. Tensor Forces and the Ground State Structure of Nuclei (R. B. Wiringa, S. C. Pieper, R. Schiavilla,\* and J. Carlson†)

We have calculated a variety of two-nucleon momentum distributions in the ground states of light nuclei with mass number  $A \leq 8$  using variational Monte Carlo wavefunctions derived from a realistic Hamiltonian with two- and three-nucleon potentials. These include distributions that are a function of either the relative momenta  $q$  between the pair or the center-of-mass momenta  $Q$  of the pair. A special case is the relative momentum distribution when the center-of-

As nucleons are added in the  $p$ -shell, they essentially decouple from the  $s$ -shell, in that the contribution to  $E_{OPE}$  from pairs where one nucleon is in the  $s$ -shell and one in the  $p$ -shell vanishes. Thus the energy prediction for  $^5\text{He}$  is  $-18 C$ , the same as for  $^4\text{He}$ , indicating that the relative stability will be determined by finer details of the force and requirements of Fermi statistics. In general, the energies of  $p$ -shell nuclei are predicted to be basically the energy of their sub-cluster components, which helps explain why light nuclei show considerable clustering. This feature is also seen in the QMC calculations with the full AV18  $NN$  potential; much of the cluster-cluster binding is provided by adding an  $NNN$  potential. The model also explains why mixing of different spatial symmetries in ground states increases as  $T$  increases across isobars.

In the  $p$ -shell, each nucleus has many excited states arising from different spin and spatial symmetry combinations. The  $P_A(ST)$  for each state is easily evaluated and the above energy estimate used to study the excitation spectrum. When various spatial symmetry states can combine to give a specific total spin, those combinations that have the least amount of very repulsive ( $00$ ) pairs will lie lowest. For example, in  $^7\text{Li}$  the states that are predominantly  $4P[421]$  symmetry are below those with  $2P[421]$  symmetry, because they have more ( $11$ ) pairs and fewer ( $00$ ) pairs. It can also be used to predict orderings of some  $sd$ -shell intruder states.

A paper describing this concept was submitted and published in 2006.<sup>1</sup>

mass of the pair is zero. Interestingly, we find the momentum distribution of  $np$  pairs is much larger than that of  $pp$  pairs for values of the relative momentum in the range  $1.5-3 \text{ fm}^{-1}$  and vanishing total momentum. This is illustrated in Fig. V-11 for nuclei from  $^3\text{He}$  to  $^8\text{Be}$ . This order of magnitude difference has a universal character originating from the tensor components present in any realistic nucleon-nucleon potential. The correlations induced by the tensor force strongly

influence the structure of  $np$  pairs, which are predominantly in deuteron-like states, building up a significant tail in the momentum distribution beyond  $1.5 \text{ fm}^{-1}$ . In contrast, the  $pp$  pairs, which are mostly in  $^1S_0$  states, have a minimum in the momentum distribution around  $2 \text{ fm}^{-1}$ . We predict these features

should be easily observable in two-nucleon knock-out processes, such as  $A(e, e'np)$  and  $A(e, e'pp)$ , and there is some preliminary evidence from experiments at Brookhaven and JLab to support this idea. A letter on this work was submitted and has been published.<sup>1</sup>

\*Thomas Jefferson National Accelerator Facility, †Los Alamos National Laboratory.

<sup>1</sup>R. Schiavilla, R. B. Wiringa, S. C. Pieper, and J. Carlson, Phys. Rev. Lett. **98**, 132501 (2007).

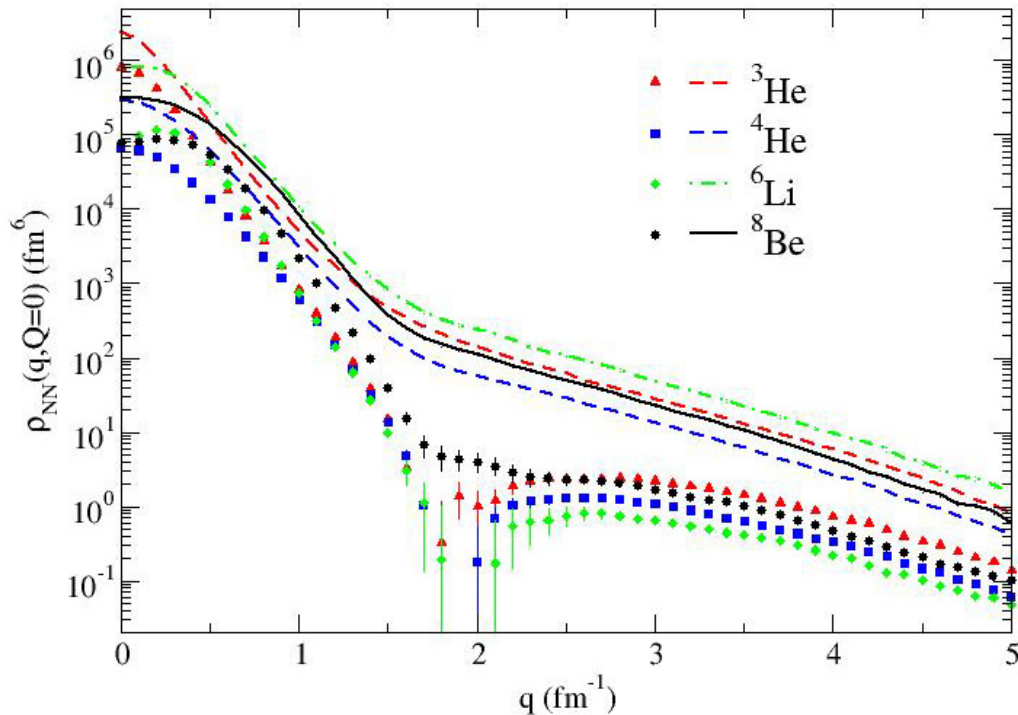


Fig. V-11. The  $np$  (lines) and  $pp$  (symbols) momentum distributions in various nuclei as functions of the relative momentum  $q$  at vanishing total pair momentum  $Q$ .

### b.7. Quantum Monte Carlo Calculations of Electroweak Transition Matrix Elements (M. Pervin, S. C. Pieper, and R. B. Wiringa)

We have been making quantum Monte Carlo calculations of M1, E2, and GT transition matrix elements in light nuclei. Variational Monte Carlo (VMC) calculations have been made in past years for electromagnetic form factors in  $^6\text{Li}$ , transition densities in  $^7\text{Li}$ , and weak decays of  $^6\text{He}$  and  $^7\text{Be}$ . Reasonable agreement with experiment at the  $\sim 10\%$  level was obtained using wavefunctions generated from the AV18+UIX Hamiltonian. Now we are performing more precise Green's function Monte Carlo (GFMC) calculations with wavefunctions generated from the

improved AV18+IL2 Hamiltonian. To the best of our knowledge, these are the first GFMC calculations of off-diagonal matrix-elements ever.

The matrix elements are extrapolated from mixed estimates that bracket the relevant electroweak operator between a variational trial state and a GFMC propagated wavefunction. Because they are off-diagonal terms, two mixed estimates are required for each transition, with a VMC initial (final) state paired with a GFMC final (initial) state. At present, we have

calculated more than a dozen M1, E2, and GT transitions between states of  ${}^6\text{He}$ ,  ${}^6\text{Li}$ ,  ${}^7\text{Li}$ , and  ${}^7\text{Be}$ . We find the  $B(E2)$  strengths, which depend sensitively upon the radius of the nucleus, are larger and closer to experimental values with the GFMC calculations compared to the older VMC results. However, the  $B(M1)$  and  $B(GT)$  strengths do not evolve much going from VMC to GFMC, although they do generally move closer to experiment. An example of the evolution of

an E2 matrix element with the propagation of the GFMC wavefunction in imaginary time is shown in Fig. V-12.

A paper on the  $A = 6, 7$  calculations is in preparation. We will extend these calculations to larger nuclei in the next year, and have already made some preliminary studies in  $A = 8$  nuclei.

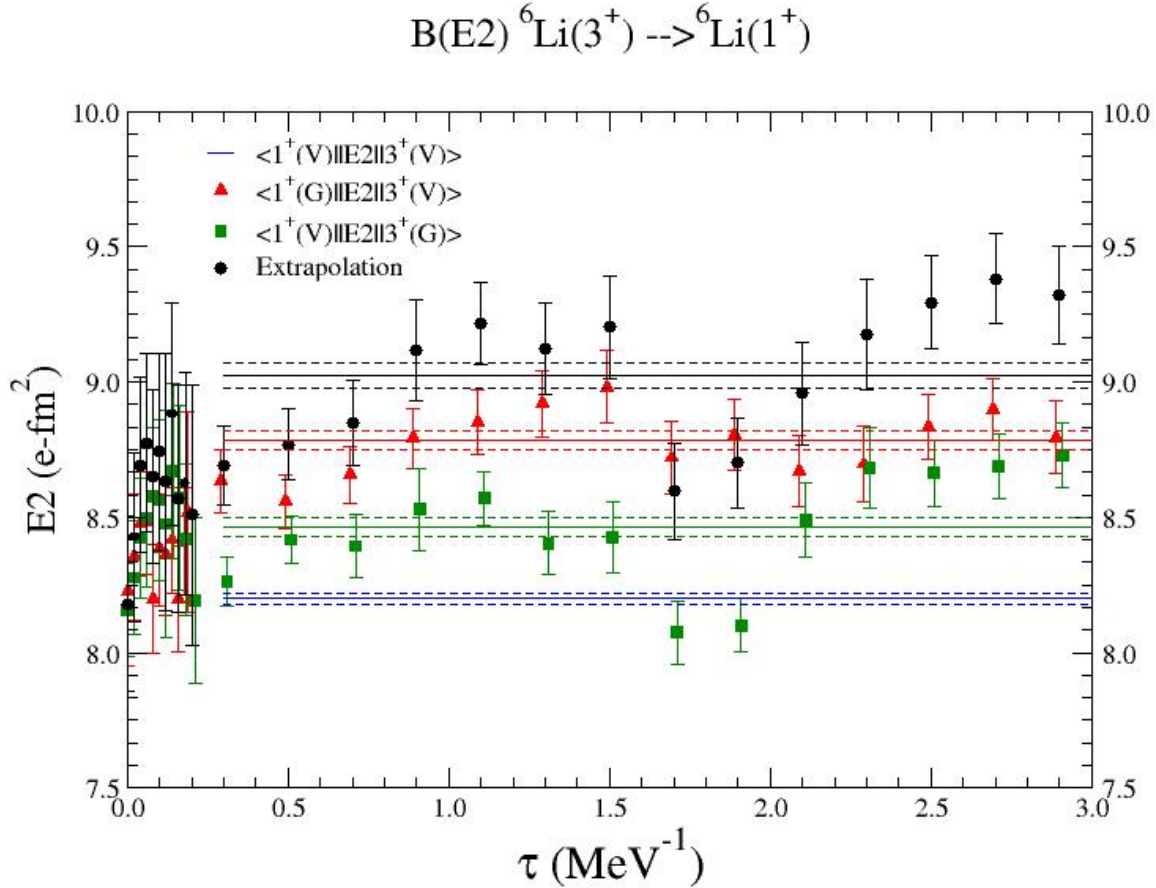


Fig.V-12. The VMC matrix element, GFMC mixed estimates, and extrapolated final result for the E2 transition from the first excited state to the ground state in  ${}^6\text{Li}$  ( $3^+ \rightarrow 1^+$ ).

### b.8. Quantum Monte Carlo Calculations of Isospin-Mixing Matrix Elements in ${}^8\text{Be}$ (R. B. Wiringa, S. C. Pieper, and M. Pervin)

There are three pairs of states in the spectrum of  ${}^8\text{Be}$  that show considerable isospin-mixing, the second and third  $2^+$  states at 16.6 and 16.9 MeV, being the most famous. These isospin-mixed states come from blending the  $T = 1$  isobaric analog of the  ${}^8\text{Li}$  ground state with the second  $T = 0$  excited state. There are also

fairly close  $1+$  and  $3+$  pairs at slightly higher energies in the  ${}^8\text{Be}$  spectrum. The isospin-mixing matrix elements that connect these pairs of states,  $E_{01}(J) = \langle \Psi(J^+; 0) | H | \Psi(J^+; 1) \rangle$ , were computed several years ago using VMC wavefunctions from the AV18+UIX Hamiltonian, which has kinetic, Coulomb,



magnetic moment, and strong charge-symmetry-breaking (CSB) contributions. However, the results underpredicted the values deduced from transition rate experiments.

Using the new methods described above, we are now recalculating these matrix elements using GFMC wavefunctions for the AV18+IL2 Hamiltonian. We find that the matrix element for the  $2^+$  states goes from  $-107$  keV in VMC to  $-115$  keV in GFMC, compared to the experimental value of  $-144$  keV. Two thirds of the calculated result is from Coulomb and one third from the other terms, so this is a sensitive place to test our

knowledge of CSB interactions.

The  $A = 8$  system is also of considerable interest as a laboratory for studying the conservation of the vector current (CVC) and the absence of second-class currents, which should be exact symmetries in the limit of good isospin. Experiments involve the weak decays of the  $2^+$  ground states of  ${}^8\text{Li}$  and  ${}^8\text{B}$  and the electromagnetic decay of the isospin-mixed  $2^+$  states in  ${}^8\text{Be}$  to the broad first  $2^+$  state in  ${}^8\text{Be}$  at 3 MeV. It is important to know how much  $T = 1$  contamination is present in this latter state; our initial GFMC calculation gives a very small  $E_{01} = -6$  keV, implying very small contamination.

### b.9. Dependence of Nuclear Binding on Hadronic Mass Variation (V. V. Flambaum\* and R. B. Wiringa)

We are studying how the binding of light ( $A \leq 8$ ) nuclei depends on possible variations of hadronic masses, including meson, nucleon, and nucleon-resonance masses. Small variations in hadronic masses may have occurred over time; the present results could help evaluate consequent changes in primordial nucleosynthesis. Larger variations may be relevant to current attempts to extrapolate properties of nucleon-nucleon interactions from lattice QCD calculations.

We carry out this study by isolating the hadronic mass dependence in three different Hamiltonians based on different nucleon-nucleon potentials. We use the Argonne  $v14$  and Argonne  $v28$  potentials of 1984, and the Argonne  $v18$  potential of 1995 accompanied by the Urbana IX three-nucleon potential. The AV14 and AV18 are standard  $NN$  potentials, while the AV28 adds explicit  $\Delta$  degrees of freedom. We calculate the energies of the  ${}^1S_0$  virtual bound state and the deuteron for these potentials by direct solution of the two-body

equations, and the energies of  $A = 3-8$  nuclei using variational Monte Carlo methods.

Results are presented as derivatives of the energy with respect to the different masses so they can be combined with different predictions of the hadronic mass-dependence on the underlying quark masses. As an example, we have used a particular set of relations obtained from a Dyson-Schwinger study of hadron masses and sigma terms.<sup>1</sup> In this case we find that nuclear binding decreases moderately rapidly as the quark mass increases, with the deuteron becoming unbound when the pion mass is increased by  $\sim 50\%$ . In the other direction, the singlet state becomes bound if the pion mass is decreased by  $\sim 10\%$ . However, the deuteron always lies below the singlet state for the range of quark masses we consider, in disagreement with some lowest-order effective field theory predictions.

\*Argonne Fellow, Physics Division, and University of New South Wales, Sydney, Australia.

<sup>1</sup>V. V. Flambaum, A. Höll, P. Jaikumar, C. D. Roberts, and S. V. Wright, *Few-Body Syst.* **38**, 31 (2006).



### C. NUCLEAR ASTROPHYSICS

The objective of this research program is to investigate nuclear processes that take place in stars, in the big bang, and in interstellar and intergalactic space. Nuclear phenomena are ubiquitous in the universe. The stars shine by nuclear energy, and the chemical compositions observed in the solar system and elsewhere are the results of nuclear processes that occurred in the big bang and inside the many generations of stars that have formed and evolved since then. Many astrophysical phenomena may only be understood by a combination of nuclear physics with methods more familiar to astrophysicists.

A particularly important problem is to determine rates for the nuclear reactions that occur in astrophysical environments. There are many applications (for example, the rapid neutron capture process) where large contributions from theoretical nuclear physics – particularly masses and cross sections – will always be necessary as input, and we maintain research interests in these areas. We have applied advances in the theoretical descriptions of light nuclei to compute cross sections important for considerations of big-bang nucleosynthesis, the solar neutrino flux, and seeding of the  $r$ -process. This work continues in close connection with our other work on light nuclei, and the main goals at present are to improve the wave functions and computational methods as described in Section b.2. In the last year, we have participated in work to improve the computational methods used to compute weak-interaction rates important for the collapse and subsequent supernova explosions of massive stars.

Understanding nucleosynthesis and energy generation in a particular astrophysical environment requires calculations of nuclear reaction networks. Even for cases in which the detailed astrophysical phenomena can only be understood from difficult calculations coupling a reaction network and hydrodynamics, simpler network calculations can identify the crucial reactions and other nuclear properties to be determined by more detailed theoretical and experimental work. Ongoing work in this area involves big-bang nucleosynthesis, nuclear burning in low-mass stars, and photon-nucleus reactions in high-energy cosmic rays.

A major goal of nucleosynthesis studies is to determine the specific physical conditions that gave rise to abundance patterns seen in nature: what mix of different kinds of stellar environments gave rise to observed chemical compositions? Large amounts of important new data on abundance patterns are now being collected, with important evidence arising from low-metallicity stars in our own galaxy, absorption-line systems backlit by distant quasars, and primitive inclusions and pre-solar grains embedded in meteorites. These data contain important clues about the nucleosynthetic history of the universe, both locally and globally, and the effort to disentangle the clues into information on stellar sources and galactic chemical evolution is necessarily coupled to our work on nucleosynthesis.

In addition, studies are underway of electroweak reaction rates relevant to astrophysical processes in dense nuclear matter. These are a part of our attempt to predict observable features of quark matter in compact astrophysical objects.

The subjects of nucleosynthesis and chemical evolution is today becoming increasingly important as probes of the star formation history of the Cosmos itself. The primordial

compositions of the first stars/first stellar generations reflect that of the Universe as it emerged from the cosmological Big Bang: hydrogen, deuterium,  $^3\text{He}$ ,  $^4\text{He}$ , and  $^7\text{Li}$ . Within galaxies, stars and supernovae play the dominant role in synthesizing the elements from carbon through uranium and in returning heavy-element-enriched matter to the interstellar gas from which subsequent generations of stars are formed. This history is written in the compositions of the stars and gas in our Galaxy and other galaxies as a function of time (“metallicity”). The contributions both from massive stars ( $M > 10 M_{\odot}$ ) and associated Type II supernovae and from thermonuclear (Type Ia) supernovae are particularly noteworthy. Observational studies with large aperture ground-based telescopes are now providing increasing amounts of information concerning both the compositions of the oldest stars in our Galaxy and nearby galaxies and the spectroscopic properties of gas clouds at high red shifts. Argonne researchers are involved with such projects as an outgrowth of their association with the Joint Institute of Nuclear Astrophysics (JINA). Our studies of the nuclear processes participating in nucleosynthesis, of the natures of the sites in which nucleosynthesis proceeds, and of the compositions of the stellar components of our Galaxy and other galaxies as a function of time (redshift) serve to inform us of the natures of the earliest stellar population of galaxies and the Cosmos.

**c.1. Sedimentation and Type I X-Ray Bursts at Low Accretion Rates** (J. W. Truran,\*  
F. Peng,† and E. F. Brown‡)

Type I X-ray bursts are understood to involve hydrogen/helium thermonuclear runaways occurring on the surfaces of accreting neutron stars in short period binary systems. Neutron stars, with their strong surface gravity, have interestingly short timescales for the sedimentation of heavy elements. Motivated by observations of Type I X-ray bursts from sources with extremely low persistent accretion luminosities,  $L_X < 10^{36}$  ergs  $s^{-1}$  ( $\sim 0.01 L_{Edd}$ ), we have studied how sedimentation effects the distribution of isotopes and the ignition of H and He in the envelope of an accreting neutron star. For local mass accretion rates  $dm/dt < 10^{-2} (dm/dt)_{Edd}$  (for which the ignition of H is unstable), where  $(dm/dt)_{Edd} = 8.8 \times 10^4$  g  $cm^{-2} s^{-1}$ , the helium and CNO elements settle out of the accreted fuel layer before the temperature is reached at which H would ignite. Using one-zone calculations of the thermonuclear burning, we identify a range of accretion

rates for which the unstable ignition of hydrogen does not trigger unstable helium burning. This range depends on the emergent flux from reactions in the deep neutron star crust; for  $F = 0.1$  MeV ( $(dm/dt)/m_u$ ), the range is  $3 \times 10^{-3} (dm/dt)_{Edd} \leq dm/dt \leq 10^{-2} (dm/dt)_{Edd}$ . We speculate that sources accreting in this range will build up a massive He layer that later produces an energetic and long X-ray burst. At mass accretion rates lower than this range, we find that the hydrogen flash leads to a strong mixed H/He flash. Surprisingly, even at accretion rates  $dm/dt \geq 0.1 (dm/dt)_{Edd}$ , although the H and He do not completely segregate, the H abundance at the base of the accumulated layer is still reduced. While following the evolution of the X-ray burst is beyond the scope of this introductory paper, we note that the reduced proton-to-seed ratio favors the production of  $^{12}\text{C}$ , an important ingredient for subsequent superbursts.

\*Argonne National Laboratory and University of Chicago, †California Institute of Technology, ‡Michigan State University.

<sup>1</sup>F. Peng, E. F. Brown, and J. W. Truran, *ApJ* **654**, 1022, (2007).

## c.2. Flame Evolution for the Deflagration Phase in Type Ia Supernova Simulations

(J. W. Truran,\* A. C. Calder,† D. M. Townsley,† O. E. B. Messer,†,‡ I. R. Seitenzahl,† F. Peng,† N. Vladimirova,† E. F. Brown,§ S. Asida,¶ and D. Q. Lamb†)

Type Ia supernovae (SNe) are bright explosions characterized by a lack of hydrogen spectral features and strong silicon P Cygni features near maximum light. The currently favored interpretation is the disruption of a near-Chandrasekhar-mass C/O white dwarf by a thermonuclear runaway. These events are fascinating in and of themselves and are important both for their contribution to the cosmic abundance of iron-peak elements and for their role as standard candles.

Models of Type Ia SNe necessarily involve a mechanism for incinerating the star by a thermonuclear runaway, and the nature of this mechanism is the subject of contemporary research. In the explosion, a thermonuclear flame propagates through the C/O fuel of the white dwarf as either a subsonic deflagration front or a supersonic detonation wave and releases sufficient energy to unbind the star. However, models involving either a pure deflagration or a pure detonation have traditionally been unable to provide an explanation for both the observed expansion velocities and the spectra produced by ejecta that is rich in both intermediate-mass and iron-peak elements.

There has been considerable progress recently in hydrodynamic simulations of deflagrations of C/O white dwarfs that model the entire star. This is a complicated endeavor, predominantly due to the vast range of length scales: the laminar flame width is  $\sim 10^3 - 10$  cm, some 8 to 12 orders of magnitude smaller than the stellar radius. Because the computational requirements for simulations with these disparate scales demand resources well beyond current capabilities, multidimensional Type Ia models must make use of an appropriate sub-grid-scale model for the evolution of the thermonuclear burning front. Moreover, large-scale simulations are very demanding of computational resources, and it is not feasible at present to include enough isotopes to allow for directly computing the reaction kinetics. A realistic model must, nevertheless, accurately describe the nuclear energy that is released, the timescale on which it is released, and the compositional changes that occur in the flame. In addition, the burned material continues to evolve after the passage of the flame due to both weak interactions and hydrodynamic evolution, and realistic simulations must describe this "post-flame" evolution.

Our efforts in this regard involved a group of JINA

researchers at the University of Chicago and Argonne National Laboratory working closely with the supernova simulation group at the FLASH Center at the University of Chicago to implement a state-of-the-art, efficient, accurate model of the nuclear burning in the diffusive flame and, after its passage, during the deflagration of a white dwarf star in a Type Ia Supernova. Such a flame model is essential for using computer simulations of the explosion to understand systematic trends in the brightness of these events, which are being heavily used to probe the expansion history of the universe. The involvement of JINA and ANL researchers has resulted in the best possible modeling of both the strong and weak nuclear interaction physics necessary to follow the early phases of the explosion, and to enable high-quality nucleosynthesis to be accomplished simultaneously with detailed hydrodynamic study of SNe Ia explosion mechanisms. In addition to the FLASH group, Type Ia supernova simulations by groups worldwide will benefit from the in-depth study of SNe Ia energetics made possible by the involvement of JINA and ANL researchers. For example, during the course of this work, we successfully matched a screened nuclear network calculation and a Coulomb-corrected nuclear statistical equilibrium calculation, a novel accomplishment in this section of literature.

Two significant papers addressing these issues have emerged from these studies: Calder *et al.*, (ApJ **656**, 313, 2007) and Townsley *et al.*, (ApJ, in press, 2007). The Calder *et al.* paper presents a study of the nuclear burning that occurs during C/O deflagrations, with the goal of providing a realistic flame model for simulations of Type Ia supernovae. Our flame model builds on the advection-diffusion-reaction model of Khokhlov and includes electron screening and Coulomb corrections to the equation of state in a self-consistent way. We calibrate this model flame – its energetics and timescales for energy release and neutronization – with self-heating reaction network calculations that include both these Coulomb effects and up-to-date weak interactions. The burned material evolves post-flame due to both weak interactions and hydrodynamic changes in density and temperature. We develop a scheme to follow the evolution, including neutronization, of the NSE state subsequent to the passage of the flame front. As a result, our model flame is suitable for deflagration simulations over a

wide range of initial central densities and can track the temperature and electron fraction of the burned material through the explosion and into the expansion of the ejecta. The Townsley *et al.* paper reports the development of an improved method for tracking the nuclear flame. A simplified 3-stage burning model and a non-static ash state are integrated with an artificially thickened ADR flame front in order to provide an accurate but efficient representation of the energy release and (electron capture induced) neutronization in and after the unresolvable flame.

The importance of such detailed considerations of the consequences of nuclear burning and neutronization via

electron captures is to provide an accurate determination of the  $^{56}\text{Ni}$  abundance in the ejecta of a Type Ia supernova. For a value of  $Y_e \approx 0.5$ , the matter in nuclear statistical equilibrium following expansion and cooling is dominated by the self-conjugate nucleus  $^{56}\text{Ni}$ . At high densities, however, electron captures on both protons and heavy nuclei effect neutronization of the matter and  $Y_e$  falls below  $0.5$ . Such neutron enrichment favors neutron-rich isotopes at the expense of  $^{56}\text{Ni}$ . Since the brightness of SNe Ia at maximum is a direct function of the mass of  $^{56}\text{Ni}$  ejected, an accurate determination of the composition of the ejecta is critical to the use of SNe Ia as distance indicators.

\*Argonne National Laboratory and University of Chicago, †University of Chicago, ‡Oak Ridge National Laboratory, §Michigan State University, ¶The Hebrew University of Jerusalem, Israel.

### c.3. 2-D Hydrodynamic Studies of Novae (J. W. Truran,\* S. A. Glasner,† and E. Livne‡)

Classical novae are a manifestation of thermonuclear runaway in accreted hydrogen-rich shells on the surfaces of white dwarfs in close binary systems. Compelling observational data indicate that the material ejected by some novae can be significantly enriched in C, N, O, or O, Ne, by <30% by mass. It was recognized early that such levels of envelope enrichment could best be explained by dredge-up of some of the underlying white dwarf matter, prior to the final stages of the thermonuclear runaway. The question of how this enrichment is realized has, however, challenged theory now for several decades, and constitutes a major roadblock to our understanding of the nova phenomenon. The three commonly recognized mechanisms for such enrichment involve: (1) diffusion, (2) gravity wave driven mixing, and (3) convective overshoot. In earlier work, researchers at the Flash Center at the University of Chicago and Argonne National Laboratory explored the possibility that the required mixing and dredge-up could result from a resonant interaction between large-scale shear flows in the accreted envelope and interfacial gravity waves. From a suite of two-dimensional simulations, we obtained a measure of the rate of mixing and the maximum mixed mass as a function of the wind velocity. The levels of envelope enrichment achieved via this mechanism were found to be quite compatible with those levels determined observationally to characterize the ejecta of classical novae.

In ongoing studies, Argonne National Laboratory and University of Chicago researchers are considering an

alternative mechanism for such mixing - driven by convective undershooting which might be expected to accompany the final stages of nova thermonuclear runaways as discussed below.

The standard model for the outbursts of novae, as we have noted, involves a hydrogen thermonuclear runaway on the surface of an accreting white dwarf in a short period binary system. While one-dimensional studies have allowed us to understand the gross features of nova explosions, it is apparent that multidimensional simulations will ultimately be required. Over the past two years, Ami Glasner and Eli Livne (The Hebrew University of Jerusalem) and Truran have been involved with 2-D calculations of the late stages of the evolution to runaway – from the onset of convection to the runaway. For this study, a 1D hydrostatic fully convective ideal profile, for which the convective flux was defined according to the Mixing Length Theory, was used as an initial model. Previous multidimensional studies of nova thermonuclear runaways (TNR) were able to simulate only the final stages, for which the timescales are very short (10 to 200 seconds), such that only the last stages of the ignition phase and the runaway to peak temperature/luminosity (from a temperature  $100\text{ K}$  to peak) could be investigated. The degree of mixing of matter from the underlying white dwarf into the envelope during the course of the runaway was therefore difficult to estimate. Typically, the initial model was taken from 1-D simulations at a stage where convection and nuclear burning had already started, at a

temperature of approximately  $10^8 K$ . A major question with this approach is the degree to which the results obtained are dependent on the choice of initial conditions. In general, the point at which the onset of convection occurs is when the temperature at the base of the envelope is of order  $3 \times 10^7 K$ , hundreds of seconds prior to the final stages of the runaway. Building on improvements in the hydro solver and better computational resources, we are now able to resolve scales that are already unstable to the shear Kelvin-Helmholtz (KH) instability, thus improving the credibility of the results concerning undershoot mixing. The time scales considered range from a phase close to

the onset of convection, when the temperature at the base of the envelope is about  $5 \times 10^7 K$ , to the runaway itself. A comparison of the evolution for simulations at initial temperatures over a range of temperatures  $3-9 \times 10^7 K$  provides a measure of convergence of these results and their consistency with regard to the consequences of runaway. We observe a universal behavior in which multi-D effects give rise to mixing that shortens the timescale to thermonuclear runaway and yields an overall level of mixing of order 30-40 percent by mass. A paper reporting our results will appear later this year.<sup>1</sup>

\*University of Chicago and Argonne National Laboratory, †The Hebrew University of Jerusalem, Israel.

<sup>1</sup>S. A. Glasner, E. Livne, and J. W. Truran, ApJ, in press, 2007.

#### c.4. *r*-Process Synthesis of the Heaviest Elements (J. W. Truran,\* K.-L. Kratz,† K. Farouqi,‡ B. Pfeiffer,† C. Sneden,§ J. J. Cowan,¶ K. Otsuki,‡ and I. Seitenzahl‡)

The origin of heavy elements in explosive environments by neutron capture processes represents one of the most challenging problems in nuclear astrophysics today. Truran and his students and postdocs at the University of Chicago are actively involved in many aspects of this research.

Abundances of heavier elements (barium and beyond) in many neutron-capture-element-rich halo stars accurately replicate the solar system *r*-process pattern. However, abundances of lighter neutron-capture elements in these same stars are not consistent with the solar system pattern. These comparisons suggest contributions from two distinct types of *r*-process synthesis events, a so-called main *r*-process for the elements above the second *r*-process peak (at mass number  $A \sim 130-140$ ) and a weak *r*-process for the lighter neutron-capture elements. We have performed *r*-process theoretical predictions to further explore the implications of the solar and stellar observations. We find that the isotopic composition of barium and the elemental Ba/Eu abundance ratios in *r*-process-rich low-metallicity stars can only be matched by computations in which the neutron densities are in the range  $23 \lesssim \log n_n \lesssim 28$ , values typical of the main *r*-process. For *r*-process conditions that successfully generate the heavy element pattern extending down to  $A = 135$ , the relative abundance of  $^{129}\text{I}$  produced in this mass region appears to be at least ~90% of the observed solar value. Finally, in the neutron number density ranges required for production of the observed solar/stellar third *r*-process-peak ( $A \sim 195$ ), the

predicted abundances of interpeak element hafnium ( $Z = 72$ ,  $A \sim 177-180$ ) follow closely those of third-peak elements and lead. Hf, observable from the ground and close in mass number to the third *r*-process-peak elements, might also be used as part of a new nuclear chronometer pair, Th/Hf, for stellar age determinations.<sup>1</sup>

An important and not yet fully investigated aspect of *r*-process nucleosynthesis is the question of fission and fission cycling and its impact on the final *r*-process abundance distributions. The relevance of fission cycling is strongly suggested by the extraordinary robustness of the observed *r*-process patterns in the very oldest stars in our Galaxy. This question is being investigated by researchers at the University of Chicago and Argonne National Laboratory. The rapid neutron capture process (*r*-process) synthesizes roughly 50% of all elements past the Fe-peak and all of the actinides. While even the site of the *r*-process remains unknown (the high entropy shell surrounding a proto-neutron star left behind by a core collapse supernovae and, to a lesser degree, neutron star mergers being currently the most promising ones), the endpoint of the *r*-process is even more uncertain. In and beyond the actinide region, fission (beta delayed, spontaneous, neutron- and neutrino induced) competes with beta decays and neutron captures, providing a way to cycle the *r*- process, as the fragments constitute new seed nuclei. However, fission barriers are strongly dependent on the mass models used, leaving the fission rates highly uncertain. The role of neutrino induced fission is even

more uncertain, since the neutrino luminosity and spectrum at the  $r$ -process site are unknown. If the timescales are right, a quasi steady flow of nuclei can be achieved. Abundance yields of steady flow  $r$ -process calculations are not sensitive to the details of the expansion, but to the nuclear microphysics, thus providing an attractive explanation of the robust nature of the strong  $r$ -process. Do steady flow calculations reproduce the strong  $r$ -process pattern? Another attractive feature of fission cycling is that it could

explain the weak  $r$ -process component without invoking a second  $r$ -process site. Fission fragments end up in the region  $50 < Z < 60$ , producing a robust yield for higher  $Z$  elements, lighter elements, however, would not experience the equalizing effect of fission cycling and remain more sensitive to other parameters such as the expansion timescale. Kaori Otsuki and collaborators at Chicago and Michigan State University are currently working on implementing an improved treatment of fission into dynamical  $r$ -process studies.

---

\*University of Chicago and Argonne National Laboratory, †University of Mainz, Germany, ‡University of Chicago, §University of Texas, ¶University of Oklahoma.

<sup>1</sup>K.-L. Kratz *et al.*, ApJ **662**, 39 (2007).



## D. NUCLEAR STRUCTURE AND HEAVY-ION REACTIONS

This research focuses on nuclear structure in unusual regimes such as nuclei near the proton and neutron driplines, deformed nuclei with strong octupole correlations, and superdeformed nuclei at high spin. We also study heavy-ion reactions near the Coulomb barrier. Much of this work is closely tied to experiments performed at ATLAS and at radioactive beam facilities.

Our studies of heavy-ion reactions include coupled-channels calculations of fusion reactions, elastic and inelastic scattering, and few nucleon transfer reactions. The calculated fusion cross sections are usually quite sensitive to the structure and the radii of the reacting nuclei, and it is often possible to reproduce the measurements fairly well by including couplings to one- and two-phonon excitations of the low-lying quadrupole and octupole modes. However, it is very challenging to reproduce the high precision fusion data that have become available in recent years. Calculations are also challenging for very heavy systems where couplings to multi-phonon excitations and multi-nucleon transfer channels can influence the fusion.

Another difficulty in the description of heavy-ion fusion reactions occurs at energies far below the Coulomb barrier, where the measured fusion cross sections fall off steeply with decreasing energy. The fall off is so steep in many cases that the S factor for fusion develops a maximum at low energy. This hindrance of the fusion is expected to be an entrance channel phenomenon because it occurs at a rather high excitation energy of the compound nucleus. We have shown that the fusion hindrance can be explained in the coupled-channels approach by using an ion-ion potential that has a shallow pocket in the entrance channel. We have applied this model and analyzed the fusion data for several of the heavy-ion systems that exhibit the fusion hindrance at low energy.

We have tested our three-body models of two-neutron halo nuclei against recent measurements of the charge radius and dipole response of  $^{11}\text{Li}$ . Both measurements are probes of the core-dineutron distance in  $^{11}\text{Li}$ . The distance we extract from the dipole response is slightly smaller than the value obtained from the charge radius measurement. The discrepancy is of the order of  $1.5\sigma$ . Our interpretation of both measurements is that the s-wave component in the two-neutron halo ground state must be fairly large.

We are continuing the development of a program for calculating many-body variational wavefunctions. This approach puts pairing and particle-hole interactions on an equal footing. These wavefunctions strictly conserve particle-number and parity. Particle number and parity are projected before variation. In studies of nuclides near the  $N = Z$  line, we also project states of good  $Q$ , the number parity of  $T = 0$  pairs, before variation. This treatment explains many of the unusual features of nuclei having almost equal numbers of protons and neutrons, such as the Wigner energy anomaly, in a simple way. It also explains a similar anomaly for odd-mass nuclides near the  $N = Z$  line.

We have developed a code for configuration mixing of the wavefunctions used to describe  $n$ - $p$  pairing. We have applied these wavefunctions to explore  $n$ - $p$  pair transfer probabilities in  $N = Z$  nuclides. We find that this quantity is very sensitive to  $T = 0$  and  $T = 1$  correlations in the many-body wavefunction. Experimental studies of the pair transfer probability in  $^{44}\text{Ti}$  will establish

the magnitude of  $T = 0$  pairing interaction correlations in nuclei near the  $N = Z$  line. Using realistic single-particle energies for nuclei in this mass region, we have made a refined estimate of the pair transfer probability to the  $T = 0$  and  $T = 1$  states in  $^{44}\text{Ti}$ .

We are developing a method that goes beyond the usual configuration mixing approach. We utilize the power of the variational method in combination with the configuration interaction method. The method determines an optimal improvement to a wavefunction with a given number of configurations. We have applied the method to the pairing force interaction and to the  $n$ - $p$  pairing interaction problem. In both cases, the results are extremely good. In the pairing case, which we studied in detail, this new approach gave well over 99.9% of the total correlation energy. In the past year, we have extended this method to cylindrically symmetric deformed nuclei, described by a Hamiltonian with particle-hole plus pairing interactions. We are finding that it is quite feasible, in terms of computer resources, to extend this variational approach to the more general interaction.

The low-lying states of odd mass nuclei provide a good test of the parametrizations of single particle potentials. Study of the spectroscopy of the heavy elements is particularly interesting, as it gives insights into the potentials that are relevant to the structure of super-heavy elements. In a collaborative effort with the experimental spectroscopy group at Argonne, we have analyzed low-lying neutron and proton single particle states in the mass 250 region. We have studied neutron single-particle states in  $^{247}\text{Cm}$  and  $^{251}\text{Cf}$ , as well as proton single particle states in  $^{249}\text{Bk}$ , and determined single-particle potentials that are consistent with these analyses. The study of  $^{251}\text{Cf}$  is particularly important as it has 153 neutrons, giving information on the neutron single particle states above the deformed gap at 152 neutrons. Nine single particle states have been identified in this nuclide. These studies constrain potentials that are used to describe superheavy elements. The same approach should prove useful for constraining potentials used to describe new regions of nuclides studied with the CARIBU facility.

#### **d.1. Signature of Shallow Potentials in Deep Sub-Barrier Fusion Reactions (H. Esbensen and Ş. Mişicu\*)**

We have completed our calculations of nuclear potentials for a series of heavy-ion systems.<sup>1</sup> The calculations are based on the M3Y double-folding potential and include corrections for exchange and a repulsive term, which is calibrated to simulate the effect of nuclear incompressibility. We refer to the potential as the M3Y+repulsion potential. The repulsive term is an essential ingredient in producing a shallow pocket and a relatively thick barrier in the entrance channel potential between two heavy ions. We find that this kind of potential explains in a natural way the hindrance of low-energy fusion which has been observed for  $^{28}\text{Si} + ^{64}\text{Ni}$ ,  $^{64}\text{Ni} + ^{64}\text{Ni}$ ,  $^{58}\text{Ni} + ^{58}\text{Ni}$ ,  $^{64}\text{Ni} + ^{89}\text{Y}$ , and  $^{64}\text{Ni} + ^{100}\text{Mo}$  systems (see Ref. 2 for a recent review).

The fusion hindrance phenomenon is characterized by

the energy  $E_s$ , where the  $S$  factor develops a maximum at low energies. Our calculations of the potential pocket show that the minimum of the pocket,  $V_{min}$ , correlates nicely with  $E_s$ . This is illustrated in Fig. V-13. It is seen that  $E_s$  is typically 3-5 MeV above the minimum of the pocket, whereas the minimum of the pocket (triangles) is some 8-15 MeV below the Coulomb barrier.

We use real potentials in the coupled-channels calculations we have performed and we describe the fusion by ingoing-wave boundary conditions, which we impose at the minimum of the pocket. Thus the calculated fusion cross section will vanish at energies that are below the minimum of the pocket. Fusion should in principle still be possible at energies below the pocket because the compound nucleus exists at even

lower energies. However, the fusion is expected to be strongly hindered at such low energies and it would require a much more complicated dynamics to describe it. We note that the fusion/absorption cross section would not have vanished below the pocket if we had

applied a complex potential in our calculations. We were unfortunately not able to reproduce the low-energy data when we used a complex potential so we were forced to abandon that approach.

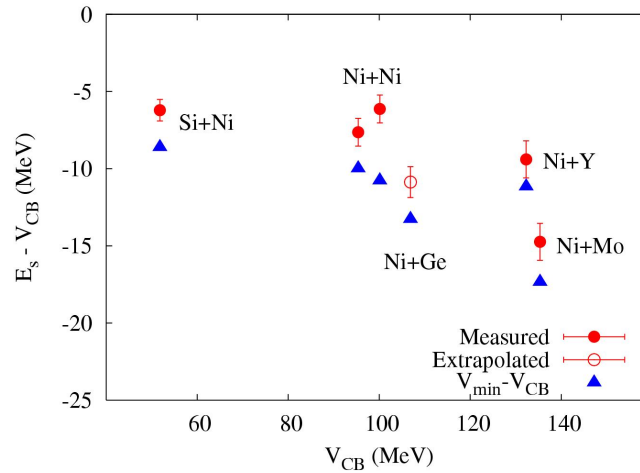


Fig. V-13. The energy  $E_s$  where the  $S$  factor for fusion develops a maximum (solid points) is compared to the minimum  $V_{min}$  of the potential pocket (triangles) for the heavy-ion systems discussed in the text. The open circle is an extrapolated value of  $E_s$  for the  $^{64}\text{Ni} + ^{74}\text{Ge}$  system.

Another signature of a shallow pocket in entrance channel potential (in addition to the fusion hindrance discussed above) is a narrowing of the spin distribution for fusion when the center-of-mass energy is below the critical energy  $E_s$ . A narrower spin distribution implies a reduction in the multiplicity of  $\gamma$ -rays emitted from the compound nucleus.

potential is that the calculated fusion cross section is suppressed at high energies compared with calculations that are based on the more conventional Akyüz-Winther potential. Moreover, the suppression helps in explaining the energy dependence of the data at high energies as illustrated in Fig. V-14.

An interesting feature of applying the M3Y+repulsion

This work has been published.<sup>1</sup>

\*National Institute of Nuclear Physics, Bucharest, Romania.

<sup>1</sup>Ş. Mişicu and H. Esbensen, Phys. Rev. C **75**, 034606 (2007).

<sup>2</sup>C. L. Jiang *et al.*, Phys. Rev. C **73**, 014613 (2006); Phys. Lett. **B640**, 18 (2006).

<sup>3</sup>M. Beckerman *et al.*, Phys. Rev. C **25**, 837 (1982).

<sup>4</sup>C. L. Jiang *et al.*, Phys. Rev. Lett. **93**, 012701 (2004).

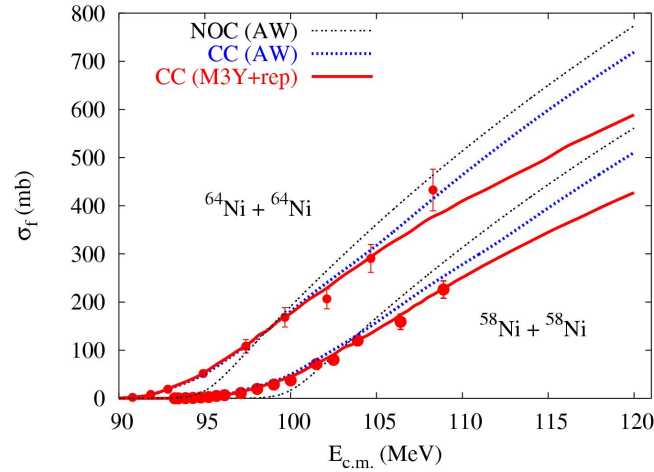


Fig. V-14. Fusion cross sections for  $^{58}\text{Ni} + ^{58}\text{Ni}$ <sup>3</sup> and  $^{64}\text{Ni} + ^{64}\text{Ni}$ .<sup>4</sup> The coupled-channels calculations that are based on the M3Y+repulsion potential (solid curves) reproduce the data, whereas the cross sections obtained with the AW potential (dashed curves), with (CC) and without (NOC) the effect of couplings, are steeper.

## d.2. Coupled-Channels Analysis of $^{16}\text{O} + ^{208}\text{Pb}$ Fusion Reactions (H. Esbensen and Ş. Mişicu\*)

The hindrance of heavy-ion fusion at extreme subbarrier energies, which has been observed at Argonne in several medium heavy systems (Si + Ni, Ni + Ni, Ni + Y, Ni + Mo),<sup>1</sup> was recently observed in the very asymmetric system  $^{16}\text{O} + ^{208}\text{Pb}$ .<sup>2</sup> The hindrance phenomenon<sup>1</sup> is characterized by the development of a maximum in the  $S$  factor at low energy, and the new data confirm this behavior as illustrated in Fig. V-15a. The open circles are the old fusion data.<sup>3</sup> The solid points are the new data<sup>2</sup> which show a very broad maximum of the  $S$  factor at low energy.

We have analyzed the  $^{16}\text{O} + ^{208}\text{Pb}$  fusion data by coupled-channels calculations. We use the M3Y double-folding potential which has been corrected for the influence of the nuclear incompressibility. This type of potential has been very successful in explaining the hindrance in the low-energy  $^{64}\text{Ni} + ^{64}\text{Ni}$  fusion data<sup>4</sup> so it is natural to test whether a similar potential can explain the  $^{16}\text{O} + ^{208}\text{Pb}$  fusion data. The total ion-ion potential we obtain is shown by the solid curve in Fig. V-15b. It has a rather shallow pocket and a much thicker Coulomb barrier than obtained with the more conventional Akyüz-Winther (AW) potential. The lowest dashed curve in Fig. V-15b is the entrance

channel potential we obtain for the M3Y double-folding potential without the correction for nuclear incompressibility. This potential is unrealistic because it produces a pocket that is even deeper than the ground state of the compound nucleus. The ground state energy of the compound nucleus is indicated in the figure by the thick horizontal line.

We calculate the fusion cross section in coupled-channels calculations by imposing ingoing-wave boundary conditions at the position of the minimum of the pocket. The calculated fusion cross section will therefore vanish at energies that are below the minimum of pocket, which is 65.1 MeV in this case. The results we obtain in different calculations are shown in the  $S$  factor representation in Fig. V-15a. They all show, as expected, a very dramatic fall off as the energy approaches 65 MeV. The bottom curve (NOC) is the result we obtain in the no-coupling limit. The next curve (Excitations) shows the effect of couplings to low-lying surface modes in projectile and target. It has a narrow peak at very low energy, which is enhanced by a factor of 30 compared to the no-coupling (NOC) limit.

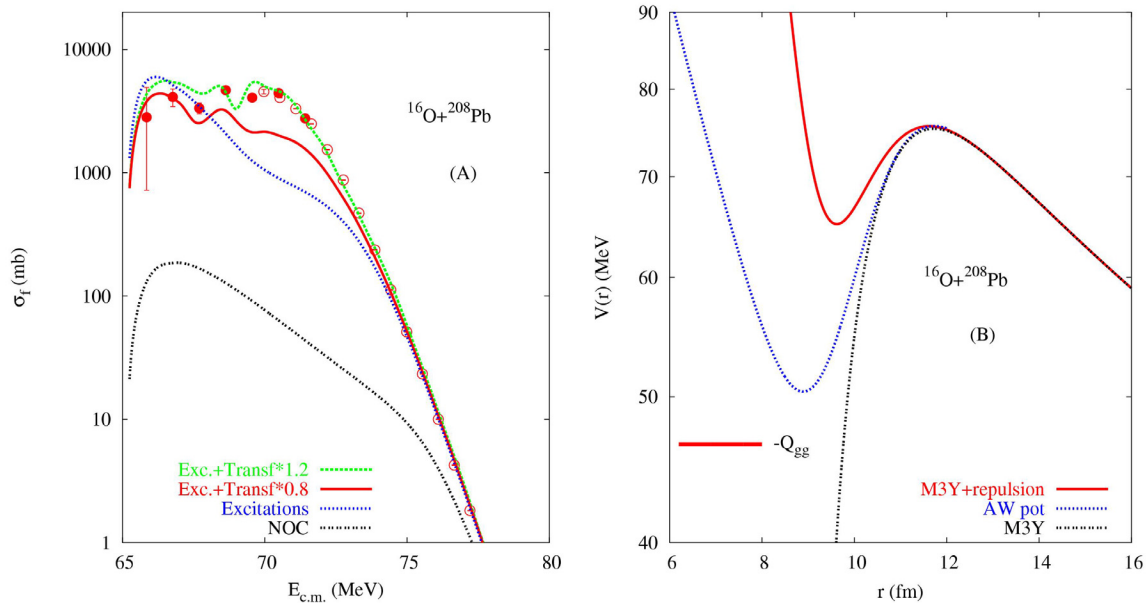


Fig. V-15. The left panel shows the  $S$  factor for the  $^{16}\text{O} + ^{208}\text{Pb}$  fusion cross sections discussed in the text. The data are from Refs. 2 and 3. The right panel shows the total ion-ion potential that was used in the calculations (solid curve,  $M3Y$ +repulsion). It is compared to the total ion-ion potentials obtained from the  $AW$  potential, and from the pure  $M3Y$  double-folding potential.

Finally, we show in Fig. V-15a the results we obtain when we include couplings to the ( $^{16}\text{O}, ^{17}\text{O}$ ) one-neutron pickup in addition to low-lying surface modes. The solid curve is based on a realistic coupling strength for the one-neutron pickup, whereas the strength for the top dashed (green) curve was inflated by 50%, in order to be able to simulate the effect of other transfer channels. It is seen that this rough estimate is in remarkably good agreement with the low energy fusion data. Thus, it is the combination of a shallow potential pocket and couplings to transfer channels that makes it possible to

explain the broad maximum of the measured low-energy  $S$  factor.

We also investigate other aspects of  $^{16}\text{O} + ^{208}\text{Pb}$  reactions at energies near the Coulomb barrier, in order to see how realistic our model calculations are. Thus we want to see how well our coupled-channels calculations can account for the total reaction cross section and the elastic scattering data. This work is in progress.

\*National Institute of Nuclear Physics, Bucharest, Romania.

<sup>1</sup>C. L. Jiang *et al.*, Phys. Rev. C **73**, 014613 (2006); Phys. Lett. **B640**, 18 (2006).

<sup>2</sup>M. Dasgupta, D. J. Hinde, C. Low, and J. O. Newton, AIP Conf. Proc. **853** (2007).

<sup>3</sup>C. R. Morton *et al.*, Phys. Rev. C **60**, 044608 (1999).

<sup>4</sup>Ş. Mişicu and H. Esbensen, Phys. Rev. Lett. **96**, 112701 (2006).

### d.3. Coupled-Channels Analysis of $^{48}\text{Ca} + ^{90,96}\text{Zr}$ Fusion Reactions (H. Esbensen and C. L. Jiang)

A common problem in the analysis of heavy-ion fusion experiments is the difficulty in reproducing all of the

data points, both at low and high energies. In order to make a good fit to the data, it is often necessary to

adjust the parameters of the ion-ion potential. The radius and the depth of the potential, for example, are sensitive parameters for determining the height of the Coulomb barrier, and small adjustments of these parameters are well justified. Another example on a parameter that is sometimes adjusted is the diffuseness of the ion-ion potential. Although the value of this parameter is well determined empirically or from double-folding potentials, it is sometimes chosen to be very large, in order to be able to reproduce the fusion data at high energy.<sup>1</sup>

In an effort to understand what causes the need for using a large diffuseness, we decided to reanalyze a recent measurement, namely, the fusion of  $^{48}\text{Ca} + ^{90,98}\text{Zr}$ .<sup>2</sup> The previous analysis<sup>2</sup> showed that the low energy  $^{48}\text{Ca} + ^{90}\text{Zr}$  fusion data could be reproduced with a realistic diffuseness of the ion-ion potential but the high energy data were then suppressed compared to the calculated cross section. The  $^{48}\text{Ca} + ^{96}\text{Zr}$  data, on the other hand, could only be reproduced with a diffuseness of the ion-ion potential that was 25% larger than the empirical value.

Our analysis shows that the  $^{48}\text{Ca} + ^{96}\text{Zr}$  fusion data can be reproduced fairly well when we use a conventional ion-ion potential, such as the Akyüz-Winther potential. The results we obtain are compared to the data in Fig. V-16. The high-energy data (panel B) are suppressed when compared to the no-coupling (NOC) calculation but the data are nicely reproduced by the coupled-channels calculation, both at high and low

energies. There is some indication of a problem at low energies (panel A), where the logarithmic slope of the data is larger than predicted by the calculation. Apart from that, we are able to make a good fit to the data using a "normal" diffuseness of the ion-ion potential. This was achieved by using coupling strengths that differ slightly from those used in the original analysis.<sup>2</sup>

The  $^{48}\text{Ca} + ^{90}\text{Zr}$  data can also be reproduced fairly accurately by the coupled-channels calculations, except at the highest energies where the data are suppressed. This is consistent with the conclusion of Ref. 2. However, when we include one- and two-proton transfer channels, with positive  $Q$ -values, we are able to reproduce the data over the entire energy range. Thus, we conclude that the use of a large diffuseness can sometimes be avoided by considering the uncertainty in the empirical coupling strengths, or by including other reaction channels (such as transfer) in the adopted coupling scheme.

The only puzzle of the original analysis<sup>2</sup> that remains is the large logarithmic slope of the low-energy  $^{48}\text{Ca} + ^{96}\text{Zr}$  fusion data. We suspect that this indicates the onset of the hindrance, which has been observed in the fusion of other heavy-ion systems. More measurements at smaller cross sections are needed in order to confirm this expectation. It is also of interest to apply the M3Y+repulsion double-folding potential<sup>3</sup> in the coupled-channels calculations in order to be able to remove this last puzzle. This work is in progress.

<sup>1</sup>O. Newton *et al.*, Phys. Rev. C **70**, 024605 (2004).

<sup>2</sup>A. M. Stefanini *et al.*, Phys. Rev. C **73**, 034606 (2006).

<sup>3</sup>Ş. Mişicu and H. Esbensen, Phys. Rev. Lett. **96**, 112701 (2006).

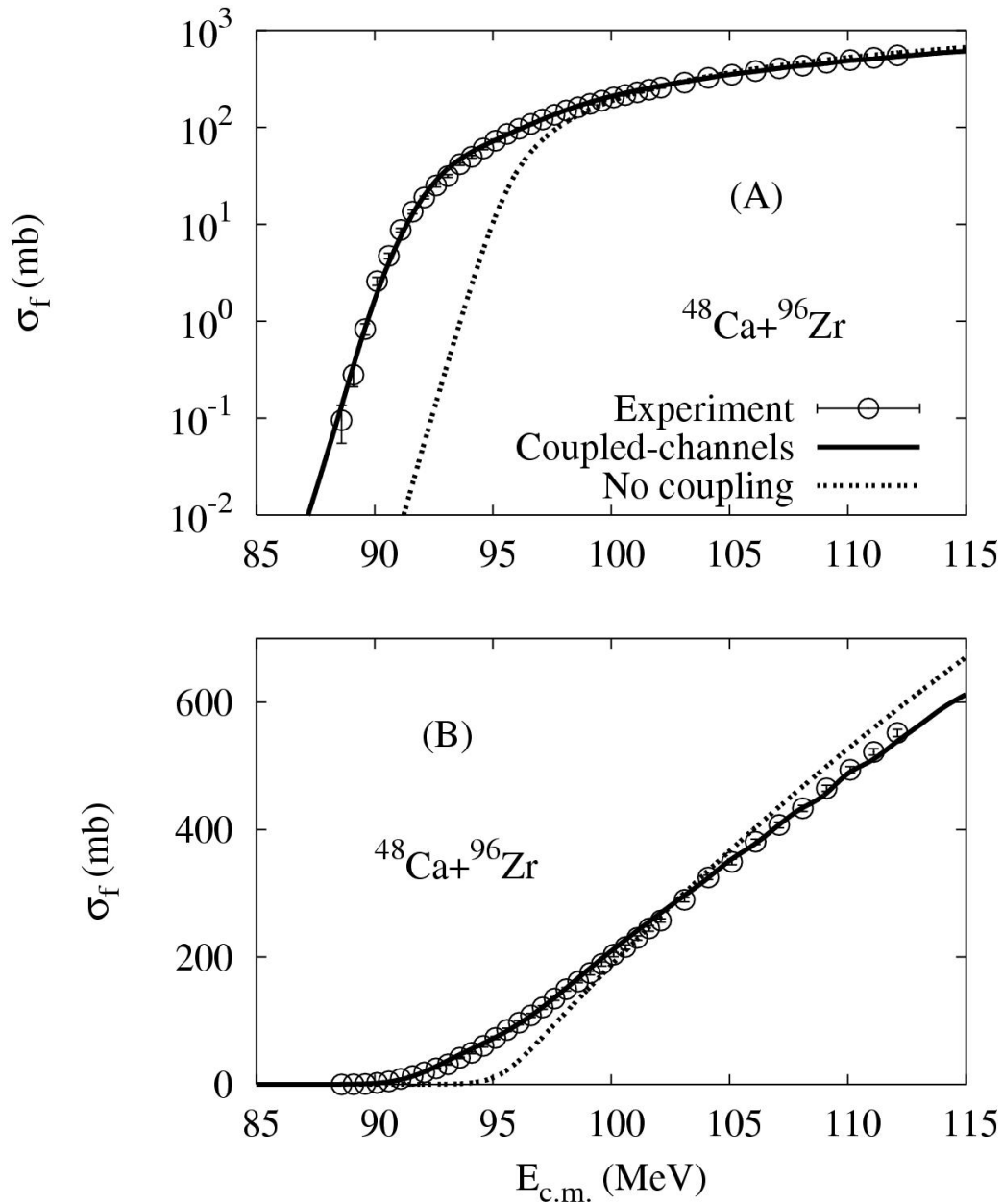


Fig. V-16. Calculated fusion cross sections for  $^{48}\text{Ca} + ^{96}\text{Zr}$  are compared to the data.<sup>1</sup> The solid curve is the coupled-channels result. The dashed curve was obtained without any couplings. The top part (A) is a logarithmic plot whereas (B) shows a linear plot of the cross sections.

#### d.4. Charge Radius and Dipole Response of $^{11}\text{Li}$ (H. Esbensen, P. Mueller, K. Hagino,\* and H. Sagawa†)

The dipole strength of  $^{11}\text{Li}$  has now been measured accurately up to 3 MeV in the  $^9\text{Li} + n + n$  three-body

final state. The measurement was performed at RIKEN at 70 MeV/nucleon on a Pb target.<sup>1</sup> The data are shown

in Fig. V-17 and they are compared to the prediction of a three-body model which we developed about 15 years ago.<sup>2</sup> The data show a strong peak near 300 keV which is reproduced surprisingly well by the calculated distribution (solid curve). The calculation includes the

effect of the final state  $nn$  interaction to all orders and also the experimental energy resolution. Without the final state  $nn$  interaction (dashed curve) we are not able to reproduce the data.

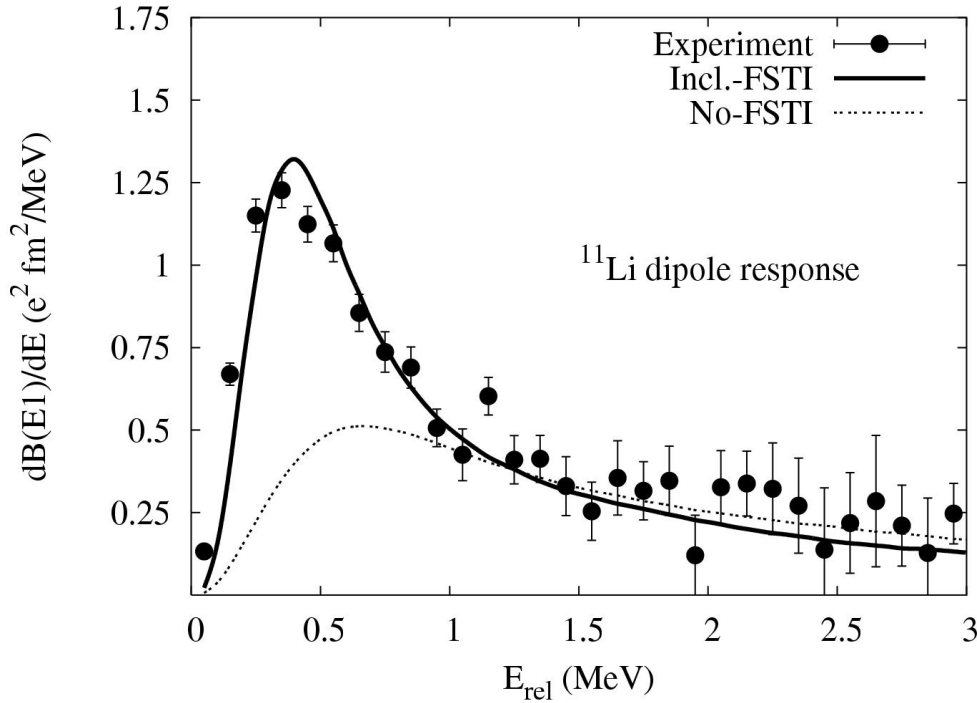


Fig. V-17. The measured dipole response of  $^{11}\text{Li}$  is compared to the calculated distribution<sup>2</sup> with (solid) and without (dashed curve) the effect of the final state neutron-neutron interaction.

The charge radius of  $^{11}\text{Li}$  was recently measured at ISAC using laser spectroscopy.<sup>3</sup> It is of interest to see whether the measured charge radius can be explained by the same three-body model that reproduces the measured dipole response,<sup>1</sup> or whether the core polarization is so strong that a three-body model is unrealistic. The fact that the measured quadrupole moments of  $^{11}\text{Li}$  and  $^9\text{Li}$  are in good agreement (within

the 15% experimental uncertainty) suggests that the effect of core polarization must be small. In a three-body model of  $^{11}\text{Li}$  we assume that the core nucleus is identical to a free  $^9\text{Li}$  nucleus. The difference between the mean square charge radii of  $^{11}\text{Li}$  and  $^9\text{Li}$  can, therefore, be expressed in terms of corrections that are caused by the valence neutrons,

$$\delta\langle r_{ch}^2 \rangle = \langle r_{ch}^r(^{11}\text{Li}) \rangle - \langle r_{ch}^2(^9\text{Li}) \rangle = \left(\frac{2}{11}\right)^2 \langle r_{c,2n}^2 \rangle + \frac{2R_n^2}{Z} + \langle r^2 \rangle_{2n}^{so}.$$

The first term is the main correction, which is due to the center-of-mass motion of the core nucleus in the presence of the two valence neutrons. It has here been expressed in terms of  $\langle r_{c,2n}^2 \rangle$ , which is the mean square distance between the core and the dineutron, *i.e.*,

the center of mass of the two valence neutrons. The second term is due to the non-zero, mean-square charge radius of a neutron,  $R_n^2 = -0.1161(22) \text{ fm}^2$ , and the last term,  $\langle r^2 \rangle_{2n}^{so}$ , is due to the spin-orbit charge density of the two valence neutrons.



The total dipole strength that was measured up to 3 MeV is  $1.42 \pm 0.18 e^2 fm^2$ . The calculated strength for the same energy range is  $1.26 e^2 fm^2$ , and the calculated mean-square core-dineutron distance is  $24.35 fm^2$ . Using simple scaling we therefore estimate that the mean square core-dineutron distance associated with the dipole response is  $27.4 \pm 3.5 fm^2$ . Inserting this estimate into the equation above, together with the other two corrections, we obtain the value  $\delta\langle r_{ch}^2 \rangle = 0.89 \pm 0.18 e^2 fm^2$ .

The difference between the mean square charge radii of  $^{11}Li$  and  $^9Li$  which we obtain from the laser spectroscopy measurement,<sup>3</sup> after applying the revised atomic physics corrections obtained in Ref. 4, is  $\delta\langle r_{ch}^2 \rangle = 1.10 \pm 0.08 fm^2$ . The agreement with the value we estimated from the dipole response

measurement is not perfect; the difference is  $0.21 \pm 0.14 fm^2$ , which is a  $1.5\sigma$  discrepancy. It remains to be seen what causes this discrepancy. An obvious candidate is core polarization, which is beyond the level of a three-body model.

We have also explored what are the implications of the two measurements for the structure of the two neutron halo ground state. Both measurements favor a fairly large  $s$ -wave component, namely, about 25% according to the dipole strength and up toward 50% according to the charge radius measurement. This is in qualitative agreement with the interpretation of other measurements, such as the  $\beta$ -decay and the momentum distributions of the fragment in  $^{11}Li$  breakup reactions. This work has been submitted for publication.

\*Tohoku University, Japan, †University of Aizu, Japan.

<sup>1</sup>T. Nakamura *et al.*, Phys. Rev. Lett. **96**, 252502 (2006).

<sup>2</sup>H. Esbensen and G. F. Bertsch, Nucl. Phys. **A542**, 310 (1992).

<sup>3</sup>R. Sanchez *et al.*, Phys. Rev. Lett. **96**, 033002 (2006).

<sup>4</sup>M. Puchalski *et al.*, Phys. Rev. Lett. **97**, 133001 (2006).

## d.5. Mean Field and Many Body Wavefunctions (R. R. Chasman)

We are continuing our long term effort to develop programs for calculating many-body variational wavefunctions. In our approach, pairing and particle-hole two-body interactions are treated on an equal footing.

In this approach, the complexity of the wavefunctions depends only on the number of levels included in the valence space. In these wavefunctions, we strictly conserve particle number and parity; projecting states of good particle number and parity before carrying out the variational calculations. By including an independent amplitude for the four particle configuration consisting of two neutrons and two protons in the same  $J_z$  sub-state, we can now explain several of the unusual features of nuclides near the  $N = Z$  line, such as the Wigner energy anomaly, in a very simple way. Most of it arises from the large interaction strength between nucleons in the same orbital. Similarly, we find that the inclusion of a three nucleon amplitude in odd-mass configurations accounts well for the extra correlation energy in such nuclides near the  $N = Z$  line.

The major limitation of shell model calculations is that the number of configurations becomes unmanageable as the valence space is increased. The wavefunctions that we are developing contain large numbers of configurations, *e.g.*,  $10^{22}$  configurations in the wavefunctions that we use for Hamiltonians that include  $n$ - $p$  pairing interactions. However, these wavefunctions are product wavefunctions and the number of independent amplitudes is quite small, *e.g.*, 150 independent amplitudes in a wavefunction that has  $10^{22}$  configurations. To fully utilize this simple wavefunction structure, a systematic approach to configuration interaction is needed. We have recently developed such an approach by extending the variational method for use in the context of configuration interaction calculations.

Many of the techniques that we have developed to treat  $n$ - $p$  (neutron-proton) pairing can be profitably applied to Hamiltonians that contain particle-hole interactions in addition to pairing interactions. We are in the process of developing a code to handle particle-hole interactions in addition to pairing.

### d.6. Variational Approach to Configuration Interaction (R. R. Chasman)

Methods for the systematic improvement of solutions to quantum-mechanical problems play an essential role in the accurate theoretical description of physical phenomena. We are developing<sup>1</sup> a class of many-body wavefunctions that are a product of terms. Each of the terms in the product is, in turn, a sum of terms. In such a case, the number of independent variational amplitudes is orders of magnitude smaller than the number of configurations in the wavefunction. In a simple pairing interaction, in a system with 32 doubly degenerate levels and 16 pairs of nucleons, there are approximately  $10^9$  configurations, but the BCS solution for this problem has only 32 independent amplitudes. For the  $n$ - $p$  pairing Hamiltonian that we have studied, there are roughly  $10^{22}$  configurations for a half-filled system with 30 four-fold degenerate levels, each capable of holding two neutrons and two protons. In our product wavefunction, there are just 150 independent amplitudes.

In a model system with pairing and particle-hole interactions, having enough levels to adequately describe the deformed actinides, there are roughly  $10^{29}$  configurations for a nuclide with half-filled neutron and proton shells. The wavefunctions that we use for such nuclides are also a product of sums. Each of the terms in the product is a sum over all configurations that can be built from the orbitals having a fixed value of  $|\Omega|$ , which is the projection of angular momentum on the nuclear symmetry axis for a deformed nucleus. For a spherical nucleus,  $|\Omega|$  is  $|j_z|$ . The number of independent amplitudes in this model actinide system is roughly  $1.2 \times 10^4$ .

We have found that such product solutions can be systematically improved by combining the approach of configuration interaction with the variational method. The basic idea is to take linear combinations of wavefunctions, all with the same general structure, to

construct more accurate solutions. We start with a variational solution of the given product form. We then calculate amplitudes for a second wavefunction having exactly the same form. The amplitudes of the second wavefunction are determined variationally as the optimal improvement to the original wavefunction for a wavefunction of that form. A third wavefunction is then calculated as the optimal improvement on the first two wavefunctions. The method can be continued indefinitely.

There are exact solutions available for a pairing Hamiltonian with constant matrix elements. We tested our approach by comparing our results with the exact energy for the model pairing Hamiltonian. We got agreement to  $1 \text{ keV}$ , by taking 80 basis states. Using only 40 basis states, the error is just  $3 \text{ keV}$ . In the case of the  $n$ - $p$  pairing Hamiltonian, there are no exact solutions available. We found that the wavefunction with 80 basis states improves the binding energy by  $1 \text{ MeV}$  relative to the wavefunction consisting of a single optimized state.

Our major effort, in the past year, has been to extend this variational approach to a Hamiltonian with pairing and particle-hole interactions. We are developing such a code and it runs reasonably quickly. We obtain 25 of the optimal variational wavefunctions on a laptop (1.7 GHz uniprocessor) in two hours, using 200 iterations to calculate each variational wavefunction. We are working to further improve the efficiency of this code.

The usual stumbling block to adding more and more wavefunctions in configuration interaction calculations is that, at some point, the overlap between the added wavefunction and those already in place approaches 1 and there is no improvement in the energy. Our variational approach does not have the problem of overlap pileup.

<sup>1</sup>R. R. Chasman, Phys. Rev. Lett. **95**, 262501 (2005).

### d.7. Neutron-Proton Pairing (R. R. Chasman)

We have developed<sup>1-3</sup> a treatment of neutron-proton pairing that explains many features of nuclear structure seen near the  $N = Z$  line. Our many-body treatment includes  $n$ - $p$  pairing, as well as like particle pairing. We do a full projection of neutron and proton particle number before the variational calculation. We also

found that there is a new quantum number that holds exactly for collective states; *i.e.*, those states in which no levels are blocked. This new quantum number ( $Q$ ) is the number parity of the  $T = 0$  and  $T = 1$   $n$ - $p$  pairs. Fixing the number parity of one  $n$ - $p$  mode fixes the other, because we conserve proton number and neutron

number exactly. This number parity is closely related to the isospin quantum number. These collective states are the ground states for  $N = Z$  nuclides. We project  $Q$  before doing a variational calculation. The form of our variational wavefunction includes an explicit amplitude for “alpha like” correlations in each level as well as the usual amplitudes for  $n$ - $n$ ,  $p$ - $p$  and  $n$ - $p$  pairs. Similarly in odd mass nuclei, we have explicit amplitudes for  ${}^3\text{He}$  and  ${}^3\text{H}$  like correlations. We have added terms to the  $n$ - $p$  pairing interaction that allow pairs of particles in the same orbitals, giving states with maximum angular momentum. Because of the exclusion principle, these must be  $n$ - $p$  pairs and  $T = 0$ .

In odd-odd  $N = Z$  nuclei, the ground state is a degenerate doublet, consisting of a  $Q = 0$  and  $Q = 1$  state, when the  $T = 0$  and  $T = 1$  pairing strengths are equal. The splitting of this ground state doublet affords some information about the relative strengths of the  $T = 0$  and  $T = 1$  pairing strengths. In even-even nuclei, there is a large splitting between the  $0^+$   $T = 1$  ground state and the  $1^+$   $T = 0$  excited state. Our model explains this feature in a transparent way. Most of the excitation energy owes to the breaking of a quartet and the single particle excitation energy involved in making a  $T = 0$  pair. In the odd-odd  $N = Z$  nuclei case, neither of these effects applies for the  $T = 0$  state.

The Wigner energy is the extra binding energy of  $N = Z$  even-even nuclei relative to neighboring nuclei. Our approach explains the magnitude of the Wigner energy very well. It arises from the extra pairing energy involved in creating a quartet of nucleons in the same orbital. There is a similar increase in the correlation

energy of odd-mass nuclei having one less nucleon than an  $N = Z$  nucleus. Our model gives a ratio of 1/2 for the two energy anomalies. We have made an analysis of experimental binding energies and find a ratio in good agreement with this prediction.

Our detailed calculations of the dependence of the binding energies on the relative strengths of the  $T = 0$  and  $T = 1$  pairing strengths shows that the differences are small as a function of the variation of the relative strengths. Other observables are needed to establish the magnitude of  $T = 0$  correlations in nuclei. To that end, we have carried out a calculation of the  $n$ - $p$  pair transfer spectroscopic factor using single-particle level spacings that are appropriate for  ${}^{44}\text{Ti}$ , for which  ${}^2\text{H}$  pair transfer studies are being carried out. In our calculation, the initial state is the ground state of  ${}^{44}\text{Ti}$ , an even-even  $N = Z$  nuclide and the final states are the lowest  $T = 1$  and  $T = 0$  states in the neighboring odd-odd ( $Z + 1, N + 1$ ) nucleus  ${}^{46}\text{V}$ . The spectroscopic probability factors show a considerable sensitivity to the relative strengths of the  $T = 0$  and  $T = 1$  pairing strengths. In Fig. V-18, we show the spectroscopic factors for  $T = 0$  and  $T = 1$  pair transfer probabilities to states in  ${}^{46}\text{V}$ . A 15% reduction of the  $T = 0$  pairing strength gives roughly a 40% reduction in the ratios of  $T = 0/T = 1$  pair transfer probability spectroscopic factor. This reduction of 15% of the  $T = 0$  pairing strength gives an excitation energy for the  $1^+$  state in agreement with experiment. In the lower portion of the figure, we display the excitation energy of the  $1^+$  state as a function of the  $T = 0$  pairing strength, keeping a fixed  $T = 1$  pairing strength.

<sup>1</sup>R. R. Chasman, Phys. Lett. **B524**, 81 (2002).

<sup>2</sup>R. R. Chasman, Phys. Lett. **B553**, 204 (2003).

<sup>3</sup>R. R. Chasman, Phys. Lett. **B577**, 47 (2003).

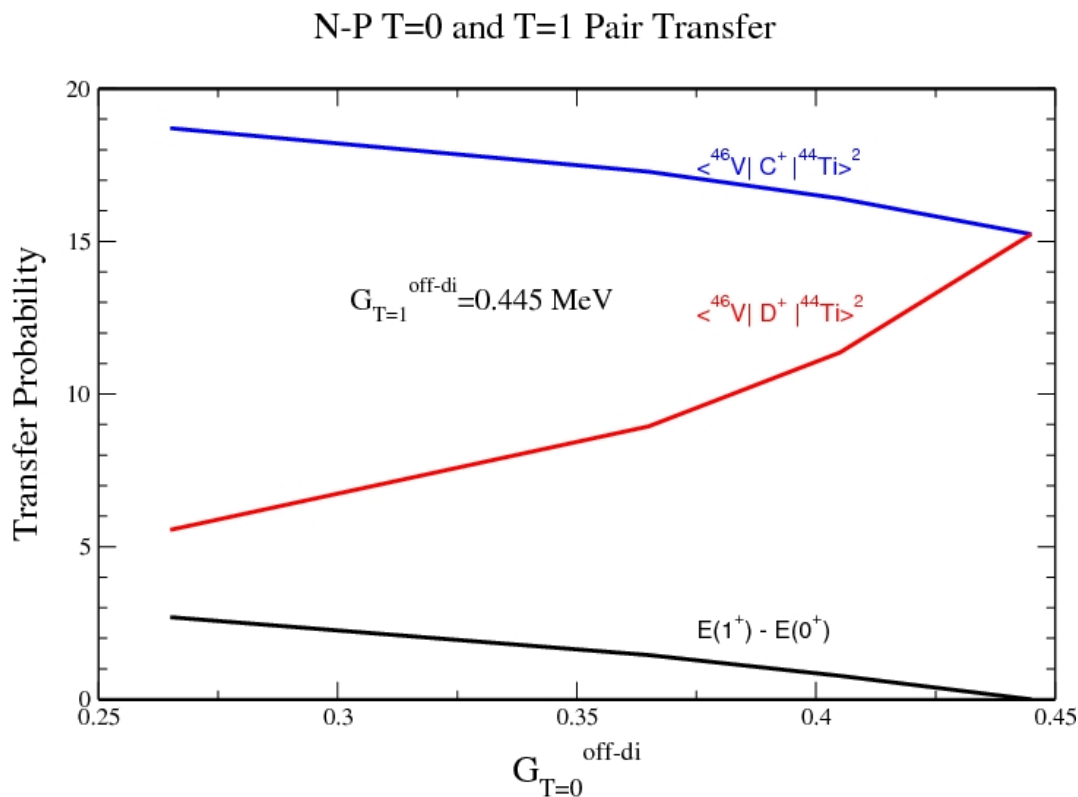


Fig. V-18. Spectroscopic Factors for  $T = 0$  and  $T = 1$   $n$ - $p$  pair transfer. The  $T = 1$  pairing interaction matrix element is held constant. The transfer probabilities are shown as a function of the  $T = 0$  pairing strength. See text for more details.

#### d.8. Energy Levels of the Heavy Elements (I. Ahmad and R. R. Chasman)

The study of single-particle states in the heavy elements is a long-term collaborative project. The low-lying states in odd-mass nuclides provide a good test of the parametrizations of single particle models. Vibrational admixtures are usually small for these states. The single-particle energy level spacings in the heavy elements provide useful guidance for single-particle potentials that are appropriate for super-heavy elements. Seven single-particle states have been identified<sup>1</sup> in  ${}^{247}\text{Cm}$ , so this nuclide provides a good test of neutron single particle potentials. The study<sup>2</sup> of  ${}^{251}\text{Cf}$  is particularly important as it has 153 neutrons, giving information on the neutron single particle states

above the deformed gap at 152 neutrons. Nine single particle states have been identified in this nuclide. Eight single-particle levels have been identified<sup>3</sup> in  ${}^{249}\text{Bk}$ . This provides a very good test of proton single-particle potentials in the very heavy elements. When pairing effects are extracted<sup>4</sup> from the observed levels in  ${}^{247}\text{Cm}$ ,  ${}^{251}\text{Cf}$  and  ${}^{249}\text{Bk}$ , the orderings and spacings of levels are in good agreement with the levels obtained from our parametrization of a deformed Woods-Saxon potential. These analyses will provide useful constraints on other parametrizations of superheavy potentials.

<sup>1</sup>I. Ahmad *et al.*, Phys. Rev. C **68**, 044306 (2003).

<sup>2</sup>I. Ahmad *et al.*, Phys. Rev. C **72**, 054308 (2005).

<sup>3</sup>I. Ahmad *et al.*, Phys. Rev. C **71**, 054305 (2005).

<sup>4</sup>R. R. Chasman, Phys. Rev. C **14**, 1935 (1976).

## E. ATOMIC THEORY AND FUNDAMENTAL QUANTUM MECHANICS

In addition to research on hadron and nuclear physics, and nuclear astrophysics, we also conduct research in atomic physics, neutron physics, and quantum computing.

Work in atomic physics includes the studies of interactions of electrons or high-energy photons with matter, in support of experiments performed at Argonne's Advanced Photon Source (APS). Theoretical studies are being conducted on the physics of the photoeffect and Compton scattering by bound electrons, focusing on topics selected in view of basic importance, timeliness, and potential in applications. Comprehensive surveys of photo-interaction data for silicon and graphite are underway. Some of the results are useful for underpinning cross sections and stopping power for charged-particle interactions, namely, basic data for radiation physics.

Ongoing theoretical work in support of a new experiment to measure the neutron electric-dipole moment (EDM) is currently focusing mostly on issues relating to the penetration of neutrons into a perfect silicon crystal in the Bragg reflection process. Preliminary reflectivity measurements at the NIST reactor have been performed and the main instrumental issues appear to have been identified. An experiment to measure the interaction of the neutron's known magnetic dipole moment with the crystalline electric field, intended both to test the principle of the EDM experiment and to calibrate the electric field, is planned for late in 2006.

Work was completed on representations of complex rational numbers as states of finite strings of two types of qubits, one for real and one for imaginary numbers. These rational string states representations were extended to a representation of real and complex numbers by defining Cauchy sequences of the rational string states. The definition of the Cauchy condition, which mirrored that used in mathematical analysis, was given for sequences of states of the form  $|s_n\rangle$ , where  $s_n: \{1, \dots, n\} \rightarrow \{0, 1\}$  is a 0 - 1 valued function, and extended to linear superpositions of sequences of these states. Much of the work to show that (equivalence classes) of these state sequences represent real and complex numbers consists in verifying that definitions of addition and multiplication and their inverses have the requisite properties and that the set is complete (the set is closed under taking of limits).

### e.1. Interactions of Photons with Matter (M. Inokuti and D. Y. Smith\*)

In support of experiments in atomic and condensed-matter physics with the use of synchrotron radiation, theoretical studies are being conducted on the physics of photo-absorption and Compton scattering, focusing on topics selected in view of basic importance, timeliness, and potential applications.

One theme of long-term studies has been the use of dispersion relations and sum rules for indices of response of matter over the entire range of photon energies. An application is the evaluation of the mean excitation energy for stopping power. New results are  $164 \pm 2 \text{ eV}$  for silicon, and  $77 \pm 4 \text{ eV}$  for graphite.<sup>1</sup>

\*University of Vermont.

<sup>1</sup>D. Y. Smith, M. Inokuti, W. Karstens, and E. Shiles, Nucl. Instrum. Methods **B250**, 1 (2006).

## e.2. Interactions of Charged Particles with Matter (M. Inokuti)

Stopping power, the total yield of ionization, and its statistical fluctuations are examples of quantities describing the penetration of charged particles through matter and are important to applications such as the detection of particles and the analysis of their charges and kinetic energies. The understanding of those quantities in terms of individual collisions and associated cross sections remains a major challenge and is the goal of our continuing effort. A recent publication<sup>1</sup> concerns the evaluation of the mean excitation energies, namely, the  $I$  values, in the Bethe stopping-power formula from the oscillator-strength spectra for 9 atoms and 23 molecules that are treated by Berkowitz.<sup>2</sup>

Extensive work for the International Commission on

Radiation Units and Measurements (ICRU) continues on the editing of its reports and on physical data such as stopping powers and various interaction cross sections.

The main line of Inokuti's life-long study concerns interactions of energetic charged particles with matter and consequent changes in the structure and properties of matter. This topic forms a basis for particle detection and analysis in experimental nuclear and particle physics, as well as for mechanistic considerations in radiation chemistry and biology, and in materials science. I am writing a manuscript for a monograph entitled "Principles of Radiation Physics". The book will be a comprehensive presentation of my major observations and findings in about 600 printed pages.

<sup>1</sup>S. Kamakura, N. Sakamoto, H. Ogawa, H. Tsuchida, and M. Inokuti, *J. Appl. Phys.* **100**, 064905 (2006).

<sup>2</sup>J. Berkowitz, *Atomic and Molecular Photoabsorption. Absolute Total Cross Sections* (Academic Press 2002).

## e.3. A Bragg Scattering Method to Search for the Neutron Electric Dipole Moment (M. Peshkin, M. Arif,\* T. W. Dombek,† D. S. Hussey,\* D. Jacobson,\* H. Kaiser,‡ D. Koetke,§ and R. K. Smither¶)

The goal of this experiment is to search for the neutron electric dipole moment by observing the precession of the neutron's spin polarization in the atomic electric fields when neutrons are Bragg reflected from a perfect silicon crystal. The anticipated rotation in a single reflection is a few microradians. By causing the neutrons to undergo some 20,000 successive reflections as they drift down a slot cut into the crystal, we anticipate achieving a sensitivity of a few times  $10^{-27}$  e-cm, comparable with the sensitivity sought in the next round of ultra-cold-neutron experiments, but with significantly different systematic errors. Our experiments are being carried out at the reactor at the NIST Center for Neutron Research, in Gaithersburg, MD.

In 2006, NIST commenced construction of a dedicated beamline and experimental area for this experiment. That construction is expected to be completed in early summer 2007. At that time we will measure the reflectivity and geometrical properties of an improved slotted silicon crystal currently being prepared at Argonne. We have previously shown experimentally that the reflectivity of a properly prepared silicon surface is greater than 0.9999. In 2007 we plan to measure the reflectivity or raise its lower bound.

We are currently preparing for an experiment to measure the interaction of the neutron's magnetic dipole moment (MDM) with the atomic electric fields by the same technique, making use of the Schwinger interaction between an electric field and a moving MDM, the latter appearing as an effective EDM. The MDM experiment will serve as a proof of principle and exploration of systematic errors for the EDM experiment, and it will also serve as a necessary calibration of the effective electric fields experienced by the neutrons in the EDM experiment. Technical details of the MDM experiment are given in a NIST report "Technical Report on the Status of the Measurement of Neutron Schwinger Scattering in Silicon," dated January 17, 2007. The MDM experiment is being done in collaboration with F. Wietfeldt of Tulane University.

We are currently procuring a set of Helmholtz coils to achieve the magnetic field quality needed for the Schwinger experiment. We have on hand, or on order, all of the necessary polarization handling equipment (polarizer, Heusler analyzer crystal, spin rotation coils, etc.). We expect to use these in 2007 to investigate the effects of neutron penetration into the crystal in Bragg scattering and begin preliminary measurements and

calibrations.

\*National Institute of Standards and Technology †University of Hawaii, ‡University of Indiana, §Valparaiso University, ¶Advanced Photon Source User Program, Argonne National Laboratory.

#### e.4. Quantum Theory Representations of Real and Complex Numbers<sup>1,2</sup> (P. Benioff)

As part of a long term project of working towards a coherent theory of physics and mathematics together, work was completed on a quantum representation of real and complex numbers as equivalence classes of Cauchy sequences of states of qubit strings that represent real and imaginary rational numbers. Complex rational number states are represented by four types of annihilation creation operators for four different types of qubits on an integer lattice;  $a_{ij}^\dagger, b_{ij}^\dagger, c_{\gamma,0}^\dagger, d_{\delta,0}^\dagger$ . Here  $i = 0,1, j$  is an integer, and  $\delta, \gamma = +, -$ . Complex rational string states are represented by  $|\gamma, s; \delta, t\rangle = c_{\gamma,0}^\dagger a_{s(l),l}^\dagger a_{s(u),u}^\dagger d_{\delta,0}^\dagger b_{t(k),k}^\dagger b_{t(v),v}^\dagger |0\rangle$ . Here  $s$  and  $t$  are 0,1 valued functions on the respective integer intervals  $[1,u]$  and  $[k,v]$ ,  $\gamma, \delta$  give the signs of the real and imaginary components and  $|0\rangle$  is the qubit vacuum state. Also,  $1 \leq 0 \leq u$  and  $k \leq 0 \leq v$ . Quantum representations of real and complex numbers are defined as equivalence classes of sequences  $\{|\gamma_n, s_n\rangle : n = 0, 1, \dots\}$  and  $\{|\gamma_n, s_n; \delta_n, t_n\rangle : n = 0, 1, \dots\}$  of qubit string states that satisfy the Cauchy condition. This definition was also extended to apply to sequences of superpositions of states of the form  $\sum_{\gamma,s,\delta,t} c_{\gamma,s,\delta,t}$

$|\gamma, s; \delta, t\rangle$ .

The above description was expanded by considering gauge transformations of the real and complex rational number representations and the corresponding transformed representations of real and complex numbers. If  $U: I \rightarrow U(2)$  is a function from the integers  $I$  to the group  $U(2)$ , then the action of  $U$  on a state  $|\gamma, s; \delta, t\rangle$  gives the state  $U|\gamma, s; \delta, t\rangle = |\gamma_U, s_U; \delta_U, t_U\rangle$ . This state represents the same complex rational number in the transformed representation as  $|\gamma, s; \delta, t\rangle$  does in the original representation. One can now define Cauchy sequences of these transformed states to obtain another quantum representation  $R_U, C_U$ , of the real and complex numbers. It is clear that for each gauge  $U$ , one has quantum representations of the real and complex numbers. All these representations are isomorphic, yet they are distinct. One can show that there is a sense in which a real number in  $R_U$ , is orthogonal to “the same” real number in  $R_{U'}$  where  $U'$  is another gauge transformation.

<sup>1</sup>P. Benioff, *Fields of Iterated Quantum Reference Frames Based on Gauge Transformations of Rational String States*, arXiv preprint quant-ph/0604135.

<sup>2</sup>P. Benioff, *Fields of Quantum Reference Frames Based on Different Representations of Rational Numbers as States of Qubit Strings*, arXiv preprint quant-ph/0611139.

#### e.5. Fields of Iterated Reference Frames Based on Quantum Theory Representations of Real and Complex Numbers<sup>1,2</sup> (P. Benioff)

These representations yield interesting structures when one considers the fact that real and complex numbers form the base of all physical theories, and of space time if space time is represented as a 4-tuple of real numbers. Let  $F$  denote a reference frame based on  $R, C$ , which are the usual real and complex numbers that are considered, by an observer in  $F$ , as “given” and with no structure beyond that required by the relevant axiom sets.  $F$  is defined to contain all physical theories as mathematical structures based on  $R, C$ , and space time as  $R^4$  if it is represented as a 4-tuple of real numbers. The above description of quantum representations,  $R_U, C_U$ , takes place in  $F$  where the relevant theories used in

the description of  $R_U, C_U$ , are based on  $R, C$ . Since  $R_U, C_U$ , are representations of the real and complex numbers, they can also serve as the base of physical theories. This gives a frame  $F_U$ , which is a collection of all physical theories as mathematical structures based on  $R_U, C_U$ . There are many such frames, one for each  $U$ . Each  $F_U$  is equivalent as the theories in each frame are equivalent. Also, an observer in  $F_U$  sees  $R_U, C_U$  as given and with no structure. The structure of  $R_U, C_U$  is visible to an observer in  $F$ .

This structure of frames emanating from frames can be iterated leading to fields of iterated reference frames

with a genealogical structure. There are several possibilities for the structure: a finite number of iterations, a one way infinite number, a two way infinite

number, and a cyclic structure. Figure V-19 is a schematic of two iterations with an ancestor frame F and two progeny generations.

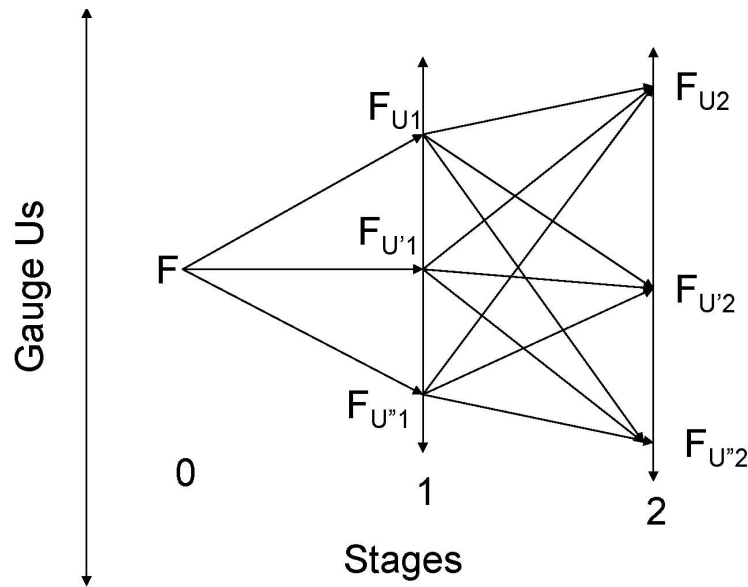


Fig. V-19. Three iteration stages of frames coming from frames. Only three frames of the infinitely many, one for each gauge U, are shown at stages 1 and 2. The arrows connecting the frames show the iteration direction of frames coming from frames.

The connection of the frame field to physics is important. Since there is no evidence of many different universes with the structure of the field, one needs to find a way to collapse the field. One method to collapse the different  $F_U$  in each generation is to use gauge invariant representations of qubit states. This

can be done by letting qubit states correspond to the irreducible representation subspaces of  $SU(2)$ . This still leaves the generations intact. Clearly, there is much work to do towards the goal of a coherent theory of physics and mathematics.

<sup>1</sup>P. Benioff, *Fields of Iterated Quantum Reference Frames Based on Gauge Transformations of Rational String States*, arXiv preprint quant-ph/0604135.

<sup>2</sup>P. Benioff, *Fields of Quantum Reference Frames Based on Different Representations of Rational Numbers as States of Qubit Strings*, arXiv preprint quant-ph/0611139.



## F. OTHER ACTIVITIES

### f.1. Third ANL/MSU/INT/JINA Rare Isotope Accelerator Workshop (H. Esbensen, K. M. Nollett, and C. D. Roberts)

This meeting was primarily organized by the Argonne Theory Group and was held in the Physics Division from April 4-7, 2006. It is one of a series of workshops that are hosted in a rotating fashion among the sponsoring institutions. The series was established to explore, explain and support the case for an advanced exotic beam facility from a theoretical-physics perspective, and to encourage the theoretical work that will be needed to interpret experiments once such a facility is built.

An advanced exotic beam facility is vital for the future of low-energy nuclear physics and will produce advances: in understanding the nature of nuclei and nuclear matter; in explaining the origins of the chemical elements and the workings of stars; and in testing the standard model of particle physics. Both the community and DOE remain firmly committed to such a facility.

The first two meetings in this series focused on specific areas of nuclear theory. The topic of the first, held at the Institute for Nuclear Theory (INT), was the astrophysical  $r$ -process. The second, held at Michigan State University (MSU), concentrated on the present state of nuclear reaction theory. Owing to the timing of this third meeting, we wanted the presentations, the discussions and, indeed, the proceedings volume<sup>1</sup> to cover a broader range of topics in current nuclear theory. Sessions were organized on: dynamic

symmetries in nuclei; fundamental symmetries; nuclear structure; and nuclear astrophysics. We recruited a collection of speakers to give a thorough overview of topics at the leading edge of nuclear theory and asked them to respond to the following question: “What questions does your research pose that only an exotic beam facility can answer?”

The picture which emerged from the presentations is that progress is being made in a broad range of distinct but overlapping areas within nuclear theory. This is captured in the contributions to the proceedings volume, which span a wide range of topics, from the lightest nuclei to some of the heaviest, from *ab initio* to phenomenological approaches, from “pure” nuclear physics to challenging astrophysical problems that require proper accounting for nuclear properties. An expansion of the range of measurable nuclear properties beyond present capabilities will present new constraints and new challenges for the theoretical approaches discussed.

We set aside thirty minutes at the end of each session for discussion in an open forum; these discussions were often lively. Such discussion, with broad representation from across the nuclear physics community, is important to maintain theory on a trajectory that will both support and profit from experiments at the next generation of experimental facilities.

<sup>1</sup>*Opportunities with Exotic Beams*, edited by T. Duguet, H. Esbensen, K. M. Nollett, and C. D. Roberts (World Scientific, New Jersey, 2007).

### f.2. Nineteenth Annual Midwest Theory Get-Together (C. D. Roberts)

The Theory Group hosted the nineteenth Annual Midwest Theory Get-Together on October 13-14, 2006. Nuclear theorists from seventeen Midwest universities and ANL met to learn about the research goals and foci of different individuals and groups throughout the region. While the organizational duties rotate amongst the participants, Argonne is the regular host site because of its meeting facilities and central location. The organizer for 2006 was Stefan Frauendorf from the University of Notre Dame. The meeting provides a

good chance for students to broaden their outlook and get some practical speaking experience in a friendly atmosphere. The format is informal, with an agenda of talks being volunteered at the beginning of the meeting. In 2006 we had forty-five registered participants: faculty, postdocs and students. Over the Friday afternoon and Saturday morning twenty-nine presentations were made, covering topics such as: *ab-initio* studies of masses and scattering based on nuclear Hamiltonians; effective field theories;

fundamental quantum mechanics; hadron physics, parton distribution functions and QCD; the nuclear shell model, nuclear pairing and nucleon matter; nuclear and quark astrophysics; quantum Monte Carlo

methods; relativistic heavy ion collisions; and relativistic quantum mechanics for few body systems. It was a successful event.

## VI. OTHER EDUCATIONAL AND COMMUNITY OUTREACH ACTIVITIES

### OVERVIEW

Education remains a key part of our mission, especially training young nuclear physicists for the next generation of research, stewardship and homeland security. We are involved in many programs, including education at undergraduate, graduate, and post-doctoral level. We are also involved in using our expertise and capabilities to support programs in local Universities and in our community.

#### a.1. Minority Program (B. Zeidman)

The primary aim of the minority program is increasing the number and quality of minority participants in physics and other sciences. This involves ongoing interactions with minority students and faculty during visits to colleges and universities with substantial minority populations and a number of other activities. Among these efforts is inclusion of qualified scientists and students from minority institutions in research being performed by ANL scientists; e.g., collaborations on experiments, short-term appointments, and internships, such as SRP and SULI. In addition, attendance at meetings of minority organizations and visits to educational institutions provide chances for individual interactions and discussion of a wide variety of topics, e.g., research opportunities at ANL and other DOE laboratories, graduate education, internships, employment possibilities, etc., that influence choices of major field and career development.

The strongest interactions with minority students result from visits to minority institutions where it is possible to have discussions in depth with individual students. During the academic year, the program involves recruiting trips to schools with substantial minority populations, many having been visited in prior years.

Included in these visits are seminars that discuss research performed by the Physics Division, particularly in the Medium Energy and Heavy Ion programs. Since ANL experiments at JLab include collaborators (both faculty and student) from some of these universities, (e.g., Florida International University, Hampton University, North Carolina A&T University, Southern University, New Orleans, UTEP) some members of the audience are often active participants in the research being discussed. Inasmuch as many students from these colleges may also have been at ANL as participants in the SRP and SULI programs, it is possible to make direct connections between the research being discussed and persons present or known to the audience. SRP and SULI students recruited under the programs performed research in several ANL divisions other than PHY during the past year, e.g. APS, HEP. Institutions recently visited include: Clark-Atlanta University; Morehouse; Spelman; North Carolina A&T; North Carolina Central; Hampton; Norfolk State; University of Texas-El Paso; New Mexico State; Lincoln; Howard University; Morgan State; Fisk; Vanderbilt; Southern University; and Dillard University.

**b.1. ANL Summer School Experience in Physics** (S. M. Fischer, C. J. Lister, A. Hecht, R. V. F. Janssens, P. Mueller, N. Patel, D. Peterson, R. Scott, D. Haskel,\* and G. McMichael†)

In order to increase the exposure of young high school students in Chicago to science and scientific careers, a one week summer school was organized in the Physics Division. The aim was to involve and encourage students, particularly from minority groups, who may not have considered a scientific career. The pilot program included students from the Hyman Rickover Naval Academy. Eight top students from 9<sup>th</sup> grade were selected by competition. The students had completed a year-long course in introductory physics. They came to Argonne each day, and were involved in a variety of projects: hands on experiments, talks about

physics, talks with scientists about their careers, and tours of experimental facilities throughout the laboratory. Dr. Rosner gave the graduation awards. Figure VI-1 is a photograph of the graduation ceremony.

This program was successful and has the potential to grow in scope, mainly by having two parallel programs running, one in the Chemistry Division and one in Physics, with a mixture of 9<sup>th</sup> and 10<sup>th</sup> grade students. In the future, we hope the program will encompass additional Chicago high schools.

\*Advanced Photon Source, Argonne National Laboratory, †Intense Pulsed Neutron Source, Argonne National Laboratory.



*Fig. VI-1. Students from the “Summer School Experience” with Susan Fischer (left), their teacher Dereck Svelnys, and Kim Lister.*

## STAFF MEMBERS OF THE PHYSICS DIVISION

Listed below is the staff of the Physics Division for the year ending December 31, 2006.  
The program headings indicate only the individual's current primary activity.

### SCIENTIFIC STAFF EXPERIMENTAL NUCLEAR PHYSICS STAFF

#### Regular Staff

- John R. Arrington, Ph.D., California Institute of Technology, 1998
- Birger B. Back, Ph.D., University of Copenhagen, Denmark, 1974
- Michael P. Carpenter, Ph.D., University of Tennessee-Knoxville, 1987
- ¶‡ Cary N. Davids, Ph.D., California Institute of Technology, 1967
- § Bela Erdelyi, Ph.D., Michigan State University, 2001
- \* Susan M. Fischer, Ph.D., University of Notre Dame, 1994
- ¶¶ Donald F. Geesaman, Ph.D., State University of New York-Stony Brook, 1976
- Kawtar Hafidi, Ph.D., University of Paris XI, France, 1999
- ‡‡ Walter F. Henning, Ph.D., Technical University of Munich, Germany, 1968
- §§ Roy J. Holt, Ph.D., Yale University, 1972
- \*\* Robert V. F. Janssens, Ph.D., University Catholique de Louvain, Belgium, 1978
- Michael P. Kelly, Ph.D., University of Washington-Seattle, 1999
- Teng Lek Khoo, Ph.D., McMaster University, Canada, 1972
- Torben Lauritsen, Ph.D., State University of New York-Stony Brook, 1990
- Christopher J. Lister, Ph.D., University of Liverpool, United Kingdom, 1977
- ⊕ Zheng-tian Lu, Ph.D., University of California-Berkeley, 1994
- ⊗ Brahim Mustapha, Ph.D., University of Paris XI, France, 1999
- Jerry A. Nolen, Jr., Ph.D., Princeton University, 1965
- Petr N. Ostroumov, Ph.D., Moscow Engineering and Physical Institute, Russia, 1982
- Richard C. Pardo, Ph.D., University of Texas-Austin, 1976
- David H. Potterveld, Ph.D., California Institute of Technology, 1988
- Karl Ernst Rehm, Ph.D., Technical University of Munich, Germany, 1973
- Paul E. Reimer, Ph.D., University of Illinois at Urbana-Champaign, 1996
- ⊕⊕ Guy Savard, Ph.D., McGill University, Canada, 1988
- ¶⊗ John P. Schiffer, Ph.D., Yale University, 1954
- Dariusz Seweryniak, Ph.D., Uppsala University, Sweden, 1994
- ¶ Kenneth W. Shepard, Ph.D., Stanford University, 1970
- Kenneth M. Teh, Ph.D., Vanderbilt University, 1988

- 
- ‡ Adjunct Professor, Vanderbilt University
  - § Joint appointment with Northern Illinois University
  - \* Continuous appointment with DePaul University
  - ¶¶ Director of the Physics Division
  - ‡‡ On leave of absence at GSI-Darmstadt, Germany
  - §§ Adjunct Professor, University of Illinois at Urbana-Champaign
  - \*\* Associate Director of the Physics Division. Adjunct Professor at Michigan State University, Vanderbilt University, and University of Notre Dame
  - ⊕ Professor Coterminous, University of Chicago
  - ⊗ Term Appointment
  - Director of the ATLAS Facility. Adjunct Professor, Michigan State University
  - ⊕⊕ Professor Coterminous, University of Chicago and Adjunct Professor, University of Manitoba, Canada
  - ¶ Retired September 2006
  - ⊗ Professor Emeritus, University of Chicago

### Special Appointments

- Irshad Ahmad, Ph.D., University of California-Berkeley, 1966
- Lowell M. Bollinger, Ph.D., Cornell University, 1951
- Cary N. Davids, Ph.D., California Institute of Technology, 1967
- Cheng-lie Jiang, Ph.D., China Institute of Atomic Energy, China, 1960
- William J. Childs, Ph.D., University of Michigan, 1956
- Donald S. Gemmell, Ph.D., Australian National University, Australia, 1960
- Harold E. Jackson, Jr., Ph.D., Cornell University, 1959
- \* Michael Paul, Ph.D., The Hebrew University of Jerusalem, Israel, 1973
- John P. Schiffer, Ph.D., Yale University, 1954
- Kenneth W. Shepard, Ph.D., Stanford University, 1970
- ☐ Ben Zeidman, Ph.D., Washington University, 1957

### THEORETICAL NUCLEAR PHYSICS STAFF

#### Regular Staff

- Henning Esbensen, Ph.D., University of Aarhus, Denmark, 1977
- Tsung-Shung Harry Lee, Ph.D., University of Pittsburgh, 1973
- Kenneth Nollet, Ph.D., University of Chicago, 2000
- Steven C. Pieper, Ph.D., University of Illinois at Urbana-Champaign, 1970
- Craig D. Roberts, Ph.D., Flinders University of South Australia, Australia, 1989
- ‡ James W. Truran, Ph.D., Yale University, 1965
- Robert B. Wiringa, Ph.D., University of Illinois at Urbana-Champaign, 1978

#### Special Appointments

- Paul Benioff, Ph.D., University of California-Berkeley, 1959
- Richard R. Chasman, Ph.D., University of California-Berkeley, 1959
- Fritz Coester, Ph.D., University of Zurich, Switzerland, 1944
- Mitio Inokuti, Ph.D., University of Tokyo, Japan, 1962
- Dieter Kurath, Ph.D., University of Chicago, 1951
- Malcolm H. Macfarlane, Ph.D., University of Rochester, 1955
- § Vijay Pandharipande, Ph.D., University of Bombay, India, 1969
- Murray Peshkin, Ph.D., Cornell University, 1951

---

\* Special Term Appointee from The Hebrew University of Jerusalem, Israel

☐ Special Term Appointee. Adjunct Professor, Hampton University

‡ Joint appointment with the University of Chicago

§ Special Term Appointee from the University of Illinois at Urbana-Champaign (deceased January 2006)

## TEMPORARY APPOINTMENTS

Mandar Bhagwat (Kent State University)

Theoretical physics studies  
(January 2006 - )

Yun Ding (the University of Chicago)

Medium-energy physics studies  
(January 2006 - )

Sebastian Gros (the University of Liverpool, United Kingdom)

Research at ATLAS  
(May 2005 - )

\* Jeffrey R. Guest (the University of Michigan)

Medium-energy physics studies  
(August 2004 - )

Prashanth Jaikumar (McGill University, Canada)

Theoretical physics studies  
(September 2004 - September 2006)

Shashikant Manikonda (Michigan State University)

Research at ATLAS  
(December 2006 - )

† Peter Mueller (Johannes Gutenberg-University, Germany)

Medium-energy physics studies  
(July 2004 - )

Donald A. Peterson (Oregon St. University)

Research at ATLAS  
(January 2004 - )

Muslema Pervin (Florida State University)

Theoretical physics studies  
(January 2006 - )

Andrew Robinson (the University of Edinburg, United Kingdom)

Research at ATLAS  
(May 2005 - )

Nicholas D. Scielzo (the University of California-Berkeley)

Medium-energy physics studies  
(July 2003 - October 2006)

Hariprakash Sharma (the University of Manitoba, Canada)

Research at ATLAS  
(July 2004 - July 2006)

---

\* Argonne Scholar-AHCPF (Arthur Holly Compton Postdoctoral Fellowship)

† Argonne Scholar-WFLPF (Willard Frank Libby Postdoctoral Fellowship)

Patricia Solvignon (Temple University)  
Medium-energy physics studies  
(July 2006 - )

Tao Sun (Michigan State University)  
Medium-energy physics studies  
(October 2006 - )

Xiaodong Tang (Texas A&M University)  
Research at ATLAS  
(May 2003 - July 2006)

Stewart V. Wright (the University of Liverpool, United Kingdom)  
Theoretical physics studies  
(September 2004 - July 2006)

Jin Xu (Brown University)  
Research at ATLAS  
(August 2005 - )

Shaofei Zhu (the University of Notre Dame)  
Research at ATLAS  
(January 2004 - December 2006)

### **TECHNICAL AND ENGINEERING STAFF**

(and areas of activity)

Kevin G. Bailey (B.S., University of Nebraska, 1989)  
Technical assistance, medium-energy physics

Donald Barnett  
ATLAS operations

\* John M. Bogaty (A.A.S., DeVry University, 1961)  
Electrical systems, ATLAS operation and development

Lee Kevin Carlquist (A.S., College of DuPage, 1986)  
ATLAS operations

\* Benny E. Clift (A.S.E.E., DeVry University, 1959)  
Electrical systems, ATLAS operation and development

\* Donald Cyborski  
Computer operations

Alex Deriy (B.S., University of Illinois-Chicago, 1988)  
ATLAS operations

Gregory Devane  
ATLAS operations

---

\* Special Term Appointee



- \* Joseph Falout (B.S.M.E., University of Illinois, 1970)  
Experimental equipment design
  
- Joel Fuerst (M.S.M.E., Northwestern University, 1990)  
Cryogenic development at ATLAS
  
- Scott M. Gerbick (B.S., Purdue University, 2003)  
ATLAS experimental equipment maintenance, technical assistance, low-energy physics
  
- John P. Greene (M.S., DePaul University, 1982)  
Target preparation
  
- \*\* Ray E. Harden (A.A.S., Milwaukee School of Engineering, 1957)  
ATLAS operations
  
- \* Dale J. Henderson (B.S., Elmhurst College, 1951)  
Detector development, technical assistance, low-energy physics
  
- \* Jack Jagger  
Consulting engineer, medium-energy physics
  
- Robert Jenkins  
ATLAS operations
  
- \*\* Mark Kedzie  
ATLAS experimental equipment development
  
- \*\* David Kurth  
Graphic specialist
  
- Anthony Krupa (A.A.S.-E.E.T., Purdue University, 1987)  
ATLAS operations
  
- Anthony Levand (B.S.M.E., University of Illinois at Urbana-Champaign, 1986)  
Experimental equipment design at ATLAS
  
- Eric Lindert (B.S., University of Wisconsin-Milwaukee, 1992)  
ATLAS operations
  
- \* Paul Markovich (B.S., Purdue University, 1972)  
Surface chemistry, ATLAS development and operation
  
- Stephen MacDonald  
Cryogenics engineer, ATLAS development and operation
  
- \* Bruce Millar  
ATLAS operations
  
- Floyd Munson, Jr. (A.A.S., DeVry University 1966; B.S., Lewis University, 1993)  
Control system for ATLAS

---

\* Special Term Appointee

\*\* Terminated (September 2006)

Thomas P. Mullen (B.S., Marquette University, 1966)  
Division ESH/QA engineer

Bruce G. Nardi (A.A.S., Morton Jr. College, 1967; A.A.S. DeVry University, 1969)  
Electronics design and maintenance

Tom O'Connor (M.S., DePaul University, 1995)  
Technical assistance, medium-energy physics

Donald Phillips (A.S., DeVry University, 1974)  
ATLAS operations

\* John Phillips (M.S., University of Illinois-Chicago, 1986)  
Consulting ESH/QA engineer

Maria Power (M.S., Illinois Institute of Technology, 1993)  
Technical assistance, ATLAS control system

John Rohrer (A.A.S., Triton College, 1987)  
Experimental equipment support, low-energy physics

Robert Scott (B.S., University of Illinois-Chicago, 1995)  
ATLAS operations

Sergey Sharamentov (M.S., Moscow Engineering Physical Institute, 1976)  
Electrical systems, ATLAS operation and development

Brent R. Shumard (B.S., University of Valparaiso, 2002)  
Detector development, technical assistance, low-energy physics

\* James R. Specht (A.A.S., DeVry University, 1964)  
Cryogenics engineer, ATLAS development and operation

Matthew Sternberg (B.S.C., University of Oregon)  
Low-energy research at ATLAS  
(October 2006 – )

\*\* Philip Strickhorn (B.S., DeVry University, 1990)  
Electrical and technical assistance, ATLAS operations

Richard Vondrasek (B.S., University of Chicago, 1990)  
ATLAS ECR source

\* Loren Weber (M.S., Northern Illinois University, 1974)  
ATLAS operations

Philip R. Wilt (Johnstown Technical School, 1973)  
Electronics design and maintenance

Bruce J. Zabransky (M.S., University of Illinois-Chicago, 1973)  
Mechanical engineer

---

\* Special Term Appointee

\*\* Terminated (September 2006)

Gary P. Zinkann (B.S., DeVry University, 1975)  
ATLAS operations supervisor

### ADMINISTRATIVE STAFF

- \* Allan Bernstein (M.B.A., Rosary College, 1986)
- \* James E. Nelson (B.A., University of Illinois-Chicago, 1975)
- \*\* Barbara Fletcher (B.A., DePaul University, 1998)  
Janet Bergman, Administrative Secretary  
Jeannie Glover, Administrative Secretary  
Debra Morrison, Administrative Secretary
- § Amy Randich, High School Student  
Elizabeth Rizzo, Administrative Assistant  
Colleen Tobolic, Administrative Secretary  
Barbara Weller, Administrative Secretary

- 
- \* Assistant Director of the Physics Division
  - \*\* Executive Secretary
  - § Terminated (September 2006)

### VISITORS AND STUDENTS

#### Long-Term Visitors (at Argonne more than 4 months)

Vladislav Asseev (Institute for Nuclear Research of the Russian Academy of Sciences, Russia)  
Accelerator development  
(October 2003 - November 2006)

- \* Van D Bistrow (University of Chicago)  
Medium-energy physics  
(July 2005 - June 2006)

- \*\* Victor Flambaum (University of South Wales, Australia)  
Theoretical physics studies  
(August 2005 - )

William Karstens (Saint Michaels College)  
Theoretical physics studies  
(July 2003 - )

Andrei Kolomiets (Institute of Theoretical and Experimental Physics, Russia)  
Research at ATLAS  
(April 2004 - April 2006)

Sergey Kondrashev (Moscow Engineering Physics Institute, Russia)  
Research at ATLAS  
(November 2006 - )

- 
- \* Guest Faculty Research Participant
  - \*\* Argonne Fellow

- † Serban Misicu (Horia Hulubei National Institute of Physics & Nuclear Engineering, Romania)  
Theoretical physics studies  
(October 2005 - March 2006)

**Short-Term Visitors** (at ANL for less than 4 months at a time)

Masato Asai (Japan Atomic Energy Research Institute, Japan)  
Low-energy research at ATLAS  
(March 2006 - July 2006)

- \* Thomas Dombek (University of Hawaii)  
Theoretical studies  
(August 2006 - )

- \* Christopher Fasano (Monmouth College)  
Theoretical studies  
(February 1999 - )

Ntombizonke Kheswa (iThemba Labs, South Africa)  
Low-energy research at ATLAS  
(April 2006 - May 2006)

Rachid Nouicer (University of Chicago)  
Low-energy research at ATLAS  
(April 1998 - January 2006)

Shuiming Hu (University of Science and Technology, China)  
Medium-energy physics  
(March 2006 - May 2006)

Timur Kulevoy (Institute of Theoretical and Experimental Physics, Russia)  
Theoretical studies  
(March 2006 - June 2006)

- \* Eugene Shiles (University of Vermont)  
Theoretical physics studies  
(August 2002 - )

- \* David Smith (University of Vermont)  
Theoretical physics studies  
(February 2002 - )

**Resident Graduate Students**

Laura Bandura (Northern Illinois University)  
Low-energy research at ATLAS  
(January 2006 - )

Zachary Conway (University of Illinois at Urbana-Champaign)  
Research at ATLAS  
(June 2003 - )

---

† Fulbright Fellow

\* Guest Faculty Research Participant

Jennifer Fallis (University of Manitoba, Canada)  
Low-energy research at ATLAS  
(January 2006 – )

Daniel Lascar (Northwestern University)  
Low-energy research at ATLAS  
(January 2006 – )

Gang Li (McGill University, Canada)  
Low-energy research at ATLAS  
(August 2006 – )

Nidhi Patel (Colorado School of Mines)  
Research at ATLAS  
(May 2005 - )

Mahuya Sengupta (Michigan State University)  
Research at ATLAS  
(November 2005 - )

Jin Wang (University of Chicago)  
Medium-energy physics  
(May 2006 – )

### **Guest Graduate Students**

Lamiaa El Fassi (Mohammed V University, Morocco)  
Medium-energy physics  
(September 2003 - )

Nkemdilim Ezeife (University of Chicago)  
Medium-energy physics  
(July 2006 - August 2006)

Jennifer Fallis (University of Manitoba, Canada)  
Low-energy research at ATLAS  
(May 2005 – August 2005)

Gitai Feinberg (The Hebrew University of Jerusalem, Israel)  
Research at ATLAS  
(May 2006 - )

Nathan Hoteling (University of Maryland)  
Research at ATLAS  
(February 2003 - )

Shlomi Halfon (The Hebrew University of Jerusalem, Israel)  
Research at ATLAS  
(May 2006 - )

Louis Jisonna (Northwestern University)  
Low-energy research at ATLAS  
(June 2000 - )

James Maloney (Northern Illinois University)  
Research at ATLAS  
(June 2006 - )

Iouri Sanjiev (St. Petersburg Nuclear Physics Institute, Russia)  
Medium-energy physics  
(January 2006 - )

Ibrahim Sulai (University of Chicago)  
Medium-energy physics  
(June 2005 - )

Jie Sun (University of Notre Dame)  
Theoretical physics studies  
(May 2006 - August 2006)

Tout Wang (University of Toronto, Canada)  
Low-energy research at ATLAS  
(May 2006 – September 2006)

### **Undergraduate Students**

Andrew Bump (DeVry University)  
Shane Caldwell (DePaul University)  
John Carr (University of Illinois-Chicago)  
Robert Carrier (St. Xavier University)  
Mark Chantell (University of Chicago)  
David Danaher (Monmouth College)  
Alan Davila (University of Texas-El Paso)  
Christopher Deatrick (Western Michigan University)  
Mark Durante (North Central College)  
Steven Fazzio (Macalester College)  
Daniel Fiorino (DePaul University)  
David Grayson (University of Illinois at Urbana-Champaign)  
Tomas Hernandez (University of Texas-El Paso)  
Sereres Johnston (Andrews University)  
Jason Kozemczak (Greenville College)  
Grant Larsen (University of Chicago)  
Roman Mongado (DeVry University)  
Patrick McCormack (North Central College)  
Holly Nolan (North Central College)  
Elena Poklonskaya (St. Petersburg Electrotechnical University (LETI), Russia)  
Ida Sefer (North Central College)  
Matthew Sternberg (University of Oregon)

## LOW-ENERGY NUCLEAR PHYSICS RESEARCH

### $^{40}\text{Ca}(\alpha,\gamma)^{44}\text{Ti}$ Reaction in the Energy Regime of Supernova Nucleosynthesis

H. Nassar, M. Paul, I. Ahmad, Y. Ben-Dov, J. Caggiano, S. Ghelberg, S. Goriely, J. P. Greene, M. Hass, A. Heger, A. Heinz, D. J. Henderson, R. V. F. Janssens, C. L. Jiang, Y. Kashiv, B. S. Nara Singh, A. Ofan, R. C. Pardo, T. Pennington, K. E. Rehm, G. Savard, R. Scott, and R. Vondrasek  
Phys. Rev. Lett. **96**, 041102/1-4 (2006)

### Breakdown of $K$ -Selection in $^{178}\text{Hf}$

A. B. Hayes, D. Cline, C. Y. Wu, J. Ai, H. Amro, C. Beausang, R. F. Casten, J. Gerl, A. A. Hecht, A. Heinz, R. Hughes, R. V. F. Janssens, C. J. Lister, A. O. Macchiavelli, D. A. Meyer, E. F. Moore, P. Napiorkowski, R. C. Pardo, Ch. Schlegel, D. Seweryniak, M. W. Simon, J. Srebrny, R. Teng, K. Vetter, and H. J. Wollersheim  
Phys. Rev. Lett. **96**, 042505/1-4 (2006)

### Stabilization of Nuclear Isovector Valence-Shell Excitations

G. Rainovski, N. Pietralla, T. Ahn, C. J. Lister, R. V. F. Janssens, M. P. Carpenter, S. Zhu, and C. J. Barton III  
Phys. Rev. Lett. **96**, 122501/1-4 (2006)

### System Size and Centrality Dependence of Charged Hadron Transverse Momentum Spectra in Au + Au and Cu + Cu Collisions from $\sqrt{s_{NN}} = 62.4$ to 200 GeV

B. B. Back *et al.* (PHOBOS Collaboration)  
Phys. Rev. Lett. **96**, 212301/1-4 (2006)

### Energy Dependence of Direct Flow Over a Wide Range of Pseudorapidity in Au + Au Collisions at RHIC

B. B. Back *et al.* (PHOBOS Collaboration)  
Phys. Rev. Lett. **97**, 012301/1-4 (2006)

### $K$ -Isomers in $^{254}\text{No}$ : Probing Single Particle Energies and Pairing Strengths in the Heaviest Nuclei

S. K. Tandel, T. L. Khoo, D. Seweryniak, G. Mukherjee, I. Ahmad, B. Back, R. Blinstrup, P. A. Butler, M. P. Carpenter, J. Chapman, P. Chowdhury, C. N. Davids, P. T. Greenlees, A. A. Hecht, A. Heinz, R.-D. Herzberg, P. Ikin, R. V. F. Janssens, G. D. Jones, F. G. Kondev, T. Lauritsen, C. J. Lister, E. F. Moore, D. Peterson, P. Reiter, U. S. Tandel, X. F. Wang, and S. F. Zhu  
Phys. Rev. Lett. **97**, 082502/1-4 (2006)

### Anomalous Isomeric Decays in $^{174}\text{Lu}$ as a Probe of $K$ Mixing and Interactions in Deformed Nuclei

G. D. Dracoulis, F. G. Kondev, G. J. Lane, A. P. Byrne, T. R. McGoram, T. Kibédi, I. Ahmad, M. P. Carpenter, R. V. F. Janssens, T. Lauritsen, C. J. Lister, D. Seweryniak, P. Chowdhury, and S. K. Tandel  
Phys. Rev. Lett. **97**, 122501/1-4 (2006)

### Isospin Symmetry of Odd-Odd Mirror Nuclei: Identification of Excited States in $N = Z - 2$ $^{48}\text{Mn}$

M. A. Bentley, C. Chandler, M. J. Taylor, J. R. Brown, M. P. Carpenter, C. Davids, J. Ekman, S. J. Freeman, P. E. Garrett, G. Hammond, R. V. F. Janssens, S. M. Lenzi, C. J. Lister, R. du Rietz, and D. Seweryniak  
Phys. Rev. Lett. **97**, 132501/1-4 (2006)

### Two-Quasiparticle $K$ -Isomers and Pairing Strengths in the Neutron-Rich Isotopes $^{174}\text{Er}$ and $^{172}\text{Er}$

G. D. Dracoulis, G. J. Lane, F. G. Kondev, A. P. Byrne, R. O. Hughes, P. Nieminen, H. Watanabe, M. P. Carpenter, R. V. F. Janssens, T. Lauritsen, D. Seweryniak, S. Zhu, P. Chowdhury, and F. R. Xu  
Phys. Lett. **B635**, 200-206 (2006)

### First Evidence of Fusion Hindrance for a Small $Q$ -Value System

C. L. Jiang, B. B. Back, H. Esbensen, R. V. F. Janssens, S. Mişicu, K. E. Rehm, P. Collon, C. N. Davids, J. Greene, D. J. Henderson, L. Jisonna, S. Kurtz, C. J. Lister, M. Notani, M. Paul, R. Pardo, D. Peterson, D. Seweryniak, B. Shumard, X. D. Tang, I. Tanihata, X. Wang, and S. Zhu  
Phys. Lett. **B640**, 18-22 (2006)

Transverse Momentum and Rapidity Dependence of Hanbury-Brown-Twiss Correlations in Au + Au Collisions at

$\sqrt{s_{NN}} = 62.4$  and 200 GeV

B. B. Back *et al.* (PHOBOS Collaboration)  
Phys. Rev. C **73**, 031901(R)/1-5 (2006)

$\alpha$  Decay of  $^{105}\text{Te}$

D. Seweryniak, K. Starosta, C. N. Davids, S. Gros, A. A. Hecht, N. Hoteling, T. L. Khoo, K. Lagergren,  
G. Lotay, D. Peterson, A. Robinson, C. Vaman, W. B. Walters, P. J. Woods, and S. Zhu  
Phys. Rev. C **73**, 061301(R)/1-3 (2006)

First Observation of Excited States in  $^{114}\text{Cs}$ : Spectroscopy of the Yrast  $\nu(h_{11/2}) \otimes \pi(h_{11/2})$  Band

J. F. Smith, A. M. Fletcher, C. J. Chiara, M. P. Carpenter, H. J. Chantler, C. N. Davids, J. L. Durell,  
D. B. Fossan, S. J. Freeman, R. V. F. Janssens, T. Koike, F. G. Kondev, D. R. LaFosse, J. C. Lisle, D. Patel,  
E. S. Paul, W. Reviol, D. G. Sarantites, D. Seweryniak, K. Starosta, R. Wadsworth, and A. N. Wilson  
Phys. Rev. C **73**, 061303(R)/1-5 (2006)

Variation with Mass of  $B(E3; 0_1^+ \rightarrow 3_1^-)$  Transition Rates in  $A = 124$ -134 Even-Mass Xenon Nuclei

W. F. Mueller, M. P. Carpenter, J. A. Church, D. C. Dinca, A. Gade, T. Glasmacher, D. T. Henderson, Z. Hu,  
R. V. F. Janssens, A. F. Lisetskiy, C. J. Lister, E. F. Moore, T. O. Pennington, B. C. Perry, I. Wiedenhöver,  
K. L. Yurkewicz, V. G. Zelevinsky, and H. Zwahlen  
Phys. Rev. C **73**, 014316/1-5 (2006)

Systematics of Heavy-Ion Fusion Hindrance at Extreme Sub-Barrier Energies

C. L. Jiang, B. B. Back, H. Esbensen, R. V. F. Janssens, and K. E. Rehm  
Phys. Rev. C **73**, 014613/1-5 (2006)

Erratum: Structure of Two-, Four-, and Six-Quasiparticle Isomers in  $^{174}\text{Yb}$  and  $K$ -Forbidden Decays  
[Phys. Rev. C **71**, 044326 (2005)]

G. D. Dracoulis, G. J. Lane, F. G. Kondev, A. P. Byrne, T. Kibédi, H. Watanabe, I. Ahmad, M. P. Carpenter,  
S. J. Freeman, R. V. F. Janssens, N. J. Hammond, T. Lauritsen, C. J. Lister, G. Mukherjee, D. Seweryniak,  
P. Chowdhury, and S. K. Tandel  
Phys. Rev. C **73**, 019901(E) (2006)

The  $^8\text{B}$  Neutrino Spectrum

W. T. Winter, S. J. Freedman, K. E. Rehm, and J. P. Schiffer  
Phys. Rev. C **73**, 025503/1-15 (2006)

Near-Yrast Structure of the  $^{109}\text{Mo}$  Nucleus

W. Urban, Ch. Droste, T. Rzaca-Urban, Zlomaniec, J. L. Durell, A. G. Smith, B. J. Varley, and I. Ahmad  
Phys. Rev. C **73**, 037302/1-4 (2006)

Spectroscopy of the Odd-Odd  $fp$ -Shell Nucleus  $^{52}\text{Sc}$  from Secondary Fragmentation

A. Gade, R. V. F. Janssens, D. Bazin, B. A. Brown, C. M. Campbell, M. P. Carpenter, J. M. Cook,  
A. N. Deacon, C.-D. Dinca, S. J. Freeman, T. Glasmacher, B. P. Kay, P. F. Mantica, W. F. Mueller, J. R. Terry,  
and S. Zhu  
Phys. Rev. C **73**, 037309/1-4 (2006)

High- $K$  Isomers and Rotational Structures in  $^{174}\text{W}$

S. K. Tandel, P. Chowdhury, E. H. Seabury, I. Ahmad, M. P. Carpenter, S. M. Fischer, R. V. F. Janssens,  
T. L. Khoo, T. Lauritsen, C. J. Lister, D. Seweryniak, and Y. R. Shimizu  
Phys. Rev. C **73**, 044306/1-19 (2006)



Half-Life and Spin of  $^{60}\text{Mn}^g$ 

S. N. Liddick, P. F. Mantica, B. A. Brown, M. P. Carpenter, A. D. Davies, M. Horoi, R. V. F. Janssens, A. C. Morton, W. F. Mueller, J. Pavan, H. Schatz, A. Stolz, S. L. Tabor, B. E. Tomlin, and M. Wiedeking  
Phys. Rev. C **73**, 044322/1-5 (2006)

Single-Particle and Collective Degrees of Freedom in  $^{101}\text{Zr}$  and  $^{103,105}\text{Mo}$ 

R. Orlandi, A. G. Smith, D. Patel, G. S. Simpson, R. M. Wall, J. F. Smith, O. J. Onakanmi, I. Ahmad, J. P. Greene, M. P. Carpenter, T. Lauritsen, C. J. Lister, R. V. F. Janssens, F. G. Kondev, D. Seweryniak, B. J. P. Gall, O. Dorveaux, and A. E. Stuchbery  
Phys. Rev. C **73**, 054310/1-12 (2006)

Reevaluation of the  $^{30}\text{P}(p,\gamma)^{31}\text{S}$  Astrophysical Reaction Rate from a Study of the  $T = 1/2$  Mirror Nuclei,  $^{31}\text{S}$  and  $^{31}\text{P}$ 

D. G. Jenkins, A. Meadowcroft, C. J. Lister, M. P. Carpenter, P. Chowdhury, N. J. Hammond, R. V. F. Janssens, T. L. Khoo, T. Lauritsen, D. Seweryniak, T. Davinson, P. J. Woods, A. Jokinen, H. Penttila, G. Martínez-Pinedo, and J. José  
Phys. Rev. C **73**, 065802/1-8 (2006)

Forward-Backward Multiplicity Correlations in  $\sqrt{s_{NN}} = 200$  GeV Au + Au Collisions

B. B. Back *et al.* (PHOBOS Collaboration)  
Phys. Rev. C **74**, 011901(R)/1-5 (2006)

Cross-Shell Excitation in Two-Proton Knockout: Structure of  $^{52}\text{Ca}$ 

A. Gade, R. V. F. Janssens, D. Bazin, R. Broda, B. A. Brown, C. M. Campbell, M. P. Carpenter, J. M. Cook, A. N. Deacon, D.-C. Dinca, B. Fornal, S. J. Freeman, T. Glasmacher, P. G. Hansen, B. P. Kay, P. F. Mantica, W. F. Mueller, J. R. Terry, J. A. Tostevin, and S. Zhu  
Phys. Rev. C **74**, 021302(R)/1-4 (2006)

## Centrality and Energy Dependence of Charged-Particle Multiplicities in Heavy Ion Collisions in the Context of Elementary Reactions

B. B. Back (for the PHOBOS Collaboration)  
Phys. Rev. C **74**, 021902(R)/1-4 (2006)

Decay Modes of  $^{250}\text{No}$ 

D. Peterson, B. B. Back, R. V. F. Janssens, T. L. Khoo, C. J. Lister, D. Seweryniak, I. Ahmad, M. P. Carpenter, C. N. Davids, A. A. Hecht, C. L. Jiang, T. Lauritsen, X. Wang, S. Zhu, F. G. Kondev, A. Heinz, J. Qian, R. Winkler, P. Chowdhury, S. K. Tandel, and U. S. Tandel  
Phys. Rev. C **74**, 014316/1-9 (2006)

Excited States and Signature Inversion in  $^{116}\text{Cs}$ 

J. F. Smith, C. J. Chiara, M. P. Carpenter, C. N. Davids, M. Devlin, D. B. Fossan, S. J. Freeman, R. V. F. Janssens, D. R. LaFosse, D. G. Sarantites, D. Seweryniak, K. Starosta, R. Wadsworth, A. N. Wilson, and R. Wyss  
Phys. Rev. C **74**, 034310/1-10 (2006)

Multiple Octupole-Type Band Structures in  $^{220}\text{Th}$ : Reflection-Asymmetric Tidal Waves?

W. Reviol, C. J. Chiara, M. Montero, D. G. Sarantites, O. L. Pechenaya, M. P. Carpenter, R. V. F. Janssens, T. L. Khoo, T. Lauritsen, C. J. Lister, D. Seweryniak, S. Zhu, and S. G. Frauendorf  
Phys. Rev. C **74**, 044305/1-8 (2006)

One-Neutron Knockout in the Vicinity of the  $N = 32$  Sub-Shell Closure:  $^9\text{Be}(^{57}\text{Cr}, ^{56}\text{Cr} + \gamma)\text{X}$ 

A. Gade, R. V. F. Janssens, D. Bazin, B. A. Brown, C. M. Campbell, M. P. Carpenter, J. M. Cook, A. N. Deacon, D.-C. Dinca, S. J. Freeman, T. Glasmacher, M. Horoi, B. P. Kay, P. F. Mantica, W. F. Mueller, J. R. Terry, J. A. Tostevin, and S. Zhu  
Phys. Rev. C **74**, 047302/1-4 (2006)

*T* = 1 States in <sup>74</sup>Rb and Their <sup>74</sup>Kr Analogs

S. M. Fischer, C. J. Lister, N. J. Hammond, R. V. F. Janssens, T. L. Khoo, T. Lauritsen, E. F. Moore, D. Seweryniak, S. Sinha, D. P. Balamuth, P. A. Hausladen, D. G. Sarantites, W. Reviol, P. Chowdhury, S. D. Paul, C. Baktash, and C.-H. Yu  
Phys. Rev. C **74**, 054304/1-10 (2006)

Multiple Band Structures in <sup>169</sup>Ta

D. J. Hartley, W. H. Mohr, J. R. Vanhoy, M. A. Riley, A. Aguilar, C. Teal, R. V. F. Janssens, M. P. Carpenter, A. A. Hecht, T. Lauritsen, E. F. Moore, S. Zhu, F. G. Kondev, M. K. Djongolov, M. Danchev, L. L. Riedinger, G. B. Hagemann, G. Sletten, P. Chowdhury, S. K. Tandel, W. C. Ma, and S. W. Ødegård  
Phys. Rev. C **74**, 054314/1-16 (2006)

Triaxiality in <sup>105</sup>Mo and <sup>107</sup>Mo from the Low to Intermediate Spin Region

J. A. Pinston, W. Urban, Ch. Droste, T. Rzaca-Urban, J. Genevey, G. Simpson, J. L. Durell, A. G. Smith, B. J. Varley, and I. Ahmad  
Phys. Rev. C **74**, 064304/1-10 (2006)

Yrast Structure of <sup>64</sup>Fe

N. Hoteling, W. B. Walters, R. V. F. Janssens, R. Broda, M. P. Carpenter, B. Fornal, A. A. Hecht, M. Hjorth-Jensen, W. Królas, T. Lauritsen, T. Pawlat, D. Seweryniak, X. Wang, A. Wöhr, J. Wrzesinski, and S. Zhu  
Phys. Rev. C **74**, 064313/1-6 (2006)

Level Structure of the Neutron-Rich <sup>56,58,60</sup>Cr Isotopes: Single-Particle and Collective Aspects

S. Zhu, A. N. Deacon, S. J. Freeman, R. V. F. Janssens, B. Fornal, M. Honma, F. R. Xu, R. Broda, I. R. Calderin, M. P. Carpenter, P. Chowdhury, F. G. Kondev, W. Królas, T. Lauritsen, S. N. Liddick, C. J. Lister, P. F. Mantica, T. Pawlat, D. Seweryniak, J. F. Smith, S. L. Tabor, B. E. Tomlin, B. J. Varley, and J. Wrzesiński  
Phys. Rev. C **74**, 064315/1-15 (2006)

Improved Measurement of the <sup>44</sup>Ti Half-Life from a 14-Year Long Study

I. Ahmad, J. P. Greene, E. F. Moore, S. Ghelberg, A. Ofan, M. Paul, and W. Kutschera  
Phys. Rev. C **74**, 065803/1-8 (2006)

Double *K*-Shell Photoionization of Silver

E. P. Kanter, I. Ahmad, R. W. Dunford, D. S. Gemmell, B. Krässig, S. H. Southworth, and L. Young  
Phys. Rev. A **73**, 022708/1-11 (2006)

Production Cross-Sections of Protactinium and Thorium Isotopes Produced in Fragmentation of <sup>238</sup>U at 1 A GeV

J. Kurcewicz, Z. Liu, M. Pfützner, P. J. Woods, C. Mazzocchi, K.-H. Schmidt, A. Kelić, F. Attallah, E. Badura, C. N. Davids, T. Davinson, J. Döring, H. Geissel, M. Görska, R. Grzywacz, M. Hellström, Z. Janas, M. Karny, A. Korgul, I. Mukha, C. Plettner, A. Robinson, E. Roeckl, K. Rykaczewski, K. Schmidt, D. Seweryniak, K. Sümmerer, and H. Weick  
Nucl. Phys. **A767**, 1-12 (2006)

## X-Ray Binaries

H. Schatz and K. E. Rehm  
Nucl. Phys. **A777**, 601-622 (2006)

Gamma-Ray Spectroscopy of the Doubly Magic Nucleus <sup>56</sup>Ni

E. K. Johansson, D. Rudolph, J. Ekman, C. Fahlander, C. Andreoiu, M. A. Bentley, M. P. Carpenter, R. J. Charity, R. M. Clark, P. Fallon, R. V. F. Janssens, F. G. Kondev, T. L. Khoo, T. Lauritsen, A. O. Macchiavelli, W. Reviol, D. G. Sarantites, D. Seweryniak, C. E. Svensson, and S. J. Williams  
Eur. Phys. J. A **27**, 157-165 (2006)

## Physics of a Rare Isotope Accelerator

D. F. Geesaman, C. K. Gelbke, R. V. F. Janssens, and B. M. Sherrill  
Ann. Rev. Nucl. and Part. Sci. **56**, 53-92 (2006)

New Information on the  $T_{1/2} = 47$  s Isomer in the  $^{136}\text{I}$  Nucleus

W. Urban, M. Saha Sarkar, S. Sarkar, T. Rzaca-Urban, J. L. Durell, A. G. Smith, J. A. Genevey, J. A. Pinston, G. S. Simpson, and I. Ahmad  
Eur. Phys. J. A **27**, 257-262 (2006)

Development of a Detection Method for  $^{244}\text{Pu}$  by Resonance Ionization Mass Spectrometry

A. Ofan, I. Ahmad, J. P. Greene, M. Paul, and M. R. Savina  
New Astronomy Reviews **50**, 640-643 (2006)

## A New Evaporator System for Target Preparation at Argonne National Laboratory

John P. Greene, Janelle Neubauer, and Dino Deligiannis  
Proceedings of the 22nd World Conference of the International Nuclear Target Development Society, Gaithersburg, MD, October 19-22, 2004; Nucl. Instrum. Methods **A561**, 58-61 (2006)

## Oxide Targets for GAMMASPHERE

J. P. Greene, K. Lister, and S. Fischer  
Proceedings of the 22nd World Conference of the International Nuclear Target Development Society, Gaithersburg, MD, October 19-22, 2004; Nucl. Instrum. Methods **A561**, 104-106 (2006)

## Identification of Nilsson States in Transcurium Nuclei

I. Ahmad  
Proceedings of the International Conference on Finite Fermionic Systems: Nilsson Model 50 Years, Lund, Sweden, June 14-18, 2005; Phys. Scr. **T125**, 78-81 (2006)

Observation of States Beyond Band Termination in  $^{156,157,158}\text{Er}$  and Strongly Deformed Structures in  $^{173,174,175}\text{Hf}$ 

M. A. Riley, M. K. Djongolov, A. O. Evans, D. J. Hartley, R. V. F. Janssens, E. S. Paul, A. Pipidis, J. Simpson, A. A. Aguilar, D. E. Appelbe, C. R. Bingham, D. B. Campbell, M. P. Carpenter, P. Chowdhury, P. T. W. Choy, R. M. Clark, M. Cromaz, D. M. Cullen, M. Danchev, G. D. Dracoulis, P. Fallon, A. Görgen, G. B. Hagemann, D. T. Joss, J. Goon, R. A. Kaye, T. L. Khoo, F. G. Kondev, R. W. Laird, K. Lagergren, T. Lauritsen, A. O. Macchiavelli, B. McClain, E. F. Moore, G. Mukherjee, E. Ngijoi-Yogo, P. J. Nolan, H. I. Park, L. L. Riedinger, G. Sletten, S. K. Tandel, P. M. Walker, D. Ward, I. Ragnarsson, F. Saric, and Jing-ye Zhang  
Proceedings of the International Conference on Finite Fermionic Systems: Nilsson Model 50 Years, Lund, Sweden, June 14-18, 2005; Phys. Scr. **T125**, 123-126 (2006)

Lifetime Measurements in  $N = Z$   $^{72}\text{Kr}$ 

C. Andreoiu, C. E. Svensson, R. A. E. Austin, M. P. Carpenter, D. Dashdorj, P. Finlay, S. J. Freeman, P. E. Garrett, A. Görgen, J. Greene, G. F. Grinyer, B. Hyland, D. Jenkins, F. Johnston-Theasby, P. Joshi, A. O. Macchiavelli, F. Moore, G. Mukherjee, A. A. Phillips, W. Reviol, D. G. Sarantites, M. A. Schumaker, D. Seweryniak, M. B. Smith, J. J. Valiente-Dobón, and R. Wadsworth  
Proceedings of the International Conference on Finite Fermionic Systems: Nilsson Model 50 Years, Lund, Sweden, June 14-18, 2005; Phys. Scr. **T125**, 127-129 (2006)

## New Results from the PHOBOS Experiment

G. Roland (for the PHOBOS Collaboration)  
Proceedings of the 18th International Conference on Ultra-Relativistic Nucleus-Nucleus Collisions, Budapest, Hungary, August 4-9, 2005; Nucl. Phys. **A774**, 113-128 (2006)

Particle Production at Very Low and Intermediate Transverse Momenta in  $d + \text{Au}$  and  $\text{Au} + \text{Au}$  Collisions

Adam Trzupek (for the PHOBOS Collaboration)  
Proceedings of the 18th International Conference on Ultra-Relativistic Nucleus-Nucleus Collisions, Budapest, Hungary, August 4-9, 2005; Nucl. Phys. **A774**, 469-472 (2006)

## System Size, Energy and Pseudorapidity Dependence of Directed and Elliptic Flow at RHIC

S. Manley (for the PHOBOS Collaboration)

Proceedings of the 18th International Conference on Ultra-Relativistic Nucleus-Nucleus Collisions, Budapest, Hungary, August 4-9, 2005; Nucl. Phys. **A774**, 523-526 (2006)Forward-Backward Multiplicity Correlations in  $\sqrt{s_{NN}}$  200 GeV Au + Au Collisions

Peter Steinberg (for the PHOBOS Collaboration)

Proceedings of the 18th International Conference on Ultra-Relativistic Nucleus-Nucleus Collisions, Budapest, Hungary, August 4-9, 2005; Nucl. Phys. **A774**, 631-634 (2006)

## Correlations and Fluctuations Over a Broad Range in Pseudorapidity Using the PHOBOS Detector

G. S. F. Stephans (for the PHOBOS Collaboration)

Proceedings of the 18th International Conference on Ultra-Relativistic Nucleus-Nucleus Collisions, Budapest, Hungary, August 4-9, 2005; Nucl. Phys. **A774**, 639-642 (2006)In-Beam  $\gamma$ -Spectroscopy of Low-Spin Mixed-Symmetry States of  $^{138}\text{Ce}$  with Gammasphere in Singles-Mode

N. Pietralla, G. Rainovski, T. Ahn, M. P. Carpenter, R. V. F. Janssens, C. J. Lister, and S. Zhu

Proceedings of the 12th International Conference on Capture Gamma-Ray Spectroscopy and Related Topics (CGS 12), Notre Dame, IN, September 4-9, 2005, eds. Andreas Woehr and Ani Aprahamian, AIP Conference Proceedings **819**, 11-15 (2006)Violations of  $K$ -Conservation in  $^{178}\text{Hf}$ 

A. B. Hayes, D. Cline, C. Y. Wu, J. Ai, H. Amro, C. Beausang, R. F. Casten, J. Gerl, A. A. Hecht, A. Heinz, R. Hughes, R. V. F. Janssens, C. J. Lister, A. O. Macchiavelli, D. A. Meyer, E. F. Moore, P. Napiorkowski, R. C. Pardo, Ch. Schlegel, D. Seweryniak, M. W. Simon, J. Srebmy, R. Teng, K. Vetter, and H. J. Wollersheim

Proceedings of the 12th International Conference on Capture Gamma-Ray Spectroscopy and Related Topics (CGS 12), Notre Dame, IN, September 4-9, 2005, eds. Andreas Woehr and Ani Aprahamian, AIP Conference Proceedings **819**, 24-29 (2006)Search for Enhanced Alpha Preformation in the  $N = Z + 1$  Nuclei  $^{113}\text{Ba}$ ,  $^{109}\text{Xe}$ ,  $^{105}\text{Te}$ 

A. A. Hecht, C. J. Lister, C. N. Davids, A. Heinz, N. Hoteling, C. Mazzocchi, J. Palombo, D. Seweryniak, J. Shergur, M. Stoyer, W. B. Walters, P. J. Woods, and S. Zhu

Proceedings of the 12th International Conference on Capture Gamma-Ray Spectroscopy and Related Topics (CGS 12), Notre Dame, IN, September 4-9, 2005, eds. Andreas Woehr and Ani Aprahamian, AIP Conference Proceedings **819**, 355-359 (2006)Rotational Damping, Ridges and the Quasi-Continuum of  $\gamma$  Rays in  $^{152}\text{Dy}$ 

T. Lauritsen, R. V. F. Janssens, T. L. Khoo, I. Ahmad, M. P. Carpenter, K. G. Kondev, C. J. Lister, E. F. Moore, D. Seweryniak, S. Zhu, T. Dössing, B. Herskind, A. M. Heinz, D. G. Jenkins, R. M. Clark, P. Fallon,

A. O. Macchiavelli, D. Ward, G. Lane, P. Chowdhury, A. Korichi, A. Lopez-Martens, and A. J. Larabee

Proceedings of the 12th International Conference on Capture Gamma-Ray Spectroscopy and Related Topics (CGS 12), Notre Dame, IN, September 4-9, 2005, eds. Andreas Woehr and Ani Aprahamian, AIP Conference Proceedings **819**, 459-463 (2006)

## Light Nuclei Studied with Nucleon Transfer Reactions Using Exotic Beams

A. H. Wuosmaa, K. E. Rehm, J. P. Greene, D. J. Henderson, R. V. F. Janssens, C. L. Jiang, L. Jisonna, E. F. Moore, R. C. Pardo, M. Paul, D. Peterson, S. C. Pieper, G. Savard, J. P. Schiffer, R. E. Segel, S. Sinha, X. Tang, and R. B. Wiringa

Proceedings of the International Conference on Frontiers in Nuclear Structure, Astrophysics, and Reactions (FINUSTAR), Kos, Greece, September 12-17, 2005, eds. S. V. Harissopoulos, P. Demetriou, and R. Julin, AIP Conference Proceedings **831**, 332-336 (2006)

## Heavy-Ion Fusion Hindrance at Extreme Sub-Barrier Energies

C. L. Jiang, B. B. Back, H. Esbensen, R. V. F. Janssens, S. Misicu, K. E. Rehm, P. Collon, C. N. Davids, J. Greene, D. J. Henderson, L. Jisonna, S. Kurtz, C. J. Lister, M. Notani, M. Paul, R. Pardo, D. Peterson, D. Seweryniak, B. Shumard, X. D. Tang, X. Wang, and S. Zhu

Proceedings of the International Conference on Reaction Mechanisms and Nuclear Structure at the Coulomb Barrier (Fusion06), San Servolo Island, Venice, Italy, March 19-23, 2006, AIP Conference Proceedings **853**, 63-38 (2006)

## Decay Modes of Narrow Molecular Resonances

S. Courtin, F. Haas, M.-D. Salsac, D. Lehbartz, A. Michalon, C. Beck, M. Rousseau, A. Sanchez I Zafra, D. G. Jenkins, R. G. Glover, P. E. Kent, D. Hutcheon, C. Davis, J. E. Pearson and the Dragon Collaboration, and C. J. Lister

Proceedings of the International Conference on Reaction Mechanisms and Nuclear Structure at the Coulomb Barrier (Fusion06), San Servolo Island, Venice, Italy, March 19-23, 2006, AIP Conference Proceedings **853**, 134-139 (2006)

Fusion-Fission of  $^{16}\text{O} + ^{197}\text{Au}$  at Sub-Barrier Energies

B. B. Back, C. L. Jiang, R. V. F. Janssens, D. J. Henderson, B. R. Shumard, C. J. Lister, D. Peterson, K. E. Rehm, I. Tanihata, X. Tang, X. F. Wang, and S. Zhu

Proceedings of the International Conference on Reaction Mechanisms and Nuclear Structure at the Coulomb Barrier (FusionN06), San Servolo Island, Venice, Italy, March 19-23, 2006, AIP Conference Proceedings **853**, 331-335 (2006)

## Microsecond and Nanosecond Isomers Populated in Fission Reactions

G. A. Jones, P. M. Walker, Zs. Podolyák, P. H. Regan, S. J. Williams, M. P. Carpenter, J. J. Carroll, R. S. Chakrawarthy, P. Chowdhury, I. J. Cullen, G. D. Dracoulis, A. B. Garnsworthy, G. Hackman, R. V. F. Janssens, T. L. Khoo, F. G. Kondev, G. J. Lane, Z. Liu, D. Seweryniak, N. J. Thompson, and S. Zhu

Proceedings of the International Conference on Reaction Mechanisms and Nuclear Structure at the Coulomb Barrier (Fusion06), San Servolo Island, Venice, Italy, March 19-23, 2006, AIP Conference Proceedings **853**, 342-349 (2006)

## Reaction Studies in Nuclear Astrophysics

K. E. Rehm

Proceedings of the International Conference on Reaction Mechanisms and Nuclear Structure at the Coulomb Barrier (Fusion06), San Servolo Island, Venice, Italy, March 19-23, 2006, AIP Conference Proceedings **853**, 350-357 (2006)

## Proton Drip Line Spectroscopy with Gammasphere and the FMA

M. P. Carpenter

Proceedings of the Conference on Nuclei at the Limits (NS06), Oak Ridge, TN, July 24-28, 2006, Book of Abstracts, p. 18 (2006)

Approaching  $^{98}\text{Ni}$  Along the  $N = 50$  Line Utilizing Deep Inelastic Reactions

M. P. Carpenter, R. V. F. Janssens, S. Zhu, B. Fornal, R. Broda, A. Galindo-Uribarri, N. Hoteling, A. Ibanez, T. L. Khoo, F. G. Kondev, T. Lauritsen, C. J. Lister, E. Padilla-Rodal, D. Seweryniak, J. P. Ureggo-Blanco, and X. Wang

Proceedings of the Conference on Nuclei at the Limits (NS06), Oak Ridge, TN, July 24-28, 2006, Book of Abstracts, p. 19 (2006)

Triple Shape Coexistence in  $^{181}\text{Tl}$ 

M. P. Carpenter, F. G. Kondev, R. V. F. Janssens, D. Seweryniak, G. Mukherjee, I. Ahmad, C. N. Davids, S. M. Fischer, S. Freeman, G. Jones, N. Hammond, D. J. Jenkins, T. L. Khoo, A. J. Larabee, T. Lauritsen, N. Liechty, C. J. Lister, E. F. Moore, P. Raddon, S. Sinha, and R. Wadsworth

Proceedings of the Conference on Nuclei at the Limits (NS06), Oak Ridge, TN, July 24-28, 2006, Book of Abstracts, p. 20 (2006)

Probing *sd-pf* Cross-Shell Interactions via Terminating Configurations in  $N \approx Z$  Scandium Isotopes

C. J. Chiara, M. Devlin, E. Ideguchi, F. Lerma, W. Reviol, S. K. Ryu, D. G. Sarantites, C. Baktash, A. Galindo-Uribarri, G. Stoitcheva, D. Rudolph, D. R. LaFosse, M. P. Carpenter, R. V. F. Janssens, T. Lauritsen, C. J. Lister, P. Reiter, D. Seweryniak, P. Fallon, A. Gørgen, A. O. Macchiavelli, and W. Satuła  
 Proceedings of the Conference on Nuclei at the Limits (NS06), Oak Ridge, TN, July 24-28, 2006,  
 Book of Abstracts, p. 24 (2006)

## Alpha-Gamma Angular Correlations Using Novel Position-Sensitive Detectors

P. Chowdhury, C. M. Wilson, R. Gramer, S. K. Tandel, N. J. Hammond, C. J. Lister, S. M. Fischer, E. F. Moore, K. M. Teh, M. McClish, K. S. Shah, and R. Farrell  
 Proceedings of the Conference on Nuclei at the Limits (NS06), Oak Ridge, TN, July 24-28, 2006,  
 Book of Abstracts, p. 25 (2006)

A New Alpha-Decaying High-Spin Isomer in the Very Neutron-Deficient Nucleus,  $^{158}\text{Ta}$ 

I. G. Darby, J. Uusitalo, D. T. Joss, R. D. Page, J. Simpson, K. Andgren, B. Cederwall, S. Eeckhaudt, T. Grahn, C. Gray-Jones, P. T. Greenlees, B. Hadinia, P. M. Jones, R. Julin, S. Juutinen, M. Leino, A.-P. Leppänen, M. Nyman, J. Pakarinen, P. Rahkila, J. Sarén, M. Sandzelius, C. Scholey, D. Seweryniak, and D. D. Warner  
 Proceedings of the Conference on Nuclei at the Limits (NS06), Oak Ridge, TN, July 24-28, 2006,  
 Book of Abstracts, p. 30 (2006)

Superdeformation and High-Spin Spectroscopy Studies on  $^{174}\text{Hf}$ 

M. K. Djongolov, D. J. Hartley, L. L. Riedinger, G. B. Hagemann, R. V. F. Janssens, F. G. Kondev, E. F. Moore, M. A. Riley, A. Aguillar, C. R. Bingham, D. B. Campbell, M. P. Carpenter, P. Chowdhury, M. Cromaz, D. M. Cullen, M. Danchev, G. D. Dracoulis, P. Fallon, J. Goon, R. A. Kaye, T. L. Khoo, R. W. Laird, T. Lauritsen, A. O. Macchiavelli, B. McClain, G. Mukherjee, E. Ngijoi-Yogo, H. I. Park, G. Sletten, S. K. Tandel, P. M. Walker, and Jing-ye Zhang  
 Proceedings of the Conference on Nuclei at the Limits (NS06), Oak Ridge, TN, July 24-28, 2006,  
 Book of Abstracts, p. 37 (2006)

## Multi-Quasiparticle Isomers and K-Conservation Paths in Stable and Neutron-Rich Yb and Lu Isotopes

G. D. Dracoulis, G. J. Lane, F. G. Kondev, A. P. Byrne, T. Kibedi, R. O. Hughes, H. Watanabe, P. Nieminen, M. P. Carpenter, R. V. F. Janssens, T. Lauritsen, C. J. Lister, D. Seweryniak, S. Zhu, and P. Chowdhury  
 Proceedings of the Conference on Nuclei at the Limits (NS06), Oak Ridge, TN, July 24-28, 2006,  
 Book of Abstracts, p. 39 (2006)

New  $T = 1$  and  $T = 0$  States in  $N = Z$   $^{74}\text{Rb}$  and the *np* Pairing Gap

S. M. Fischer, C. J. Lister, P. Chowdhury, N. J. Hammond, R. V. F. Janssens, T. L. Khoo, F. G. Kondev, T. Lauritsen, E. F. Moore, D. Seweryniak, S. Sinha, D. P. Balamuth, P. A. Hausladen, D. G. Sarantites, W. Reviol, S. D. Paul, and C. Baktash  
 Proceedings of the Conference on Nuclei at the Limits (NS06), Oak Ridge, TN, July 24-28, 2006,  
 Book of Abstracts, p. 45 (2006)

Proton Cross-Shell Excitations: The Study of  $^{52}\text{Ca}$ 

A. Gade, R. V. F. Janssens, D. Bazin, R. Broda, B. A. Brown, C. M. Campbell, M. P. Carpenter, J. M. Cook, A. N. Deacon, D.-C. Dinca, B. Fornal, S. J. Freeman, T. Glasmacher, P. G. Hansen, B. P. Kay, P. F. Mantica, J. R. Terry, S. J. Freeman, T. Glasmacher, P. G. Hansen, B. P. Kay, P. F. Mantica, J. R. Terry, J. A. Tostevin, and S. Zhu  
 Proceedings of the Conference on Nuclei at the Limits (NS06), Oak Ridge, TN, July 24-28, 2006,  
 Book of Abstracts, p. 52 (2006)

Internal Conversion Coefficient Measurements of Transitions in  $^{167}\text{Lu}$ 

G. Gürdal, C. W. Beausang, D. S. Brenner, H. Ai, M. Carpenter, R. F. Casten, B. Crider, D. J. Hartley, A. A. Hecht, R. V. F. Janssens, A. Heinz, T. Lauritsen, C. J. Lister, R. Raabe, J. X. Saladin, D. Seweryniak, E. Williams, and S. Zhu  
 Proceedings of the Conference on Nuclei at the Limits (NS06), Oak Ridge, TN, July 24-28, 2006,  
 Book of Abstracts, p. 63 (2006)

Decay of the  $r$ -Process Waiting Point Nucleus  $^{138}\text{Sn}$  and Adjacent Nuclei

A. A. Hecht, J. Shergur, A. Wöhr, W. B. Walters, K.-L. Kratz, N. Hoteling, B. A. Brown, B. Pfeiffer, O. Arndt, J. Cederkall, S. Hennrich, O. Keller, L. M. Fraile, P. Hoff, A. Joinet, U. Köster, and M. A. Stoyer  
Proceedings of the Conference on Nuclei at the Limits (NS06), Oak Ridge, TN, July 24-28, 2006,  
Book of Abstracts, p. 68 (2006)

On the Role of the  $g_{9/2}$  Neutron Orbital in the Structure of Fe Isotopes Toward  $N = 40$ 

N. Hoteling, W. B. Walters, A. A. Hecht, M. Carpenter, R. Janssens, T. Lauritsen, D. Seweryniak, X. Wang, S. Zhu, R. Broda, B. Fornal, W. Krolas, and J. Wrzesinski  
Proceedings of the Conference on Nuclei at the Limits (NS06), Oak Ridge, TN, July 24-28, 2006,  
Book of Abstracts, p. 73 (2006)

## Superdeformation in Nuclei: Order Embedded in Chaos

T. L. Khoo  
Proceedings of the Conference on Nuclei at the Limits (NS06), Oak Ridge, TN, July 24-28, 2006,  
Book of Abstracts, p. 81 (2006)

Identification of the  $(\pi h_{11/2})^2 \otimes (v i_{13/2})^2, I^\pi = 22^+$  Isomer in  $^{204}\text{Hg}$ 

G. J. Lane, K. H. Maier, B. Fornal, M. Rejmund, R. Broda, A. P. Byrne, M. P. Carpenter, G. D. Dracoulis, R. V. F. Janssens, and J. Wrzesiński  
Proceedings of the Conference on Nuclei at the Limits (NS06), Oak Ridge, TN, July 24-28, 2006,  
Book of Abstracts, p. 86 (2006)

High-K Multi-Quasiparticle States and Anomalous  $\gamma$ -Ray Decays in  $^{184}\text{W}$ 

G. J. Lane, J. T. Werner, G. D. Dracoulis, F. G. Kondev, A. P. Byrne, R. O. Hughes, H. Watanabe, P. Nieminen, M. P. Carpenter, R. V. F. Janssens, T. Lauritsen, D. Seweryniak, S. Zhu, and P. Chowdhury  
Proceedings of the Conference on Nuclei at the Limits (NS06), Oak Ridge, TN, July 24-28, 2006,  
Book of Abstracts, p. 87 (2006)

Rotational Damping, Ridges and the Quasicontinuum of  $\gamma$  Rays in  $^{152}\text{Dy}$ 

T. Lauritsen, R. V. F. Janssens, T. L. Khoo, I. Ahmad, M. P. Carpenter, P. Chowdhury, T. Dossing, P. Fallon, A. M. Heinz, B. Herskind, D. G. Jenkins, F. G. Kondev, A. Korichi, A. J. Larabee, C. J. Lister, A. Lopez-Martens, A. O. Macchiavelli, E. F. Moore, D. Seweryniak, D. Ward, and S. Zhu  
Proceedings of the Conference on Nuclei at the Limits (NS06), Oak Ridge, TN, July 24-28, 2006,  
Book of Abstracts, p. 89 (2006)

Strongly Deformed Bands in  $^{163}\text{Tm}$ : Particle Excitation vs. Wobbling?

N. S. Pattabiraman, Y. Gu, S. Frauendorf, U. Garg, T. Li, B. K. Nayak, X. Wang, S. Zhu, S. S. Ghugre, R. V. F. Janssens, R. S. Chakrawarthy, M. Whithead, A. O. Macchiavelli, and D. Ward  
Proceedings of the Conference on Nuclei at the Limits (NS06), Oak Ridge, TN, July 24-28, 2006,  
Book of Abstracts, p. 124 (2006)

New Superdeformed Bands in  $^{131,132}\text{Ce}$ 

E. S. Paul, A. O. Evans, B. M. McGuirk, A. J. Boston, L. Nelson, P. J. Nolan, K. Lagergren, W. T. Cluff, A. Pipidis, M. A. Riley, D. T. Joss, J. Simpson, F. Johnson-Theasby, R. Wadsworth, G. Rainovski, K. Starosta, M. P. Carpenter, A. A. Hecht, R. V. F. Janssens, F. G. Kondev, T. Lauritsen, E. F. Moore, S. Zhu, and I. Ragnarsson  
Proceedings of the Conference on Nuclei at the Limits (NS06), Oak Ridge, TN, July 24-28, 2006,  
Book of Abstracts, p. 126 (2006)

Alpha Decay of  $^{257}\text{Rf}$ 

J. Qian, A. Heinz, R. Winkler, J. Vinson, A. B. Gamsworthy, R. V. F. Janssens, D. Peterson, D. Seweryniak, M. Asai, B. Back, M. P. Carpenter, G. Savard, A. A. Hecht, C.-L. Jiang, T. L. Khoo, F. G. Kondev, T. Lauritsen, C. J. Lister, A. Robinson, X. Wang, and S. Zhu  
Proceedings of the Conference on Nuclei at the Limits (NS06), Oak Ridge, TN, July 24-28, 2006,  
Book of Abstracts, p. 131 (2006)

Test of Nuclear Chirality in  $^{104}\text{Rh}$  by Study of the Electromagnetic Transitions Properties

G. Rainovski, T. Ahn, M. P. Carpenter, A. Costin, M. Danchev, A. Dewald, R. V. F. Janssens, T. Koike, C. J. Lister, O. Möller, N. Pietralla, C. Vaman, R. Wadsworth, and S. Zhu  
Proceedings of the Conference on Nuclei at the Limits (NS06), Oak Ridge, TN, July 24-28, 2006,  
Book of Abstracts, p. 134 (2006)

The "Octupole Transitional" Nuclei  $^{219,220}\text{Th}$ 

W. Reviol, C. J. Chiara, D. G. Sarantites, O. L. Pechenaya, M. P. Carpenter, R. V. F. Janssens, T. L. Khoo, C. J. Lister, D. Seweryniak, S. Zhu, and S. G. Frauendorf  
Proceedings of the Conference on Nuclei at the Limits (NS06), Oak Ridge, TN, July 24-28, 2006,  
Book of Abstracts, p. 136 (2006)

Ground State Proton Radioactivity from  $^{121}\text{Pr}$ 

A. P. Robinson, P. J. Woods, C. N. Davids, D. Seweryniak, M. P. Carpenter, A. Hecht, R. V. F. Janssens, D. Peterson, S. Sinha, W. B. Walters, and S. Zhu  
Proceedings of the Conference on Nuclei at the Limits (NS06), Oak Ridge, TN, July 24-28, 2006,  
Book of Abstracts, p. 138 (2006)

Multi-Quasiparticle States in  $^{254}\text{No}$ : K-Conservation, Single Particle Energies and Pairing Strengths

S. K. Tandel, T. L. Khoo, D. Seweryniak, G. Mukherjee, I. Ahmad, B. Back, R. Blinstrup, P. A. Butler, M. P. Carpenter, J. Chapman, P. Chowdhury, C. N. Davids, P. T. Greenlees, A. A. Hecht, A. Heinz, R.-D. Herzberg, P. Ikin, R. V. F. Janssens, G. D. Jones, F. G. Kondev, T. Lauritsen, C. J. Lister, E. F. Moore, D. Peterson, P. Reiter, U. S. Tandel, X. Wang, and S. Zhu  
Proceedings of the Conference on Nuclei at the Limits (NS06), Oak Ridge, TN, July 24-28, 2006,  
Book of Abstracts, p. 167 (2006)

## Delayed Alignments and Search for Oblate Rotation in Neutron-Rich Hf Nuclei

U. S. Tandel, P. Chowdhury, S. K. Tandel, D. Cline, C. Y. Wu, M. P. Carpenter, R. V. F. Janssens, T. L. Khoo, T. Lauritsen, C. J. Lister, D. Seweryniak, and S. Zhu  
Proceedings of the Conference on Nuclei at the Limits (NS06), Oak Ridge, TN, July 24-28, 2006,  
Book of Abstracts, p. 168 (2006)

Configurations and Decay Hindrances of High-K States in  $^{180}\text{Hf}$ 

S. K. Tandel, P. Chowdhury, M. P. Carpenter, A. Deacon, S. J. Freeman, N. J. Hammond, R. V. F. Janssens, G. D. Jones, T. L. Khoo, F. G. Kondev, T. Lauritsen, C. J. Lister, E. F. Moore, D. Seweryniak, J. F. Smith, and S. Zhu  
Proceedings of the Conference on Nuclei at the Limits (NS06), Oak Ridge, TN, July 24-28, 2006,  
Book of Abstracts, p. 169 (2006)

Multi-Quasiparticle States in  $^{254}\text{No}$ : K-Conservation, Single Particle Energies and Pairing Strengths

S. K. Tandel, T. L. Khoo, D. Seweryniak, G. Mukherjee, I. Ahmad, B. Back, R. Blinstrup, P. A. Butler, M. P. Carpenter, J. Chapman, P. Chowdhury, C. N. Davids, P. T. Greenlees, A. A. Hecht, A. Heinz, R.-D. Herzberg, P. Ikin, R. V. F. Janssens, G. D. Jones, F. G. Kondev, T. Lauritsen, C. J. Lister, E. F. Moore, D. Peterson, P. Reiter, U. S. Tandel, X. Wang, and S. Zhu  
Proceedings of the Conference on Nuclei at the Limits (NS06), Oak Ridge, TN, July 24-28, 2006,  
Book of Abstracts, p. 170 (2006)

New Spectroscopic Studies of the  $N = Z$  Nuclei  $^{74}\text{Rb}$ ,  $^{76}\text{Sr}$  and  $^{78}\text{Y}$ 

R. Wadsworth, B. S. Nara Singh, A. N. Steer, D. G. Jenkins, P. Davies, R. Glover, N. S. Pattabiraman, T. Grahn, P. T. Greenlees, P. Jones, R. Julin, M. Leino, M. Nyman, J. Pakarinen, P. Rahkila, C. Scholey, J. Sorri, J. Uusitalo, P. A. Butler, M. Dimmock, R.-D. Herzberg, D. T. Joss, R. D. Page, J. Thomson, R. Lemmon, J. Simpson, B. Blank, B. Cederwall, B. Hadinia, M. Sandzelius, A. V. Afanasjev, C. Andreoiu, P. E. Garrett, C. E. Svensson, R. A. E. Austin, M. P. Carpenter, F. Moore, D. Seweryniak, A. O. Macchiavelli, D. Ward, W. Reviol, D. Sarantites, and A. Gorgen  
Proceedings of the Conference on Nuclei at the Limits (NS06), Oak Ridge, TN, July 24-28, 2006,  
Book of Abstracts, p. 182 (2006)



## Strength of Octupole Correlations in the Actinides

X. Wang, S. Zhu, R. V. F. Janssens, I. Wiedenhöver, M. P. Carpenter, I. Ahmad, S. J. Freeman, J. P. Greene, T. L. Khoo, F. G. Kondev, T. Lauritsen, C. J. Lister, D. Seweryniak, U. Garg, A. Bernstein, P. Wilson, E. Diffenderfer, C. Teal, A. Larabee, and B. Meredith  
Proceedings of the Conference on Nuclei at the Limits (NS06), Oak Ridge, TN, July 24-28, 2006,  
Book of Abstracts, p. 183 (2006)

## Study of Neutron-Rich sd-pf Shell Nuclei Using Multi-Nucleon Transfer Reactions

M. Wiedeking, E. Rodriguez-Vieitez, P. Fallon, R. M. Clark, M. Cromaz, M. Descovich, I-Y. Lee, M.-A. Deleplanque, A. O. Macchiavelli, F. S. Stephens, D. Ward, M. P. Carpenter, R. V. F. Janssens, X. Wang, S. Zhu, D. Cline, R. Teng, and C. Y. Wu  
Proceedings of the Conference on Nuclei at the Limits (NS06), Oak Ridge, TN, July 24-28, 2006,  
Book of Abstracts, p. 186 (2006)

Triaxial Strongly Deformed Bands in  $^{171,172}\text{Hf}$ ?

Y. C. Zhang, W. C. Ma, M. P. Carpenter, P. Chowdhury, D. Cullen, M. K. Djongolov, G. B. Hagemann, D. J. Hartley, R. V. F. Janssens, T. L. Khoo, F. G. Kondev, T. Lauritsen, E. F. Moore, E. Ngijoi-Yogo, S. Odegard, S. V. Rigby, D. G. Roux, D. T. Scholes, J. A. Winger, R. B. Yadav, and S. Zhu  
Proceedings of the Conference on Nuclei at the Limits (NS06), Oak Ridge, TN, July 24-28, 2006,  
Book of Abstracts, p. 195 (2006)

Deep Inelastic Reactions with CHICO: The Case of  $^{48}\text{Ca} + ^{208}\text{Pb}$ 

S. Zhu, R. V. F. Janssens, M. P. Carpenter, J. A. Becker, D. Cline, A. B. Hayes, A. Hecht, A. Gade, T. Lauritsen, C. J. Lister, R. Macri, D. Seweryniak, X. Wang, and C. Y. Wu  
Proceedings of the Conference on Nuclei at the Limits (NS06), Oak Ridge, TN, July 24-28, 2006,  
Book of Abstracts, p. 197 (2006)

Structure of the Even-Even Neutron-Rich  $^{56,58,60}\text{Cr}$  Isotopes

S. Zhu, A. N. Deacon, R. V. F. Janssens, S. J. Freeman, R. Broda, M. P. Carpenter, I. R. Calderin, B. Fornal, T. Lauritsen, C. J. Lister, D. Seweryniak, J. F. Smith, S. L. Tabor, and B. J. Varley  
Proceedings of the Conference on Nuclei at the Limits (NS06), Oak Ridge, TN, July 24-28, 2006,  
Book of Abstracts, p. 198 (2006)

## Reaction Studies with Light, Unstable Nuclei

K. Ernst Rehm  
2006 Annual Meeting of the Division of Nuclear Physics of the American Physical Society, Nashville, TN,  
October 25-28, 2006; Bull. Am. Phys. Soc. **51**, 10 (2006)

## High Spin Structure in Neutron Rich Zn Isotopes

A. A. Hecht, N. Hoteling, W. B. Walters, M. P. Carpenter, R. V. F. Janssens, T. Lauritsen, D. Seweryniak, X. Wang, S. Zhu, B. Fornal, R. Broda, W. Krolas, J. Wrzesinski, A. Woehr, N. J. Stone, and J. Stone  
2006 Annual Meeting of the Division of Nuclear Physics of the American Physical Society, Nashville, TN,  
October 25-28, 2006; Bull. Am. Phys. Soc. **51**, 36 (2006)

Update on the Structure of N-Rich  $^{52-56}\text{Ti}$ 

S. Zhu, R. V. F. Janssens, M. P. Carpenter, S. Freeman, B. Fornal, A. Deacon, B. Kay, J. Kozemczak, A. Larabee, T. Lauritsen, A. Robinson, D. Seweryniak, J. Smith, D. Steppenbeck, and X. Wang  
2006 Annual Meeting of the Division of Nuclear Physics of the American Physical Society, Nashville, TN,  
October 25-28, 2006; Bull. Am. Phys. Soc. **51**, 36 (2006)

A New Measurement of the E1 Component of the  $^{12}\text{C}(\alpha,\gamma)^{16}\text{O}$  Reaction

X. D. Tang, M. Notani, K. E. Rehm, I. Ahmad, J. Greene, A. A. Hecht, D. Henderson, R. V. F. Janssens, C. L. Jiang, E. F. Moore, N. Patel, R. C. Pardo, G. Savard, J. P. Schiffer, S. Sinha, M. Paul, L. Jisonna, R. E. Segel, C. Brune, A. Champagne, and A. Wuosmaa  
2006 Annual Meeting of the Division of Nuclear Physics of the American Physical Society, Nashville, TN,  
October 25-28, 2006; Bull. Am. Phys. Soc. **51**, 39 (2006)

## Alpha-Gamma Coincidence Spectroscopy Using a Si PSAPD and Ge DSSD Combination

C. M. Wilson, P. Chowdhury, R. Gramer, S. K. Tandel, N. J. Hammond, C. J. Lister, S. M. Fischer, E. F. Moore, K. M. Teh, L. McClish, K. S. Shah, and R. Farrell  
2006 Annual Meeting of the Division of Nuclear Physics of the American Physical Society, Nashville, TN, October 25-28, 2006; Bull. Am. Phys. Soc. **51**, 84 (2006)

Internal Conversion Coefficient Measurements of Transitions in  $^{167}\text{Lu}$ 

G. Gürdal, C. W. Beausang, D. S. Brenner, H. Ai, R. F. Casten, A. Heinz, E. Williams, B. Crider, R. Raabe, D. J. Hartley, M. Carpenter, R. V. F. Janssens, T. Lauritsen, C. J. Lister, D. Seweryniak, S. Zhu, A. A. Hecht, and J. X. Saladin  
2006 Annual Meeting of the Division of Nuclear Physics of the American Physical Society, Nashville, TN, October 25-28, 2006; Bull. Am. Phys. Soc. **51**, 89 (2006)

Quadrupole Moments of Normal Deformed and Triaxial Strongly Deformed Bands in  $^{167}\text{Lu}$ 

E. Ngijoi-Yogo, W. C. Ma, D. G. Roux, R. B. Yadav, Y. Zhang, G. B. Hagemann, C. R. Hansen, B. Herskind, G. Sletten, H. Amro, D. A. Meyer, G. Gürdal, C. W. Beausang, D. J. Hartley, C. Engelhardt, H. Hübel, A. Neusser, P. Bringel, M. P. Carpenter, T. L. Khoo, T. Lauritsen, and E. F. Moore  
2006 Annual Meeting of the Division of Nuclear Physics of the American Physical Society, Nashville, TN, October 25-28, 2006; Bull. Am. Phys. Soc. **51**, 89 (2006)

Four-, Six- and Eight-Quasiparticle Isomers in  $^{174}\text{Lu}$ 

F. G. Kondev, I. Ahmad, M. P. Carpenter, R. V. F. Janssens, T. Lauritsen, C. J. Lister, D. Seweryniak, G. D. Dracoulis, G. J. Lane, A. P. Byrne, T. Kibedi, P. Chowdhury, and S. K. Tandel  
2006 Annual Meeting of the Division of Nuclear Physics of the American Physical Society, Nashville, TN, October 25-28, 2006; Bull. Am. Phys. Soc. **51**, 90 (2006)

Nucleon Alignment and Shape Competition at High Spin in  $^{180}\text{Hf}$ 

U. S. Tandel, P. Chowdhury, S. K. Tandel, S. Sheppard, D. Cline, C. Y. Wu, M. P. Carpenter, R. V. F. Janssens, T. L. Khoo, T. Lauritsen, C. J. Lister, D. Seweryniak, and S. Zhu  
2006 Annual Meeting of the Division of Nuclear Physics of the American Physical Society, Nashville, TN, October 25-28, 2006; Bull. Am. Phys. Soc. **51**, 90 (2006)

## Search for Highly Deformed Rotational Structures in Tungsten Isotopes

S. K. Tandel, A. J. Knox, U. S. Tandel, C. Parnell-Lampen, P. Chowdhury, D. J. Hartley, J.-Y. Zhang, M. P. Carpenter, R. V. F. Janssens, T. L. Khoo, T. Lauritsen, C. J. Lister, D. Seweryniak, X. Wang, and S. Zhu  
2006 Annual Meeting of the Division of Nuclear Physics of the American Physical Society, Nashville, TN, October 25-28, 2006; Bull. Am. Phys. Soc. **51**, 90 (2006)

Alpha Decay of  $^{257}\text{Rf}$ 

J. Qian, A. Heinz, R. Winkler, J. Vinson, A. B. Gamsworthy, R. V. F. Janssens, D. Peterson, D. Seweryniak, B. Back, M. P. Carpenter, G. Savard, A. A. Hecht, C. L. Jiang, T. L. Khoo, F. G. Kondev, T. Lauritsen, C. J. Lister, A. Robinson, X. Wang, and S. Zhu  
2006 Annual Meeting of the Division of Nuclear Physics of the American Physical Society, Nashville, TN, October 25-28, 2006; Bull. Am. Phys. Soc. **51**, 91 (2006)

Octupole Strength in the  $^{238,240,242}\text{Pu}$ 

X. Wang, S. Zhu, R. V. F. Janssens, M. P. Carpenter, I. Ahmad, J. P. Greene, T. L. Khoo, F. G. Kondev, T. Lauritsen, C. J. Lister, D. Seweryniak, S. J. Freeman, U. Garg, I. Wiedenhöver, A. Bernstein, P. Wilson, E. Diffenderfer, C. Teal, A. Larabee, and B. Meredith  
2006 Annual Meeting of the Division of Nuclear Physics of the American Physical Society, Nashville, TN, October 25-28, 2006; Bull. Am. Phys. Soc. **51**, 91 (2006)

## On Line Yield Measurements of UC Targets

H. K. Carter, E. H. Spejewski, A. Kronenberg, D. W. Stracener, W. Talbert, H.-H. Hsu, J. Nolen, J. Greene, and T. Burtseva

2006 Annual Meeting of the Division of Nuclear Physics of the American Physical Society, Nashville, TN, October 25-28, 2006; Bull. Am. Phys. Soc. **51**, 103 (2006)

Two-Quasiparticle States in  $^{252,254}\text{No}$  and the Stability of Superheavy Nuclei

T. L. Khoo, S. K. Tandel, A. Robinson, D. Seweryniak, and F. G. Kondev

2006 Annual Meeting of the Division of Nuclear Physics of the American Physical Society, Nashville, TN, October 25-28, 2006; Bull. Am. Phys. Soc. **51**, 112 (2006)



**OPERATION AND DEVELOPMENT OF ATLAS  
and  
ACCELERATOR PHYSICS AND EXOTIC BEAM TECHNOLOGY**

Atomic Layer Deposition of W on Nanoporous Carbon Aerogels

J. W. Elam, J. A. Libera, M. J. Pellin, A. V. Zinovev, J. P. Greene, and J. A. Nolen  
*Appl. Phys. Lett.* **89**, 053124/1-3 (2006)

Global Theory of Extended Generating Functions

Bela Erdelyi  
*Int. J. Pure and Appl. Math.* **33**, 553-578 (2006)

Application of a New Procedure for Design of 325 MHz RFQ

P. N. Ostroumov, V. N. Aseev, and A. A. Kolomiets  
*Jrnl. of Instr.* **1**, P04002 (2006)

Physics Design of the 8-GeV H-Minus Linac

P. N. Ostroumov  
*New Jrnl. of Phys.* **8**, 281 (2006)

Computational Needs for the RIA Accelerator Systems

P. N. Ostroumov, J. A. Nolen, and B. Mustapha  
Proceedings of the 8th International Computational Accelerator Physics Conference (ICAP-04),  
St. Petersburg, Russia, June 29-July 2, 2004; *Nucl. Instrum. Methods* **A558**, 25-31 (2006)

ECRIS Operation with Multiple Frequencies

R. C. Vondrasek, R. Scott, and R. C. Pardo  
Proceedings of the 11th International Conference on Ion Sources (ICIS05), Caen, France,  
September 12-16, 2005; *Rev. Sci. Instrum.* **77**, 03A337/1-4 (2006)

Monte Carlo Beam Capture and Charge Breeding Simulation

J. S. Kim, C. Liu, D. H. Edgell, and R. Pardo  
Proceedings of the 11th International Conference on Ion Sources (ICIS05), Caen, France,  
September 12-16, 2005; *Rev. Sci. Instrum.* **77**, 03B106/1-5 (2006)

The Rare Isotope Accelerator

D. F. Geesaman  
Proceedings of the 34th ICFA Advanced Beam Dynamics Workshop on "High Power Superconducting Ion,  
Proton, and Multi-Species Linacs" (HPSL2005), Naperville, IL, May 22-24, 2005, p. OP5 (2006)

Error Simulations and Beam Loss Studies in the RIA Driver Linac

B. Mustapha, P. N. Ostroumov, and V. N. Aseev  
Proceedings of the 34th ICFA Advanced Beam Dynamics Workshop on "High Power Superconducting Ion,  
Proton, and Multi-Species Linacs" (HPSL2005), Naperville, IL, May 22-24, 2005, pp. TP2/1-4 (2006)

Failure Mode and Recovery in the RIA Driver Linac

B. Mustapha and P. N. Ostroumov  
Proceedings of the 34th ICFA Advanced Beam Dynamics Workshop on "High Power Superconducting Ion,  
Proton, and Multi-Species Linacs" (HPSL2005), Naperville, IL, May 22-24, 2005, pp. TWA4/1-5 (2006)

Availability Optimization of a High Power Driver

E. S. Lessner and P. N. Ostroumov

Proceedings of the 34th ICFA Advanced Beam Dynamics Workshop on "High Power Superconducting Ion, Proton, and Multi-Species Linacs" (HPSL2005), Naperville, IL, May 22-24, 2005, pp. TWA5/1-4 (2006)

Applications of Differential Algebraic Methods in Beam Physics

B. Erdelyi

Proceedings of the 34th ICFA Advanced Beam Dynamics Workshop on "High Power Superconducting Ion, Proton, and Multi-Species Linacs" (HPSL2005), Naperville, IL, May 22-24, 2005, pp. TWA6/1-4 (2006)

TRACK: The New Beam Dynamics Code

V. N. Assev, P. N. Ostroumov, E. S. Lessner, and B. Mustapha

Proceedings of the 34th ICFA Advanced Beam Dynamics Workshop on "High Power Superconducting Ion, Proton, and Multi-Species Linacs" (HPSL2005), Naperville, IL, May 22-24, 2005, pp. TWA8/1-4 (2006)

Remote Control of the ATLAS Superconducting Accelerator

F. H. Munson, R. C. Pardo, M. A. Power, R. C. Raffenetti, and R. J. Carrier

Proceedings of the 10th International Conference on Accelerator and Large Experimental Physics Control Systems (ICALEPCS2005), Geneva, Switzerland, October 10-14, 2005, pp. PO1.075-7/1-5 (2006)

Design of the Driver Linac for the Rare Isotope Accelerator

P. N. Ostroumov, J. A. Nolen, and K. W. Shepard

Proceedings of the 39th ICFA Advanced Beam Dynamics Workshop on "High Intensity High Brightness Hadron Beams" (HB2006), Tsukuba, Japan, May 29-June 2, 2006, pp. 89-93 (2006)

Design and Development of an 8-GeV Superconducting H-Linac

P. N. Ostroumov, G. Apollinari, G. W. Foster, and R. Webber

Proceedings of the 39th ICFA Advanced Beam Dynamics Workshop on "High Intensity High Brightness Hadron Beams" (HB2006) Tsukuba, Japan, May 29-June 2, 2006, pp. 134-136 (2006)

Superconducting Spoke Cavities

Mike Kelly

Proceedings of the 39th ICFA Advanced Beam Dynamics Workshop on "High Intensity High Brightness Hadron Beams" (HB2006), Tsukuba, Japan, May 29-June 2, 2006, pp. 337-340 (2006)

Lattice Design in a Multi-GeV H-Minus Linac

P. N. Ostroumov and G. W. Foster

34th ICFA Advanced Beam Dynamics Workshop on "High Power Superconducting Ions, Proton, and Multi-Species Linacs" (HPSL2005), Naperville, IL, May 22-24, 2005, Abstract MWA2 (2006)

Design of the Driver Linac for the Rare Isotope Accelerator

P. N. Ostroumov, J. A. Nolen, and K. W. Shepard

39th ICFA Advanced Beam Dynamics Workshop on "High Intensity High Brightness Hadron Beams" (HB2006), Tsukuba, Japan, May 29-June 2, 2006, Abstract TUAY03 (2006)

Physics Design of a Multi-GeV Superconducting H-Minus Linac

P. N. Ostroumov, G. Apollinari, G. W. Foster, and R. Webber

39th ICFA Advanced Beam Dynamics Workshop on "High Intensity High Brightness Hadron Beams" (HB2006), Tsukuba, Japan, May 29-June 2, 2006, Abstract TUBY02 (2006)

Shielding Design for the CARIBU Project

Eugene Moore, Samuel Baker, Richard Pardo, Guy Savard, and the CARIBU Collaboration

2006 Annual Meeting of the Division of Nuclear Physics of the American Physical Society, Nashville, TN, October 25-28, 2006; Bull. Am. Phys. Soc. **51**, 85 (2006)

**MEDIUM-ENERGY NUCLEAR PHYSICS RESEARCH**

## Double-Hadron Leptoproduction in the Nuclear Medium

A. Airapetian *et al.* (HERMES Collaboration)  
Phys. Rev. Lett. **96**, 162301/1-5 (2006)

Search for the  $\Theta^+$  Pentaquark in the  $\gamma d \rightarrow \Lambda n K^+$  Reaction Measured with CLAS

S. Niccolai *et al.* (CLAS Collaboration)  
Phys. Rev. Lett. **97**, 032001/1-6 (2006)

## Measurement of Deeply Virtual Compton Scattering with a Polarized Proton Target

S. Chen *et al.* (CLAS Collaboration)  
Phys. Rev. Lett. **97**, 072002/1-6 (2006)

Search for  $\Theta^{++}$  Pentaquarks in the Exclusive Reaction  $\gamma p \rightarrow K^+ K^- p$ 

V. Kubarovsky *et al.* (CLAS Collaboration)  
Phys. Rev. Lett. **97**, 102001/1-5 (2006)

Determination of the Pion Charge Form Factor at  $Q^2 = 1.60$  and  $2.45$  (GeV/c)<sup>2</sup>

T. Horn *et al.* (Jefferson Lab  $F_\pi$  Collaboration)  
Phys. Rev. Lett. **97**, 192001/1-4 (2006)

Measurement of the  $x$ - and  $Q^2$ -Dependence of the Asymmetry  $A_1$  on the Nucleon

K. V. Dharmawardane *et al.* (CLAS Collaboration)  
Phys. Lett. **B641**, 11-17 (2006)

Measurement of the Lifetimes of the Lowest  $^3P_1$  State of Neutral Ba and Ra

N. D. Scielzo, J. R. Guest, E. C. Schulte, I. Ahmad, K. Bailey, D. L. Bowers, R. J. Holt, Z.-T. Lu,  
T. P. O'Connor, and D. H. Potterveld  
Phys. Rev. A **73**, 010501(R)/1-4 (2006)

## Experimental Constraints on Nonlinearities Induced by Two-Photon Effects in Elastic and Inelastic Rosenbluth Separations

V. Tvaskis, J. Arrington, M. E. Christy, R. Ent, C. E. Keppel, Y. Liang, and G. Vittorini  
Phys. Rev. C **73**, 025206/1-6 (2006)

## Low-Q Scaling, Duality, and the EMC Effect

J. Arrington, R. Ent, C. E. Keppel, J. Mammei, and I. Niculescu  
Phys. Rev. C **73**, 035205/1-6 (2006)

Moments of Nuclear and Nucleon Structure Functions at Low  $Q^2$  and the Momentum Sum Rule

I. Niculescu, J. Arrington, R. Ent, and C. E. Keppel  
Phys. Rev. C **73**, 045206/1-5 (2006)

Search for the  $\Theta^+$  Pentaquark in the Reactions  $\gamma p \rightarrow \bar{K}^0 K^+ n$  and  $\gamma p \rightarrow \bar{K}^0 K^0 p$ 

R. DeVita *et al.* (CLAS Collaboration)  
Phys. Rev. D **74**, 032001/1-16 (2006)

Longitudinal Spin Transfer to the  $\Lambda$  Hyperon in Semi-Inclusive Deep-Inelastic Scattering

A. Airapetian *et al.*  
Phys. Rev. D **74**, 072004/1-11 (2006)

Beam of Metastable Krypton Atoms Extracted from a Microwave-Driven Discharge

Y. Ding, K. Bailey, A. M. Davis, S.-M. Hu, Z.-T. Lu, and T. P. O'Connor  
Rev. Sci. Instrum. **77**, 126105/1-2 (2006)

A New Parameterization of the Nucleon Elastic Form Factors

R. Bradford, A. Bodek, H. Budd, and J. Arrington  
Proceedings of the 4th International Workshop on Neutrino-Nucleus Interactions in the Few-GeV Region, Okayama, Japan, September 26-29, 2005; Nucl. Phys. **B159**, 127-132 (2006)

Measurement of  $\Delta S$  in the Nucleon at HERMES from Semi-Inclusive DIS

H. E. Jackson (on behalf of the HERMES Collaboration)  
Proceedings of the 17th International Conference on Particles and Nuclei (PANIC'05), Santa Fe, NM, October 23-30, 2005, eds. Peter D. Barnes, Martin D. Cooper, Robert A. Eisenstein, Hubert van Hecke, and Gerard J. Stephenson, AIP Conference Proceedings **842**, 363-365 (2006)

Opportunities with Drell-Yan Scattering: Probing the Sea Quark Distributions of the Proton

P. E. Reimer (on behalf of the Fermilab E866 and E906 Collaborations)  
Proceedings of the 17th International Conference on Particles and Nuclei (PANIC'05), Santa Fe, NM, October 23-30, 2005, eds. Peter D. Barnes, Martin D. Cooper, Robert A. Eisenstein, Hubert van Hecke, and Gerard J. Stephenson, AIP Conference Proceedings **842**, 369-371 (2006)

Progress Towards Laser Trapping of  $^{225}\text{Ra}$  for an Electric Dipole Moment Measurement

N. D. Scielzo, I. Ahmad, K. Bailey, D. L. Bowers, J. R. Guest, R. J. Holt, Z.-T. Lu, T. P. O'Connor, D. H. Potterveld, and E. C. Schulte  
Proceedings of the 17th International Conference on Particles and Nuclei (PANIC'05), Santa Fe, NM, October 23-30, 2005, eds. Peter D. Barnes, Martin D. Cooper, Robert A. Eisenstein, Hubert van Hecke, and Gerard J. Stephenson, AIP Conference Proceedings **842**, 787-789 (2006)

Laser-Trapping of Radium and the Path to a Next Generation Electric Dipole Moment Measurement

J. R. Guest, N. D. Scielzo, I. Ahmad, K. Bailey, J. P. Greene, R. J. Holt, Z.-T. Lu, T. P. O'Connor, D. H. Potterveld, and J. Wang  
Proceedings of the 2006 International Conference on Trapped Charge Particles and Fundamental Physics, Tigh-Na-Mara, Parksville, BC, Canada, September 3-8, 2006, Book of Abstracts, p. 4 (2006)

Towards a Laser Spectroscopic Determination of the  $^8\text{He}$  Nuclear Charge Radius

P. Mueller, K. Bailey, R. J. Holt, R. V. F. Janssens, Z.-T. Lu, T. P. O'Connor, J. P. Schiffer, I. Sulai, M.-G. Saint Laurent, J.-Ch. Thomas, A. C. C. Villari, O. Naviliat-Cuncic, X. Flechard, S.-M. Hu, G. W. F. Drake, and M. Paul  
2006 Annual Meeting of the Division of Nuclear Physics of the American Physical Society, Nashville, TN, October 25-28, 2006; Bull. Am. Phys. Soc. **51**, 20 (2006)

Laser Trapping of Ra-225 and Ra-226 Progress Towards an Electric Dipole Moment Measurement

J. R. Guest, N. D. Scielzo, I. Ahmad, K. Bailey, J. P. Greene, R. J. Holt, Z.-T. Lu, T. P. O'Connor, and D. H. Potterveld  
2006 Annual Meeting of the Division of Nuclear Physics of the American Physical Society, Nashville, TN, October 25-28, 2006; Bull. Am. Phys. Soc. **51**, 110 (2006)



**THEORETICAL PHYSICS**

## Strange Star Surface: A Crust with Nuggets

Prashanth Jaikumar, Sanjay Reddy, and Andrew W. Steiner  
Phys. Rev. Lett. **96**, 041101/1-4 (2006)

## Hindrance of Heavy-Ion Fusion Due to Nuclear Incompressibility

S. Mişicu and H. Esbensen  
Phys. Rev. Lett. **96**, 112701/1-4 (2006)

## Pair Production and Optical Lasers

D. B. Blaschke, A. V. Prozorkevich, C. D. Roberts, S. M. Schmidt, and S. A. Smolyansky  
Phys. Rev. Lett. **96**, 140401/1-4 (2006)

## Reply to Comment by M. Gai

H. Esbensen, G. F. Bertsch, and K. A. Snover  
Phys. Rev. Lett. **96**, 159202 (2006)

## Calculation of Isotope Shifts and Relativistic Shifts in C I, C II, C III and C IV

J. C. Berengut, V. V. Flambaum, and M. G. Kozlov  
Phys. Rev. A **73**, 012504/1-13 (2006)

## Direct Urca Neutrino Rate in Color Superconducting Quark Matter

P. Jaikumar, C. D. Roberts, and A. Sedrakian  
Phys. Rev. C **73**, 042801(R)/1-5 (2006)

## From Finite Nuclei to the Nuclear Liquid Drop: Leptodermous Expansion Based on the Self-Consistent Mean-Field Theory

P.-G. Reinhard, M. Bender, W. Nazarewicz, and T. Vertse  
Phys. Rev. C **73**, 014309/1-11 (2006)

## Interplay of Compressional and Vortical Nuclear Currents in Overtones of the Isoscalar Giant Dipole Resonance

Şerban Mişicu  
Phys. Rev. C **73**, 024301/1-12 (2006)

## Pair Counting, Pion-Exchange Forces and the Structure of Light Nuclei

R. B. Wiringa  
Phys. Rev. C **73**, 034317/1-11 (2006)

## Global Study of Quadrupole Correlation Effects

M. Bender, G. F. Bertsch, and P.-H. Heenen  
Phys. Rev. C **73**, 034322/1-26 (2006)

## Dynamical Coupled-Channel Approach to Hadronic and Electromagnetic Kaon-Hyperon Production on the Proton

B. Juliá-Díaz, B. Sanghai, T.-S. H. Lee, and F. Tabakin  
Phys. Rev. C **73**, 055204/1-20 (2006)

## Coulomb Problem for Vector Bosons

M. Yu. Kuchiev and V. V. Flambaum  
Phys. Rev. D **73**, 093009/1-16 (2006)

## Short-Lived Nuclei in the Early Solar System: Possible AGB Sources

G. J. Wasserburg, M. Busso, R. Gallino, and K. M. Nollett  
Nucl. Phys. **A777**, 5-69 (2006)

## Modern Theories of Low-Energy Astrophysical Reactions

L. E. Marcucci, Kenneth M. Nollett, R. Schiavilla, and R. B. Wiringa  
Nucl. Phys. **A777**, 111-136 (2006)

## Early Infrared Spectral Development of V1187 Scorpii (Nova Scorpii 2004 No. 2)

D. K. Lynch *et al.*  
Astrophys. J. **638**, 987-1003 (2006)

## From First Stars to the Spite Plateau: A Possible Reconciliation of Halo Stars Observations with Predictions from Big Bang Nucleosynthesis

L. Piau, T. C. Beers, D. S. Balsara, T. Sivarani, J. W. Truran, and J. W. Ferguson  
Astrophys. J. **653**, 300-315 (2006)

## Possible Evidence for "Dark Radiation" from Big Bang Nucleosynthesis Data

V. V. Flambaum and E. V. Shuryak  
Europhys. Lett. **74**, 813-816 (2006)

## Sigma Terms of Light-Quark Hadrons

V. V. Flambaum, A. Höll, P. Jaikumar, C. D. Roberts, and S. V. Wright  
Few-Body Systems **38**, 31-51 (2006)

## Spin-Zero Particles Must Be Bosons: A New Proof within Nonrelativistic Quantum Mechanics

M. Peshkin  
Foundations of Physics **36**, 19-29 (2006)

## Complex Rational Numbers in Quantum Mechanics

P. Benioff  
Int. J. Mod. Phys. B **20**, 1730-1741 (2006)

## Mean Excitation Energies for Stopping Power of Atoms and Molecules Evaluated from Oscillator-Strength Spectra

Sachie Kamakura, Naoki Sakamoto, Hidemi Ogawa, Hidetsugu Tsuchida, and Mitio Inokuti  
J. Applied Phys. **100**, 064905/1-12 (2006)

## Narrow Atomic Transitions with Enhanced Sensitivity to Variation of the Fine Structure Constant

E. J. Angstmann, V. A. Dzuba, V. V. Flambaum, A. Yu. Nevsky, and S. G. Karshenboim  
J. Phys. B **39**, 1937-1944 (2006)

## Coulomb Problem for Vector Bosons in Standard Model

Michael Kuchiev and Victor Flambaum  
Modern Phys. Lett. A **21**, 781-788 (2006)

## Probing Variations in Fundamental Constants with Radio and Optical Observations of Quasar Absorption Lines

P. Tzanavaris, J. K. Webb, M. T. Murphy, V. V. Flambaum, and S. J. Curran  
Mon. Not. R. Astron. Soc. **374**, 634-646 (2007)

Pentaquark  $\Theta^+$  (1540) Production in  $\gamma N \rightarrow K \bar{K} N$  Reactions

Yongseok Oh, K. Nakayama, and T.-S. H. Lee  
Physics Reports **423**, 49-89 (2006)

## Bethe's Contributions to Atomic and Molecular Physics

M. Inokuti and B. Bederson  
Phys. Scr. **73**, C98-C106 (2006)

## Mean Excitation Energy for the Stopping Power of Light Elements

D. Y. Smith, M. Inokuti, W. Karstens, and E. Shiles

Proceedings of the 13th International Conference on Radiation Effects in Insulators (REI-2005), Santa Fe, NM, August 28-September 2, 2005; Nucl. Instrum. Methods **B250**, 1-5 (2006)

## Dynamical Model of Electroweak Pion Production in the Resonance Region

T. Sato, B. Szczerbinska, K. Kubodera, and T.-S. H. Lee

Proceedings of the 4th International Workshop on Neutrino-Nucleus Interactions in the Few-GeV Region, Okayama, Japan, September 26-29, 2005; Nucl. Phys. **B159**, 141-146 (2006)

## Schwinger Functions and Light-Quark Bound States, and Sigma Terms

A. Höll, P. Maris, C. D. Roberts, and S. V. Wright

Proceedings of the Cairns Topical Workshop on Light-Cone QCD and Nonperturbative Hadron Physics (LC 2005), Cairns, Australia, July 7-15, 2005; Nucl. Phys. **B161**, 87-44 (2006)

## Surface Structure of Quark Stars with Magnetic Fields

P. Jaikumar

Proceedings of the 9th Workshop on High Energy Physics Phenomenology (WHEPP-9), Bhubaneswar, India, January 3-14, 2006; Pramana - J. Phys. **67**, 937-949 (2006)

## Radiative Capture Versus Coulomb Dissociation

H. Esbensen

Proceedings of the 12th International Conference on Capture Gamma-Ray Spectroscopy and Related Topics (CGS 12), Notre Dame, IN, September 4-9, 2005, eds. Andreas Woehr and Ani Aprahamian, AIP Conference Proceedings **819**, 518-522 (2006)

## Sensitivity to Multiphonon Excitations and Incompressibility in Fusion Reactions

H. Esbensen and S. Mişicu

Proceedings of the International Conference on Reaction Mechanisms and Nuclear Structure at the Coulomb Barrier (Fusion06), San Servolo Island, Venice, Italy, March 19-23, 2006, AIP Conference Proceedings **853**, 13-20 (2006)

## A Perspective on Hadron Physics

A. Höll, C. D. Roberts, and S. V. Wright

Proceedings of the Xth Mexican Workshop on Particles and Fields, Morelia, Michoacán, Mexico, November 7-12, 2005, eds. Adnan Bashir, Victor Villanueva, Luis Villaseñor, Miguel A. Pérez, and Luis Urrutia, AIP Conference Proceedings **857**, 46-61 (2006)

## Variation of Fundamental Constants

V. V. Flambaum

Proceedings of the XX International Conference on Atomic Physics (ICAP 2006), Innsbruck, Austria, July 16-21, 2006, eds. Christian Roos, Hartmut Häffner, and Rainer Blatt, AIP Conference Proceedings **869**, 29-36 (2006)

Models for Extracting  $N^*$  Parameters from Meson-Baryon Reactions

T.-S. H. Lee

Proceedings of the Workshop on the Physics of Excited Nucleons (NSTAR2005), Tallahassee, FL, October 12-15, 2005, eds. S. Capstick, V. Crede, and P. Eugenio (World Scientific 2006) pp. 1-15

## Quantum Monte Carlo Studies of Bound and Unbound Nuclear States

Kenneth M. Nollett

Conference on Nuclei at the Limits (NS06), Oak Ridge, TN, July 24-28, 2006, Book of Abstracts, p. 115 (2006)

Scattering and Reactions in Ab Initio Nuclear Theory

Kenneth M. Nollett

2006 Annual Meeting of the Division of Nuclear Physics of the American Physical Society, Nashville, TN, October 25-28, 2006; Bull. Am. Phys. Soc. **51**, 10 (2006)

Ab Initio Calculations of Electroweak Matrix Elements

Muslema Pervin, R. B. Wiringa, Steven C. Pieper, and Kenneth M. Nollett

2006 Annual Meeting of the Division of Nuclear Physics of the American Physical Society, Nashville, TN, October 25-28, 2006; Bull. Am. Phys. Soc. **51**, 20 (2006)

A Unitary and Relativistic Model for  $\pi\eta N$  and  $\pi\pi N$  Photoproduction

Alvin Kiswandhi, Simon Capstick, and T.-S. Harry Lee

2006 Annual Meeting of the Division of Nuclear Physics of the American Physical Society, Nashville, TN, October 25-28, 2006; Bull. Am. Phys. Soc. **51**, 28 (2006)

N- $\Delta$  Transition Form Factors

Mandar S. Bhagwat

2006 Annual Meeting of the Division of Nuclear Physics of the American Physical Society, Nashville, TN, October 25-28, 2006; Bull. Am. Phys. Soc. **51**, 80 (2006)



**Physics Division**

Argonne National Laboratory  
9700 South Cass Avenue, Bldg. 203  
Argonne, IL 60439-4843

[www.anl.gov](http://www.anl.gov)



UChicago ►  
Argonne<sub>LLC</sub>

A U.S. Department of Energy laboratory  
managed by UChicago Argonne, LLC